Of Mice and Women: Understanding Pregnancy-Induced Changes in Glyburide PK/PD for the Improved Management of Gestational Diabetes Mellitus (GDM)

Diana Lyn Shuster

A dissertation

submitted in partial fulfillment of the

requirements for the degree of

Doctor of Philosophy

University of Washington

2014

Reading Committee:

Qingcheng Mao, Chair

Kenneth E. Thummel

Danny D. Shen

Program Authorized to Offer Degree:

Pharmaceutics

University of Washington

Abstract (350 words)

Of Mice and Women: Understanding Pregnancy-Induced Changes in Glyburide PK/PD for the Improved Management of Gestational Diabetes Mellitus (GDM)

Diana Lyn Shuster

Chair of the Supervisory Committee:
Qingcheng Mao, PhD. Associate Professor
Pharmaceutics

Pregnancy-induced changes in drug PK is explained by changes in physiology and expression of metabolic enzymes and transporters. We determined mRNA expression of enzymes and transporters in the maternal liver, kidney, small intestine, and placenta of pregnant mice by microarray analysis. A full summary of gene expression changes is listed in Supplemental Tables 1-14. Glyburide is commonly prescribed to treat gestational diabetes mellitus, a major complication of pregnancy. Gestational age-dependent changes in glyburide PK have not been characterized. We examined pregnancy-induced changes in the maternal-fetal disposition of glyburide and its primary metabolites using a pregnant mouse model, and found maternal CL, V_{β}, and V_{ss} approximately doubled by mid-late gestation. Glyburide depletion rate in mouse liver microsomes increased as gestation progressed, suggesting increased CL is related to increased hepatic metabolism. Fetal exposure to glyburide was low, but doubled from mid to late pregnancy. Fetal exposure/metabolism of glyburide is also not well characterized. We determined the kinetic parameters of CYP3A enzymes for glyburide depletion; characterized

glyburide metabolism by human fetal livers; and identified the enzyme responsible. M5 was the predominant metabolite generated by fetal CYP3A7 and human fetal liver microsomes (HFLMs). CYP3A7 protein levels in HFLMs were highly correlated with glyburide Cl_{int}, 16α-OH DHEA formation, and 4′-OH MDZ formation. CYP3A5 and CYP3A7 genotype, fetal sex, gestational age, and post-mortem interval did not alter CYP3A7 protein expression or glyburide Cl_{int}. In recent years, oral hypoglycemic agents such as glyburide and metformin have gained increasing popularity for the treatment of GDM. Data is quite limited regarding the PD of glyburide and metformin during pregnancy. We completed an interim analysis of glyburide monotherapy, metformin monotherapy, or glyburide/metformin combination therapy in women with gestational diabetes compared to healthy pregnant women and non-pregnant women with type-2 diabetes mellitus receiving metformin. Pharmacodynamic analyses of blood glucose, insulin, and C-peptide data were performed, and estimates of insulin sensitivity (SI), beta-cell responsivity (Φ_t), and disposition index (DI) were compared across treatment groups. The full study is still ongoing. Overall, this body of research provides novel insight for the optimization of oral hypoglycemic therapies in the management of gestational diabetes mellitus.

Dedication

In loving memory of my incredible mother, Janis

For my father, Mark, and my beloved sisters, Susan and Laura

For my husband, Brent, whose unconditional support was a gift I will never forget

Table of Contents

Chapter 1: Introduction

Portions of this work were previously published by Shuster et al., 2011 (citation below).

Diana L. Shuster, Mary F. Hebert and Qingcheng Mao (2011). Glyburide Disposition During Pregnancy, Gestational Diabetes, Prof. Miroslav Radenkovic (Ed.), ISBN: 978-953-307-581-5, InTech, DOI: 10.5772/20926. Available from: http://www.intechopen.com/books/gestational-diabetes/glyburide-disposition-during-pregnancy

1.1 Introduction

During pregnancy, 5-14% of women are diagnosed with gestational diabetes mellitus (GDM) and the incidence has been increasing in recent years [1, 2]. While insulin treatment is still the "gold standard" therapy for controlling maternal glycemia, the increasing use of oral anti-diabetic agents such as glyburide and metformin has begun to change standard care [3]. Anti-diabetic drugs are often titrated over a prolonged period of time to achieve glycemic control. Prolonged hyperglycemia increases the likelihood of adverse fetal/neonatal and maternal outcomes. Thus, quickly achieving glycemic control during pregnancy can significantly reduce the occurrence of certain adverse perinatal and maternal outcomes [4].

Glyburide is a second generation oral sulfonylurea that lowers blood sugar levels by stimulating the pancreas to secrete insulin [5]. Considerable data in the literature suggest that glyburide may be a safe alternative to insulin for the treatment of GDM due to its similar

efficacy to insulin and its low fetal distribution [6]. Physiological and biochemical changes that occur during pregnancy alter the pharmacokinetics of glyburide, thus potentially affecting the safety and efficacy of the drug for both the mother and the fetus. Understanding pregnancy-induced changes in the disposition of glyburide (including fetal exposure) will be important for optimizing dosage guidelines during pregnancy. This chapter summarizes current knowledge on the safety and efficacy of glyburide for the treatment of GDM, as well as glyburide disposition during pregnancy, and outlines the specific aims of this dissertation research that were conducted to address important knowledge gaps.

1.2 Pregnancy-induced changes in drug pharmacokinetics

Throughout gestation, pregnant women experience substantial changes to their physiology and biochemistry in order to support fetal growth and maturation. The implications of such changes during pregnancy on medication selection, safety, and efficacy, however, are not well characterized. According to one international study, 81.2% of women used at least one prescription or over-the-counter medication while pregnant, and 17% of those medications were used to treat chronic or long-term illness [7]. Another study in the United States reported that between 2006 and 2008, 50% of women reported taking four or more medications (including prescription and over-the-counter) at some point during pregnancy [8]. Therefore, there is a growing need to understand pregnancy-induced changes in maternal drug disposition and efficacy during pregnancy, as well as fetal exposure and toxicity.

Physiological changes of pregnancy

All aspects of drug absorption, distribution, metabolism, and excretion (ADME) can be affected by physiological changes during pregnancy. The magnitude of these changes is largely determined by the physiochemical properties of a drug in conjunction with gestational age-dependent physiological changes. Drug dissolution and absorption following oral administration may be both altered by decreases in gastric emptying time and intestinal motility during pregnancy, as well as increases in gastric pH [9]. The volume of distribution and drug partitioning between blood and tissues could be affected by increases in blood volume (~50%) and total fat content during pregnancy [10]. Albumin concentrations decrease during pregnancy in part because of diluted plasma volume and its decreased synthesis in the liver, which could result in increase in the plasma unbound fraction (f_u) for some drugs [9]. Increases in f_u will in turn increase clearance of low extraction ratio or orally administered drugs. High extraction ratio drugs whose clearance is limited by perfusion to the liver and kidney may also experience a shortened half-life during pregnancy due to major increases in cardiac output (~40%) [10]. The well-characterized physiological changes that occur during pregnancy lead to predictable changes in the pharmacokinetics and efficacy of drugs in pregnant women prior to administration.

Changes in gene expression during pregnancy

In addition to physiologically-based changes in PK, there is also evidence of changes in ADME gene expression during pregnancy that could affect drug PK and efficacy. Several studies have already shown that expression and activities of drug-metabolizing enzymes and transporters are altered during pregnancy [11-13]. In humans, these include cytochrome P450 (CYP)

enzymes such as CYP2A6, CYP2D6, CYP3A4, and CYP2C9 (increased activity), as well as CYP1A2 and CYP2C19 (decreased activity) [9, 14, 15]. Additionally, the expression and/or activity of phase II enzymes such as UGT1A4 and UGT 2B4 have been shown to increase during pregnancy [16]. Such changes have been shown to alter drug pharmacokinetics during pregnancy [17, 18]. Because there are ethical and logistical barriers to studying gene expression during pregnancy in humans, rodent models are frequently used. One challenge in translating expression data between species, however, is the absence of orthologs for some of the major players in drug metabolism and disposition, (i.e. CYP3A4). Despite this challenge, there are still similarities in pregnancy-induced changes in gene expression across species. Hepatic CYP3A activity in pregnant mice increases nearly two-fold compared to non-pregnant mice, which is comparable to the changes seen in humans [19-21]. Likewise, hepatic *Cyp1a2* mRNA decreases in mouse pregnancy is consistent with CYP1A2 activity in pregnant women [11, 22].

Fewer studies have been done in humans or rodents to elucidate changes in the expression of drug transporters during pregnancy. The mainstay of research has focused on ATP-binding cassette (ABC) transporters such as P-glycoprotein (P-gp) and Breast Cancer Resistance Protein (BCRP). In humans, P-gp-mediated renal secretion of digoxin increases during late gestation [12]. In pregnant mice, however, P-gp protein levels do not seem to be significantly affected in the liver, kidney, and small intestine, and mRNA expression actually decreases in the kidney [19, 21]. Despite these differences, the role of P-gp and BCRP in determining fetal drug exposure has been extensively studied in mouse models because of the similar efflux function of these transporters in mouse and human placenta [23-26]. Importantly, in mice, rats and humans, placental mRNA and protein expression of BCRP decreases from mid gestation towards term

[27-31]. There are still many drug transporters whose expression and activity have not been characterized throughout pregnancy.

The main limitation of the aforementioned studies is the scarcity of gestational age-dependent data in gene expression. In recent years, there have been attempts to understand gene or protein expression throughout gestation [19, 22, 29, 32], however this body of research is not comprehensive, and rather, focused on a limited number or category of genes. After considering the similarities between pregnant mice and women in regards to drug PK during pregnancy, I have chosen the pregnant mouse as an appropriate animal model to study gestational age-dependent changes in the expression of drug disposition genes. **Therefore, the objective of Chapter 2 was to characterize gestational age-dependent expression of drug-metabolizing enzymes and transporters in maternal tissues of pregnant mice using microarray analysis.**

1.3 Gestational diabetes mellitus (GDM) and treatment options

The American College of Obstetricians and Gynecologists (ACOG) committee on practice defines GDM as "carbohydrate intolerance that begins or is first recognized during pregnancy" [33]. GDM and type 2 diabetes mellitus are believed to share similar disease pathologies characterized by insulin resistance and/or deficiencies in pancreatic production/secretion of insulin. Insulin resistance is normal to some extent during pregnancy as a means of ensuring that glucose is freely available to the developing fetus; however, in women predisposed to diabetes, the degree of insulin resistance can be so high that treatment is necessary to maintain euglycemia.

Traditionally, women are screened for GDM based on the presence of risk factors such as age, weight, family history of diabetes, perinatal loss and previously large babies; however, this

practice only detects ~50% of cases. Because risk factors do not predict all instances of GDM and symptoms are minimal, simple diagnostic tests for glucose tolerance are used during routine obstetric visits to aid in the diagnosis of GDM. Women are generally screened between 24-28 weeks gestation in a non-fasted state using an oral glucose challenge test (OGCT) or in a fasted state using the oral glucose tolerance test (OGTT). Typically, women drink a solution containing 50-100 g/dL of glucose and blood glucose concentrations are measured for up to three hours. The threshold for diagnosis depends on the screening test administered [34].

If left untreated, GDM presents a danger to both the mother and baby, particularly the risk of hypertension, preeclampsia, urinary tract infections, cesarean delivery and development of type 2 diabetes mellitus later in life in mothers, as well as macrosomia, neonatal hypoglycemia, childhood obesity and type 2 diabetes mellitus in the offspring [1, 35-37]. Diet therapy is the first line of treatment for GDM and is adequate for controlling glucose concentrations in the majority of patients. Those failing diet therapy are managed with the addition of pharmacotherapy [38]. Traditionally, insulin therapy has been the "gold standard" for the management of GDM, when diet therapy and exercise fail to achieve maternal glycemic control. Pregnant women have difficulty adhering to insulin therapy regimens, though, because of the challenges with route of administration (intravenous) and schedule. Therefore, oral hypoglycemic agents such as glyburide and metformin are being increasingly used to treat GDM, and have been shown to have similar efficacy and safety as insulin, as well as lower cost and easier route of administration [3, 6]. The safety of insulin for use in pregnancy has been well established and is without the risk of transfer across the placenta. The FDA has not approved the use of glyburide or metformin for the treatment of women with GDM. Despite this, glyburide use off-label for the treatment of GDM has risen from 7.4% in 2000 to 64.5% in 2011 [39].

1.4 Glyburide and its clinical pharmacokinetics

Glyburide is a second generation oral sulfonylurea (Figure 1-1). Glyburide is indicated for the treatment of type 2 diabetes mellitus and stimulates insulin production in the pancreas [5]. Specifically, glyburide inhibits ATP-sensitive potassium channels on the surface of pancreatic beta-islet cells, leading to cellular membrane depolarization. Depolarization at the cellular membrane prompts voltage-gated calcium channels to open, increasing the intracellular calcium concentration, which stimulates the release of insulin into the portal vein. The FDA approved dosage range is 1.25 - 20 mg per day. When higher dosages of glyburide are required, patients are typically switched to insulin.

Glyburide is a small lipophilic molecule (LogP = 4.8, MW = 494 Da) that is highly bound to plasma proteins (99.8% plasma protein binding). Glyburide is well absorbed, with an oral bioavailability of approximately 95% for micronized tablets [40]. It exhibits biphasic elimination kinetics, with an initial distribution half-life ($t_{1/2\alpha}$) of roughly 30 min and a terminal elimination half-life ($t_{1/2\beta}$) of approximately 10 hours [5, 41]. Glyburide has a small volume of distribution (0.2 L/kg), despite its lipophilic nature, and has negligible renal clearance.

Glyburide is extensively metabolized in the liver with a low hepatic extraction ratio. Three enzymes are believed to be primarily responsible for the metabolism of glyburide: CYP3A4, CYP2C9, and CYP2C19. CYP2C9 is highly polymorphic and multiple clinical studies have shown that subjects expressing CYP2C9*3, which is associated with lower catalytic activity compared to wild-type CYP2C9*1 [42], demonstrated a nearly 40% decrease in the oral clearance of glyburide and 2-3 fold increase in plasma area under the curve (AUC) [43-45]. These clinical studies suggest that CYP2C9 contributes significantly to glyburide metabolism *in*

vivo. On the other hand, *in vitro* studies using human liver microsomes have shown that CYP3A4 contributes greater than 50% of glyburide metabolism, while CYP2C9 contributes a much smaller percentage [46-48]. Additionally, Lilja et al. showed that oral administration of clarithromycin, an inhibitor of CYP3A but not CYP2C9, significantly increased C_{max} and the plasma AUC of glyburide [49]. An epidemiological study [50] and case reports [51, 52] all indicated that the concomitant use of glyburide with clarithromycin (a CYP3A4 inhibitor) was associated with severe hypoglycemia. Thus, CYP3A also appears to contribute to glyburide metabolism *in vivo*. It is therefore likely that glyburide is metabolized *in vivo* through the joint actions of hepatic CYP3A and CYP2C9.

In vitro metabolism studies using human liver microsomes or recombinant systems revealed that, besides CYP3A4 and CYP2C9, glyburide was also metabolized by other cytochrome P450 enzymes such as CYP3A5, CYP2C8 and CYP2C19, but to a much lesser extent [46-48]. Zharikova et al. determined five primary metabolites of glyburide formed in human liver microsomes: M1 (4-*trans*-hydrocyclohexyl glyburide), M2a (4-*cis*-hydrocyclohexyl glyburide), M2b (3-*cis*-hydrocyclohexyl glyburide), M3 (3-*trans*-hydrocyclohexyl glyburide), M4 (2-*trans*-hydrocyclohexyl glyburide) and M5 (ethylene-hydroxylated glyburide) [48, 53]. The structures of these primary metabolites are shown in Figure 1-1. CYP3A4 preferentially forms M5, followed by M1, but is capable of forming all primary metabolites. CYP2C9 catalyzes the formation of M1-M3. CYP2C8 catalyzes the formation of M1, M2b, M3 and M4; and CYP2C19 catalyzes the formation of M2a, M2b and M3 [48, 53]. Two metabolites of glyburide, M1 and M2b, are believed to be pharmacologically active and are ultimately excreted into the bile and urine (~50% each) [5, 54]. The fate of the remaining metabolites, as well as their potential pharmacologic activity has not been established.

1.5 Glyburide pharmacokinetics during pregnancy

Data is quite limited regarding the PK of glyburide during pregnancy, particularly in relation to gestational age. Hebert et al. estimated a 2-fold increase in the oral clearance of glyburide in women with GDM in the third trimester of pregnancy compared to non-pregnant women with type 2 diabetes mellitus [17]. The formation clearance of M1, a pharmacologically active metabolite, was also increased more than 2-fold in the women with GDM. The underlying mechanism of glyburide's increased clearance is not certain, but could be due to increased CYP3A and CYP2C9 activity during pregnancy [12, 55]. To test this hypothesis, glyburide PK and hepatic metabolism was examined in pregnant mice. Similar to humans, the expression and activity of several CYP3A isoforms are significantly increased during pregnancy in mice, which made the pregnant mouse a suitable animal model to investigate glyburide PK during pregnancy [19, 56]. Indeed, Zhou et al. found that the clearance of glyburide was doubled in pregnant mice (gestation day 15) compared to non-pregnant controls [20], and glyburide metabolism via depletion studies with hepatic S-9 fractions was markedly higher in pregnant mice (gestation day 15) compared to non-pregnant mice. Furthermore, glyburide depletion was also inhibited to a large extent by ketoconazole, a CYP3A inhibitor, suggesting that the increased hepatic clearance of glyburide during pregnancy may likely be due to increased hepatic CYP3A activity [20]. Though the mechanism of increased clearance appears to be CYP3A related, the time-course of these pregnancy-induced changes remains largely undescribed. **Therefore, the objective of Chapter 3 was to investigate gestational age-dependent changes in the maternal-fetal disposition of glyburide.**

Hebert et al. have also shown that glyburide concentrations are measurable in umbilical cord blood at the time of delivery (umbilical cord to maternal plasma concentration ratio equaled 0.7 ± 0.4), suggesting that glyburide can cross the placenta [17]. Many ATP-binding cassette (ABC) efflux transporters such as P-gp, BCRP, and multidrug resistance proteins (MRPs) are highly expressed on the apical membrane of placental syncytiotrophoblasts and serve to protect the fetus by expelling compounds from the fetal compartment to the maternal circulation [57-60]. Using transfected cell lines treated with selective transporter inhibitors, inside-out placental membrane vesicles, and *ex vivo* placental perfusion models, Gedeon et al. showed that glyburide is preferentially transported by BCRP and to a small degree by MRP1, 2, and 3 as well [61-63]. Additionally, Gedeon et al. showed that MRP's play a minor role in fetal exposure to glyburide [63]. Zhou et al. also confirmed that glyburide is a substrate for human BCRP and the murine homolog of BCRP (Bcrp1) [25]. Hemauer et al. showed that MRP1 seemingly plays a greater role in the efflux of glyburide than P-gp or BCRP, making the predominant placental efflux transporter of glyburide debatable [64]. Zhou et al. also characterized glyburide disposition in wild-type and *Bcrp1*$^{-/-}$ pregnant mice (gestation day 15) and found that the fetal AUC of glyburide was 2-fold higher in *Bcrp1*$^{-/-}$ mice compared to wild-type mice [25]. Whether BCRP is the predominant efflux transporter of glyburide in human placenta is still uncertain. In mice, however, BCRP seems to be the predominant placental transporter that determines fetal exposure to glyburide.

Human term placentas have also been used in several studies to characterize placental metabolism of glyburide [48, 53, 65]. Zharikova et al. reported that placental microsomes metabolized glyburide primarily to M5 (~87% relative abundance), and that CYP19 was the primary enzyme responsible [48, 53]. The intrinsic clearance of CYP19 was only 1.8% of the

overall intrinsic clearance of human liver microsomes for glyburide, however. Thus, the placenta appears to play a minor role in the maternal disposition of glyburide, but placental formation of M5 could have clinical implications for fetal exposure to glyburide and its metabolites.

Additionally, fetal metabolism of glyburide, particularly in the fetal liver, may have important effects on overall fetal exposure to glyburide and its metabolites. CYP3A7 is the predominant CYP enzyme in the human fetal liver [66-68]. Previous studies have shown that glyburide is a substrate of CYP3A4 and CYP3A5 [47], which suggests that glyburide is also a substrate of CYP3A7. CYP3A7 has been shown to oxidize CYP3A4 substrates, but with different oxidation site preferences [67], suggesting that if CYP3A7 did metabolize glyburide, it may create a unique metabolite profile. Several *in vitro* studies have also shown that human fetal livers can metabolize endogenous molecules, drugs, and procarcinogens [69, 70]. Given that glyburide can cross the placental barrier [17, 62], **the objective of Chapter 4 was to investigate CYP3A7-mediated metabolism of glyburide metabolism in human fetal livers and evaluate the corresponding metabolite profile.**

1.6 The safety and efficacy of glyburide during pregnancy

Maternal and neonatal safety

Several studies have been conducted to investigate the adverse effects of glyburide versus insulin on maternal health. Some of the most common adverse outcomes reported are hypoglycemia, preeclampsia, weight gain and cesarean delivery. Langer et al. observed hypoglycemia in 20% of women treated with insulin compared to only 4% of those treated with glyburide [71]. Additionally, Yogev et al. reported that 63% of insulin-treated subjects with

GDM experienced asymptomatic hypoglycemia versus 28% of glyburide-treated patients [72]. On the other hand, Ogunyemi et al. was unable to show a significant difference in hypoglycemic events between insulin and glyburide groups (31% versus 38%, respectively) [73]; and other clinical studies did not observe any hypoglycemic events all together [74, 75]. Although the results varied, possibly due to differences in the definition of hypoglycemia, these studies appear to support the notion that glyburide therapy generally causes fewer maternal hypoglycemic events than insulin therapy. Regarding other maternal adverse outcomes, Langer et al. showed no difference in the incidence of preeclampsia among women treated with insulin or glyburide [71], Bertini et al. found no significant difference in maternal weight gain [75], and multiple studies showed no significant differences in cesarean delivery rate [71, 73-75].

Various clinical studies have also analyzed the effects of glyburide and insulin on neonatal adverse outcomes. Of the perinatal morbidities recorded, neonatal hypoglycemia and LGA infants appear to be the most common, though incidence rates vary between studies. Coetzee and Jackson treated over 600 pregnant women suffering from GDM or type 2 diabetes mellitus with glyburide, metformin or insulin therapy, and evaluated neonatal outcomes [76]. Their results suggest metformin was the safest (0 still births, 1 neonatal death, and 33 per 1,000 perinatal morbidities), followed by glyburide (1 still birth, 0 neonatal deaths, and 43 per 1,000 perinatal morbidities) and finally insulin (1 still birth, 4 neonatal deaths, and 59 per 1,000 perinatal morbidities). The authors also reported zero cases of serious neonatal hypoglycemia in the group of subjects receiving glyburide [76]. Langer et al. also showed no difference in the incidence rate of hypoglycemia in infants whose mothers were treated with either insulin or glyburide [71]. In contrast, Bertini et al. observed neonatal hypoglycemia in 8 newborns, 6 of which were from their glyburide treatment group [75]. Likewise, Ogunyemi et al. reported that

28% of infants from the glyburide treatment group experienced hypoglycemia versus 13% in the insulin group [73]. Due to conflicting evidence, it is still uncertain whether glyburide causes infant hypoglycemia more often than insulin.

Bertini et al. also demonstrated that a significantly higher percentage of fetuses in the glyburide treatment group were large for gestational age (LGA) infants compared to the insulin group (25% versus 3.7%, respectively) [75]; however, Langer et al. reported comparable incidence rates of LGA between treatment groups [71]. All the clinical studies mentioned consistently reported higher average infant birth weights in the glyburide group than the insulin group, but the difference was small (an average of ~100 g) and not statistically significant [71, 73-75].

Overall, the maternal and neonatal safety of glyburide does not substantially differ from insulin therapy. There is no long-term safety data, however, for infants whose mothers were treated with glyburide. Thus, further studies are needed to assess the long-term effects of maternal glyburide administration on child and adolescent development (neurologic and behavioral) as well as the incidence rate of type 2 diabetes mellitus and obesity.

Clinical efficacy during pregnancy

There have been several randomized controlled clinical trials examining the efficacy of glyburide for the treatment of GDM during pregnancy [71, 73-75]. Perhaps the most influential study was performed by Langer et al., who showed no statistically significant difference in fasting, preprandial, 2-hour postprandial and mean blood glucose concentrations between the glyburide and insulin groups, concluding that glyburide was as effective as insulin for the treatment of GDM [71]. Two smaller clinical studies also observed no difference in fasting and

2-hour postprandial blood glucose concentrations [74, 75]. In contrast, Ogunyemi et al. reported significantly higher blood glucose concentrations (fasting and 2-hour postprandial) in patients receiving glyburide compared to insulin [73]. One study reported that the failure rate of glyburide therapy in women with GDM reached as high as ~20% even with similarities in maternal demographics across treatment groups (e.g. age, weight and parity) [75, 77]. Moore et al. also measured the efficacy of metformin versus glyburide for the treatment of gestational diabetes. The failure rate of women taking metformin (n = 75) was 2.1 times higher than the glyburide group (n = 74) [78]. The study failed to include a control group that received insulin as the standard of care, therefore, conclusions regarding the efficacy of metformin and/or glyburide compared to insulin could not be made.

Retrospective studies have also been conducted to assess the efficacy of glyburide in women with GDM [79, 80]. While several of the randomized controlled trials found glucose concentrations were either similar or higher in women receiving glyburide compared to insulin, Jacobson et al. noted in a retrospective study (n = 584) that women receiving glyburide had significantly lower post-treatment fasting and postprandial blood glucose levels, and that the failure rate of glyburide was 12% [79]. Additionally, Ramos et al. retrospectively examined the effectiveness of glyburide (n = 44) versus insulin (n = 78) in women with GDM who previously received a 50 g 3-hour OGCT, and found there were no significant differences between treatment with respect to blood glucose levels; however the failure rate of glyburide was again 16% [80]. Retrospective studies are often not adequately powered, though, and do not possess adequate controls, making general conclusions regarding the efficacy of glyburide more difficult.

In light of glyburide failure rates, there is a need to better understand what factors determine treatment failure versus clinical control. Kahn et al. conducted a prospective cohort study (n = 75) that demonstrated that fasting blood glucose levels ≥ 110 mg/dL in women with GDM were associated with higher glyburide failure rates [81]. The authors also reported that women who were older, had more than one child and were diagnosed with GDM earlier in their pregnancy were more likely to fail glyburide therapy. These women also had a higher mean fasting blood glucose, suggesting that these women may already have difficulty producing and releasing sufficient levels of endogenous insulin. Therefore a drug that stimulates insulin secretion such as glyburide might not be effective (Kahn et al., 2006). Another study by Rochon et al. suggested that only higher mean blood glucose levels (≥ 200 mg/dL in the 50 g 1-hour OGCT) were indicators of glyburide failure [82]. Considering the heterogeneous pathology of GDM (insulin resistance and/or beta-cell dysfunction), there may be times when glyburide therapy (which improves beta-cell function) may not be the appropriate medication to control blood glucose levels. **Therefore, the objective of Chapter 5 was to provide a quantitative interim analysis of an ongoing clinical study comparing the efficacy of glyburide, metformin or glyburide/metformin combination therapy in women with GDM.**

1.7 Conclusions

Although insulin therapy has been the "gold standard" for the treatment of GDM, the increasing use of oral anti-diabetic agents such as glyburide and metformin has begun to change the standard of care. Clinical studies demonstrate that glyburide is a safe alternative to insulin therapy for the treatment of GDM due to its similar efficacy to insulin, relatively low fetal exposure, lower cost and ease of administration. The pharmacokinetic properties of glyburide

resulting in low fetal exposure include: high plasma protein binding, a relatively short elimination half-life, and efflux transport by ABC transporters such as BCRP in the placenta. Glyburide is also metabolized in the placenta by CYP19, which may limit fetal exposure to the parent compound but simultaneously expose the fetus to metabolites. Although the currently used glyburide dosage range for pregnant women with GDM may have comparable maternal, fetal and neonatal outcomes as insulin therapy, there are still concerns that have yet to be addressed, such as the PK changes during pregnancy, the mechanisms behind fetal exposure to glyburide and metabolites, and clinical effectiveness of glyburide used alone and in combination with metformin The studies described in following thesis chapters were designed to address these concerns.

Physiological changes that occur during pregnancy may alter the pharmacokinetics of glyburide, thus affecting the safety and efficacy of the drug for both the mother and the fetus. In **Chapter 2**, gestational age-dependent changes in gene expression of metabolic enzymes and drug transporters in the maternal liver, kidney, small intestine, and placenta of pregnant mice were studied using microarray approaches. The results of which will be important for understanding mechanistic determinants of altered glyburide PK during pregnancy. A recent clinical study has demonstrated that the apparent oral clearance of glyburide is increased two-fold in pregnant women with gestational diabetes as compared to non-pregnant women with type 2 diabetes mellitus [17]. The mechanism of such a change in glyburide disposition during pregnancy has not been fully understood, but is likely related to increased expression and activity of cytochrome P450 enzymes in the liver, such as CYP2C9 and CYP3A. In **Chapter 3**, gestational age-dependent changes in maternal-fetal glyburide PK were evaluated in the pregnant mouse model, as well as the distribution and exposure of glyburide metabolites. The gestational

age-dependent changes in maternal-fetal disposition of glyburide were interpreted in conjugation with the microarray gene expression analysis. In **Chapter 4**, the capacity of the human fetal liver to metabolize glyburide via CYP3A7 was explored to further our understanding of determinants for fetal exposure to glyburide and its metabolites. Taken together, these studies imply the need for dosage optimization of glyburide during pregnancy. In **Chapter 5**, preliminary pharmacodynamic (PD) analyses of serum glucose, insulin, and C-peptide levels were performed in women with GDM receiving glyburide, metformin, or glyburide/metformin combination therapy to estimate markers of drug efficacy: insulin sensitivity (SI), beta-cell responsivity (Φ_{total}), and disposition index (DI).

In summary, glyburide has been increasingly used for the treatment of GDM with similar safety and efficacy to insulin therapy. The mechanistic understanding of pregnancy-induced changes in the disposition and efficacy of this drug are explored in this thesis work, and will be important for the optimization of dosage guidelines during pregnancy.

Figures for Chapter 1

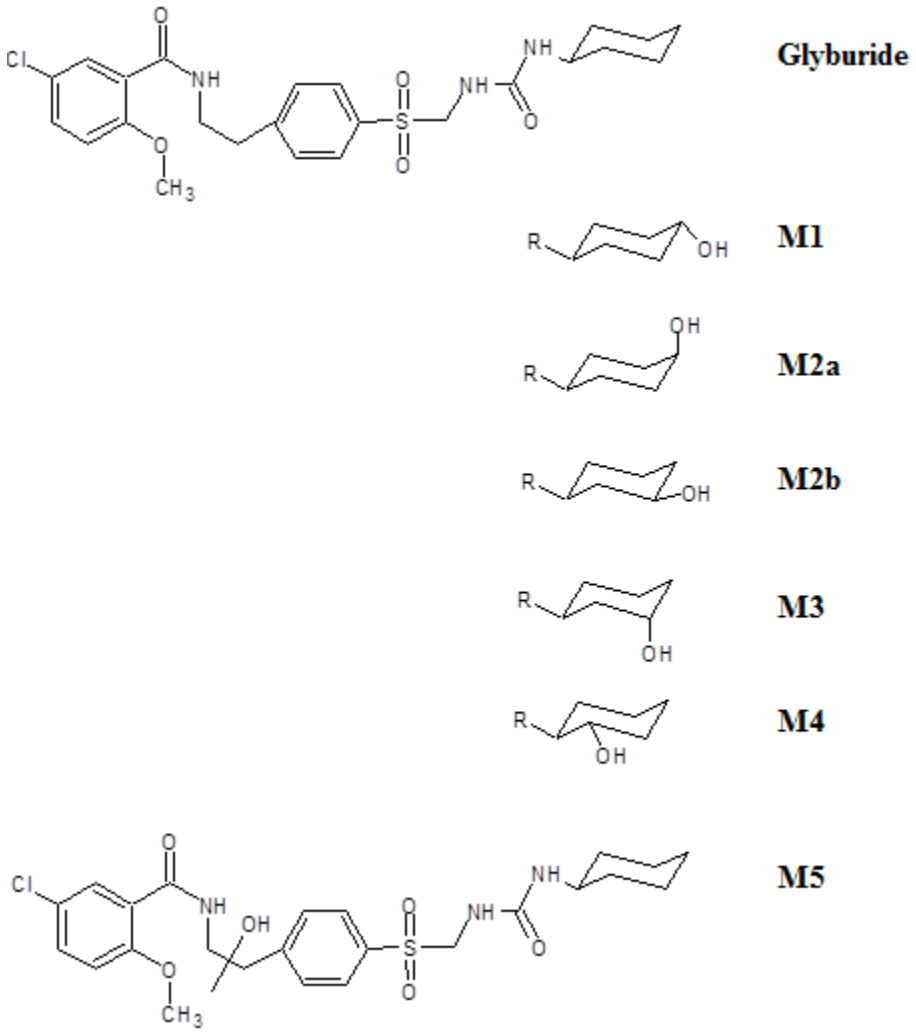

Figure 1-1. The structures of glyburide and its primary metabolites. M1, 4-trans-hydrocyclohexyl glyburide); M2a, 4-cis-hydrocyclohexyl glyburide; M2b, 3-cis-hydrocyclohexyl glyburide; M3, 3-trans-hydrocyclohexyl glyburide; M4, 2-trans-hydrocyclohexyl glyburide; and M5, ethylene-hydroxylated glyburide.

References

[1] Paglia MJ, Coustan DR. Gestational diabetes: evolving diagnostic criteria. Curr Opin Obstet Gynecol. 2011;23:72-5.
[2] Jovanovic L, Pettitt DJ. Gestational diabetes mellitus. JAMA. 2001;286:2516-8.
[3] Maymone AC, Baillargeon JP, Menard J, Ardilouze JL. Oral hypoglycemic agents for gestational diabetes mellitus? Expert Opin Drug Saf. 2011;10:227-38.
[4] Karakash SD, Einstein FH. Diabetes in pregnancy: glycemia control guidelines and rationale. Curr Opin Endocrinol Diabetes Obes. 2011.
[5] Feldman JM. Glyburide: a second-generation sulfonylurea hypoglycemic agent. History, chemistry, metabolism, pharmacokinetics, clinical use and adverse effects. Pharmacotherapy. 1985;5:43-62.
[6] Nicholson W, Baptiste-Roberts K. Oral hypoglycaemic agents during pregnancy: The evidence for effectiveness and safety. Best Pract Res Clin Obstet Gynaecol. 2011;25:51-63.
[7] Lupattelli A, Spigset O, Twigg MJ, Zagorodnikova K, Mardby AC, Moretti ME, et al. Medication use in pregnancy: a cross-sectional, multinational web-based study. BMJ open. 2014;4:e004365.
[8] Mitchell AA, Gilboa SM, Werler MM, Kelley KE, Louik C, Hernandez-Diaz S, et al. Medication use during pregnancy, with particular focus on prescription drugs: 1976-2008. American journal of obstetrics and gynecology. 2011;205:51 e1-8.
[9] Anderson GD. Pregnancy-induced changes in pharmacokinetics: a mechanistic-based approach. Clin Pharmacokinet. 2005;44:989-1008.
[10] Klieger C, Pollex E, Kazmin A, Koren G. Hypoglycemics: pharmacokinetic considerations during pregnancy. Ther Drug Monit. 2009;31:533-41.
[11] Tracy TS, Venkataramanan R, Glover DD, Caritis SN. Temporal changes in drug metabolism (CYP1A2, CYP2D6 and CYP3A Activity) during pregnancy. American journal of obstetrics and gynecology. 2005;192:633-9.
[12] Hebert MF, Easterling TR, Kirby B, Carr DB, Buchanan ML, Rutherford T, et al. Effects of pregnancy on CYP3A and P-glycoprotein activities as measured by disposition of midazolam and digoxin: a University of Washington specialized center of research study. Clin Pharmacol Ther. 2008;84:248-53.
[13] Feghali MN, Mattison DR. Clinical therapeutics in pregnancy. Journal of biomedicine & biotechnology. 2011;2011:783528.
[14] Dempsey D, Jacob P, 3rd, Benowitz NL. Accelerated metabolism of nicotine and cotinine in pregnant smokers. The Journal of pharmacology and experimental therapeutics. 2002;301:594-8.
[15] Hodge LS, Tracy TS. Alterations in drug disposition during pregnancy: implications for drug therapy. Expert Opin Drug Metab Toxicol. 2007;3:557-71.
[16] Anger GJ, Piquette-Miller M. Pharmacokinetic studies in pregnant women. Clin Pharmacol Ther. 2008;83:184-7.
[17] Hebert MF, Ma X, Naraharisetti SB, Krudys KM, Umans JG, Hankins GD, et al. Are we optimizing gestational diabetes treatment with glyburide? The pharmacologic basis for better clinical practice. Clin Pharmacol Ther. 2009;85:607-14.

[18] Unadkat JD, Wara DW, Hughes MD, Mathias AA, Holland DT, Paul ME, et al. Pharmacokinetics and safety of indinavir in human immunodeficiency virus-infected pregnant women. Antimicrob Agents Chemother. 2007;51:783-6.
[19] Zhang H, Wu X, Wang H, Mikheev AM, Mao Q, Unadkat JD. Effect of pregnancy on cytochrome P450 3a and P-glycoprotein expression and activity in the mouse: mechanisms, tissue specificity, and time course. Mol Pharmacol. 2008;74:714-23.
[20] Zhou L, Zhang Y, Hebert MF, Unadkat JD, Mao Q. Increased glyburide clearance in the pregnant mouse model. Drug Metab Dispos. 2010;38:1403-6.
[21] Mathias AA, Maggio-Price L, Lai Y, Gupta A, Unadkat JD. Changes in pharmacokinetics of anti-HIV protease inhibitors during pregnancy: the role of CYP3A and P-glycoprotein. J Pharmacol Exp Ther. 2006;316:1202-9.
[22] Koh KH, Xie H, Yu AM, Jeong H. Altered cytochrome P450 expression in mice during pregnancy. Drug metabolism and disposition: the biological fate of chemicals. 2011;39:165-9.
[23] Jonker JW, Smit JW, Brinkhuis RF, Maliepaard M, Beijnen JH, Schellens JH, et al. Role of breast cancer resistance protein in the bioavailability and fetal penetration of topotecan. J Natl Cancer Inst. 2000;92:1651-6.
[24] Smit JW, Huisman MT, van Tellingen O, Wiltshire HR, Schinkel AH. Absence or pharmacological blocking of placental P-glycoprotein profoundly increases fetal drug exposure. The Journal of clinical investigation. 1999;104:1441-7.
[25] Zhou L, Naraharisetti SB, Wang H, Unadkat JD, Hebert MF, Mao Q. The breast cancer resistance protein (Bcrp1/Abcg2) limits fetal distribution of glyburide in the pregnant mouse: an Obstetric-Fetal Pharmacology Research Unit Network and University of Washington Specialized Center of Research Study. Mol Pharmacol. 2008;73:949-59.
[26] Zhang Y, Wang H, Unadkat JD, Mao Q. Breast cancer resistance protein 1 limits fetal distribution of nitrofurantoin in the pregnant mouse. Drug Metab Dispos. 2007;35:2154-8.
[27] Cygalova L, Ceckova M, Pavek P, Staud F. Role of breast cancer resistance protein (Bcrp/Abcg2) in fetal protection during gestation in rat. Toxicol Lett. 2008;178:176-80.
[28] Yasuda S, Itagaki S, Hirano T, Iseki K. Expression level of ABCG2 in the placenta decreases from the mid stage to the end of gestation. Biosci Biotechnol Biochem. 2005;69:1871-6.
[29] Wang H, Wu X, Hudkins K, Mikheev A, Zhang H, Gupta A, et al. Expression of the breast cancer resistance protein (Bcrp1/Abcg2) in tissues from pregnant mice: effects of pregnancy and correlations with nuclear receptors. American journal of physiology Endocrinology and metabolism. 2006;291:E1295-304.
[30] Kalabis GM, Petropoulos S, Gibb W, Matthews SG. Breast cancer resistance protein (Bcrp1/Abcg2) in mouse placenta and yolk sac: ontogeny and its regulation by progesterone. Placenta. 2007;28:1073-81.
[31] Meyer zu Schwabedissen HE, Jedlitschky G, Gratz M, Haenisch S, Linnemann K, Fusch C, et al. Variable expression of MRP2 (ABCC2) in human placenta: influence of gestational age and cellular differentiation. Drug Metab Dispos. 2005;33:896-904.
[32] Aleksunes LM, Cui Y, Klaassen CD. Prominent expression of xenobiotic efflux transporters in mouse extraembryonic fetal membranes compared with placenta. Drug metabolism and disposition: the biological fate of chemicals. 2008;36:1960-70.

[33] ACOG Practice Bulletin. Clinical management guidelines for obstetrician-gynecologists. Number 30, September 2001 (replaces Technical Bulletin Number 200, December 1994). Gestational diabetes. Obstetrics and gynecology. 2001;98:525-38.
[34] Moyer VA, Force USPST. Screening for gestational diabetes mellitus: U.S. Preventive Services Task Force recommendation statement. Annals of internal medicine. 2014;160:414-20.
[35] The Hyperglycemia and Adverse Pregnancy Outcome (HAPO) Study. Int J Gynaecol Obstet. 2002;78:69-77.
[36] Hyperglycaemia and Adverse Pregnancy Outcome (HAPO) Study: associations with maternal body mass index. BJOG. 2010;117:575-84.
[37] Hyperglycemia and Adverse Pregnancy Outcome (HAPO) Study: associations with neonatal anthropometrics. Diabetes. 2009;58:453-9.
[38] Lang T, Hitzl M, Burk O, Mornhinweg E, Keil A, Kerb R, et al. Genetic polymorphisms in the multidrug resistance-associated protein 3 (ABCC3, MRP3) gene and relationship to its mRNA and protein expression in human liver. Pharmacogenetics. 2004;14:155-64.
[39] Camelo Castillo W, Boggess K, Sturmer T, Brookhart MA, Benjamin DK, Jr., Jonsson Funk M. Trends in glyburide compared with insulin use for gestational diabetes treatment in the United States, 2000-2011. Obstetrics and gynecology. 2014;123:1177-84.
[40] Jonsson A, Rydberg T, Ekberg G, Hallengren B, Melander A. Slow elimination of glyburide in NIDDM subjects. Diabetes Care. 1994;17:142-5.
[41] Prendergast BD. Glyburide and glipizide, second-generation oral sulfonylurea hypoglycemic agents. Clinical pharmacy. 1984;3:473-85.
[42] Cavallari LH, Limdi NA. Warfarin pharmacogenomics. Curr Opin Mol Ther. 2009;11:243-51.
[43] Kirchheiner J, Brockmoller J, Meineke I, Bauer S, Rohde W, Meisel C, et al. Impact of CYP2C9 amino acid polymorphisms on glyburide kinetics and on the insulin and glucose response in healthy volunteers. Clin Pharmacol Ther. 2002;71:286-96.
[44] Niemi M, Cascorbi I, Timm R, Kroemer HK, Neuvonen PJ, Kivisto KT. Glyburide and glimepiride pharmacokinetics in subjects with different CYP2C9 genotypes. Clin Pharmacol Ther. 2002;72:326-32.
[45] Yin OQ, Tomlinson B, Chow MS. CYP2C9, but not CYP2C19, polymorphisms affect the pharmacokinetics and pharmacodynamics of glyburide in Chinese subjects. Clin Pharmacol Ther. 2005;78:370-7.
[46] Naritomi Y, Terashita S, Kagayama A. Identification and relative contributions of human cytochrome P450 isoforms involved in the metabolism of glibenclamide and lansoprazole: evaluation of an approach based on the in vitro substrate disappearance rate. Xenobiotica. 2004;34:415-27.
[47] Zhou L, Naraharisetti SB, Liu L, Wang H, Lin YS, Isoherranen N, et al. Contributions of human cytochrome P450 enzymes to glyburide metabolism. Biopharm Drug Dispos. 2010;31:228-42.
[48] Zharikova OL, Fokina VM, Nanovskaya TN, Hill RA, Mattison DR, Hankins GD, et al. Identification of the major human hepatic and placental enzymes responsible for the biotransformation of glyburide. Biochem Pharmacol. 2009;78:1483-90.
[49] Lilja JJ, Niemi M, Fredrikson H, Neuvonen PJ. Effects of clarithromycin and grapefruit juice on the pharmacokinetics of glibenclamide. British journal of clinical pharmacology. 2007;63:732-40.

[50] Schelleman H, Bilker WB, Brensinger CM, Wan F, Hennessy S. Anti-infectives and the risk of severe hypoglycemia in users of glipizide or glyburide. Clin Pharmacol Ther. 2010;88:214-22.
[51] Bussing R, Gende A. Severe hypoglycemia from clarithromycin-sulfonylurea drug interaction. Diabetes Care. 2002;25:1659-61.
[52] Leiba A, Leibowitz A, Grossman E. An unusual case of hypoglycemia in a diabetic patient. Ann Emerg Med. 2004;44:427-8.
[53] Zharikova OL, Ravindran S, Nanovskaya TN, Hill RA, Hankins GD, Ahmed MS. Kinetics of glyburide metabolism by hepatic and placental microsomes of human and baboon. Biochem Pharmacol. 2007;73:2012-9.
[54] Rydberg T, Jonsson A, Roder M, Melander A. Hypoglycemic activity of glyburide (glibenclamide) metabolites in humans. Diabetes Care. 1994;17:1026-30.
[55] Feghali MN, Mattison DR. Clinical therapeutics in pregnancy. J Biomed Biotechnol. 2011;2011:783528.
[56] Shuster DL, Bammler TK, Beyer RP, Macdonald JW, Tsai JM, Farin FM, et al. Gestational age-dependent changes in gene expression of metabolic enzymes and transporters in pregnant mice. Drug Metab Dispos. 2013;41:332-42.
[57] Mao Q. BCRP/ABCG2 in the placenta: expression, function and regulation. Pharmaceutical research. 2008;25:1244-55.
[58] Ceckova-Novotna M, Pavek P, Staud F. P-glycoprotein in the placenta: expression, localization, regulation and function. Reprod Toxicol. 2006;22:400-10.
[59] Behravan J, Piquette-Miller M. Drug transport across the placenta, role of the ABC drug efflux transporters. Expert Opin Drug Metab Toxicol. 2007;3:819-30.
[60] Ni Z, Mao Q. ATP-binding Cassette Efflux Transporters in Human Placenta. Curr Pharm Biotechnol. 2010.
[61] Gedeon C, Behravan J, Koren G, Piquette-Miller M. Transport of glyburide by placental ABC transporters: implications in fetal drug exposure. Placenta. 2006;27:1096-102.
[62] Gedeon C, Anger G, Piquette-Miller M, Koren G. Breast cancer resistance protein: mediating the trans-placental transfer of glyburide across the human placenta. Placenta. 2008;29:39-43.
[63] Gedeon C, Anger G, Lubetsky A, Miller MP, Koren G. Investigating the potential role of multi-drug resistance protein (MRP) transporters in fetal to maternal glyburide efflux in the human placenta. J Obstet Gynaecol. 2008;28:485-9.
[64] Hemauer SJ, Patrikeeva SL, Nanovskaya TN, Hankins GD, Ahmed MS. Role of human placental apical membrane transporters in the efflux of glyburide, rosiglitazone, and metformin. American journal of obstetrics and gynecology. 2010;202:383 e1-7.
[65] Jain S, Zharikova OL, Ravindran S, Nanovskya TN, Mattison DR, Hankins GD, et al. Glyburide metabolism by placentas of healthy and gestational diabetics. Am J Perinatol. 2008;25:169-74.
[66] Komori M, Nishio K, Kitada M, Shiramatsu K, Muroya K, Soma M, et al. Fetus-specific expression of a form of cytochrome P-450 in human livers. Biochemistry. 1990;29:4430-3.
[67] Leeder JS, Gaedigk R, Marcucci KA, Gaedigk A, Vyhlidal CA, Schindel BP, et al. Variability of CYP3A7 expression in human fetal liver. J Pharmacol Exp Ther. 2005;314:626-35.

[68] Hakkola J, Raunio H, Purkunen R, Saarikoski S, Vahakangas K, Pelkonen O, et al. Cytochrome P450 3A expression in the human fetal liver: evidence that CYP3A5 is expressed in only a limited number of fetal livers. Biol Neonate. 2001;80:193-201.
[69] Shimada T, Yamazaki H, Mimura M, Wakamiya N, Ueng YF, Guengerich FP, et al. Characterization of microsomal cytochrome P450 enzymes involved in the oxidation of xenobiotic chemicals in human fetal liver and adult lungs. Drug Metab Dispos. 1996;24:515-22.
[70] Yang HY, Lee QP, Rettie AE, Juchau MR. Functional cytochrome P4503A isoforms in human embryonic tissues: expression during organogenesis. Mol Pharmacol. 1994;46:922-8.
[71] Langer O, Conway DL, Berkus MD, Xenakis EM, Gonzales O. A comparison of glyburide and insulin in women with gestational diabetes mellitus. N Engl J Med. 2000;343:1134-8.
[72] Yogev Y, Ben-Haroush A, Chen R, Rosenn B, Hod M, Langer O. Undiagnosed asymptomatic hypoglycemia: diet, insulin, and glyburide for gestational diabetic pregnancy. Obstetrics and gynecology. 2004;104:88-93.
[73] Ogunyemi D, Jesse M, Davidson M. Comparison of glyburide versus insulin in management of gestational diabetes mellitus. Endocr Pract. 2007;13:427-8.
[74] Anjalakshi C, Balaji V, Balaji MS, Seshiah V. A prospective study comparing insulin and glibenclamide in gestational diabetes mellitus in Asian Indian women. Diabetes Res Clin Pract. 2007;76:474-5.
[75] Bertini AM, Silva JC, Taborda W, Becker F, Lemos Bebber FR, Zucco Viesi JM, et al. Perinatal outcomes and the use of oral hypoglycemic agents. J Perinat Med. 2005;33:519-23.
[76] Coetzee EJ, Jackson WP. The management of non-insulin-dependent diabetes during pregnancy. Diabetes Res Clin Pract. 1985;1:281-7.
[77] Kremer CJ, Duff P. Glyburide for the treatment of gestational diabetes. American journal of obstetrics and gynecology. 2004;190:1438-9.
[78] Moore LE, Clokey D, Rappaport VJ, Curet LB. Metformin compared with glyburide in gestational diabetes: a randomized controlled trial. Obstetrics and gynecology. 2010;115:55-9.
[79] Jacobson GF, Ramos GA, Ching JY, Kirby RS, Ferrara A, Field DR. Comparison of glyburide and insulin for the management of gestational diabetes in a large managed care organization. American journal of obstetrics and gynecology. 2005;193:118-24.
[80] Ramos GA, Jacobson GF, Kirby RS, Ching JY, Field DR. Comparison of glyburide and insulin for the management of gestational diabetics with markedly elevated oral glucose challenge test and fasting hyperglycemia. J Perinatol. 2007;27:262-7.
[81] Kahn BF, Davies JK, Lynch AM, Reynolds RM, Barbour LA. Predictors of glyburide failure in the treatment of gestational diabetes. Obstetrics and gynecology. 2006;107:1303-9.
[82] Rochon M, Rand L, Roth L, Gaddipati S. Glyburide for the management of gestational diabetes: risk factors predictive of failure and associated pregnancy outcomes. American journal of obstetrics and gynecology. 2006;195:1090-4.

Chapter 2: Gestational Age-Dependent Changes in Gene Expression of Metabolic Enzymes and Transporters in Pregnant Mice

This work was previously published by Shuster et al., in *Drug Metabolism and Disposition* **41**:332–342, February 2013.

2.1 Introduction

Significant physiological changes during pregnancy are essential to support and protect the developing fetus [1]. Changes in maternal physiology include, among others, increased renal blood flow and glomerular filtration rate (GFR) [2], as well as increased hepatoportal venous blood flow (Carlin and Alfirevic, 2008). These physiological changes alter important drug pharmacokinetic (PK) determinants such as GFR, oral absorption, plasma volume, and plasma protein binding [3-5]. Considerable data in the literature also suggest that expression and activities of drug-metabolizing enzymes and transporters are altered during pregnancy [6-8]. In

humans, cytochrome P450 (CYP) enzymes such as CYP2A6, CYP3A4, CYP2D6, and CYP2C9 demonstrate increased activities during pregnancy, whereas the activities of CYP1A2 and CYP2C19 are decreased [3, 9, 10]. These changes result in altered drug PK during pregnancy [11, 12].

The trends in human pregnancy regarding expression/activity of metabolic enzymes and drug transporters appear to be similar in pregnant mice. Hepatic CYP3A activity in pregnant mice, for example, is increased to a similar extent as CYP3A in humans (compared to non-pregnant controls) [13-15]. In addition, hepatic *Cyp1a2* mRNA is decreased during mouse pregnancy, which is consistent with CYP1A2 activity in pregnant women [6, 16]. Fewer studies have been done in humans and animals, though, to investigate changes in activity of drug transporters in the liver, kidney, and small intestine during pregnancy. P-glycoprotein (P-gp) is perhaps the most studied of all transporters, but discrepancies exist between mice and humans. In humans, P-gp-mediated renal secretion of digoxin increased during late gestation [7]. However, during mouse pregnancy, not only were P-gp protein levels unaffected in the liver, kidney, and small intestine, but mRNA expression actually decreased in the kidney [13, 15]. Despite this difference, the role of ATP-binding cassette (ABC) transporters (i.e. P-gp and BCRP) in determining fetal drug exposure has been extensively studied in mouse models because of the similar efflux function of these transporters in mouse and human placenta [17-20].

Current research merely provides snapshots of gene expression or protein activity at select times during pregnancy [14, 19]. Only in the last several years has there been any attempt to understand gene or protein expression throughout gestation [13, 16, 21, 22]. This body of research targeted specific CYP isoforms, as well as important solute carrier (SLC) and ABC

transporters. None of these studies, however, offer a comprehensive overview of trends in expression as gestation progresses for *all* mouse isoforms related to drug metabolism and disposition. After considering the similarities between pregnant mice and women, we chose the pregnant mouse as an appropriate animal model to study gestational age-dependent changes in expression of drug disposition genes. Therefore, the goal of this study was to analyze the global gene expression profiles of maternal tissues and placenta at different gestational ages using microarray approaches.

Though the focus of our study was to investigate gestational age-dependent changes in metabolic enzymes and transporters relevant to drug disposition, we were also cognizant of the fact that changes in *Cyp*, *Abc*, *Slc*, or *Slco* gene expression during pregnancy could potentially impact the homeostasis of endogenous substances such as bile acids and steroid hormones. Characterization of genes involved in bile acid synthesis and distribution during pregnancy may provide a physiologic basis for understanding complications that arise during pregnancy such as intrahepatic cholestasis of pregnancy. Characterization of steroid hormone production during pregnancy supports mechanistic explanations of gestational age-dependent expression of metabolic enzymes and transporters. Thus, we systematically investigated expression of all metabolic enzymes and transporters in the mouse maternal tissues and placenta across gestation, demonstrating significant changes in the expression of many genes including those important for drug, bile acid, and steroid hormone metabolism and transport. These data also provide novel insights into potential changes in drug PK during pregnancy, and support the growing foundation of evidence clinicians need to make decisions regarding drug dosage selection during pregnancy.

2.2 Materials and Methods

Animal studies

FVB wild-type mice, 7-10 weeks of age, were purchased from Taconic Farms (Hudson, NY), and cared for in accordance with the Guide for the Care and Use of Laboratory Animals published by the National Research Council. The animal protocol for this project was approved by the Institutional Animal Care and Use Committee at the University of Washington (protocol number 4035-01). Briefly, mice were maintained under 12-hour light/dark cycles, and food was provided *ad libitum*. Female mice, 7-10 weeks of age, were mated with male mice of the same age overnight. Gestation day (gd) 1 was defined as the presence of a sperm plug following overnight housing. Gd 0 was defined as non-pregnant mice. Progression of pregnancy was monitored by visual inspection and body weight increase. On gd 0, 7.5, 10, 15, and 19, female mice (n = 5-6 per gestational age) were sacrificed under anesthesia (isoflurane) by cardiac puncture, and the maternal liver, kidney, and small intestine were collected. The placentas were collected on gd 10, 15, and 19. All tissues were rinsed with phosphate-buffered saline, snap-frozen in liquid nitrogen, and stored at -80°C until use.

Total RNA extraction

Total RNA was isolated from the snap-frozen mouse tissues using the miRNeasy mini kit (Qiagen, Valencia, CA) according to the manufacturer's instructions for purification of total RNA from animal tissues. The integrity of RNA samples was assessed with an Agilent 2100 Bioanalyzer (Agilent Technologies Inc., Santa Clara, CA),which is the recognized standard in the field. RNA integrity was evaluated using the RNA integrity number (RIN) and by observing

distinct and sharp 18s and 28s ribosomal RNA peaks. The RIN of all samples was greater than 9. RNA quantity and purity were determined with a Thermo Scientific NanoDrop™ 1000 Spectrophotometer (Thermo Fisher Scientific Inc., Wilmington, DE) by measuring OD_{260}, as well as $OD_{260/280}$ and $OD_{260/230}$ ratios, respectively. Samples with $OD_{260/280}$ ratios greater than 1.9 and $OD_{260/230}$ ratios greater than 1.6 were considered acceptable for further processing. Five RNA samples per gestation day that passed these stringent quality control measures were selected from each tissue group for further processing.

Microarray hybridization and data analysis

Processing of the RNA samples was carried out according to the AffymetrixGeneChip Whole Transcript Sense Target labeling protocol (http://www.affymetrix.com/index.affx) as reported previously [23]. The arrays were scanned with an AffymetrixGeneChip® 3000 scanner. Image generation and feature extraction were performed using the AffymetrixGeneChip Command Console (**AGCC**) software. Affymetrix Mouse Gene 1.0 ST Arrays were used for this study. The output files from **AGCC** were further processed using the Bioconductor oligo package [24]. Raw data were normalized using quantile normalization and then summarized at the transcript level using a Robust Multi-array Average (RMA) method [25]. For the maternal tissues, we made univariate comparisons of gd 7.5, 10, 15, and 19 to gd 0 using the Bioconductor limma package, which fits an analysis of variance model to the data and then computes individual contrasts. For the placenta, univariate comparisons of gd 10 and 15 to gd 19 were also made using Bioconductor. The limma package uses an empirical Bayes adjustment on the variance estimate (based on all genes on the array) to increase power to detect true differences [26]. P-values were adjusted for multiplicity with the program q-value which allows the selection

of statistically significant genes while controlling the estimated false discovery rate (FDR) [27, 28].

The adjusted p-values or the FDR values are only interpretable when genes are ranked by unadjusted p-values, from the smallest to the largest. The corresponding FDR value for an unadjusted p-value of 0.05 varies for each gestational age and tissue. A given FDR value states that the group of genes listed above the corresponding unadjusted p-value cut-off has a particular FDR associated with it. This FDR value represents a percentage of genes within the group list whose fold-changes in expression are there by chance alone, i.e. false positive results. FDR values are therefore displayed as supplemental data for each gestation day comparison to gd 0 for maternal tissues or gd 19 for placenta (Supplemental Data PDF file, Tables 1-14). Microarray data presented in this study were deposited in the National Center for Biotechnology Information Gene Expression Omnibus data repository under accession number GSE41438.

Filtration criteria for differentially expressed genes

Expression patterns of differentially expressed genes were visualized by creating heatmaps of relevant genes. Ordering of genes in these plots was determined by hierarchical clustering of the gene expression values. For the overall gene expression trends shown in heatmaps, genes with a larger than 2-fold or less than 0.5-fold change in expression compared to gd 0, an unadjusted p-value less than 0.05, and a $\log_2$ average fluorescent intensity greater than 4, for at least one gestation day, were considered to be differentially expressed for the maternal liver, kidney, and small intestine. Because the placenta is an organ undergoing development as gestation progresses, the number of differentially expressed genes in this tissue, as determined using the above criteria, was much larger than the number of genes in the maternal tissues. To

limit the number of differentially expressed genes in the placenta to something comparable to the maternal tissues, we implemented a more stringent statistical criteria, namely, genes with a larger than 2-fold or less than 0.5-fold change on gd 10 or 15 compared to gd 19, an unadjusted p-value less than 0.00005, and a $\log_2$ average fluorescent intensity greater than 4, for at least one gestation day. Fluorescent intensity is an indication of signal strength and data integrity. Higher fluorescent intensity ensures that a detected change is not background noise and is therefore an important factor to consider before further examination of gene expression data.

For changes in gene expression shown in relevant tables**,** expression of metabolic enzyme and transporter genes, namely, *Cyp*, *Ugt*, and *Sult* enzymes as well as *Abc*, *Slc*, and *Slco* transporters, were filtered based on a lower fold-change criteria that included genes demonstrating larger than 1.5-fold or less than 0.65-fold changes in expression, as well as unadjusted p-values less than 0.05 for maternal tissues and placenta, and average $\log_2$ fluorescent intensities greater than 4, for at least one gestation day compared to gd 0 (maternal tissues) or gd 19 (placenta).

In order to examine *Cyp*, *Abc*, and *Slc* genes that are important for drug metabolism and transport, but do not meet previous filtration criteria needed for inclusion in tables, we selected specific genes known to be involved in drug metabolism and disposition (e.g., *Cyp1*, *Cyp2*, and *Cyp3* isoforms) and filtered them according to unadjusted p-values less than 0.01 and $\log_2$ average fluorescent intensities greater than 4, for at least one gestation day compared to gd 0 for maternal tissues and gd 19 for placenta. Fold-changes in expression of these genes were smaller, but are meaningful to understand drug PK during pregnancy and were therefore presented in relevant figures.

Quantitative real-time PCR validation

To validate microarray gene expression data, quantitative real-time PCR was used. We selected 3 genes from the 25 maternal liver tissues (n = 5 for gd 0, 7.5, 10, 15, and 19) and 7 genes from the 15 placental tissues (n = 5 for gd 10, 15, and 19), which totaled 180 microarray gene expression data for validation. The three genes selected for RNA quantification in the maternal liver were *Abcc3*, *Cyp17a1*, and *Cyp2d40*. The seven genes selected for RNA quantification in the placenta were *Abcb1a*, *Abcb1b*, *Abcg2*, *Cyp2s1*, *Slc22a3*, *Slco1a4*, and *Slco2b1*. These genes were selected because they either demonstrated large changes in the microarray data or are important for xenobiotic metabolism and transport. Fluorogenic 5' nuclease-based assays were employed as previously described [23, 29, 30]. *Actb* (*β-actin*) amplification plots derived from serial dilutions of an established reference sample were used to create a linear regression formula to calculate expression levels. Variations in *β-actin* gene expression throughout gestation were small (< 25% in the maternal liver and < 18% in the placenta) (data not shown), and *β-actin* was therefore selected as an internal control to normalize the data for the respective tissue.

2.3 Results

Validation of microarray data by quantitative real-time PCR (qRT-PCR)

Gene expression levels determined by microarray analysis correlated well with mRNA levels determined by qRT-PCR (Pearson's R coefficient of 0.99 and 0.95 for the liver and placenta, respectively) (Figure 2-1). A direct comparison of the approaches is shown in Figures

2-2 and 2-3. *Cyp17a1*, *Cyp2d40*, and *Abcc3* (*Mrp3*) expression in the maternal liver is shown in Figure 2-2; placental expression of *Cyp2s1*, *Abcb1a* (*Mdr1a*), *Abcb1b* (*Mdr1b*), *Abcg2* (*Bcrp1*), *Slc22a3* (*Oct3*), *Slco1a4* (*Oatp4c1*), and *Slco2b1* (*Oatp2b1*) is shown in Figure 2-3. In both tissues, the absolute magnitude of change in expression was consistently greater for the qRT-PCR data compared to the microarray data. Both approaches also agreed on the direction of change (up- or down-regulation), except for *Cyp2d40* on gd 7.5 in the maternal liver as well as *Abcg2* and *Slco1a4* on gd 15 in the placenta where changes in gene expression were small. Taken together, these results establish the accuracy and reliability of our microarray analysis.

Overall gestational age-dependent trends in gene expression

Hierarchical one-dimensional clustering of differentially expressed genes for each tissue is shown in Figure 2-4. Gene expression levels in the liver and small intestine were similar between replicate samples within the same gestational age group. Changes in expression in the liver and small intestine (up- or down-regulation) were more robust as gestation progressed, peaking on gd 15 and/or gd 19 (Figure 2-4A and 2-4C). Interestingly, the kidney exhibited a bimodal pattern of gene expression that peaked on gd 10 and gd 19 (Figure 2-4B). This apparent trend is the result of replicate samples gd 10_3 and gd 10_6. In addition, the expression on gd 15 in the placenta was not very different from term placenta (gd 19); however, large differences were visible on gd 10 compared to gd 19 (Figure 2-4D). Figure 2-4D also shows that the pattern of expression between placenta sample replicates was very similar, except for gd19_1, which appeared to be more robust in comparison to the other replicates in the gd 19 group. Although expression in the placenta was lower on gd 10, this is in comparison to gd 19 placenta levels, indicating that gene expression in the placenta is actually increasing throughout the course of

pregnancy. All tissues demonstrated a preference for up-regulation during pregnancy; however, the pattern of changes in gene expression throughout gestation was uniquely different for the kidney.

The filtration criteria used to generate heatmaps in Figure 2-4 were also used to count the number of differentially expressed genes for each gestation day. In the liver, 56, 103, 216, and 138 genes were differentially expressed on gd 7.5, 10, 15, and 19, respectively. In the kidney, there were 17, 163, 38, and 74 genes differentially expressed on gd 7.5, 10, 15, and 19, respectively. The small intestine had 37, 55, 47, and 75 differentially expressed genes on gd 7.5, 10, 15, and 19, respectively. In the placenta, 856 genes were differentially expressed on gd 10, but only 8 genes were differentially expressed on gd 15. As a whole, this study identified 1,883 differentially expressed genes in the maternal tissues and placenta.

Drug metabolism during pregnancy

Major gene families involved in drug metabolism (*Cyp*, *Ugt*, and *Sult*) were analyzed for gestational age-dependent changes in expression. Raw microarray data from these gene families were filtered based on three criteria. First, on at least one gestation day, fold changes in expression (compared to gd 0 for maternal tissues and gd 19 for placenta) had to be greater than 1.5 or less than 0.65. Second, these fold changes had to have a corresponding unadjusted p-value that was less than 0.05. Third, for a particular fold change that was significant, the associated average $\log_2$ fluorescent intensity had to be larger than 4. The resulting genes are shown in Tables 2-1 through 2-4 for genes in the maternal liver, kidney, small intestine, and placenta, respectively.

In the maternal liver, *Cyp* and *Slc* gene families were most significantly altered during pregnancy; however, only a few genes had larger than two-fold changes in expression. By far the largest up-regulation occurred for *Cyp17a1*, which was increased 3.3-fold, 8.2-fold, and 10.4-fold on gd 7.5/10, gd 15, and gd 19, respectively. *Cyp4a12a/b* was decreased by 70-80% as gestation progressed, which was the largest down-regulation in *Cyp* gene expression. *Cyp2b13*, *Cyp2c50*, *Cyp2c54*, *Cyp2c55*, *Cyp2d9*, and *Cyp4a12* expression was also decreased throughout gestation. Many of the *Cyp* isoforms thought to be involved in drug metabolism, such as the *Cyp1*, *Cyp2*, and *Cyp3* families, did not demonstrate large enough changes in gene expression to be included in Table 2-1. Therefore, time-dependent trends in the expression of *Cyp1*, *Cyp2*, and *Cyp3* families are shown in Figure 2-5, which was generated with only two filtration criteria, namely, the unadjusted p-value associated with a fold change had to be less than 0.01 and the average $\log_2$ fluorescent intensity had to be greater than 4 for at least one gestational age. These criteria allowed us to examine with confidence smaller, but significant, changes in gene expression related to drug metabolism. The data in Figure 2-5 indicate that many genes from the *Cyp1*, *Cyp2b*, *Cyp2c*, and *Cyp2d* families are down-regulated as gestation progresses (Figure 2-5A-C). This pattern is also true for *Cyp3a11* (Figure 2-5A). While the majority of *Cyp* genes were down-regulated during pregnancy, *Cyp2d40*, *Cyp3a16*, *Cyp3a41a*, *Cyp3a41b*, and *Cyp3a44* were up-regulated (Figure 2-5D). Overall, changes in hepatic gene expression of *Cyp* isoforms important for drug metabolism were rather small (down-regulated by less than 50% or up-regulated less than 1.5-fold).

Cyp expression in the maternal kidney was very dynamic during pregnancy (Table 2-2). A few genes, namely *Cyp2d9*, *Cyp2d12*, and *Cyp3a41a/b*, were altered in a gestational age-dependent manner. *Cyp3a41a/b* was highly up-regulated by ~12-fold on gd 19. In the small

intestine, only *Cyp1a1*, *Cyp2a5*, *Cyp2c55*, and *Cyp2j6* displayed larger than1.5-fold changes in expression during pregnancy (Table 2-3). The *Cyp* isoforms that were most notably changed in the placenta during pregnancy are likely responsible for xenobiotic detoxification (*Cyp2s1*), arachidonic acid metabolism (*Cyp4a14*), bile acid synthesis (*Cyp7b1*), steroid biosynthesis (*Cyp11a1*, *Cyp11b1*, and *Cyp17a1*), and retinoic acid and vitamin D regulation (*Cyp26a1* and *Cyp2r1*) (Table 2-4). In contrast to the liver, all *Cyp* enzymes in the placenta, except for *Cyp2s1* and *Cyp7b1*, were up-regulated during mid-gestation (gd 10) and decreased to term expression levels by mid to late gestation (gd 15). Placental *Cyp1*, *Cyp2*, and *Cyp3* gene families were further evaluated for gestational age-dependent trends in expression (Figure 2-5E). All *Cyp* isoforms in the placenta were up-regulated on gd 10 compared to gd 19, with two exceptions. *Cyp1a1* peaked on gd 15 rather than gd 10, and *Cyp3a57* was down-regulated on gd 10 (rather than up-regulated) compared to gd 19.

Across tissues, *Sult* and *Ugt* expression was relatively unaffected by pregnancy. In the maternal liver, *Sult1d1* was decreased by as much as 60% on gd 15 (Table 2-1). In the kidney and small intestine, only a few *Sult* and *Ugt* isoforms were altered during pregnancy, but their relevance to drug metabolism is not well understood (Tables 2-2 and 2-3). In the placenta, *Sult1a1*, *Sult5a1*, and *Ugt1a9* were only affected on gd 10 during pregnancy (Table 2-4). Specifically, *Sult1a1* was down-regulated by 50% on gd 10 compared to gd 19, and *Sult5a1* and *Ugt1a9* were up-regulated more than 2-fold. Overall, the number of *Sult* and *Ugt* genes in the maternal tissues and placenta affected by pregnancy was small, but the magnitude of changes in expression for these genes was quite large.

Drug transport during pregnancy

Gestational age-dependent expression of important drug transporter genes such as ATP-binding cassette (*Abc*) and solute carrier transporters (*Slc* and *Slco*) were characterized using the same fold-change, unadjusted p-value, and fluorescent intensity filtration criteria as the metabolic enzymes. *Abc* transporter expression in maternal tissues appeared relatively unaffected by pregnancy compared to non-pregnant controls (gd 0), except for *Abcc3* (*Mrp3*) and *Abcb1a/1b* (mouse *P-gp* or *Mdr1a/1b*) (Table 2-1 through 2-3). In the maternal liver, expression of *Abcc3* and *Abcb1a* was decreased by ~70% and 40%, respectively, on gd 15. When the fold-change filtration criteria was removed and the unadjusted p-value criteria was lowered to less than 0.01, *Abcc6* (*Mrp6*) was down-regulated by 20-30% on gd 10 and 15 (Figure 2-6A). In the maternal kidney, *Abcb1a* expression was consistently decreased by 30-40 % throughout mid to late gestation (Figure 2-6C, Table 2-2). *Abcc4* expression in the maternal kidney was also decreased by 20-30% on gd 10 and 15 and returned to non-pregnant levels by term (Figure 2-6C). Changes in transporter expression in the small intestine were minimal compared to the liver and kidney (Table 2-3). There were many changes, however, in placental *Abc* transporters (Figure 2-6D, Table 2-4). Specifically, *Abcb1a* and *Abcb1b* were 70% and 80% lower, respectively, on gd 10 compared to gd19. *Abcc5* (*Mrp5*) expression was 3-fold higher on gd 10 compared to gd 19. It appears that most *Abc* transporters in the placenta, with a few exceptions, tend to be suppressed during mid to late gestation (gd 10 and 15) and then return to the control levels by birthing, i.e., gd 19.

Expression of many *Slc* and *Slco* transporter genes in the maternal liver and kidney was significantly altered throughout gestation (Tables 2-1 and 2-2). In the liver, a large portion of

these *Slc* transporters were nutrient transporters, rather than xenobiotic transporters. *Slco1b2* (*Oatp1b2*, ortholog of human *OATP1B3*), *Slc10a1* (*Ntcp*), and *Slc47a1* (*Mate1*), were down-regulated by ~25% on gd 15 and gd 19 (Figure 2-6B). In the maternal kidney, many *Slc* and *Slco* transporters demonstrated only moderate gestational age-dependent changes in expression (Table 2-2). *Slco4c1* (*Oatp4c1*), on the other hand, showed decreased expression (~60-70%) across gestation (Figure 2-6C). In the small intestine, several *Slc* transporter genes demonstrated gestational age-dependent changes in expression; however, their role in xenobiotic transport is not known. For example, *Slc6a9*, *Slc10a5*, and *Slc12a6* were down-regulated by 20-30% on gd 10 and/or gd 15, while *Slc25a43*, *Slc31a1*, *Slc35c2*, and *Slc36a1* expression increased as much as 2.3-fold during pregnancy (Table 2-3). In the placenta, *Slc22a3* (*Oct3*) expression was 80% lower on gd 10 compared to gd 19 (Table 2-4). In contrast, *Slc22a5* (*Octn2*) and *Slc6a2* (*Net*) were both up-regulated more than 2.5-fold on gd 10 (Figure 2-6F). Overall, relatively few *Slc* and *Slco* transporter genes known to be involved in drug transport were affected during pregnancy. Changes in expression of *Slco1b2* in the liver, *Slco4c1* in the kidney, and *Slc22a3* in the placenta, however, may affect drug pharmacokinetics during pregnancy.

Metabolism and transport of endogenous substances during pregnancy

Gestational age-dependent trends were also observed for genes involved in the metabolism and transport of endogenous substances such as bile acids and steroid hormones. According to our data, bile acid production may be altered during pregnancy, particularly in late gestation. For example, *Cyp7a1* and *Cyp7b1*, the hepatic enzymes responsible for the rate-limiting step in bile acid synthesis, were significantly induced as much as 1.5-fold across gestation. The expression of bile acid phase I metabolic enzyme, *Cyp3a11*, decreased by ~ 30%

in a gestational-age dependent manner (Table 2-1 and 2-5). The expression of bile acid transporters also changed. *Abcb1a* (*Mdr1a*), a canalicular bile acid efflux transporter, decreased by 40% on gd 15 (Table 2-5), and *Abcc3* (*Mrp3*), the primary transporter responsible for basolateral efflux of bile acids from hepatocytes into the systemic circulation, decreased by 30%, 70%, and 60% on gd 10, 15, and 19, respectively (Figure 2-6A, Table 2-5). Expression of bile acid hepatic uptake transporters *Slc10a1* (*Ntcp*) and *Slco1b2* (*Oatp1b2*) was decreased slightly by ~20-30% on gd 15 and 19 (Table 2-5).

Fold-changes in steroidogenic enzyme expression were quite large in the maternal liver and placenta; however, the number of genes that changed throughout gestation was low. In the maternal liver, *Cyp17a1*, which oxidizes progesterone and pregnenolone to their 17α-OH metabolites, was induced 3- to 10-fold across gestation (Table 2-1). In the placenta, expression of *Cyp11a1*, which converts cholesterol to pregnenolone, was 2.8-fold higher on gd 10 compared to gd 19, yet 30% lower than term levels on gd 15 (Table 2-4). Likewise, *Cyp17a1* was 2.7-fold higher on gd 10 compared to gd 19 (Table 2-4). Therefore, both *Cyp11a1* and *Cyp17a1* in the placenta were down-regulated during pregnancy, but their expression returns approximately to control levels by gd 15. The effects of pregnancy on hepatic and placental expression of aromatase (*Cyp19a1*), an enzyme that converts androstendione to estrogens, were very small (data not shown). Murine orthologs of other important human steroidogenic enzymes, such as 3β-hydroxysteroid dehydrogenase (3β-HSD) and 17β-hydroxysteroid dehydrogenase (17β-HSD), are not known. Several mouse isoforms of *Hsd* genes were affected in a statistically significant way during pregnancy (Supplemental Data PDF file, Tables 13 and 14).

2.4 Discussion

In the present study, we have performed the first comprehensive gestational age-dependent analysis of metabolic enzyme and transporter gene expression in the maternal liver, kidney, small intestine, and placenta of pregnant mice using microarray analysis. Ten genes were selected for validation by qRT-PCR based on their robust changes in expression and/or involvement in drug metabolism or transport. Fold-changes in the qRT-PCR data were consistently higher than those in the microarray data, but the direction of changes was similar between the two approaches (Figures 2-2 and 2-3). These differences in magnitude are possibly due to higher detection sensitivity of qRT-PCR [31]. We did not expect differences in the reliability/accuracy of the microarray data across tissues because sample preparation was the same for all tissues; therefore, qRT-PCR validation for the liver and placenta was considered adequate. As a secondary validation, we confirmed our results with previously well-characterized genes affected during pregnancy. These included induction of *Cyp3a16* [13] and *Cyp8b1* [32] in the liver and down-regulation of *Abcc3* in the liver [32], *Abcb1a* in the kidney [13], and *Abcc5* in the placenta [22] (Tables 2-1 through 2-4).

In the kidney, a bimodal pattern of gene expression on gd 10 and 19 was produced by two kidney samples, gd10_3 and gd10_6. This inter-animal variability appears to be specific for the kidney because the liver, small intestine, and placenta collected from the same mice did not exhibit such a pattern. The reason for such an observation is not known; however, recent computational studies do predict that cooperative binding of transcription factors to DNA promotes a bimodal gene expression response in eukaryotic systems [33]. Thus, the same might explain the bimodal pattern of gene expression in the mouse kidney observed in this study.

The data from the small intestine and placenta should be interpreted with caution for the following reasons: The entire small intestine was used to isolate total RNA, resulting in a mixing of RNA from mucosal epithelium, submucosa (connective tissue), and smooth muscle. Our data therefore do not precisely reflect changes in gene expression in the more functionally relevant enterocytes (from a drug disposition perspective), nor does it reflect changes in specific regions along the small intestine. Consequently, we placed less of an emphasis on the small intestine data. The formation of placenta is different between mice and humans, which complicates translation of the placental data to human pregnancy. For example, development of the prominent chorionic villus structure occurs quickly in human pregnancy (by day 21 of 270), but not until gd 11.5 in the mouse. This may explain why the mouse placenta had more differentially expressed genes on gd 10 versus gd 15, and call into question whether it is relevant to analyze gene expression before gd 11.5. Interpretation of drug transport across the mouse placenta on gd 15 and 19 is still relevant to human placenta, as both mice and humans use syncytiotrophoblasts to modulate the exchange of nutrients, hormones, and xenobiotics between the mother and fetus.

Our study is the first to characterize gestational age-dependent changes in gene expression for all metabolic enzymes and transporters. Zhang et al. reported that while *Cyp3a16*, *Cyp3a41*, and *Cyp3a44* were induced in the maternal liver during pregnancy, *Cyp3a11*, *Cyp3a13*, and *Cyp3a25* were down-regulated [13]. This is consistent with our results (Figure 2-5). Koh et al. examined gestational age-dependent expression of hepatic *Cyp1a2*, *Cyp2a5*, *Cyp2b10*, *Cyp2c37*, *Cyp2d22*, *Cyp2e1*, *Cyp3a11*, and *Cyp3a41* using qRT-PCR [16]. Again, their observations mirror our data (Figure 2-5). In the placenta, *Cyp* up-regulation during mid-gestation is also consistent with previous studies [34]. We are the first, however, to examine *Cyp* gene expression in the maternal kidney. Interestingly, *Cyp3a41a* and *Cyp3a41b* were markedly

induced in late gestation. Implications of *Cyp3a41a/b* induction are not known, but might include altered renal xenobiotic metabolism, increased bioactivation of nephrotoxic pathways, or increased sodium retention to control blood pressure [35].

We also used our microarray data to explore CYP-mediated steroid hormone biosynthesis during pregnancy. CYP17A1 is a critical enzyme for steroid hormone biosynthesis. The large induction of hepatic *Cyp17a1* (~3 to 10-fold) suggests increased production of 17α-hydroxyprogesterone and 17α-hydroxypregnenolone during mouse pregnancy, which is consistent with reported increase in circulating 17α-OH progesterone in humans during pregnancy [36]. Increased levels of 17α-OH metabolites could ultimately increase estrogen production in the maternal liver; however, down-regulation of placental *Cyp17a1* throughout gestation favors progesterone formation, not estrogen. Therefore, our microarray data support the general pattern of steroid hormone biosynthesis during pregnancy, that is, while progesterone and estrogen are increasingly produced as gestation progresses, the majority of progesterone is made by the placenta in late gestation [37]. Nevertheless, interpretation of placental steroidogenesis in mice should be done with caution as one study has shown that the pattern of gestational age-dependent expression of some steroidogenic enzymes can be opposite between mice and humans [38].

Our results revealed that *Abc* transporter gene expression was decreased during pregnancy, particularly *Abcc3* in the liver, *Abcb1a* in the kidney, and *Abcc5* in the placenta. Similarly, several *Slc* or *Slco* transporters important for drug disposition were moderately decreased during pregnancy (such as *Slco1b2* in the liver and *Slco4c1* in the kidney). *Slc22a3* (*Oct3*) and *Slc6a2* (*Net*) in the placenta were down-regulated and up-regulated, respectively, to a

larger extent. The small number of transporters affected by pregnancy may still be enough, though, to explain reported increases in hepatic bile acid concentrations in late pregnancy in mice [32, 39]. Consistent with these previous studies, our data support increased bile acid synthesis (*Cyp7b1*) and decreased basolateral and canalicular bile acid efflux (*Abcc3* and *Abcb1a*) during mouse pregnancy. Decreased expression of hepatic uptake transporters in the maternal liver may therefore be an adaptive response to manage increased intrahepatocellular bile acid concentrations.

Translation of our findings to human pregnancy is not straightforward. One reason is that gene expression and protein levels are not always correlative [40]. In the placenta, *Abcb1a/1b* expression increases, however, its protein expression has been shown to decrease as gestation progresses [13]. Microarray data therefore may not entirely reflect pregnancy's effect on protein expression/activity. In addition, the number of *Cyp1*, *Cyp2*, and *Cyp3* isoforms in mice is greater than that in humans, and there are potential species differences in substrate specificity and/or enzymatic activity. All these factors make it challenging to predict drug metabolism during human pregnancy using the mouse data. If our microarray data does predict CYP activity, then xenobiotic substrates of CYP1 or CYP2 isoforms (which exhibit decreased activity in human pregnancy) may need to be given at smaller doses during pregnancy. Prediction for CYP3A substrates is less certain, because *Cyp3a16*, *Cyp3a41a/b*, and *Cyp3a44* are up-regulated during pregnancy, yet *Cyp3a11* and *Cyp3a13* are down-regulated. Also, fold-changes in *Cyp3a* gene expression do not reflect the magnitude of increase we and others have shown for *in vivo* CYP3A activity in pregnant mice and humans [11, 14, 15]. Therefore, the *Cyp* isoform(s) that best represent *in vivo* CYP3A activity should be carefully evaluated.

Mouse *Cyp3a11* is most closely related to human *CYP3A4* with 76% amino acid identity and may be the dominant contributor to CYP3A activity in mouse liver [41]. However, CYP3A11 is likely not the mouse CYP3A isoform responsible for increased CYP3A activity in pregnant mice, as its gene expression was down-regulated over gestation. *Cyp3a13* and *Cyp3a16* appear less important because hepatic *Cyp3a13* levels are 5-10-fold lower than *Cyp3a11* in non-pregnant female mice; and *Cyp3a16* is considered a fetal isoform [41]. On the other hand, *Cyp3a41a/b* and *Cyp3a44* are female-specific isoforms expressed solely in the liver, and they are known to be induced by growth hormone, glucocorticoids, and estradiol [42-44]. Indeed, in mice maternal estradiol plasma concentrations triple from gd 10 to gd 17 [45], which parallels the trend of hepatic induction of *Cyp3a41a/b* and *Cyp3a44* during gestation (Figure 2-5D). Clearly, isoform-specific quantitation of protein levels and activity is needed to further evaluate which isoforms are responsible for the *in vivo* CYP3A activity in pregnant mice.

In summary, we have determined global gene expression profiles in the maternal tissues and placenta of pregnant mice, providing a genetic basis for understanding gestational-age dependent physiological and pharmacological changes during pregnancy. These data also offer a means to study the mechanisms of regulation behind such changes. Based on our findings, mid to late gestation (gd 10-15) may be the best time to study the full impact of mouse pregnancy on drug metabolism and disposition.

Tables and Figures for Chapter 2

Table 2-1. Gestational age-dependent changes of metabolic enzyme and transporter genes in the maternal liver.

Gene Symbol	Gd 7.5		Gd 10		Gd 15		Gd 19	
	Fold Change	*p*	Fold Change	*p*	Fold Change	*p*	Fold Change	*p*
Cyp2b13	0.7	(0.024)	0.5	(< 0.001)	0.3	(< 0.001)	0.3	(< 0.001)
Cyp2c50	0.9	(0.133)	0.6	(< 0.001)	0.4	(< 0.001)	0.5	(< 0.001)
Cyp2c54	0.9	(0.047)	0.7	(< 0.001)	0.6	(< 0.001)	0.7	(< 0.001)
Cyp2c55	0.8	(0.302)	0.8	(0.284)	0.5	(0.001)	0.7	(0.033)
Cyp2d9	0.7	(< 0.001)	0.5	(< 0.001)	0.5	(< 0.001)	0.6	(< 0.001)
Cyp2d40	1.0	(0.808)	1.5	(0.002)	1.7	(< 0.001)	1.9	(< 0.001)
Cyp2g1	1.0	(0.66)	1.2	(0.094)	1.6	(< 0.001)	1.2	(0.027)
Cyp3a16	1.4	(< 0.001)	1.4	(< 0.001)	1.6	(< 0.001)	1.4	(< 0.001)
Cyp4a12a	0.2	(< 0.001)	0.3	(< 0.001)	0.2	(< 0.001)	0.2	(< 0.001)
Cyp4a12b	0.3	(< 0.001)	0.3	(< 0.001)	0.3	(< 0.001)	0.3	(< 0.001)
Cyp4a14	1.7	(0.24)	1.3	(0.598)	0.3	(0.021)	0.6	(0.237)
Cyp4a31	1.5	(0.004)	1.6	(0.002)	1.8	(< 0.001)	1.9	(< 0.001)
Cyp4f15	0.9	(0.242)	0.7	(< 0.001)	0.6	(< 0.001)	0.8	(0.066)
Cyp7b1	1.5	(0.003)	1.3	(0.046)	1.5	(0.002)	1.5	(0.006)
Cyp8b1	0.9	(0.322)	1.1	(0.598)	1.4	(0.064)	1.6	(0.006)

Cyp17a1	3.3	(< 0.001)	3.3	(< 0.001)	8.2	(< 0.001)	10.4	(< 0.001)
Cyp26a1	1.0	(0.962)	2.1	(0.082)	2.9	(0.015)	1.1	(0.752)
Cyp39a1	0.8	(0.103)	0.5	(< 0.001)	0.3	(< 0.001)	0.4	(< 0.001)
Cyp51	1.0	(0.84)	0.8	(0.176)	0.8	(0.069)	0.6	(0.001)
Sult1d1	0.9	(0.195)	0.6	(< 0.001)	0.4	(< 0.001)	0.7	(0.021)
Ugt2b37	1.5	(0.004)	1.5	(0.005)	0.9	(0.354)	1.0	(0.836)
Abca8a	0.9	(0.249)	0.7	(0.018)	0.5	(< 0.001)	0.8	(0.103)
Abcb1a	1.1	(0.431)	0.9	(0.573)	0.6	(0.008)	0.9	(0.356)
Abcb6	0.9	(0.032)	0.8	(0.006)	0.6	(< 0.001)	0.8	(< 0.001)
Abcc3	0.9	(0.412)	0.7	(0.01)	0.3	(< 0.001)	0.4	(< 0.001)
Abcg5	0.8	(0.157)	0.7	(0.013)	0.6	(< 0.001)	0.8	(0.092)
Abcg8	0.8	(0.259)	0.6	(0.002)	0.8	(0.134)	1.0	(0.815)
Slc1a2	0.9	(0.362)	1.1	(0.329)	1.7	(< 0.001)	2.1	(< 0.001)
Slc3a1	1.7	(0.009)	1.7	(0.007)	1.8	(0.003)	2.1	(0.001)
Slc6a9	1.1	(0.612)	2.1	(< 0.001)	4.3	(< 0.001)	2.8	(< 0.001)
Slc7a2	0.7	(0.014)	0.5	(< 0.001)	0.6	(0.001)	0.7	(0.068)
Slc7a8	1.3	(0.005)	1.5	(< 0.001)	1.2	(0.023)	1.0	(0.979)
Slc9a3r1	1.0	(0.843)	0.9	(0.419)	0.6	(< 0.001)	0.8	(0.009)
Slc13a2	1.0	(0.663)	1.2	(0.162)	1.5	(< 0.001)	1.1	(0.564)
Slc15a1	1.0	(0.832)	0.9	(0.542)	1.7	(0.018)	1.0	(0.897)
Slc15a4	0.7	(0.006)	0.6	(< 0.001)	0.6	(< 0.001)	0.8	(0.029)
Slc16a1	1.1	(0.422)	1.4	(0.002)	1.7	(< 0.001)	1.3	(0.018)
Slc16a12	1.0	(0.932)	0.7	(0.002)	0.4	(< 0.001)	0.7	(0.009)
Slc16a13	0.9	(0.237)	1.2	(0.011)	1.6	(< 0.001)	1.3	(0.001)
Slc16a6	1.2	(0.363)	3.4	(< 0.001)	8.9	(< 0.001)	2.7	(< 0.001)
Slc17a1	1.0	(0.658)	0.8	(0.057)	0.5	(< 0.001)	0.7	(< 0.001)
Slc17a2	1.0	(0.872)	0.7	(0.002)	0.4	(< 0.001)	0.6	(< 0.001)
Slc17a4	0.8	(0.036)	1.4	(0.003)	1.6	(< 0.001)	1.3	(0.01)
Slc17a8	0.7	(0.009)	0.6	(0.001)	0.6	(< 0.001)	0.7	(0.012)
Slc19a2	0.8	(0.103)	0.7	(0.003)	0.6	(< 0.001)	0.9	(0.181)
Slc22a15	0.9	(0.131)	0.8	(0.024)	0.6	(< 0.001)	0.9	(0.083)
Slc22a2	1.1	(0.677)	1.0	(0.978)	3.6	(< 0.001)	1.9	(< 0.001)
Slc22a23	1.1	(0.484)	1.1	(0.389)	1.6	(< 0.001)	1.2	(0.008)
Slc24a3	0.9	(0.426)	0.9	(0.314)	1.7	(< 0.001)	1.3	(0.009)
Slc24a6	1.1	(0.579)	0.5	(< 0.001)	0.5	(< 0.001)	1.2	(0.295)
Slc25a4	0.6	(0.005)	0.8	(0.116)	0.7	(0.008)	0.6	(0.004)
Slc25a25	0.7	(0.223)	1.0	(0.898)	1.3	(0.31)	0.6	(0.026)
Slc25a30	1.5	(0.011)	1.3	(0.092)	1.8	(< 0.001)	1.4	(0.019)
Slc25a32	0.7	(0.006)	0.7	(0.002)	0.6	(< 0.001)	0.8	(0.057)

Slc25a47	0.8	(0.063)	0.6	(0.001)	0.5	(< 0.001)	0.8	(0.226)
Slc30a10	1.2	(0.118)	1.5	(0.001)	1.1	(0.362)	0.9	(0.288)
Slc34a2	1.3	(0.211)	2.6	(< 0.001)	1.7	(0.034)	1.1	(0.657)
Slc35c2	0.9	(0.215)	1.2	(0.013)	1.7	(< 0.001)	1.5	(< 0.001)
Slc36a1	1.1	(0.161)	1.5	(< 0.001)	2.1	(< 0.001)	1.5	(< 0.001)
Slc37a1	1.5	(0.018)	2.5	(< 0.001)	4.0	(< 0.001)	1.9	(< 0.001)
Slc37a4	0.8	(0.028)	0.8	(0.052)	0.6	(< 0.001)	0.9	(0.452)
Slc38a4	0.9	(0.216)	0.7	(0.001)	0.4	(< 0.001)	0.6	(< 0.001)
Slc39a14	1.1	(0.213)	1.4	(0.001)	1.7	(< 0.001)	1.3	(0.022)
Slc39a4	0.8	(0.011)	0.8	(0.002)	0.6	(< 0.001)	0.8	(< 0.001)
Slc40a1	1.0	(0.732)	1.1	(0.054)	1.5	(< 0.001)	1.0	(0.988)
Slc41a1	1.3	(0.011)	1.6	(< 0.001)	1.6	(< 0.001)	1.3	(0.01)
Slc41a2	1.8	(0.073)	5.2	(< 0.001)	8.3	(< 0.001)	3.7	(< 0.001)
Slc41a3	1.1	(0.159)	1.2	(0.06)	1.6	(< 0.001)	2.2	(< 0.001)
Slc43a1	1.0	(0.813)	1.3	(0.008)	1.7	(< 0.001)	1.7	(< 0.001)
Slc43a3	1.1	(0.375)	1.0	(0.69)	0.6	(< 0.001)	0.7	(< 0.001)
Slc46a3	0.9	(0.123)	0.8	(0.02)	0.5	(< 0.001)	0.8	(0.006)
Slco1a4	1.0	(0.901)	0.8	(0.074)	0.5	(< 0.001)	0.9	(0.367)

This list of *Cyp*, *Sult*, *Ugt*, *Abc*, *Slc*, and *Slco* genes was generated using the following filtration criteria: fold-change > 1.5 or < 0.65, unadjusted $p < 0.05$, and $\log_2$ average fluorescent intensity > 4 on at least one gestation day (gd). Shown are fold-changes compared to gd 0. Fold-change is defined as the ratio of fluorescent intensity of the gene on a gestation day to that on gd 0. *p*, unadjusted p-value.

Table 2-2. Gestational age-dependent changes of metabolic enzymes and transporter genes in the maternal kidney.

Gene Symbol	Gd 7.5		Gd 10		Gd 15		Gd 19	
	Fold Change	*p*	Fold Change	*p*	Fold Change	*p*	Fold Change	*p*
Cyp1a2	1.1	(0.842)	3.4	(0.019)	1.1	(0.817)	2.1	(0.128)
Cyp2a12	1.2	(0.775)	4.0	(0.032)	1.4	(0.604)	2.9	(0.089)
Cyp2b9	1.3	(0.727)	5.3	(0.022)	1.6	(0.483)	3.7	(0.067)
Cyp2b10	0.9	(0.779)	1.8	(0.026)	1.0	(0.911)	1.1	(0.667)
Cyp2b13	1.0	(0.909)	2.9	(0.013)	1.1	(0.752)	1.4	(0.431)
Cyp2c29	1.1	(0.924)	4.5	(0.042)	1.5	(0.571)	3.6	(0.082)
Cyp2c37	1.1	(0.795)	2.1	(0.028)	1.1	(0.858)	1.4	(0.287)
Cyp2c39	1.2	(0.802)	6.3	(0.022)	1.5	(0.6)	5.0	(0.041)
Cyp2c40	1.2	(0.772)	5.1	(0.027)	1.7	(0.455)	4.2	(0.05)
Cyp2c50	1.2	(0.796)	3.5	(0.028)	1.1	(0.846)	2.0	(0.205)
Cyp2c54	1.1	(0.842)	3.0	(0.039)	1.1	(0.872)	1.8	(0.281)
Cyp2c67	1.0	(0.995)	3.1	(0.036)	1.2	(0.664)	2.1	(0.15)
Cyp2c70	1.3	(0.634)	4.3	(0.018)	1.4	(0.571)	2.8	(0.089)
Cyp2d9	0.8	(0.036)	0.7	(0.002)	0.6	(< 0.001)	0.7	(0.002)
Cyp2d12	1.6	(< 0.001)	1.4	(< 0.001)	1.3	(0.003)	1.6	(< 0.001)
Cyp2d13	1.1	(0.794)	2.0	(0.039)	1.1	(0.836)	1.5	(0.238)
Cyp2f2	1.2	(0.788)	3.8	(0.026)	1.4	(0.552)	3.0	(0.063)
Cyp3a11	1.2	(0.747)	4.8	(0.021)	1.7	(0.402)	3.5	(0.063)

Cyp3a25	1.1	(0.888)	4.1	(0.025)	1.2	(0.708)	2.3	(0.165)
Cyp3a25	1.1	(0.888)	4.1	(0.025)	1.2	(0.708)	2.3	(0.165)
Cyp3a41a	1.8	(0.434)	9.5	(0.006)	3.4	(0.118)	11.3	(0.004)
Cyp3a41b	1.8	(0.439)	9.9	(0.007)	3.5	(0.123)	12.4	(0.004)
Cyp4f14	1.4	(0.128)	2.4	(0.001)	1.5	(0.117)	1.7	(0.028)
Cyp4f15	1.1	(0.801)	2.0	(0.009)	1.0	(0.937)	1.3	(0.268)
Cyp4v3	1.2	(0.344)	1.8	(0.012)	1.2	(0.366)	1.5	(0.077)
Cyp7a1	1.3	(0.678)	3.3	(0.04)	1.4	(0.538)	2.7	(0.087)
Cyp7b1	1.1	(0.554)	1.6	(0.032)	1.0	(0.989)	1.2	(0.433)
Cyp24a1	0.8	(0.454)	0.5	(0.053)	0.4	(0.024)	1.5	(0.306)
Sult3a1	1.4	(0.682)	6.9	(0.028)	2.4	(0.302)	7.4	(0.022)
Ugt2a3	1.0	(0.962)	3.0	(0.033)	1.1	(0.908)	1.7	(0.313)
Ugt2b1	1.3	(0.681)	5.6	(0.016)	1.3	(0.705)	3.2	(0.095)
Ugt2b5	1.2	(0.525)	1.7	(0.047)	1.2	(0.494)	1.4	(0.208)
Ugt2b36	1.5	(0.505)	4.8	(0.019)	1.5	(0.495)	3.4	(0.062)
Abcb1a	0.8	(0.037)	0.7	(< 0.001)	0.6	(< 0.001)	0.7	(< 0.001)
Abcb4	1.1	(0.704)	2.0	(0.013)	1.2	(0.56)	1.5	(0.157)
Slc4a11	0.6	(0.037)	0.9	(0.483)	0.5	(0.006)	0.5	(0.005)
Slc5a3	0.6	(< 0.001)	0.8	(0.038)	0.6	(< 0.001)	0.5	(< 0.001)
Slc5a8	0.8	(0.031)	0.8	(0.062)	0.6	(< 0.001)	0.7	(< 0.001)
Slc6a15	0.6	(0.024)	0.6	(0.059)	0.4	(0.001)	0.4	(< 0.001)
Slc7a12	0.6	(0.118)	0.8	(0.569)	0.6	(0.073)	0.4	(0.008)
Slc16a1	1.2	(0.249)	1.2	(0.158)	1.2	(0.161)	1.9	(< 0.001)
Slc17a2	1.1	(0.672)	1.6	(0.021)	1.0	(0.939)	1.0	(0.921)
Slc22a13	0.7	(0.162)	0.8	(0.389)	0.6	(0.021)	0.6	(0.009)
Slc22a7	1.0	(0.977)	1.2	(0.502)	0.8	(0.299)	0.6	(0.043)
Slc25a25	0.5	(< 0.001)	0.7	(0.005)	0.7	(0.004)	0.6	(0.002)
Slc27a5	1.1	(0.732)	2.3	(0.042)	1.1	(0.814)	1.5	(0.279)
Slc38a4	1.1	(0.759)	3.0	(0.018)	1.2	(0.73)	2.0	(0.133)
Slc40a1	1.4	(< 0.001)	1.4	(< 0.001)	1.6	(< 0.001)	1.6	(< 0.001)
Slco1a6	0.8	(0.287)	0.9	(0.511)	0.7	(0.069)	0.6	(0.008)
Slco4c1	0.4	(< 0.001)	0.4	(< 0.001)	0.3	(< 0.001)	0.4	(< 0.001)

This list of *Cyp*, *Sult*, *Ugt*, *Abc*, *Slc*, and *Slco* genes was generated using the following filtration criteria: fold-change > 1.5 or < 0.65, unadjusted $p < 0.05$, and average $\log_2$ fluorescent intensity > 4 for at least one gestation day (gd). Shown are fold-changes compared to gd 0. Fold-change is

defined as the ratio of the average fluorescence intensity of the gene at a gestation day to that at gd 0. *p*, unadjusted p-value.

Table 2-3. Gestational age-dependent changes of metabolic enzymes and transporter genes in the maternal small intestine.

Gene Symbol	Gd 7.5		Gd 10		Gd 15		Gd 19	
	Fold Change	*p*	Fold Change	*p*	Fold Change	*p*	Fold Change	*p*
Cyp1a1	1.9	(0.145)	2.9	(0.017)	0.8	(0.555)	1.0	(0.909)
Cyp2a5	1.2	(0.44)	1.3	(0.212)	1.6	(0.031)	1.7	(0.028)
Cyp2c55	2.1	(0.13)	2.7	(0.046)	1.5	(0.378)	1.5	(0.372)
Cyp2j6	1.0	(0.857)	1.0	(0.955)	0.6	(0.012)	0.7	(0.072)
Sult1c2	0.8	(0.346)	0.7	(0.089)	0.6	(0.017)	0.5	(0.003)
Ugt2b5	0.8	(0.29)	0.8	(0.214)	0.6	(0.013)	0.5	(0.002)
Ugt2b35	0.9	(0.432)	0.9	(0.467)	0.6	(0.008)	0.7	(0.042)
Ugt2b36	0.7	(0.042)	0.7	(0.054)	0.6	(0.021)	0.6	(0.008)
Abcc2	0.9	(0.51)	0.9	(0.484)	0.6	(0.02)	0.8	(0.33)
Slc5a4a	1.3	(0.307)	2.4	(0.002)	1.5	(0.097)	2.1	(0.008)
Slc6a9	0.8	(0.057)	0.6	(< 0.001)	1.0	(0.864)	0.8	(0.02)
Slc10a5	0.9	(0.34)	0.9	(0.433)	0.6	(< 0.001)	0.8	(0.151)
Slc12a6	0.8	(0.041)	0.8	(0.008)	0.6	(< 0.001)	0.8	(0.084)
Slc13a1	0.8	(0.436)	0.6	(0.057)	0.9	(0.672)	0.5	(0.041)
Slc16a3	1.4	(0.063)	1.5	(0.016)	1.1	(0.575)	1.4	(0.067)
Slc25a43	1.2	(0.05)	1.5	(< 0.001)	1.8	(< 0.001)	1.8	(< 0.001)

Slc31a1	1.1	(0.087)	1.5	(< 0.001)	1.5	(< 0.001)	1.5	(< 0.001)
Slc35c2	1.4	(0.132)	1.6	(0.042)	1.2	(0.507)	1.3	(0.238)
Slc35e3	1.0	(0.905)	0.9	(0.473)	0.6	(0.04)	0.9	(0.538)
Slc36a1	1.8	(0.132)	2.3	(0.034)	1.4	(0.335)	1.4	(0.374)

This list of *Cyp*, *Sult*, *Ugt*, *Abc*, *Slc*, and *Slco* genes was generated using the following filtration criteria: fold-change > 1.5 or < 0.65, unadjusted $p < 0.05$, and average $\log_2$ fluorescent intensity > 4 for at least one gestation day (gd). Shown are fold-changes compared to gd 0. Fold-change is defined as the ratio of the average fluorescence intensity of the gene at a gestation day to that at gd 0. *p*, unadjusted p-value.

Table 2-4. Gestational age-dependent changes of metabolic enzymes and transporter genes in the placenta.

Gene Symbol	Gd 10		Gd 15	
	Fold Change	*p*	Fold Change	*p*
Cyp1a1	1.1	(0.257)	1.9	(< 0.001)
Cyp2b10	4.0	(0.003)	1.2	(0.664)
Cyp2r1	4.5	(< 0.001)	1.2	(0.384)
Cyp2s1	0.1	(< 0.001)	0.7	(0.006)
Cyp4a14	1.6	(0.022)	0.9	(0.468)
Cyp4v3	2.3	(0.001)	1.1	(0.55)
Cyp7b1	0.5	(0.001)	0.7	(0.019)
Cyp11a1	2.8	(0.001)	0.7	(0.188)
Cyp11b1	7.2	(< 0.001)	1.2	(0.677)
Cyp17a1	2.7	(0.001)	1.1	(0.59)
Cyp20a1	1.7	(< 0.001)	1.2	(0.008)
Cyp26a1	1.8	(< 0.001)	1.0	(0.945)
Cyp27a1	1.9	(< 0.001)	0.8	(0.048)
Cyp51	2.2	(< 0.001)	1.4	(0.01)
Sult1a1	0.5	(0.001)	0.6	(0.006)
Sult5a1	3.5	(< 0.001)	1.0	(0.698)

Ugt1a9	2.1	(0.007)	1.1	(0.73)
Abca1	0.6	(< 0.001)	0.7	(0.002)
Abca2	1.7	(0.001)	1.0	(0.945)
Abca3	0.4	(< 0.001)	0.8	(0.043)
Abca5	1.8	(< 0.001)	1.0	(0.774)
Abca6	1.5	(< 0.001)	0.9	(0.458)
Abca9	0.5	(< 0.001)	0.8	(0.149)
Abcb1a	0.3	(< 0.001)	1.0	(0.839)
Abcb1b	0.2	(< 0.001)	1.2	(0.375)
Abcb8	0.6	(0.002)	1.1	(0.33)
Abcb10	0.5	(< 0.001)	0.9	(0.172)
Abcc5	3.0	(< 0.001)	0.9	(0.694)
Abcd2	0.6	(0.021)	0.5	(0.01)
Abcg1	0.3	(< 0.001)	0.6	(0.001)
Slc1a1	0.1	(< 0.001)	0.5	(0.004)
Slc1a4	0.2	(< 0.001)	0.5	(0.002)
Slc1a5	0.4	(0.003)	1.0	(0.967)
Slc2a1	0.4	(< 0.001)	1.1	(0.574)
Slc2a5	1.7	(0.002)	1.0	(0.812)
Slc2a12	5.2	(< 0.001)	0.9	(0.673)
Slc4a1	0.5	(0.001)	1.2	(0.345)
Slc4a2	0.4	(< 0.001)	1.2	(0.466)
Slc4a4	0.4	(< 0.001)	0.7	(0.119)
Slc4a5	0.5	(< 0.001)	1.0	(0.96)
Slc5a3	0.2	(< 0.001)	0.8	(0.124)
Slc5a6	0.2	(< 0.001)	0.6	(0.005)
Slc5a8	1.7	(0.002)	0.9	(0.62)
Slc6a2	2.8	(< 0.001)	2.0	(0.007)
Slc6a12	2.5	(0.021)	1.3	(0.486)
Slc6a14	0.3	(0.002)	1.1	(0.792)
Slc7a1	0.3	(0.001)	1.0	(0.968)
Slc7a2	0.2	(< 0.001)	1.2	(0.615)
Slc7a5	0.4	(0.007)	1.2	(0.53)
Slc9a2	0.5	(0.004)	1.2	(0.366)
Slc9a3	0.5	(0.008)	1.0	(0.938)
Slc9a3r1	0.5	(< 0.001)	0.8	(0.177)
Slc9a6	0.3	(< 0.001)	1.0	(0.874)
Slc9a8	0.6	(< 0.001)	0.9	(0.17)
Slc10a6	2.0	(0.002)	0.6	(0.014)
Slc11a1	0.6	(0.012)	0.7	(0.14)

Slc12a7	0.4	(0.001)	1.5	(0.091)
Slc13a4	0.1	(< 0.001)	1.4	(0.433)
Slc15a2	0.6	(< 0.001)	1.0	(0.998)
Slc16a1	0.5	(0.002)	1.2	(0.228)
Slc16a3	0.2	(< 0.001)	1.4	(0.063)
Slc16a4	0.1	(< 0.001)	0.9	(0.702)
Slc16a9	0.1	(< 0.001)	1.1	(0.78)
Slc16a10	0.3	(< 0.001)	1.1	(0.861)
Slc16a12	0.1	(< 0.001)	0.9	(0.609)
Slc18a1	0.4	(0.01)	0.8	(0.36)
Slc18a2	0.4	(< 0.001)	1.1	(0.465)
Slc19a1	3.0	(< 0.001)	1.4	(0.171)
Slc19a2	0.3	(< 0.001)	0.9	(0.569)
Slc19a3	0.2	(< 0.001)	1.2	(0.41)
Slc20a1	0.4	(< 0.001)	0.7	(0.056)
Slc20a2	0.7	(0.013)	0.6	(0.009)
Slc22a3	0.2	(< 0.001)	1.2	(0.58)
Slc22a4	0.5	(0.012)	0.8	(0.449)
Slc22a5	2.7	(< 0.001)	1.3	(0.078)
Slc22a18	0.4	(0.001)	1.9	(0.002)
Slc22a21	1.8	(< 0.001)	1.1	(0.191)
Slc22a23	0.6	(0.016)	0.9	(0.628)
Slc23a2	2.4	(0.002)	1.1	(0.636)
Slc23a3	0.2	(0.003)	0.5	(0.187)
Slc25a1	1.8	(< 0.001)	1.2	(0.035)
Slc25a12	1.7	(0.001)	1.4	(0.036)
Slc25a13	1.6	(0.001)	1.3	(0.075)
Slc25a17	0.6	(0.002)	1.0	(0.906)
Slc25a29	2.3	(< 0.001)	1.0	(0.872)
Slc25a31	0.5	(< 0.001)	1.0	(0.892)
Slc25a33	3.9	(< 0.001)	1.1	(0.44)
Slc25a35	0.5	(0.003)	1.1	(0.532)
Slc25a36	0.6	(< 0.001)	0.9	(0.431)
Slc25a37	0.3	(< 0.001)	0.8	(0.359)
Slc25a40	0.6	(0.004)	0.7	(0.079)
Slc25a43	0.6	(< 0.001)	1.1	(0.241)
Slc26a2	0.2	(< 0.001)	0.9	(0.336)
Slc26a7	0.1	(< 0.001)	1.8	(0.118)
Slc27a3	0.5	(0.001)	1.4	(0.044)
Slc27a6	0.3	(0.001)	1.3	(0.353)

Slc28a3	0.4	(0.001)	2.2	(0.003)
Slc29a1	2.8	(< 0.001)	1.2	(0.323)
Slc29a3	0.5	(0.001)	1.1	(0.377)
Slc30a3	3.1	(< 0.001)	0.4	(0.006)
Slc33a1	2.5	(< 0.001)	1.0	(0.885)
Slc34a2	0.2	(< 0.001)	1.2	(0.478)
Slc35b1	2.1	(< 0.001)	1.1	(0.602)
Slc37a1	0.4	(< 0.001)	0.9	(0.113)
Slc37a3	0.4	(< 0.001)	1.0	(0.663)
Slc38a3	2.1	(0.003)	1.3	(0.261)
Slc38a4	0.2	(< 0.001)	1.2	(0.514)
Slc39a2	6.2	(< 0.001)	1.3	(0.33)
Slc39a4	0.2	(< 0.001)	0.5	(0.03)
Slc39a6	2.0	(0.014)	1.1	(0.585)
Slc39a7	1.9	(< 0.001)	1.0	(0.778)
Slc39a11	1.6	(< 0.001)	1.1	(0.303)
Slc39a14	2.1	(0.019)	1.4	(0.219)
Slc40a1	0.1	(< 0.001)	1.0	(0.846)
Slc41a1	0.3	(0.001)	0.7	(0.239)
Slc43a2	0.4	(0.001)	0.7	(0.085)
Slc43a3	1.7	(< 0.001)	0.9	(0.558)
Slc44a2	2.7	(0.002)	1.1	(0.639)
Slc44a3	0.3	(< 0.001)	1.1	(0.425)
Slc45a3	0.5	(0.003)	1.0	(0.84)
Slc45a4	0.3	(< 0.001)	1.0	(0.982)
Slc46a3	0.5	(0.008)	0.7	(0.12)
Slc48a1	0.6	(0.001)	0.8	(0.062)
Slco4a1	0.3	(0.006)	1.1	(0.81)

This list of *Cyp*, *Sult*, *Ugt*, *Abc*, *Slc*, and *Slco* genes was generated using the following filtration criteria: fold-change > 1.5 or < 0.65, unadjusted $p < 0.05$, and average $\log_2$ fluorescent intensity > 4 for at least one gestation day (gd). Shown are fold-changes compared to gd 19. Fold-change is defined as the ratio of the average fluorescence intensity of the gene at a gestation day to that at gd 19. *p*, unadjusted p-value.

Table 2-5. Summary of gestational age-dependent expression of genes in the maternal liver involved in bile acid synthesis, metabolism, and transport.

Gene Symbol	Gd 7.5		Gd 10		Gd 15		Gd 19	
	Fold Change	*p*	Fold Change	*p*	Fold Change	*p*	Fold Change	*p*
Bile acid synthesis								
Cyp7a1	1.0	(0.916)	1.3	(0.044)	1.5	(0.004)	1.0	(0.874)
Cyp7b1	1.5	(0.003)	1.3	(0.046)	1.5	(0.002)	1.5	(0.006)
Cyp8b1	0.9	(0.322)	1.1	(0.598)	1.4	(0.064)	1.6	(0.006)
Cyp27a1	0.8	(0.003)	0.7	(< 0.001)	0.7	(< 0.001)	0.7	(< 0.001)
Cyp39a1	0.8	(0.103)	0.5	(< 0.001)	0.3	(< 0.001)	0.4	(< 0.001)
Bile acid Phase I metabolism								
Cyp2b10	0.7	(0.014)	0.8	(0.115)	0.8	(0.204)	0.9	(0.66)
Cyp3a11	0.8	(0.049)	0.8	(0.004)	0.7	(< 0.001)	0.7	(0.001)
Canalicular bile acid efflux into bile								
Abcb1a	1.1	(0.431)	0.9	(0.573)	0.6	(0.008)	0.9	(0.356)
Abcb1b	1.0	(0.887)	1.0	(0.957)	1.0	(0.985)	1.1	(0.146)
Abcb11	1.0	(0.542)	0.9	(0.319)	0.9	(0.346)	0.9	(0.05)
Abcc2	0.9	(0.049)	0.9	(0.044)	1.0	(0.931)	0.9	(0.229)

Basolateral bile acid efflux into circulation								
Abcc3	0.9	(0.412)	0.7	(0.01)	0.3	(< 0.001)	0.4	(< 0.001)
Abcc4	1.4	(0.014)	1.4	(0.017)	1.1	(0.68)	1.0	(0.94)
Basolateral bile acid uptake into hepatocyte								
Slc10a1	1.0	(0.274)	0.9	(0.063)	0.7	(< 0.001)	0.9	(0.011)
Slco1b2	1.0	(0.836)	0.9	(0.025)	0.8	(< 0.001)	0.8	(< 0.001)
Slco1c1	0.9	(0.293)	0.9	(0.032)	0.9	(0.226)	1.0	(0.627)

Shown are fold-changes compared to gd 0. Fold-change is defined as the ratio of the average fluorescence intensity of the gene at a gestation day to that at gd 0. *p*, unadjusted p-value.

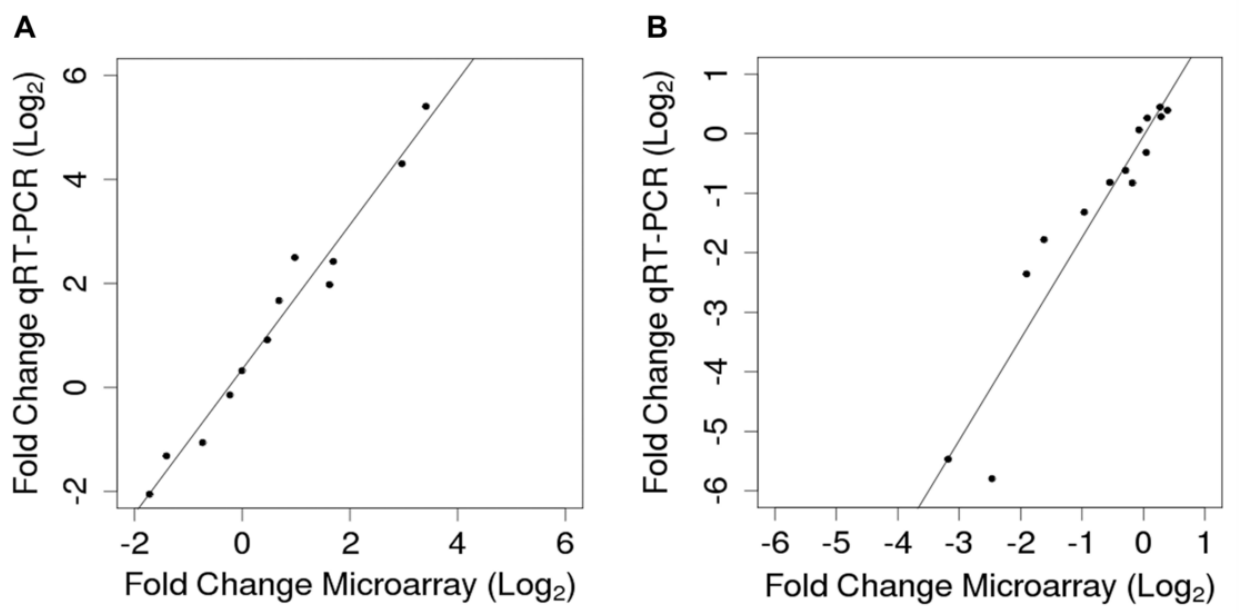

Figure 2-1. Correlation between quantitative real-time PCR (qRT-PCR) and microarray in the maternal liver and placenta.

Shown are expression means from five animals for selected genes in the liver **(A)** on gd 7.5, 10, 15, and 19, and placenta **(B)** on gd 10 and 15. Both panels are expressed as $\log_2$ fold changes

compared to gd 0 (liver) or gd 19 (placenta). The Pearson R correlation coefficient is 0.99 and 0.95 in the liver and placenta, respectively.

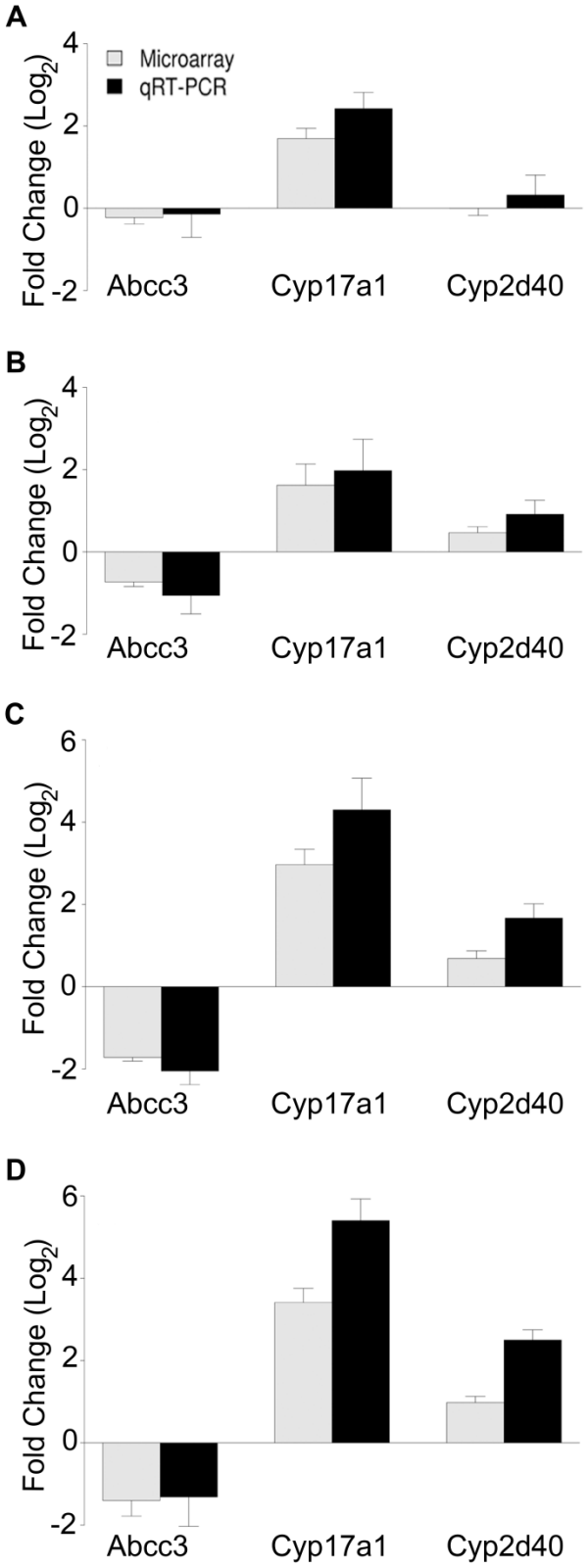

Figure 2-2. Comparison of microarray and qRT-PCR gene expression data in the maternal liver.

Shown are means ± S.D. of gene expression data from five maternal liver samples on gd 7.5 **(A)**, gd 10 **(B)**, gd 15 **(C)**, and gd 19 **(D)** compared to those on gd 0 and expressed as $\log_2$ fold-changes.

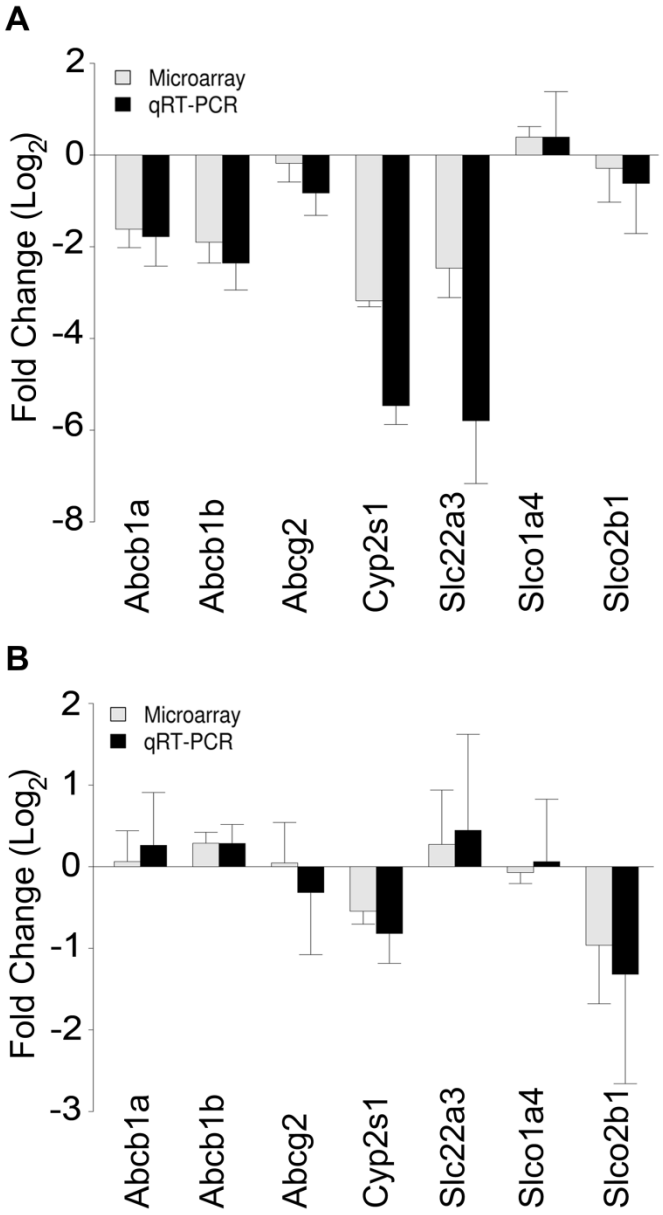

Figure 2-3. Comparison of microarray and qRT-PCR gene expression data in the placenta.

Shown are means ± S.D. of gene expression data from five placenta samples on gd 10 **(A)** and gd 15 **(B)** compared to those on gd 19 and expressed as $\log_2$ fold-changes.

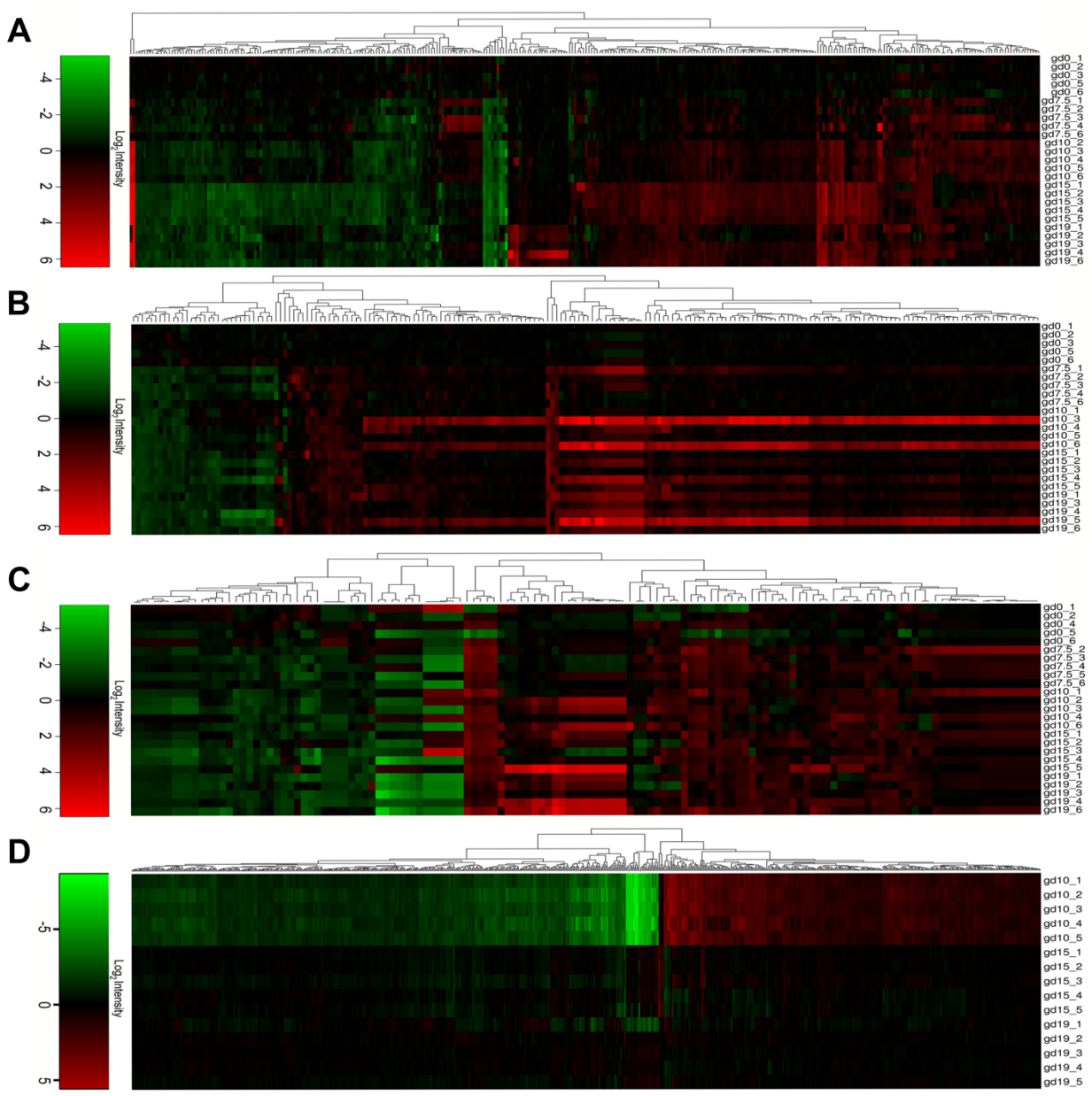

Figure 2-4. One-dimensional heatmaps of differentially expressed genes.

Liver **(A)**; kidney **(B)**; small intestine **(C)**; and placenta **(D)**. Each individual replicate (n = 5 per gestation day) was compared with the average expression on gd 0 (A-C) or gd 19 (D). Differentially expressed gene lists were generated based on the following inclusion criteria: fold-change > 2 or < 0.5 with an unadjusted p-value < 0.05 (unadjusted p < 0.00005 for placenta), and

the $\log_2$ average fluorescent intensity > 4. Red indicates an increase, and green indicates a decrease in gene expression. Color intensity is displayed on a $\log_2$ scale.

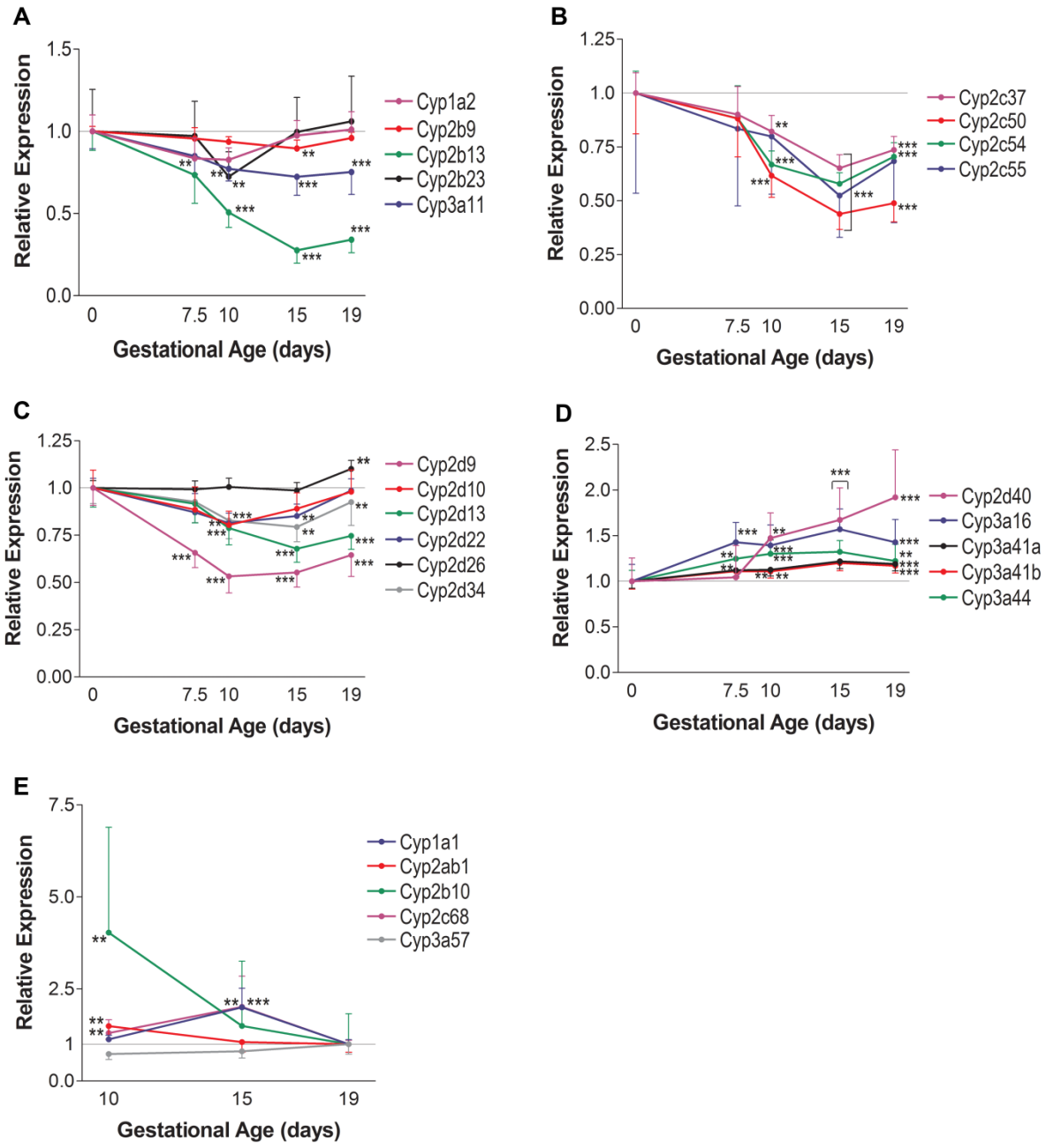

Figure 2-5. Gestational age-dependent trends in cytochrome P450 gene expression in the maternal liver and placenta.

Shown are expression means ± S.E. for selected genes in the liver **(A-D)** and placenta **(E)** from five animals. All panels are expressed as relative fold changes compared to gd 0 (liver) or gd 19

(placenta). Data points in brackets share the same statistical significance. **, unadjusted p-value < 0.01; ***, unadjusted p-value < 0.001.

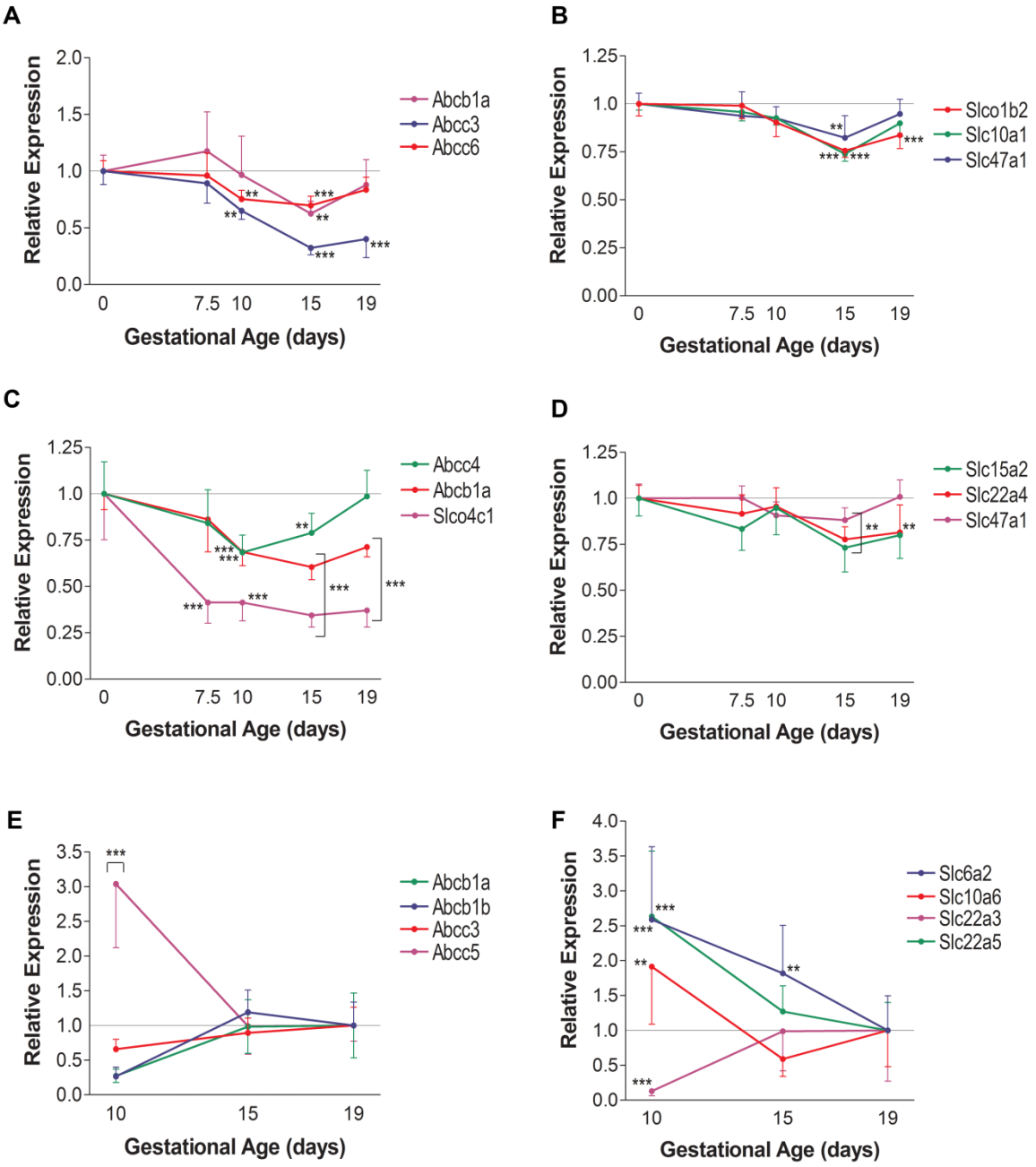

Figure 2-6. Gestational age-dependent trends in ATP-binding cassette and solute carrier transporter gene expression in the maternal liver, kidney, and placenta.

Shown are expression means ± S.E. for selected genes in the liver **(A and B)**, kidney **(C and D)**, and placenta **(E and F)** from five animals. All panels are expressed as relative fold changes

compared to gd 0 (liver and kidney) or gd 19 (placenta). Data points in brackets share the same statistical significance. **, unadjusted p-value < 0.01; ***, unadjusted p-value < 0.001.

References

[1] Carlin A, Alfirevic Z. Physiological changes of pregnancy and monitoring. Best Pract Res Clin Obstet Gynaecol. 2008;22:801-23.
[2] Davison JM, Hytten FE. The effect of pregnancy on the renal handling of glucose. Br J Obstet Gynaecol. 1975;82:374-81.
[3] Anderson GD. Pregnancy-induced changes in pharmacokinetics: a mechanistic-based approach. Clin Pharmacokinet. 2005;44:989-1008.
[4] Anger GJ, Piquette-Miller M. Pharmacokinetic studies in pregnant women. Clin Pharmacol Ther. 2008;83:184-7.
[5] Klieger C, Pollex E, Kazmin A, Koren G. Hypoglycemics: pharmacokinetic considerations during pregnancy. Ther Drug Monit. 2009;31:533-41.
[6] Tracy TS, Venkataramanan R, Glover DD, Caritis SN. Temporal changes in drug metabolism (CYP1A2, CYP2D6 and CYP3A Activity) during pregnancy. American journal of obstetrics and gynecology. 2005;192:633-9.
[7] Hebert MF, Easterling TR, Kirby B, Carr DB, Buchanan ML, Rutherford T, et al. Effects of pregnancy on CYP3A and P-glycoprotein activities as measured by disposition of midazolam and digoxin: a University of Washington specialized center of research study. Clin Pharmacol Ther. 2008;84:248-53.
[8] Feghali MN, Mattison DR. Clinical therapeutics in pregnancy. Journal of biomedicine & biotechnology. 2011;2011:783528.
[9] Dempsey D, Jacob P, 3rd, Benowitz NL. Accelerated metabolism of nicotine and cotinine in pregnant smokers. The Journal of pharmacology and experimental therapeutics. 2002;301:594-8.
[10] Hodge LS, Tracy TS. Alterations in drug disposition during pregnancy: implications for drug therapy. Expert Opin Drug Metab Toxicol. 2007;3:557-71.
[11] Hebert MF, Ma X, Naraharisetti SB, Krudys KM, Umans JG, Hankins GD, et al. Are we optimizing gestational diabetes treatment with glyburide? The pharmacologic basis for better clinical practice. Clin Pharmacol Ther. 2009;85:607-14.
[12] Unadkat JD, Wara DW, Hughes MD, Mathias AA, Holland DT, Paul ME, et al. Pharmacokinetics and safety of indinavir in human immunodeficiency virus-infected pregnant women. Antimicrob Agents Chemother. 2007;51:783-6.
[13] Zhang H, Wu X, Wang H, Mikheev AM, Mao Q, Unadkat JD. Effect of pregnancy on cytochrome P450 3a and P-glycoprotein expression and activity in the mouse: mechanisms, tissue specificity, and time course. Mol Pharmacol. 2008;74:714-23.
[14] Zhou L, Zhang Y, Hebert MF, Unadkat JD, Mao Q. Increased glyburide clearance in the pregnant mouse model. Drug Metab Dispos. 2010;38:1403-6.
[15] Mathias AA, Maggio-Price L, Lai Y, Gupta A, Unadkat JD. Changes in pharmacokinetics of anti-HIV protease inhibitors during pregnancy: the role of CYP3A and P-glycoprotein. J Pharmacol Exp Ther. 2006;316:1202-9.
[16] Koh KH, Xie H, Yu AM, Jeong H. Altered cytochrome P450 expression in mice during pregnancy. Drug metabolism and disposition: the biological fate of chemicals. 2011;39:165-9.
[17] Jonker JW, Smit JW, Brinkhuis RF, Maliepaard M, Beijnen JH, Schellens JH, et al. Role of breast cancer resistance protein in the bioavailability and fetal penetration of topotecan. J Natl Cancer Inst. 2000;92:1651-6.

[18] Smit JW, Huisman MT, van Tellingen O, Wiltshire HR, Schinkel AH. Absence or pharmacological blocking of placental P-glycoprotein profoundly increases fetal drug exposure. The Journal of clinical investigation. 1999;104:1441-7.
[19] Zhou L, Naraharisetti SB, Wang H, Unadkat JD, Hebert MF, Mao Q. The breast cancer resistance protein (Bcrp1/Abcg2) limits fetal distribution of glyburide in the pregnant mouse: an Obstetric-Fetal Pharmacology Research Unit Network and University of Washington Specialized Center of Research Study. Mol Pharmacol. 2008;73:949-59.
[20] Zhang Y, Wang H, Unadkat JD, Mao Q. Breast cancer resistance protein 1 limits fetal distribution of nitrofurantoin in the pregnant mouse. Drug Metab Dispos. 2007;35:2154-8.
[21] Wang H, Wu X, Hudkins K, Mikheev A, Zhang H, Gupta A, et al. Expression of the breast cancer resistance protein (Bcrp1/Abcg2) in tissues from pregnant mice: effects of pregnancy and correlations with nuclear receptors. American journal of physiology Endocrinology and metabolism. 2006;291:E1295-304.
[22] Aleksunes LM, Cui Y, Klaassen CD. Prominent expression of xenobiotic efflux transporters in mouse extraembryonic fetal membranes compared with placenta. Drug metabolism and disposition: the biological fate of chemicals. 2008;36:1960-70.
[23] Anderson GD, Farin FM, Bammler TK, Beyer RP, Swan AA, Wilkerson HW, et al. The effect of progesterone dose on gene expression after traumatic brain injury. Journal of neurotrauma. 2011;28:1827-43.
[24] Carvalho BS, Irizarry RA. A framework for oligonucleotide microarray preprocessing. Bioinformatics. 2010;26:2363-7.
[25] Irizarry RA, Hobbs B, Collin F, Beazer-Barclay YD, Antonellis KJ, Scherf U, et al. Exploration, normalization, and summaries of high density oligonucleotide array probe level data. Biostatistics. 2003;4:249-64.
[26] Smyth GK. Linear models and empirical bayes methods for assessing differential expression in microarray experiments. Statistical applications in genetics and molecular biology. 2004;3:Article3.
[27] Tusher VG, Tibshirani R, Chu G. Significance analysis of microarrays applied to the ionizing radiation response. Proc Natl Acad Sci U S A. 2001;98:5116-21.
[28] Dabney AR, Storey JD. A reanalysis of a published Affymetrix GeneChip control dataset. Genome biology. 2006;7:401.
[29] Stamper BD, Park SS, Beyer RP, Bammler TK, Farin FM, Mecham B, et al. Differential expression of extracellular matrix-mediated pathways in single-suture craniosynostosis. PLoS One. 2011;6:e26557.
[30] Cole TB, Beyer RP, Bammler TK, Park SS, Farin FM, Costa LG, et al. Repeated developmental exposure of mice to chlorpyrifos oxon is associated with paraoxonase 1 (PON1)-modulated effects on cerebellar gene expression. Toxicol Sci. 2011;123:155-69.
[31] Evans SJ, Datson NA, Kabbaj M, Thompson RC, Vreugdenhil E, De Kloet ER, et al. Evaluation of Affymetrix Gene Chip sensitivity in rat hippocampal tissue using SAGE analysis. Serial Analysis of Gene Expression. The European journal of neuroscience. 2002;16:409-13.
[32] Aleksunes LM, Yeager RL, Wen X, Cui JY, Klaassen CD. Repression of Hepatobiliary Transporters and Differential Regulation of Classic and Alternative Bile Acid Pathways in Mice During Pregnancy. Toxicol Sci. 2012.
[33] Gutierrez PS, Monteoliva D, Diambra L. Cooperative binding of transcription factors promotes bimodal gene expression response. PLoS One. 2012;7:e44812.

[34] Hakkola J, Raunio H, Purkunen R, Pelkonen O, Saarikoski S, Cresteil T, et al. Detection of cytochrome P450 gene expression in human placenta in first trimester of pregnancy. Biochem Pharmacol. 1996;52:379-83.
[35] Clore J, Schoolwerth A, Watlington CO. When is cortisol a mineralocorticoid? Kidney Int. 1992;42:1297-308.
[36] Dorr HG, Heller A, Versmold HT, Sippell WG, Herrmann M, Bidlingmaier F, et al. Longitudinal study of progestins, mineralocorticoids, and glucocorticoids throughout human pregnancy. J Clin Endocrinol Metab. 1989;68:863-8.
[37] Raunig JM, Yamauchi Y, Ward MA, Collier AC. Assisted reproduction technologies alter steroid delivery to the mouse fetus during pregnancy. J Steroid Biochem Mol Biol. 2011;126:26-34.
[38] Malassine A, Frendo JL, Evain-Brion D. A comparison of placental development and endocrine functions between the human and mouse model. Hum Reprod Update. 2003;9:531-9.
[39] Milona A, Owen BM, Cobbold JF, Willemsen EC, Cox IJ, Boudjelal M, et al. Raised hepatic bile acid concentrations during pregnancy in mice are associated with reduced farnesoid X receptor function. Hepatology. 2010;52:1341-9.
[40] Schwanhausser B, Busse D, Li N, Dittmar G, Schuchhardt J, Wolf J, et al. Global quantification of mammalian gene expression control. Nature. 2011;473:337-42.
[41] Martignoni M, Groothuis GM, de Kanter R. Species differences between mouse, rat, dog, monkey and human CYP-mediated drug metabolism, inhibition and induction. Expert Opin Drug Metab Toxicol. 2006;2:875-94.
[42] Sakuma T, Endo Y, Mashino M, Kuroiwa M, Ohara A, Jarukamjorn K, et al. Regulation of the expression of two female-predominant CYP3A mRNAs (CYP3A41 and CYP3A44) in mouse liver by sex and growth hormones. Arch Biochem Biophys. 2002;404:234-42.
[43] Sakuma T, Kitajima K, Nishiyama M, Endo Y, Miyauchi K, Jarukamjorn K, et al. Collaborated regulation of female-specific murine Cyp3a41 gene expression by growth and glucocorticoid hormones. Biochem Biophys Res Commun. 2004;314:495-500.
[44] Jarukamjorn K, Sakuma T, Jaruchotikamol A, Ishino Y, Oguro M, Nemoto N. Modified expression of cytochrome P450 mRNAs by growth hormone in mouse liver. Toxicology. 2006;219:97-105.
[45] Barkley MS, Geschwind, II, Bradford GE. The gestational pattern of estradiol, testosterone and progesterone secretion in selected strains of mice. Biol Reprod. 1979;20:733-8.

Chapter 3: Maternal-Fetal Disposition of Glyburide in Pregnant Mice is Dependent on Gestational Age

This work was previously published by Shuster et al., in *The Journal of Pharmacology and Experimental Therapeutics,* 350**(2)**:425-434, August 2014.

3.1 Introduction

Gestational diabetes mellitus (GDM) complicates 5-14% of human pregnancies [1, 2]. Like Type-2 diabetes, the pathology of GDM is a combination of increased insulin resistance and decreased insulin sensitivity. If left untreated, GDM poses significant risks to the mother, fetus, and neonate. Such risks include maternal hypertension, preeclampsia, and cesarean delivery; fetal/neonatal morbidities include macrosomia, hypoglycemia, as well as increased risk of metabolic syndrome, Type-2 diabetes, and obesity for the offspring later in life [3, 4]. While insulin resistance occurs in normal pregnancy, women with GDM experience insulin resistance beyond their ability to compensate with increased insulin production, leading to hyperglycemia. Although insulin has been the standard of care for pharmacotherapeutic treatment of GDM, oral

anti-diabetic agents such as glyburide have gained increasing popularity because of their ease of administration, lower cost, and comparable efficacy to insulin [5].

Diagnosis of GDM generally takes place during the second trimester of pregnancy. It has been well established that physiological, biochemical, and hormonal changes during pregnancy can alter the pharmacokinetics (PK) of drugs throughout gestation (e.g., increased hepatic blood flow and glomerular filtration, and/or changes in the expression of drug-metabolizing enzymes and transporters) [6]. However, data is quite limited regarding the PK of glyburide during pregnancy, particularly in relation to gestational age. One study estimated a 2-fold increase in the oral clearance of glyburide in women with GDM in the third trimester of pregnancy, compared to non-pregnant women with Type-2 Diabetes Mellitus [7]. Formation clearance of 4-*trans*-hydroxycyclohexyl glyburide (M1), a pharmacologically active metabolite, was also increased more than 2-fold in the GDM group. Glyburide crosses the human placenta, but at a much slower rate compared to the placental transfer marker antipyrine [8]. This was not expected given the low molecular weight and high lipophilicity of glyburide. Moreover, the low rate of placental transfer could be explained by extremely high plasma protein binding of glyburide [8] and efflux transport at the apical membrane of the syncytiotrophoblasts in humans and mice. The ATP-Binding Cassette (ABC) transporters breast cancer resistance protein (BCRP) and P-glycoprotein (P-gp) have been implicated as placental barriers to glyburide [9-12]. Although multidrug resistance proteins (MRP1 and MRP3) also transport glyburide [11{Hemauer, 2010 #603, 12], human placenta perfusion studies suggest that MRPs may only play a minor role in the transport of glyburide across the human placenta [13]. The time-course and mechanism by which pregnancy changes glyburide PK throughout gestation remain largely unexplained. Therefore,

the main objective of this study was to investigate gestational age-dependent changes in maternal-fetal disposition of glyburide and the mechanisms behind these changes.

Since hepatic CYP3A and CYP2C9 activities are significantly induced during pregnancy [14, 15], CYP induction could be one possible mechanism for the increased maternal glyburide clearance during pregnancy. Like in humans, glyburide clearance in pregnant mice was similarly doubled on gestation day (gd) 15 compared to non-pregnant controls [16], suggesting that the pregnant mouse may be an appropriate animal model to study glyburide PK during pregnancy. The mRNA levels of several hepatic *Cyp3a* isoforms and CYP3A activity in pregnant mice are significantly increased in a gestational age-dependent manner compared with non-pregnant controls [17, 18]. Therefore, we used pregnant mice to study gestational age-dependent effects on maternal-fetal disposition of glyburide.

In vitro microsomal incubation studies suggest that glyburide is extensively metabolized in the liver by CYP3A4, CYP2C9, and CYP2C19 to six major metabolites: 4-*trans*-hydroxycyclohexyl glyburide (M1), 4-*cis*-hydroxycyclohexyl glyburide (M2a), 3-*cis*-hydroxycyclohexyl glyburide (M2b), 3-*trans*-hydroxycyclohexyl glyburide (M3), 2-*trans*-hydroxycyclohexyl glyburide (M4), and ethylene-hydroxylated glyburide (M5) [19, 20]. Because M1 and M2b are potentially pharmacologically active [21] and limited data exists regarding metabolite PK in pregnant and non-pregnant individuals, we also examined maternal-fetal disposition of metabolites.

In the present study, we first determined maternal-fetal PK of glyburide and its metabolites throughout gestation in pregnant mice. We then investigated whether the intrinsic clearance of glyburide in microsomes isolated from the livers of pregnant mice was increased in

a gestational age-dependent manner. The data obtained in this study will facilitate mechanistic understanding of changes in maternal-fetal PK of glyburide and its metabolites throughout gestation, which is imperative for gestational age-dependent therapeutic strategies.

3.2 Materials and Methods

Materials

Glyburide (Gly) and glipizide were purchased from Sigma-Aldrich (St. Louis, MO). Glyburide metabolites: 4-*trans*-hydroxycyclohexyl glyburide (M1), 4-*cis*-hydroxycyclohexyl glyburide (M2a), 3-*cis*-hydroxycyclohexyl glyburide (M2b), and 3-*trans*-hydroxycyclohexyl glyburide (M3) were purchased from Toronto Research Chemicals (Toronto, Ontario, Canada). 2-*Trans*-hydroxycyclohexyl glyburide (M4), and ethylene-hydroxylated glyburide (M5) are not commercially available, and therefore were not included in our metabolite analyses. Internal standards glyburide-*d11* and 4-*trans*-hydroxycyclohexyl glyburide-*d3*,*13C* were also purchased from Toronto Research Chemicals. [Cyclohexyl-2,3-^{3}H(N)]-glyburide ([^{3}H]-Gly) (50 Ci/mmol) was obtained from PerkinElmer Life (Waltham, MA). β-nicotinamide adenine dinucleotide 2′-phosphate reduced (NADPH) tetrasodium salt hydrate, potassium phosphate monobasic (KH_2PO_4), and ethylenediaminetetraacetic acid (EDTA) were purchased from Sigma-Aldrich. Optima-grade (or HPLC grade) methanol, dimethyl sulfoxide, polyethylene glycol 400, ethanol, *n*-hexane, methylene chloride, formic acid, ammonium formate and water were obtained from Thermo Fisher Scientific (Waltham, MA) or Acros Organics (Pittsburgh, PA). Phosphate-buffered saline (PBS) was purchased from Corning Cellgro (Manassas, VA).

Animal Studies

Wild-type FVB mice, 7-10 weeks of age, were purchased from Taconic Farms (Germantown, NY) and cared for in accordance with the Guide for the Care and Use of Laboratory Animals published by the National Research Council. The animal protocol for this study was approved by the Institutional Animal Care and Use Committee at the University of Washington. Briefly, mice were maintained under 12-hour light/dark cycles, and food was provided *ad libitum*. Female mice, 7-10 weeks of age, were mated with male mice of the same age overnight using a female to male ratio of 2:1. Gestation day (gd) 1 was defined as the presence of a sperm plug following overnight housing; non-pregnant mice were defined as gd 0. Progression of pregnancy was monitored by visual inspection and body weight increase. Body weight was recorded on the day of dosing.

Glyburide was dissolved in 0.5 % (v/v) dimethyl sulfoxide, 10% (v/v) ethanol, 39.5% (v/v) saline, and 50% (v/v) polyethylene glycol 400 at a concentration of 0.5 mg/ml. Under anesthesia (2-5% isoflurane), pregnant (gd 7.5, 10, 15, and 19) or non-pregnant (gd 0) mice were administered 20 μg glyburide per mouse by retro-orbital injection (40 μl each injection). The 20 μg dose was selected to achieve maternal plasma concentrations in the 10-1,000 ng/ml range which is comparable to steady-state plasma concentrations observed in pregnant women during the third trimester of pregnancy, as we demonstrated in previous studies with pregnant and non-pregnant mice receiving a glyburide dose of 1 mg/kg body weight [7, 9, 16]. The same dose of glyburide (20 μg) was used across gestational ages because the increase in body weight during pregnancy is mainly due to the presence of placenta and fetuses, which do not significantly contribute to the overall distribution volume and metabolic clearance of glyburide. Additionally,

in clinical practice, glyburide is not administered based on body weight, therefore maintaining the same dose across gestation better mimics clinical scenarios. Depth of anesthesia was evaluated using the front-toe pinch method. At various times (0.5, 5, 10, 20, 40, 60, 120, 180, and 240 min) after glyburide administration, animals (n = 3-5 per time point) were sacrificed under anesthesia by cardiac puncture (i.e., a total of ~30 samples for each gd). Maternal blood was collected in heparinized microcentrifuge tubes (BD Biosciences, San Jose, CA) and centrifuged at 1,000 × g for 10 minutes at 4°C. Plasma was collected and stored at -80°C until further analysis. Individual whole fetuses were collected from mice dosed on gd 15 and 19. Maternal mouse livers were also collected (n = 5-6 per gd) for microsomal preparation from mice that had not been dosed with glyburide. Tissues were immediately rinsed with phosphate-buffered saline (PBS), snap-frozen in liquid nitrogen, and stored at -80°C until use.

Quantification of glyburide and metabolites in maternal plasma and fetal homogenates

Glyburide and metabolite quantification in maternal plasma and fetal homogenates was performed using a previously validated HPLC-MS method, with some modifications [22]. Most notable was the use of protein precipitation for the isolation of glyburide and metabolites from maternal plasma and fetal homogenates in place of liquid-liquid extraction. In brief, for every 100 µl of maternal plasma, 450 µl of methanol and 20 µl of working internal standards (0.5 ng/µl glyburide-*d11* and 0.15 ng/µl 4-*trans*-hydroxycyclohexyl glyburide-*d3*,*13C*) were added into a 1.5 ml microcentrifuge tube. Plasma samples were briefly vortexed and centrifuged at 20,800 × g for 10 min at 4°C. Supernatants were transferred to disposable clean glass tubes and evaporated using nitrogen gas. Samples were reconstituted in 75 µl initial mobile phase and 2 µl were

injected per sample for HPLC-MS analysis. A calibration curve was prepared identically using human plasma as a matrix with a dynamic range of 10-4,000 ng/ml for glyburide and 1.2-120 ng/ml for M1-M3.

Individual whole fetuses were homogenized in 1.5-2.5 ml of PBS using an Omni Bead Ruptor Homogenizer (Omni International, Kennesaw, GA). For every 500 µl of fetal homogenates, 50 µl of 2 M HCl, 4 mL of 60/40 (v/v) *n*-hexane/methylene chloride, and 20 µl of working internal standard (0.5 ng/µl glyburide-*d11*) were added in a 13 × 100-mm borosilicate glass culture tube. Fetal samples were vortexed 30 s and centrifuged at 1,970 × g for 10 min at 4°C. Supernatants were transferred to disposable clean glass tubes and evaporated using nitrogen gas. Each sample was reconstituted in 75 µl of 1% formic acid in methanol and 2 µl were injected per sample for HPLC-MS analysis. A calibration curve for glyburide was prepared using 500 µl of blank fetal homogenate (matched by gestational age) as matrix, over a dynamic range of 0.05-2 ng glyburide. Calibration according to analyte amount was chosen for fetal tissue analysis to accommodate the variations in fetal tissue specimen size and homogenate dilutions. No matrix effect was observed; i.e., glyburide extraction recovery and instrument response did not vary over the range of fetal homogenate concentrations prepared on samples taken from gd 15 and 19 (0.06-0.6 g fetus/ml PBS).

The previously validated HPLC-MS method did not include quantification of M2a and M3 for lack of commercially available standards at the time [22]. Those standards are now available; therefore, we modified the above method slightly to incorporate the separation and quantification of M1-M3 in maternal plasma. These metabolites were quantifiable in maternal plasma, but not detectable in fetal tissue samples.

In brief, HPLC-MS was performed using an Agilent series 1100 HPLC interfaced with an Agilent G1956B single quadrupole mass spectrometer (Agilent Technologies, Palo Alto, CA). Separation of glyburide and all metabolites in maternal plasma and fetal homogenates was achieved using an Ace 3 C8 column (150 mm × 2.1 mm, 3 micron) with gradient elution. The mobile phases consisted of methanol containing 5 mM ammonium formate (B) and water containing 5 mM ammonium formate at pH 6.0 (A). The flow rate was set to 0.4 ml/min. The gradient was 42.5% methanol for the first 5 min, then increased linearly to 90% for 5.1 min, and finally decreased back to 42.5% for the remainder of the 11-min run time. The mass spectrometer was run in API-ES positive ionization mode with a capillary voltage of 3500 V and a fragmentation voltage of 90 V for M1-M3 and *trans*-4-hydroxy glyburide-*d3,13C* or 115 V for glyburide and glyburide-*d11*. The drying gas temperature was 350ºC, the nitrogen drying gas flow rate was 12 L/min, and the nebulizer pressure was 35 pound-force per square-inch-gauge. Ions monitored were 494 *m*/z for glyburide, 505 *m*/z for glyburide-*d11*, 510 *m*/z for M1-M3, and 514 *m*/z *trans*-4-hydroxy glyburide *d3,13C*. Select ion chromatograms generated from sample extracts and that demonstrate the separation of glyburide and metabolites are presented in Figure 3-1. The lower limit of quantification in maternal plasma was 10 ng/ml for glyburide and 1.2 ng/ml for M1-M3 (Figure 3-2). Blank human plasma spiked with glyburide and metabolites was used for quality control samples for maternal plasma and fetal homogenate analyses. Inter- and intra-day variability of glyburide and metabolites were less than 5% and 2%, respectively.

Plasma Protein Binding

Mouse plasma protein binding was determined by ultrafiltration using Microcon-10 kDa Centrifugal Filters with Ultracel-10 membranes (EMD Millipore Corporation, Billerica, MA).

[^{3}H]-Glyburide (1 ng) in methanol was aliquoted into 1.5 ml Eppendorf® tubes and evaporated to dryness. Maternal plasma collected after glyburide administration on gd 0, 7.5, 10, 15 and 19 was added to each tube to a total volume of 220 µl. Samples were briefly vortexed and allowed to equilibrate for 30 min at 37°C. Two 100 µl aliquots from each sample were transferred to ultrafiltration cartridges, equilibrated for 30 min at 37°C, and centrifuged at 1,000 × g for 10 min. Eight microliters of filtrate and unfiltered plasma were counted on a liquid scintillation counter. The fraction unbound (f_u) of glyburide was calculated as the percentage of radioactivity of the filtrate to the radioactivity of the corresponding unfiltered plasma. Non-specific binding of [^{3}H]-Gly was determined using PBS rather than plasma, and was 15.8 ± 4.8% (n = 5 determinations done in duplicate).

Glyburide depletion kinetics in maternal mouse liver microsomes

Microsomes were prepared from individual maternal mouse livers (n = 5-6 per gd) as previously described [23, 24]. Briefly, approximately 1 g of mouse liver tissue was homogenized in 3 ml of homogenization buffer (50 mM KPi buffer containing 0.25 M sucrose and 1 mM EDTA) using an Omni Bead Ruptor Homogenizer (Omni International, Kennesaw, GA). The homogenate was centrifuged at 15,000 × g for 30 min at 4°C, and the supernatant at 120,000 × g for 70 min at 4°C. Microsomal pellets were carefully resuspended in washing buffer (10 mM KPi, 0.1 mM KCl, and 1 mM EDTA, pH 7.4) and centrifuged again at 120,000 × g for 70 min at 4°C. Microsomal pellets were finally resuspended in 1 ml of storage buffer (50 mM KPi, 0.25 M sucrose, and 10 mM EDTA, pH 7.4), and stored at -80°C until use. Microsomal protein concentrations were determined using the Pierce BCA Protein Assay Kit (Thermo Scientific, Rockford, IL) with bovine serum albumin as the standard.

Glyburide depletion reaction mixtures contained 0.3 mg/ml microsomal protein and 0.5 µM glyburide (dissolved in <1% v/v methanol) in 200 µl of 100 mM KH_2PO_4 buffer (1 mM EDTA, pH 7.4). The concentration of glyburide selected was below the K_m values of CYP3A4 and CYP3A5 for glyburide depletion, which are both reported to be ~5 µM [25]. After pre-incubating for 5 min, reactions were initiated by adding NADPH to a final concentration of 1 mM. Incubations without NADPH were used as negative controls. Reactions were stopped at 0, 3, 6, 10, 15, 20, and 30 min with 200 µl of ice-cold methanol. Following the addition of 20 µl of glipizide (internal standard, 1 ng/µl), samples were briefly vortexed and centrifuged at 20,800 × g for 10 min at 4°C. The supernatant was transferred to a 96-well plate and 1 µl was injected for analysis by HPLC-MS. Glyburide concentration remaining at the various time points was analyzed graphically on a semilogarithmic plot. The first-order rate constant for glyburide depletion (k_{dep}, 1/min) was estimated by least-squares regression of the log-linear portion of the depletion curve. The intrinsic clearance (CL_{int}) was calculated using the following equation:

CL_{int} = [k_{dep} × incubation volume in ml]/amount of microsomal protein in mg

Statistically significant differences of CL_{int} between gd 0 and other gestation days were determined using the Kruskal-Wallis test followed by the Dunn's Multiple Comparison test assuming a significance level of 0.05.

Quantification of glyburide in mouse liver microsomes

Chromatographic separation of glyburide in extracts of mouse liver microsomal incubates was achieved using an Agilent Extend C18 column (50 mm × 2.1 mm, 5 micron) with gradient elution. The mobile phases consisted of methanol (B) and water containing 0.1% formic acid (A). The flow rate was set to 0.4 ml/min. The gradient was 30% methanol for the first 2 min,

increased linearly to 75% for 3 min, held for 1 min at 75% methanol, and finally decreased back to 30% for the remainder of the 9-min run time. The mass spectrometer was run in API-ES positive ionization mode with a capillary voltage of 3500 V and a fragmentation voltage of 90 V for glyburide and glipizide. The drying gas temperature was 350ºC, the nitrogen drying gas flow rate was 10 L/min, and the nebulizer pressure was 35 pound-force per square-inch-gauge. Ions monitored were 494 *m*/z for glyburide and 446 *m*/z for glipizide.

Pharmacokinetic and statistical analysis of glyburide and metabolites in pregnant mice

Maternal PK parameters were estimated for each gd using a pooled data bootstrap method as previously described [26], with some modifications. Briefly, the following steps were used to obtain PK parameter estimates: 1) Concentration-time points from one gd group were sampled randomly with replacement 30 times using R programming software [27]; 2) A two-compartment model was fit to the bootstrapped pseudo concentration-time profiles using the following equation and upper constraint: $C_t = Ae^{-\alpha t} + Be^{-\beta t}$, ($A+B \leq 12{,}500$ ng/ml), where C_t is the plasma concentration at time *t* after dosing. The upper constraint for the sum of A and B was set to the highest possible blood concentration of glyburide in a 20 g female mouse given a 20 µg retro-orbital dose, i.e., 20 µg distributed in a blood volume of 1.6 ml or 8% of mouse total body weight; 3) A, B, α, β and average body weight of mice in the given pseudo-profile were used to calculate $AUC_{0\text{-}240\ min}$, CL with and without body weight normalization (CL and CL_{bw}), central volume of distribution with and without body weight normalization (V_c and $V_{c,\ bw}$), volume of distribution at steady-state or beta phase with and without body weight normalization (V_{ss} and $V_{ss,\ bw}$ or V_β and $V_{\beta,\ bw}$), and mean body residence time (MBRT). The average body weight of

the mice used to generate the pseudo-profile was also used to calculate body weight normalized estimates of clearance and volume of distribution; 4) Steps 1-3 were repeated 10,000 times to create a distribution of PK parameter estimates; 5) Based on the distribution of PK parameter estimates, 95% confidence intervals were obtained for all PK parameters. The above five steps were repeated for all gd groups. To determine whether PK parameters for pregnant mice (gd 7.5, 10, 15, and 19) were significantly different from those of non-pregnant mice (gd 0), we calculated two-sided *p*-values using permutation tests with 10,000 replications [28]. If the *p*-value was less than 0.05, the difference was considered to be statistically significant.

Maternal metabolite AUCs for each gd group and fetal glyburide AUCs for gd 15 and 19 were estimated using the same bootstrapping method as described above. Fetal glyburide concentrations were determined in individual fetuses and averaged by litter prior to bootstrap analysis. Due to the complexity of maternal metabolite kinetics and fetal glyburide kinetics, only non-compartmental analyses were feasible. We chose to estimate AUCs using the linear trapezoidal rule. To evaluate if compartmental and non-compartmental approaches produce comparable results, the AUCs of glyburide in maternal plasma were estimated using non-compartmental analysis as well. This allowed calculations of the maternal metabolite to glyburide AUC ratios as well as the fetal to maternal glyburide AUC ratios. Statistical significance between maternal metabolite AUCs and metabolite to glyburide AUC ratios estimated on gd 7.5, 10, 15 or 19 versus gd 0 were determined as described in the above paragraph. Likewise, statistical comparisons of fetal glyburide AUCs or AUC ratios between gd 15 and 19 were conducted using the same method.

Differences in fetal glyburide concentrations were compared between gd 15 and 19 at each of nine time points (from 0 to 240 minutes) and evaluated for statistical significance. Because glyburide was quantified in individual fetuses, fetal concentrations derived from the same litter were not considered statistically independent. For that reason, a generalized-estimating-equation (GEE) approach was used to account for that dependence. Differences in fetal glyburide concentrations between gd 15 and 19 at each time point (between 0 and 240 minutes) were therefore determined using GEE with an independent correlation structure. The same approach was used to model differences between fetal-maternal glyburide concentration ratios on gd 15 and 19 at each time point. In both cases, the R package geepack [29, 30] was used to perform the calculations, and calculated *p*-values were adjusted for multiple testing using a Bonferroni correction.

3.3 Results

Maternal glyburide disposition changed in a gestational age-dependent manner.

Wild-type FVB mice of various gestational ages (gd 0, 7.5, 10, 15 and 19) were administered 20 μg glyburide per mouse by retro-orbital injection. As shown in Figure 3-3, within each gd group, maternal plasma glyburide concentrations decreased over time from 0 to 240 min in a biexponential fashion. As gestation advanced, glyburide concentrations showed progressive decrease at nearly every time point; the largest differences between gestational ages occurred in the first 60 min after dosing. These changes are reflected by decreases in the coefficient of the slow exponential term (B) when the bootstrapped plasma concentration data

were fit to a biexponetnial equation. However, distribution (α) and elimination (β) rate constants remained unchanged during pregnancy (Table 3-1). All the derived two-compartmental model parameters for the maternal plasma glyburide PK are shown in Table 3-1. The $AUC_{0\text{-}240\ min}$ of glyburide steadily decreased throughout gestation by as much as 50% on gd 15 and 19 compared to non-pregnant controls (20.7, 21.2, and 47.9 μg·min/ml on gd 15, 19, and 0, respectively; $p = 0.001$). Accordingly, glyburide CL increased more than 2-fold on gd 15 and 19 compared to non-pregnant controls (0.97, 0.94, and 0.42 ml/min on gd 15, 19, and 0, respectively; $p < 0.05$). Body weight normalized estimates of CL (CL_{bw}) also demonstrated a gestational age-dependent increase (~1.5-fold increase on gd 15 and 19 versus gd 0). V_c was unaffected by pregnancy; however, V_β and V_{ss} showed a significant 2-fold increase on gd 10 and nearly tripled on gd 15 and 19 compared to non-pregnant controls. MBRT did not significantly change throughout gestation since the distribution and elimination rate constants did not vary across gestational ages. Maternal plasma protein binding (f_u) of glyburide was not significantly affected by pregnancy throughout gestation.

Maternal metabolite exposure relative to glyburide exposure was unchanged during pregnancy

Primary metabolites of glyburide, M1, M2a, M2b and M3, were also quantified in all maternal plasma samples collected. As shown in Figure 3-4, within each gd group, maternal plasma concentrations of all four metabolites first increased to a maximum at times around 30-60 min and then decreased over time to 240 min. The concentrations of all four metabolites (0-4 ng/ml) were approximately 1,000 times lower compared to those of glyburide (10-6,000 ng/ml). Similar to glyburide, metabolite concentrations at most time points tended to decrease as

gestation progressed; however, the differences in metabolite concentrations and $AUC_{0\text{-}240\ min}$ estimates compared to non-pregnant controls were greatest on gd 15 and slightly reversed on gd 19 (rather than the sustained increase on gd 15 and 19 in the case of glyburide). Indeed, $AUC_{0\text{-}240\ min}$ for M1 significantly decreased by 200% on gd 15 and 150% on gd 19 compared to gd 0 (129 and 141 ng·min/ml compared to 251 ng·min/ml, respectively) (Table 3-2). $AUC_{0\text{-}240\ min}$ of M2a, M2b, and M3 all decreased by 300% on gd 15 compared to gd 0 (Table 3-2). Though the metabolite to glyburide AUC ratios for M1 and M2a on gd 10 or for M2b and M3 on gd 15 were significantly increased or decreased, respectively, these ratios were <1% for all metabolites across all gestational ages. Maternal plasma AUCs of glyburide estimated using non-compartmental analysis shown in Table 3-2 were comparable to those calculated using a two-compartmental model shown in Table 3-1.

Fetal exposure to glyburide doubled from mid to late gestation

On gd 15 and 19, individual fetuses were collected simultaneously to determine fetal exposure to glyburide and metabolites. Concentrations of glyburide in fetal homogenates ranged from ~1-10 ng/g fetus, and were lower overall on gd 15 compared to gd 19 (Figure 3-5A). The fetal-to-maternal plasma concentration ratios of glyburide on gd 19 were also generally greater than those on gd 15 at several time points from 0.5 to 240 min (Figure 3-5B). Consequently, the fetal $AUC_{0\text{-}240\ min}$ of glyburide on gd 19 was significantly increased 2-fold compared to gd 15 (905 versus 462 ng·min/g, respectively; $p < 0.001$) (Table 3-3). The fetal-to-maternal plasma $AUC_{0\text{-}240\ min}$ ratio of glyburide doubled from gd 15 to 19 as well (1.8% versus 3.7%, respectively; $p = 0.007$). Fetal concentrations of all four metabolites were below the detection limit for all time points on gd 15 and 19.

Gestational age-dependent changes in maternal glyburide metabolism

We hypothesized that increased glyburide CL in pregnant mice versus non-pregnant controls is the result of increased CYP-mediated metabolism of glyburide in the liver. To test this hypothesis, glyburide depletion rate was measured in microsomes prepared from maternal livers collected on gd 0, 7.5, 10, 15 and 19. Mean time courses of glyburide depletion during incubation with liver microsomes for the five gestational age groups are shown in Figure 3-6A. There was indeed a gestational age-dependent increase in glyburide CL_{int} in the liver, which doubled by gd 19 versus gd 0 (0.17 versus 0.09 ml/min/mg protein, respectively) (Figure 3-6B).

3.4 Discussion

Previous clinical studies showed that the oral clearance of glyburide increased 2-fold during the third trimester in pregnant women with GDM compared to non-pregnant controls [7]. Diagnosis and treatment of GDM most often occur in the second trimester [31]. In addition, women at risk for developing GDM or with a previous history of GDM may be screened and treated earlier in pregnancy [31]. Therefore, it is important to understand glyburide PK changes throughout gestation, and how such changes affect glycemic control. In this study, we characterized maternal-fetal glyburide disposition throughout gestation in a pregnant mouse model, since it is not feasible to obtain data at this level of detail in pregnant women.

We found that the maternal plasma PK of glyburide changes in a gestational age-dependent manner, with the largest alterations occurring in mid-late gestation on gd 15 and 19 (Figure 3-3 and Table 3-1). In particular, maternal glyburide CL, V_{β}, and V_{ss} steadily increased over gestation and were approximately doubled by mid-late gestation. Glyburide is a low hepatic

ER drug (ER = ~0.1) with no significant renal CL. Therefore, the increase in maternal systemic CL could be accounted for by changes in fraction unbound in plasma and CL_{int} of glyburide in the liver. The fraction unbound (f_u) did not increase throughout gestation (Table 3-1), which was somewhat unexpected, considering that plasma albumin is known to decrease during pregnancy [32]. However, the f_u of glyburide also did not change in pregnant women with GDM compared to non-pregnant controls [7]. The reasons why the f_u was unaffected by pregnancy are not clear. It is possible that glyburide can bind to other lipoproteins in the plasma and/or there are biochemical changes in maternal plasma that have offsetting modulation on plasma protein binding of glyburide. Since the f_u of glyburide in maternal plasma did not significantly change throughout gestation, the increase in maternal glyburide CL and CL_{bw} is most likely caused by an increase in hepatic CL_{int}. Indeed, the glyburide depletion rate in mouse liver microsomes steadily increased as gestation progressed (Figure 3-6). Using ketoconazole as a CYP3A inhibitor, we previously showed that glyburide was primarily metabolized by CYP3A in mouse liver [16]. This is consistent with the finding that hepatic CYP3A activity is significantly induced by pregnancy both in humans and mice [14, 17]. The present study further confirmed that hepatic CYP3A activity in pregnant mice is induced in a gestational age-dependent manner. It is not known which mouse CYP3A isoforms are responsible for increased glyburide metabolism during pregnancy as we and others have shown that mRNA levels of *Cyp3a16, Cyp3a41,* and *Cyp3a44* are induced, while *Cyp3a11, Cyp3a13,* and *Cyp3a25* genes are down-regulated in a gestational age-dependent manner [17, 18]. Increases in V_{ss} and V_{β} most likely reflect increases in total body water and fat content during pregnancy, and further suggest that distribution of glyburide into maternal tissues is increased during pregnancy.

Although the pharmacodynamics and therapeutic window of glyburide have not been well characterized, it is possible that 1.5-2-fold increases in glyburide CL (and CL_{bw}) and corresponding decreases in AUC warrant consideration when determining appropriate therapeutic management of glyburide in pregnant women. If our animal data indeed reflect gestational age-dependent changes in maternal glyburide CL and AUC in humans, dosing adjustments may be required as early as the first or second trimester. This would be particularly important for pregnant women treated with glyburide starting in the first or second trimester.

Understanding maternal disposition of primary metabolites of glyburide is also important as some metabolites (e.g. M1 and M2b) are pharmacologically active [21, 33]. We had expected that increased glyburide CL across gestation would lead to either no change or increase in formation of M1-M3, if they are all derived from pathways that are up-regulated; instead, maternal plasma AUCs of each of the measured metabolites decreased progressively reaching a nadir by gd 15 and slightly reversed by gd 19 (Figure 3-5 and Table 3-2).

AUC of a metabolite represents the balance of its formation and elimination rates. A decrease in metabolite AUC can possibly be explained by an increase in elimination clearance of the metabolite. Accelerated metabolite elimination could be due to increased secondary oxidative metabolism, increased Phase II conjugation, and/or increased renal clearance of the metabolites. In humans, M1 undergoes glucuronidation mediated by uridine 5'-diphospho-glucuronosyltransferases (UGTs) and M2b is excreted unchanged in the urine [22]. UGT1A1 and UGT1A4 expression is indeed induced during human pregnancy [15]; however, mRNA levels of UGTs in pregnant mice are relatively unchanged [18]. Mechanisms of renal clearance (i.e. active tubular secretion and/or reabsorption) remain unknown for all glyburide metabolites in humans

and mice. Further investigation is required to elucidate the mechanisms of the putative increase in metabolite elimination.

Another possible explanation for a decrease in metabolite AUC as gestation progresses is that the increase in glyburide CL is due to an increase in normally minor metabolic pathway(s) not represented by the measured metabolites; that is, up-regulation of competing pathway(s) resulting in a decrease in formation of the measured metabolites. M1, M2a, M2b, M3, M4 and M5 are the primary metabolites of glyburide produced by the human liver, and glyburide is metabolized primarily to M5 in human placenta by CYP19 [19]. It is therefore possible that decreases in concentrations of M1-M3 could be due to increased formation of M4 and/or M5 in maternal liver and placenta. However, without commercially available standards for M4 and M5, we were unable to quantify gestational age-dependent changes in maternal concentrations of M4 and M5.

Table 3-2 also presents the metabolite-to-glyburide AUC ratio, which is governed by the ratio of a given metabolite's formation clearance to its elimination clearance. It is a quantitative index reflecting either the joint or opposing effects of simultaneous changes in formation and elimination clearances of a primary metabolite. Mean AUC ratios for M1and M2a were elevated on gd 10 and declined to near the gd 0 values by gd 15 and 19. This suggests that the increase in formation clearance of these two metabolites outpaced the increase in their elimination clearances by gd 10; moreover, the changes in formation and elimination clearances became comparable as gestation progressed beyond gd 10. For M2b and M3, their AUC ratios declined across all the gestation days studied, suggesting that there was a greater increase in elimination clearance compared to formation clearance.

Fetal exposure to glyburide was <5% of maternal exposure, but was doubled on gd 19 versus gd 15 (Table 3-3 and Figure 3-5). This change is consistent with the finding that protein expression of BCRP in mouse placenta on gd 15 is 2-3 times greater than that on gd 19 [34]. Glyburide is a substrate of mouse and human BCRP, which limit the transport of glyburide across the placenta barrier [9, 11, 12]. As BCRP protein expression decreases from gd 15 to gd 19, glyburide penetration across the placenta to the fetus increases. P-gp could also contribute to the gestational age-dependent changes in fetal exposure to glyburide because both human and mouse P-gp expression in the placenta decreases as gestation progresses [17, 35, 36]. M1-M3 were not detectable in fetal homogenates, suggesting that fetal exposure to these primary metabolites is negligible due to their low concentrations in maternal circulations. Since glyburide is highly bound to plasma proteins with a low volume of distribution, the actual fetal plasma concentrations may be higher than what we observed in fetal homogenates. Indeed, one clinical study showed that the mean ratio of umbilical cord glyburide concentration at delivery to maternal plasma glyburide concentration was ~0.7 [7], indicating that a substantial amount of glyburide can cross the placenta to the fetus. Therefore, while total fetal exposure in human pregnancy is not known, there could be times following drug administration that fetal concentrations are nearly as high as maternal plasma concentrations. While the current dosage of glyburide is safe for use during pregnancy, dosage increases based on gestational age could raise concerns for fetal safety. In addition, since BCRP expression in human placenta decreases from ~28 weeks of gestation towards term [37], increased fetal exposure to glyburide in late pregnancy would be expected and may pose a safety concern that conflicts with the consideration to increase glyburide doses during pregnancy for improved maternal efficacy.

In summary, we have demonstrated gestational age-dependent maternal-fetal glyburide PK in pregnant mice. Results of this study suggest the possible need for increased glyburide dosages even in early pregnancy should the same PK changes occur in humans, and that the pregnant mouse is an appropriate animal model to study glyburide disposition during pregnancy.

Tables and Figures for Chapter 3

Table 3-1. Gestational age-dependent pharmacokinetics of glyburide in maternal plasma using a two-compartmental model

Parameter	Gd 0		Gd 7.5			Gd 10			Gd 15			Gd 19		
	Mean	± SD or (95% CI)	Mean	± SD or (95% CI)	*p*	Mean	± SD or (95% CI)	*p*	Mean	± SD or (95% CI)	*p*	Mean	± SD or (95% CI)	*p*
$AUC_{0\text{-}240\ min}$ (μg·min/ml)	47.9	(40.5-54.1)	**37.2**	**(30.6-42.1)**	**0.021**	**29.5**	**(23.1-35.0)**	**0.002**	**20.7**	**(16.1-26.3)**	**0.001**	**21.2**	**(16.3-25.5)**	**0.001**
CL (ml/min)	0.42	(0.37-0.49)	**0.54**	**(0.48-0.65)**	**0.025**	**0.68**	**(0.57-0.87)**	**0.003**	**0.97**	**(0.76-1.24)**	**0.025**	**0.94**	**(0.79-1.23)**	**0.020**
CL_{bw} (ml/min/g)	0.018	(0.016-0.021)	**0.022**	**(0.020-0.027)**	**0.038**	**0.026**	**(0.022-0.033)**	**0.010**	**0.030**	**(0.024-0.039)**	**0.036**	**0.028**	**(0.023-0.036)**	**0.030**
Vc (ml)	2.1	(1.7-5.2)	4.0	(2.4-32.9)	0.124	3.9	(1.7-56.3)	0.205	5.2	(2.7-50.2)	0.137	3.5	(1.8-8.7)	0.398
$Vc_{, bw}$ (ml/g)	0.09	(0.07-0.22)	0.17	(0.10-1.33)	0.143	0.15	(0.07-2.24)	0.240	0.161	(0.084-1.630)	0.310	0.102	(0.052-0.254)	0.837
V_{β} (ml)	35.5	(29.1-48.3)	43.7	(34.7-57.0)	0.219	**68.8**	**(51.7-103.3)**	**0.012**	**89.9**	**(67.2-152)**	**0.039**	**93.6**	**(65.0-170)**	**0.030**
$V_{\beta, bw}$ (ml/g)	1.51	(1.24-2.06)	1.82	(1.45-2.37)	0.270	**2.61**	**(1.95-3.93)**	**0.023**	2.81	(2.10-4.84)	0.089	2.73	(1.92-4.88)	0.146
V_{ss} (ml)	21.2	(18.2-27.1)	29.2	(23.2-41.2)	0.067	**39.8**	**(28.3-61.7)**	**0.014**	**56.2**	**(38.4-84.6)**	**0.013**	**49.3**	**(33.3-71.5)**	**0.014**
$V_{ss, bw}$ (ml/g)	0.90	(0.77-1.15)	1.22	(0.97-1.71)	0.090	**1.51**	**(1.09-2.31)**	**0.033**	1.75	(1.20-2.69)	0.052	1.44	(0.98-2.13)	0.135
A (ng/ml)	9020	(3432-11154)	4602	(454-7999)	0.150	4851	(250-11317)	0.210	3680	(251-7316)	0.155	5556	(1565-10891)	0.280
α (1/min)	0.67	(0.38-0.83)	0.60	(0.20-0.84)	0.600	0.68	(0.19-0.98)	0.939	0.84	(0.18-1.35)	0.750	0.82	(0.37-1.28)	0.657
B (ng/ml)	431	(325-543)	382	(283-462)	0.465	**243**	**(169-299)**	**0.007**	**189**	**(127-238)**	**0.023**	**159**	**(93-216)**	**0.020**
β (1/min)	0.012	(0.009-0.014)	0.012	(0.01-0.014)	0.712	0.010	(0.007-0.012)	0.287	0.011	(0.006-0.015)	0.756	0.010	(0.006-0.013)	0.558
MBRT (1/min)	50.8	(44.9-59.3)	54.3	(46.7-64.4)	0.532	58.7	(48.3-72.9)	0.288	58.1	(43.0-75.5)	0.548	52.2	(40.8-63.7)	0.870
F_u (%)	2.19	± 0.25	2.45	± 0.67	0.394	2.27	± 0.59	0.766	2.00	± 0.11	0.260	2.27	± 0.52	0.741
Body Wt (g)	24	± 2.2	24	± 1.2		26	± 1.7		32	± 2.3		34	± 4.7	

Data reported as mean ± SD or (95% confidence interval). PK parameters on gd 7.5, 10, 15 or 19 with statistically significant ($p < 0.05$) differences versus gd 0 were bolded. Gd, gestation day; bw, body weight normalized; D, dose; AUC, area under the concentration-time curve; CL, clearance; V, volume of distribution; MBRT, mean body residence time; f_u, fraction unbound ; *p*-values, *p*. Fraction unbound data are shown as mean ± S.D. from 6 maternal plasma samples for each gestation day, with duplicate determinations for each maternal plasma sample. Body weight data are means ± SD from n ≈ 30 mice per gestation day.

Table 3-2. Gestational age-dependent AUCs of glyburide and metabolites in maternal plasma using non-compartmental analyses

Parameter	Gd 0		Gd 7.5			Gd 10			Gd 15			Gd 19		
	Mean	**(95% CI)**	**Mean**	**(95% CI)**	***p***	**Mean**	**(95% CI)**	***p***	**Mean**	**(95% CI)**	***p***	**Mean**	**(95% CI)**	***p***
GLY AUC (ng·min/ml)	55169	(46859-65378)	**39729**	**(32827-46781)**	**0.013**	**29308**	**(25112-33771)**	**<0.001**	**25302**	**(19276-31635)**	**<0.001**	**24216**	**(19689-30361)**	**<0.001**
M1 AUC (ng·min/ml)	251	(204-294)	187	(156-219)	0.084	232	(205-258)	0.596	**129**	**(88-172)**	**0.006**	**141**	**(114-163)**	**0.011**
M2a AUC (ng·min/ml)	359	(305-401)	**221**	**(166-265)**	**0.001**	**256**	**(206-295)**	**0.007**	**101**	**(61-149)**	**<0.001**	**131**	**(97-169)**	**<0.001**
M2b AUC (ng·min/ml)	238	(208-274)	**159**	**(134-188)**	**0.009**	**141**	**(112-177)**	**0.005**	**47**	**(30-63)**	**<0.001**	**83**	**(66-99)**	**<0.001**
M3 AUC (ng·min/ml)	251	(223-285)	**188**	**(148-237)**	**0.044**	**137**	**(107-170)**	**0.002**	**50**	**(32-67)**	**<0.001**	**70**	**(57-82)**	**<0.001**
M1/GLY AUC Ratio (%)	0.44	(0.37-0.51)	0.46	(0.37-0.55)	0.793	**0.77**	**(0.67-0.88)**	**<0.001**	0.49	(0.36-0.64)	0.534	0.57	(0.43-0.69)	0.091
M2a/GLY AUC Ratio (%)	0.63	(0.53-0.71)	0.54	(0.40-0.67)	0.270	**0.85**	**(0.70-0.98)**	**0.028**	**0.39**	**(0.25-0.55)**	**0.036**	0.53	(0.38-0.70)	0.298
M2b/GLY AUC Ratio (%)	0.42	(0.35-0.48)	0.39	(0.32-0.47)	0.576	0.47	(0.37-0.57)	0.485	**0.18**	**(0.12-0.24)**	**0.003**	0.33	(0.25-0.42)	0.231
M3/GLY AUC Ratio (%)	0.44	(0.37-0.51)	0.46	(0.36-0.60)	0.767	0.45	(0.36-0.55)	0.867	**0.19**	**(0.13-0.25)**	**0.003**	**0.28**	**(0.21-0.35)**	**0.041**

Data are reported as mean (95% confidence interval). Parameters on gd 7.5, 10, 15 or 19 with statistically significant ($p < 0.05$) differences versus gd 0 were bolded. The metabolite to glyburide AUC ratios were corrected for differences in the molarity between glyburide (494 g/mol) and metabolites (510 g/mol). Gd, gestation day; AUC, area under the concentration-time curve; *p*-values (*p*).

Table 3-3. Gestational age-dependent maternal-fetal AUCs of glyburide using non-compartmental analyses

Parameter	Gd 15		Gd 19		
	Mean	**(95% CI)**	**Mean**	**(95% CI)**	***p***
Maternal $AUC_{0\text{-}240\ min}$ (ng·min/ml)	26129	(20129 - 32478)	24216	(19576 - 30273)	0.657
Fetal $AUC_{0\text{-}240\ min}$ (ng·min/g)	462	(349 - 529)	**905**	**(726 - 1013)**	**<0.001**
Fetal/Maternal AUC Ratio (%)	1.8	(1.4 - 2.2)	**3.7**	**(2.8 - 4.6)**	**0.007**

Data reported as mean (95% confidence interval). Statistically significant ($p < 0.05$) differences between gd 19 and 15 were bolded. Gd, gestation day; AUC, area under the concentration-time curve; *p*-values (*p*).

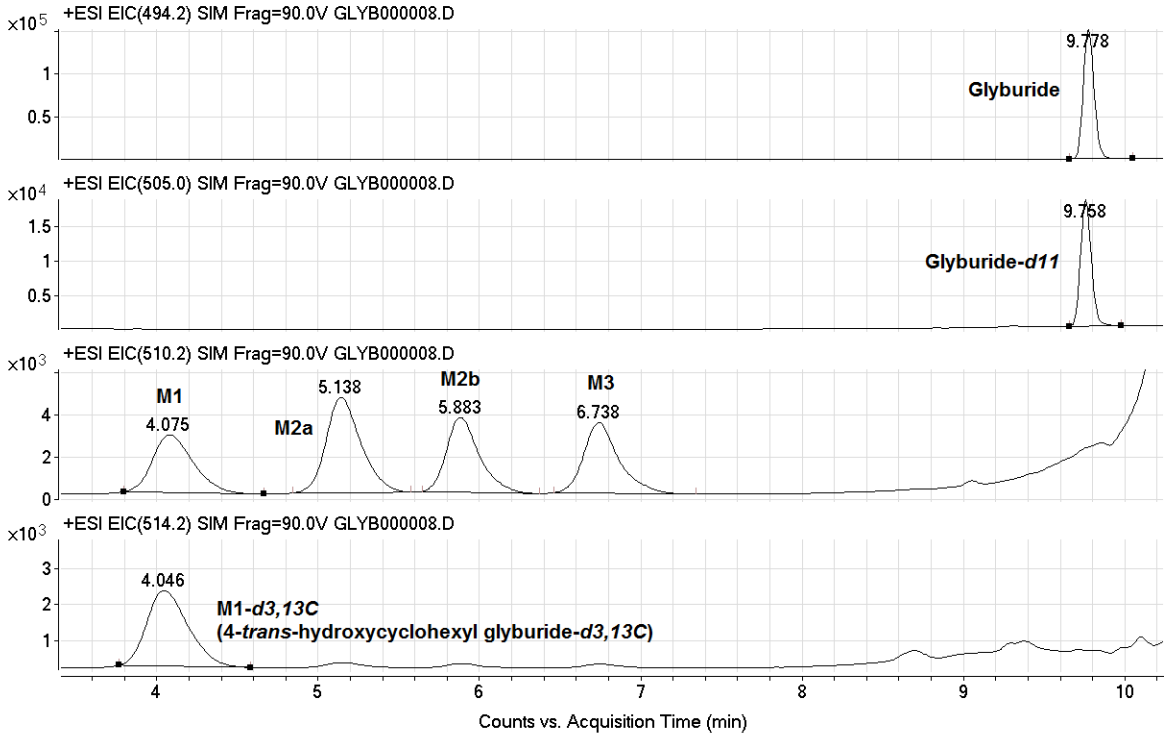

Figure 3-1. Extracted ion chromatograms (EICs) of glyburide, metabolites, and internals standards.

EIC taken from highest calibration standard injection (corresponding to 4,000 ng/ml glyburide).

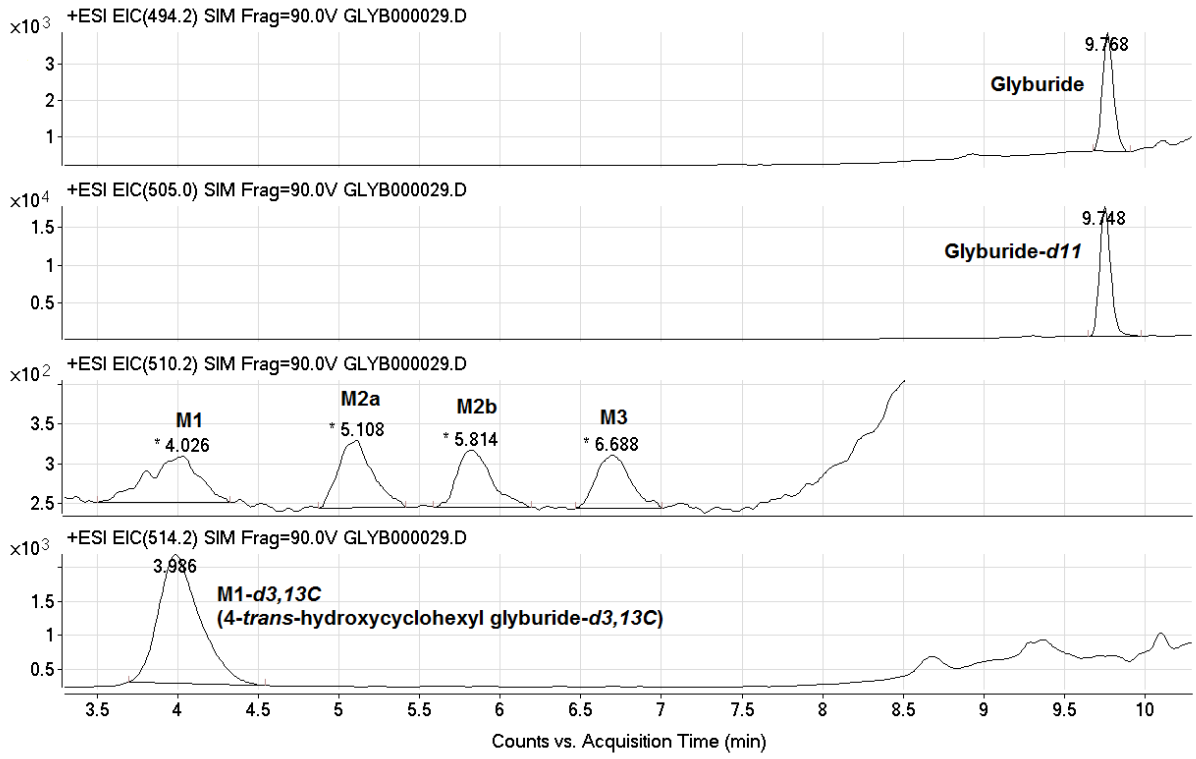

Figure 3-2. Extracted ion chromatograms of glyburide, metabolites, and internals standards corresponding to the lower limit of quantification (LLOQ) in maternal plasma.

The LLOQ was 10 ng/ml glyburide and 1.2 ng/ml M1-M3 in maternal plasma.

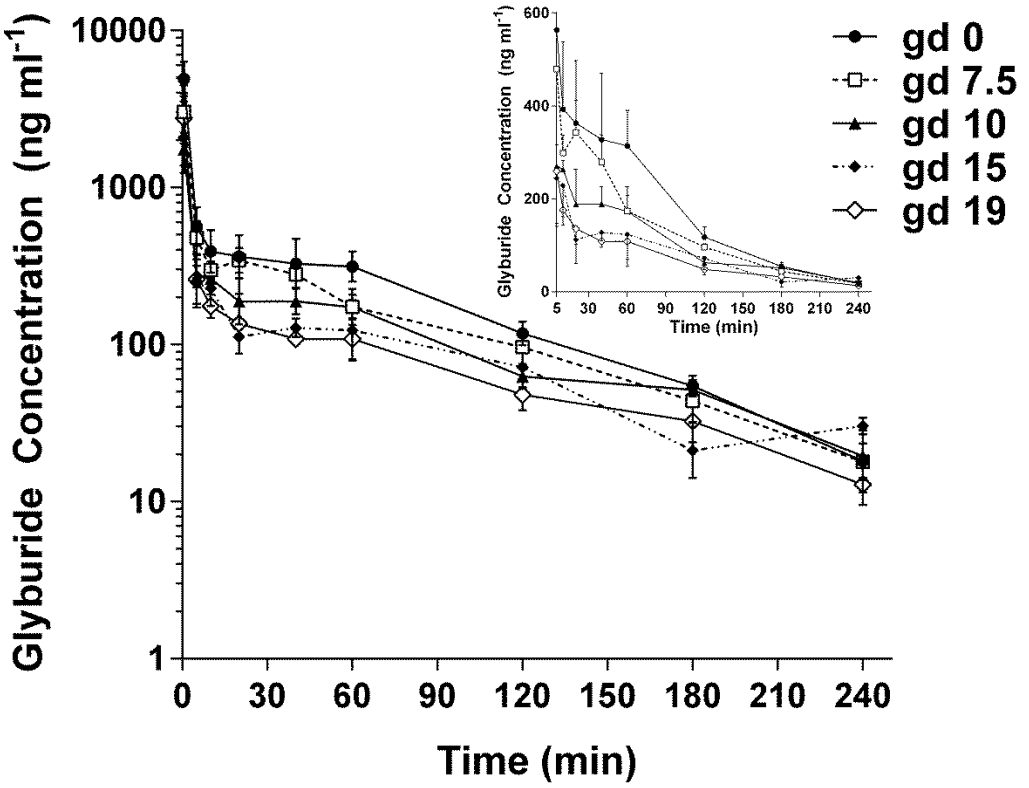

Figure 3-3. Maternal plasma concentration-time profiles of glyburide in wild-type FVB pregnant mice throughout gestation.

Mice were administered 20 μg of glyburide per mouse by retro-orbital injection. Data from gestation day 0 (gd 0) (solid circles), gd 7.5 (open squares), gd 10 (solid triangles), gd 15 (solid diamonds), and gd 19 (open diamonds) are shown as mean ± S.D. (n = 3-5 mice per time point). The main figure shows a semilogarithmic plot and the insert in the upper right-hand corner shows a rectilinear plot (including data from 5 – 240 min). Non-pregnant mice are referred to as gd 0.

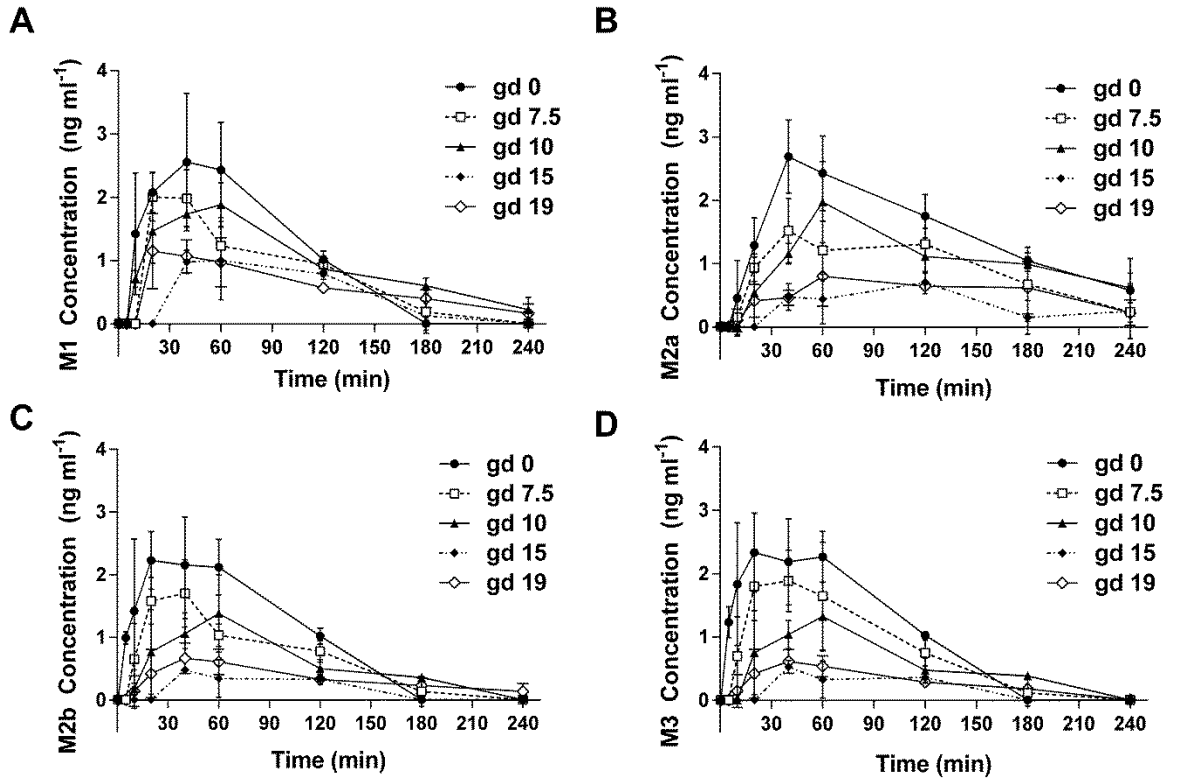

Figure 3-4. Maternal plasma concentration-time profiles of metabolites M1-M3 in wild-type FVB pregnant mice throughout gestation.

A, M1; **B**, M2a; **C**, M2b; **D**, M3. Data from gestation day 0 (gd 0) (solid circles), gd 7.5 (open squares), gd 10 (solid triangles), gd 15 (solid diamonds), and gd 19 (open diamonds) are shown as mean ± S.D. (n = 3-5 mice per time point). Non-pregnant mice are referred to as gd 0.

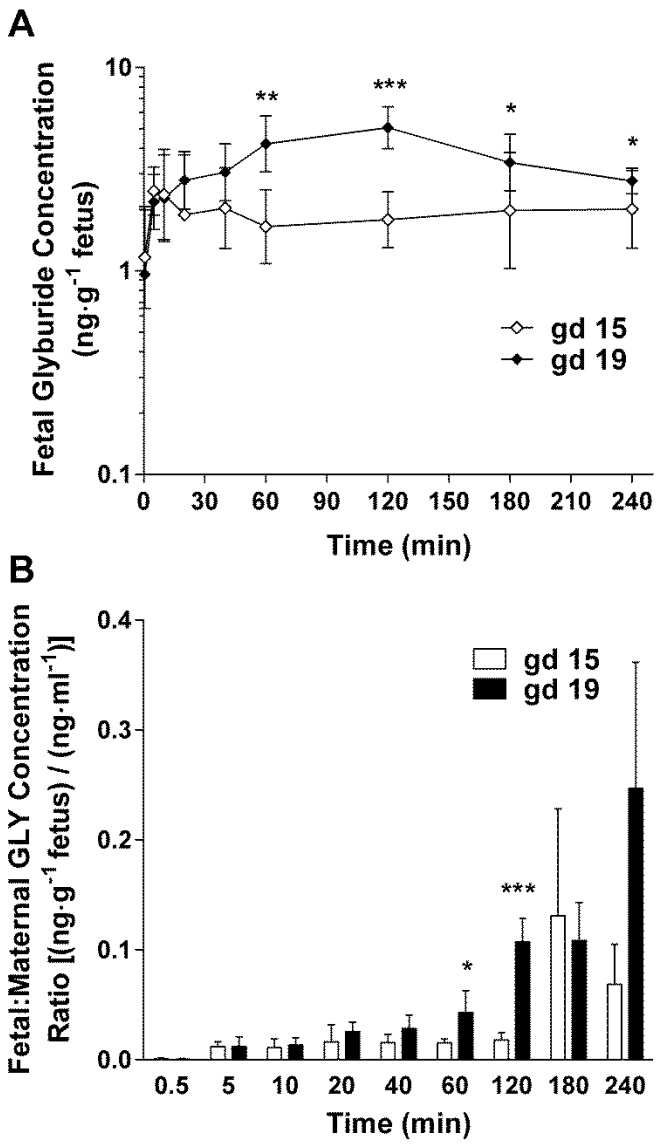

Figure 3-5. Fetal glyburide concentration-time profiles and fetal-to-maternal plasma concentration ratios in mid-late gestation.

Data from gestation day (gd) 15 (open diamonds) and gd 19 (solid diamonds) are shown as mean ± S.D. (n = 20-40 fetuses per time point). **A**, semilogarithmic plot of fetal glyburide concentration over time; **B**, fetal to maternal plasma glyburide concentration ratios. Statistically significant differences in fetal concentrations and fetal-to-maternal plasma concentration ratios

between gd 15 and 19 were determined using a generalized estimating-equation (GEE) approach with an independent correlation structure. P-values were adjusted for multiple testing using a Bonferroni correction assuming a significance level of 0.05. * $p < 0.05$; ** $p < 0.01$; *** $p < 0.001$.

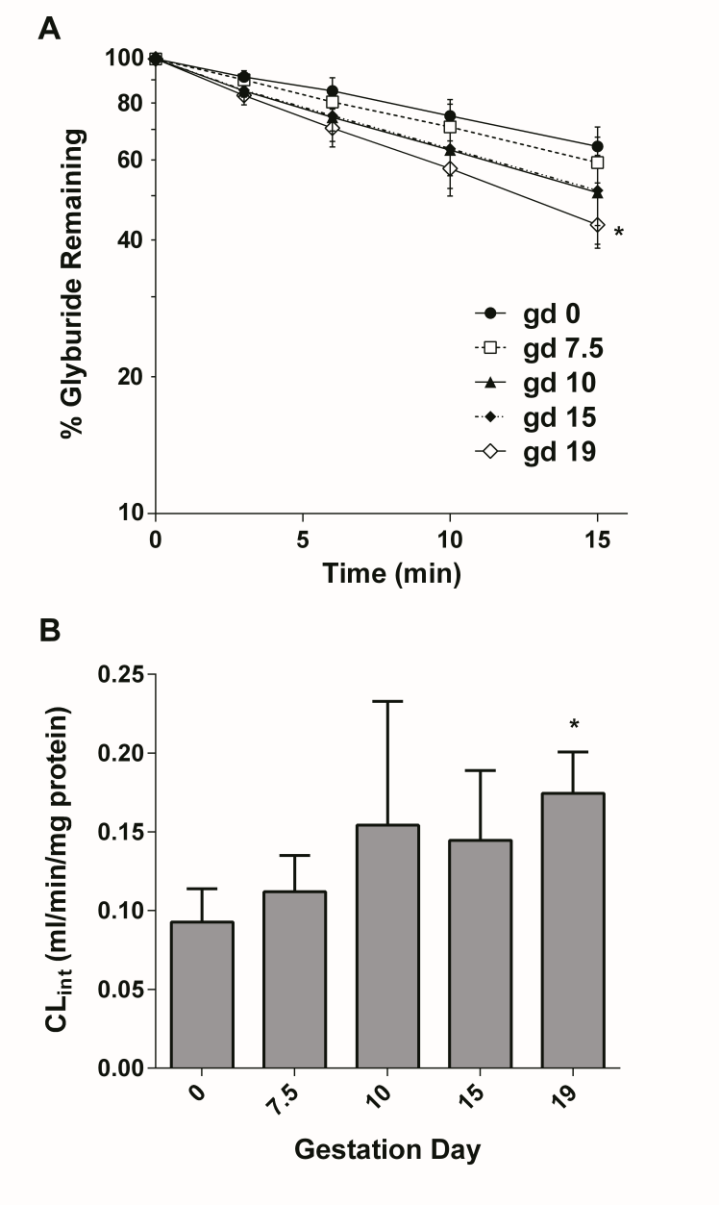

Figure 3-6. Gestational age-dependent depletion kinetics of glyburide in mouse liver microsomes.

A, semilogarithmic plot of glyburide depletion over time in mouse liver microsomes. Data from gestation day 0 (gd 0) (solid circles), gd 7.5 (open squares), gd 10 (solid triangles), gd 15 (solid diamonds), and gd 19 (open diamonds) are shown as mean ± S.D. (n = 4-6 livers per gd). **B**, gestational age-dependent changes in glyburide CL_{int}. Shown are mean ± S.D. (n = 4-6 livers per

gd). Statistically significant differences between gd 0 and gd 7.5, 10, 15 or 19, as indicated by an asterisk (*), were determined by the Kruskal-Wallis test followed by the Dunn's Multiple Comparison test assuming a significance level of 0.05. Non-pregnant mice are referred to as gd 0.

References

[1] Jovanovic L, Pettitt DJ. Gestational diabetes mellitus. JAMA. 2001;286:2516-8.
[2] Paglia MJ, Coustan DR. Gestational diabetes: evolving diagnostic criteria. Curr Opin Obstet Gynecol. 2011;23:72-5.
[3] The Hyperglycemia and Adverse Pregnancy Outcome (HAPO) Study. Int J Gynaecol Obstet. 2002;78:69-77.
[4] ACOG Practice Bulletin. Clinical management guidelines for obstetrician-gynecologists. Number 30, September 2001 (replaces Technical Bulletin Number 200, December 1994). Gestational diabetes. Obstetrics and gynecology. 2001;98:525-38.
[5] Langer O, Conway DL, Berkus MD, Xenakis EM, Gonzales O. A comparison of glyburide and insulin in women with gestational diabetes mellitus. N Engl J Med. 2000;343:1134-8.
[6] Klieger C, Pollex E, Kazmin A, Koren G. Hypoglycemics: pharmacokinetic considerations during pregnancy. Ther Drug Monit. 2009;31:533-41.
[7] Hebert MF, Ma X, Naraharisetti SB, Krudys KM, Umans JG, Hankins GD, et al. Are we optimizing gestational diabetes treatment with glyburide? The pharmacologic basis for better clinical practice. Clin Pharmacol Ther. 2009;85:607-14.
[8] Nanovskaya TN, Nekhayeva I, Hankins GD, Ahmed MS. Effect of human serum albumin on transplacental transfer of glyburide. Biochem Pharmacol. 2006;72:632-9.
[9] Zhou L, Naraharisetti SB, Wang H, Unadkat JD, Hebert MF, Mao Q. The breast cancer resistance protein (Bcrp1/Abcg2) limits fetal distribution of glyburide in the pregnant mouse: an Obstetric-Fetal Pharmacology Research Unit Network and University of Washington Specialized Center of Research Study. Mol Pharmacol. 2008;73:949-59.
[10] Gedeon C, Anger G, Piquette-Miller M, Koren G. Breast cancer resistance protein: mediating the trans-placental transfer of glyburide across the human placenta. Placenta. 2008;29:39-43.
[11] Gedeon C, Behravan J, Koren G, Piquette-Miller M. Transport of glyburide by placental ABC transporters: implications in fetal drug exposure. Placenta. 2006;27:1096-102.
[12] Hemauer SJ, Patrikeeva SL, Nanovskaya TN, Hankins GD, Ahmed MS. Role of human placental apical membrane transporters in the efflux of glyburide, rosiglitazone, and metformin. American journal of obstetrics and gynecology. 2010;202:383 e1-7.
[13] Gedeon C, Anger G, Lubetsky A, Miller MP, Koren G. Investigating the potential role of multi-drug resistance protein (MRP) transporters in fetal to maternal glyburide efflux in the human placenta. J Obstet Gynaecol. 2008;28:485-9.
[14] Hebert MF, Easterling TR, Kirby B, Carr DB, Buchanan ML, Rutherford T, et al. Effects of pregnancy on CYP3A and P-glycoprotein activities as measured by disposition of midazolam and digoxin: a University of Washington specialized center of research study. Clin Pharmacol Ther. 2008;84:248-53.
[15] Feghali MN, Mattison DR. Clinical therapeutics in pregnancy. J Biomed Biotechnol. 2011;2011:783528.
[16] Zhou L, Zhang Y, Hebert MF, Unadkat JD, Mao Q. Increased glyburide clearance in the pregnant mouse model. Drug Metab Dispos. 2010;38:1403-6.
[17] Zhang H, Wu X, Wang H, Mikheev AM, Mao Q, Unadkat JD. Effect of pregnancy on cytochrome P450 3a and P-glycoprotein expression and activity in the mouse: mechanisms, tissue specificity, and time course. Mol Pharmacol. 2008;74:714-23.

[18] Shuster DL, Bammler TK, Beyer RP, Macdonald JW, Tsai JM, Farin FM, et al. Gestational age-dependent changes in gene expression of metabolic enzymes and transporters in pregnant mice. Drug Metab Dispos. 2013;41:332-42.
[19] Zharikova OL, Fokina VM, Nanovskaya TN, Hill RA, Mattison DR, Hankins GD, et al. Identification of the major human hepatic and placental enzymes responsible for the biotransformation of glyburide. Biochem Pharmacol. 2009;78:1483-90.
[20] Ravindran S, Zharikova OL, Hill RA, Nanovskaya TN, Hankins GD, Ahmed MS. Identification of glyburide metabolites formed by hepatic and placental microsomes of humans and baboons. Biochem Pharmacol. 2006;72:1730-7.
[21] Rydberg T, Jonsson A, Roder M, Melander A. Hypoglycemic activity of glyburide (glibenclamide) metabolites in humans. Diabetes Care. 1994;17:1026-30.
[22] Naraharisetti SB, Kirby BJ, Hebert MF, Easterling TR, Unadkat JD. Validation of a sensitive LC-MS assay for quantification of glyburide and its metabolite 4-transhydroxy glyburide in plasma and urine: an OPRU Network study. J Chromatogr B Analyt Technol Biomed Life Sci. 2007;860:34-41.
[23] Thummel KE, Kharasch ED, Podoll T, Kunze K. Human liver microsomal enflurane defluorination catalyzed by cytochrome P-450 2E1. Drug Metab Dispos. 1993;21:350-7.
[24] Paine MF, Khalighi M, Fisher JM, Shen DD, Kunze KL, Marsh CL, et al. Characterization of interintestinal and intraintestinal variations in human CYP3A-dependent metabolism. J Pharmacol Exp Ther. 1997;283:1552-62.
[25] Zhou L, Naraharisetti SB, Liu L, Wang H, Lin YS, Isoherranen N, et al. Contributions of human cytochrome P450 enzymes to glyburide metabolism. Biopharm Drug Dispos. 2010;31:228-42.
[26] Mager H, Goller G. Resampling methods in sparse sampling situations in preclinical pharmacokinetic studies. J Pharm Sci. 1998;87:372-8.
[27] R Core Team. R: A language and environment for statistical computing. Vienna, Austria: R Foundation for Statistical Computing; 2014.
[28] Westfall PH, Young SS. Resampling-based multiple testing : examples and methods for P-value adjustment. New York: Wiley; 1993.
[29] Halekoh U, Hojsgaard S, Yan J. The R Package geepack for Generalized Estimating Equations. J Stat Softw. 2006;15:1-11.
[30] Yan J, Fine J. Estimating equations for association structures. Stat Med. 2004;23:859-74.
[31] Metzger BE, Buchanan TA, Coustan DR, de Leiva A, Dunger DB, Hadden DR, et al. Summary and recommendations of the Fifth International Workshop-Conference on Gestational Diabetes Mellitus. Diabetes Care. 2007;30 Suppl 2:S251-60.
[32] Anderson GD. Pregnancy-induced changes in pharmacokinetics: a mechanistic-based approach. Clin Pharmacokinet. 2005;44:989-1008.
[33] Balant L, Fabre J, Loutan L, Samimi H. Des 4-trans-hydroxy-glibenclamide show hypoglycemic activity? Arzneimittelforschung. 1979;29:162-3.
[34] Wang H, Wu X, Hudkins K, Mikheev A, Zhang H, Gupta A, et al. Expression of the breast cancer resistance protein (Bcrp1/Abcg2) in tissues from pregnant mice: effects of pregnancy and correlations with nuclear receptors. American journal of physiology Endocrinology and metabolism. 2006;291:E1295-304.
[35] Mathias AA, Hitti J, Unadkat JD. P-glycoprotein and breast cancer resistance protein expression in human placentae of various gestational ages. Am J Physiol Regul Integr Comp Physiol. 2005;289:R963-9.

[36] Aleksunes LM, Cui Y, Klaassen CD. Prominent expression of xenobiotic efflux transporters in mouse extraembryonic fetal membranes compared with placenta. Drug metabolism and disposition: the biological fate of chemicals. 2008;36:1960-70.
[37] Meyer zu Schwabedissen HE, Grube M, Dreisbach A, Jedlitschky G, Meissner K, Linnemann K, et al. Epidermal growth factor-mediated activation of the map kinase cascade results in altered expression and function of ABCG2 (BCRP). Drug Metab Dispos. 2006;34:524-33.

Chapter 4: Identification of CYP3A7 for Glyburide Metabolism in Human Fetal Livers

4.1 Introduction

During pregnancy, 5-14% of women will be diagnosed with gestational diabetes mellitus (GDM) [1, 2]. Glyburide is an oral hypoglycemic drug that is prescribed more commonly for the treatment of GDM [3]. Though glyburide exhibits nearly comparable efficacy to insulin, the incidence rates of adverse fetal effects associated with glyburide verses insulin therapy, such as neonatal hypoglycemia and large for gestational age infants, are conflicting [4-8]. At present, there are no long-term safety data for infants whose mothers were treated with glyburide. In addition, studies are needed to understand the mechanistic determinants of fetal exposure that impact the fetal safety of glyburide.

Glyburide is extensively metabolized in the maternal liver by CYP3A4, CYP2C9, and CYP2C19 to several metabolites, such as 4-*trans*-hydroxycyclohexyl glyburide (M1), 4-*cis*-hydroxycyclohexyl glyburide (M2a), 3-*cis*-hydroxycyclohexyl glyburide (M2b), 3-*trans*-hydroxycyclohexyl glyburide (M3), 2-*trans*-hydroxycyclohexyl glyburide (M4), and ethylene-hydroxylated glyburide (M5); though there may be more [9, 10]. As treatment of GDM with glyburide is optimized, there will be several factors that could be important determinants of fetal exposure to glyburide and its metabolites, (and ultimately its safety profile), including maternal exposure, transplacental clearance, placental metabolism, and fetal elimination. Maternal exposure to conventional doses of glyburide during human pregnancy is reduced compared to

non-pregnant women, suggesting the need for increased doses [11]. Glyburide concentrations, which are measurable in umbilical cord blood at the time of delivery, suggest that glyburide can cross the placenta [11]. ATP-binding cassette (ABC) efflux transporters, particularly breast cancer resistance protein (BCRP) and P-glycoprotein (P-gp) are highly expressed in the placenta and may limit fetal glyburide exposure to some extent [12-18]. Since the expression of ABC transporters in the placenta changes as gestation progresses [15] and the placenta grows larger with gestational age, penetration of glyburide into the fetal compartment across the placental barrier may also change over gestation. In addition, glyburide can be metabolized in human term placenta [9, 10, 19, 20], specifically by the cytochrome P450 (CYP) enzyme CYP19 (aromatase). Although the relative contribution of placental drug-metabolizing enzymes to the overall maternal disposition of glyburide may in fact be minimal, glyburide metabolism in such close proximity to the fetus could possibly affect fetal exposure to glyburide and its metabolites. Metabolite transplacental clearances have not been determined, however. Finally, fetal exposure to glyburide may also be influenced by fetal liver metabolism upon entrance into the fetal circulation. At present, little is known about glyburide metabolism in human fetal livers.

CYP3A7 is the predominant CYP enzyme in the human fetal liver [21-23]. CYP3A5 has also been found in the human fetal liver [24], but at much lower amounts relative to CYP3A7. In a panel of human fetal livers (n ~10), the mRNA levels of CYP3A5 were approximately 700-fold lower than those of CYP3A7, and CYP3A5 protein was detected in just one liver (CYP3A5 genotype was not determined) [23]. Previous studies using adult human liver microsomes (HLMs) and recombinant enzymes have shown that glyburide is a substrate of CYP3A4 and CYP3A5 [9, 25], suggesting the plausibility of glyburide metabolism by other CYP3A isoforms such as CYP3A7. Indeed, CYP3A7 has been shown to metabolize endogenous substrates of

CYP3A4, such as testosterone and dehydroepiandrosterone (DHEA), but with different oxidation site preferences [22, 26]. Several *in vitro* studies have also shown that both embryonic (less than 60 days) and fetal livers can metabolize endogenous compounds (i.e. testosterone, retinoic acid, and DHEA) and xenobiotics (i.e. warfarin, benzyloxyresorufin, and coumarin), as well as activate promutagens and procarcinogens [27, 28]. CYP3A7 preferentially metabolizes testosterone to its 2α–OH metabolite, rather than its 6β–OH metabolite, which is primarily produced by CYP3A4 [22], suggesting the metabolic profile of glyburide in human fetal livers could differ from that in adult livers. Given that glyburide can cross the placental barrier [11, 29] and that CYP3A7 expression/activity is variable in human fetal livers [22], it is important to investigate CYP3A7-mediated metabolism of glyburide and characterize the variability of glyburide metabolism in human fetal livers. Understanding fetal metabolism of glyburide is clinically relevant because this may govern fetal exposure to not only glyburide, but its major metabolites such as M1 and M2b, which are believed to be pharmacologically active [30].

In this study, we determined the kinetics of glyburide depletion by CYP3A4, CYP3A5, and CYP3A7 supersomes, measured the Cl_{int} of glyburide in human fetal liver microsomes (HFLMs), and compared the metabolite profiles generated by CYP3A supersomes, HFLMs, and HLMs. We examined the correlation between glyburide Cl_{int} and metabolism of DHEA (a known CYP3A7 probe substrate) as well as midazolam (a CYP3A substrate) in human fetal livers. To better understand sources of variability in fetal metabolism, we also investigated the relationship between glyburide Cl_{int} and CYP3A7 protein levels in human fetal livers, fetal liver gestational age, fetal sex, CYP3A7 genotype, and other fetal demographics. Results from this study will have important clinical implications for informing fetal exposure and the fetal safety profile of glyburide in early and mid-gestation.

4.2 Materials and Methods

Materials

Glyburide and glipizide (internal standard) were purchased from Sigma-Aldrich (St. Louis, MO). The following glyburide metabolites were purchased from TLC PharmaChem (Vaughan, Ontario, Canada): 4-*trans*-hydroxycyclohexyl glyburide (M1), 3-*cis*-hydroxycyclohexyl glyburide (M2b), and 3-*trans*-hydroxycyclohexyl glyburide (M3). 4-*cis*-hydroxycyclohexyl glyburide (M2a) was a generous gift from Mary Hebert. [Cyclohexyl-2,3-^{3}H(N)]-glyburide ([^{3}H]-Gly) (50 Ci/mmol) was obtained from PerkinElmer Life and Analytical Sciences (Waltham, MA). Midazolam (MDZ) was purchased from Sigma-Aldrich (St. Louis, MO). 1′-OH Midazolam (1′-OH MDZ) and 4′-OH Midazolam (4′-OH MDZ) were purchased from Ultrafine (Manchester, England). Internal standards for the metabolites of MDZ, $^{15}N_3$-1′-OH MDZ and $^{15}N_3$-4′-OH MDZ, were prepared as previously described [31]. Dehydroepiandrosterone (DHEA) and its metabolite, 16α-hydroxydehydroepiandrosterone (16α-OH DHEA) were purchased from Steraloids (Newport, RI). Iodoacetamide, dithiothreitol and sequencing grade trypsin were purchased from Pierce Biotechnology (Rockford, IL). Ammonium bicarbonate was purchased from Acros Organics (Geel, Belgium). Sodium deoxycholate was purchased from MP Biologicals (Santa Ana, California). Synthetic light peptides for CYP enzyme quantification were procured from New England Peptides (Boston, MA), with purity established by amino acid analysis. Heavy stable isotope labeled amino acids, [$^{13}C_6{}^{15}N_2$]-lysine and [$^{13}C_6{}^{15}N_4$]-arginine, were purchased from Pierce Biotechnology, Inc. (Rockford, IL). β-Nicotinamide adenine dinucleotide 2′-phosphate reduced (NADPH) tetrasodium salt hydrate, potassium phosphate monobasic and dibasic, ethylenediaminetetraacetic acid (EDTA), and HPLC-grade formic acid were purchased from Sigma-Aldrich (St. Louis, MO). Potassium phosphate dibasic, ethyl

acetate, and HPLC-grade methanol, acetonitrile, and ammonium formate were obtained from Thermo Fisher Scientific (Waltham, MA). CYP3A4, CYP3A5 and CYP3A7 Supersomes™ were purchased from BD Biosciences (San Jose, California). Pooled HLMs were purchased from Xenotech (Lenexa, KS).

Preparation of human fetal liver microsomes (HFLMs)

Sixteen human fetal livers from first and second trimester pregnancies were obtained from the University of Washington Birth Defects Research Laboratory. HFLMs were prepared as described previously [32, 33]. Briefly, approximately 1 g of fetal liver tissue was homogenized in 3 ml of homogenization buffer (50 mM KPi buffer containing 0.25 M sucrose and 1 mM EDTA, pH 7.4) using an Omni Bead Ruptor Homogenizer (Omni International, Kennesaw, GA). The homogenate was centrifuged at 15,000 × g for 30 min at 4° C, and the supernatant at 120,000 × g for 70 min at 4° C. Microsomal pellets were resuspended in 1 ml storage buffer (50 mM KPi buffer, 0.25 M sucrose, and 10 mM EDTA, pH 7.4), and stored at -80° C until use. Microsomal protein concentrations were determined using the Pierce BCA Protein Assay Kit (Thermo Scientific, Rockford, IL) with bovine serum albumin as the standard.

DNA isolation and CYP3A genotyping of human fetal livers

DNA was isolated from 16 human fetal liver samples using a Qiagen (Valencia, California) DNeasy Blood and Tissue Kit according to the manufacturer's recommendations. For allele nomenclature, the CYPallele Nomenclature Guidelines (http://www.imm.ki.se/cypalleles) were used with *CYP3A5*1* and *CYP3A7*1* as reference sequences. Genotyping for alleles *CYP3A5*3* (C__26201809_30) and **6* (C__30203950_10) as well as *CYP3A7*2*

(C__25474551_10) and **1C* (T>A: C__30634321_20; G>T: C__30634326_10) was performed using pre-developed TaqMan assays purchased from Invitrogen (Grand Island, NY).

Quantification of CYP protein in human fetal liver microsomes by HPLC-MS/MS

Simultaneous quantification of multiple CYP enzymes was carried out using a surrogate peptide-based HPLC-MS/MS method. The surrogate light peptides were first selected based on previously reported criteria [34, 35]. The corresponding heavy peptides containing labeled [$^{13}C_6{}^{15}N_2$]-lysine or [$^{13}C_6{}^{15}N_4$]-arginine residues were used as internal standards. Prior to CYP quantification, fetal liver microsomal samples were diluted to 2 mg/ml, and 20 µl (40 µg of protein) was subsequently digested using a previously validated protocol with a few modifications [36]. Briefly, microsomal samples were denatured and reduced via incubation with 4 µl of 100 mM dithiothreitol, 10 µl of sodium deoxycholate (2.6 % w/v) and 10 µl of ammonium bicarbonate buffer (100 mM) at 95° C for 5 min. The protein samples were then cooled and alkylated using 4 µl of 200 mM iodoacetamide at room temperature in the dark. The samples were digested with 10 µl of trypsin in a final volume of 48 µl at 37° C for 22 hours. The reaction was stopped by the addition of 20 µl of peptide internal standard cocktail (prepared in 50% acetonitrile in water containing 0.1% formic acid) and 10 µl of the neat solvent, i.e., 50% acetonitrile in water containing 0.1% formic acid. The samples were vortexed and centrifuged at 3500 × g for 5 min. Calibration curve standards were prepared by spiking standard working solutions of peptides into a solution containing all of the above mentioned reagents plus microsomal storage buffer to replace microsomal sample. Eight calibration concentrations ranging from approximately 0.3 to 600 fmol peptide (on column) were used for various CYP

enzymes. For each standard, working stock solutions of the peptide (10 µl) were added in the last step instead of the neat solvent. The supernatant was transferred to HPLC vials and stored at -20° C until further analysis by HPLC-MS/MS. Digestion and quantification were performed in triplicate for each HFLM sample. Two pooled (n = 10) HLM samples from adult donors were also processed similarly to serve as quality controls for the HPLC-MS/MS method.

The CYP protein quantification assays were performed on a triple-quadrupole LC-MS instrument (Agilent 6460A) coupled to an Agilent 1290 Infinity LC system (Agilent Technologies), in ESI positive ionization mode. Approximately 2 µg of the trypsin digest (5 µl) was injected onto the column (Kinetex 1.7 µ, C18 100A; 100 × 2.1 mm, Phenomenex, Torrance, CA). Mobile phases consisted of water (A) and acetonitrile (B) (both containing 0.1% formic acid) at a flow rate of 0.3 ml/min. The gradient was 3% mobile phase B for 2.0 min, followed by gradient elution program with mobile phase B concentration of 3 to 18% (2.0-4.0 min), 18 to 22% (4.0-8.0 min), 22 to 24% (8.0-10 min), 24% (10-12.2 min), 24 to 34% (12.2-12.5 min) and 34 to 38% (12.5-15.0 min). This was followed by washing with 80% mobile phase B for 0.9 min and re-equilibration for 4.9 min. Surrogate peptides and internal standards were monitored in multiple reaction monitoring (MRM) mode using instrument parameters provided in Table 4-1. HPLC-MS/MS data were processed using the MassHunter (Agilent Technologies) and Skyline software.

Glyburide depletion kinetics in CYP3A supersomes and HFLMs, and quantification by HPLC-MS

Incubations and reaction conditions were adapted from published methods [22, 25]. Briefly, supersome reaction mixtures contained varying glyburide concentrations (0.01-20 µM)

dissolved in methanol (<1% v/v), CYP3A4, CYP3A5, or CYP3A7 supersomes, and 100 mM potassium phosphate buffer (1 mM EDTA, pH 7.4), in a final volume of 200 µl. The concentrations of CYP3A4, CYP3A5 or CYP3A7 supersomes in reaction mixtures were 10, 30, and 50 pmol/ml, respectively. HFLM reaction mixtures were prepared similarly, except that only one concentration of glyburide was used (0.05 µM) with 0.8 mg/ml of microsomal protein. After pre-incubation in a shaking 37° C water bath for 5 min, reactions were initiated by adding NADPH to a final concentration of 1 mM. Supersome reactions were stopped at 0, 5, 10, 15, 20, 30, and 45 min; HFLM reactions were stopped at 0, 15, 30, and 45 min, both with 200 µl of ice-cold methanol (for glyburide concentrations ≤ 0.5 µM) or 1 ml of ice-cold methanol (for glyburide concentrations > 0.5 µM). Incubations without NADPH at 0 and 45 min served as negative controls. No depletion was observed in the absence of NADPH. Following the addition of 20 µl of glipizide (internal standard, 1 ng/µl in methanol), samples were briefly vortexed and centrifuged at 20,800 × g for 10 min at 4° C. The supernatant was transferred to a 96-well plate and 1 µl was injected for analysis by HPLC-MS. To determine CYP3A supersome kinetics, three experiments were performed for each CYP3A isoform. In a given experiment, triplicate determinations were performed for each time point. To determine the intrinsic clearance (Cl_{int}) of glyburide in individual HFLMs, one experiment was performed using duplicate determinations for each time point. Due to the limited amount of fetal liver microsomal protein, only one depletion experiment was performed for each HFLM. Glyburide concentrations were quantified using a validated HPLC-MS assay as previously described [37]. Two calibration curves (low and high) were prepared using potassium phosphate buffer as a matrix over the concentration ranges of 2.5 – 500 ng/ml (5 nM – 1 µM) and 25 – 10,000 ng/ml (0.05 – 20 µM) glyburide.

Glyburide concentrations remaining at various time points were analyzed graphically on a semilogarithmic plot. The first-order rate constant for glyburide depletion (k_{dep}, min^{-1}) was estimated by least-squares regression of the entire depletion curve using the Graphpad Prism 6.04 software (La Jolla, CA). For CYP3A supersome kinetics, depletion rates were converted to reaction velocities (v) using the following equation:

$$v = (k_{dep} \cdot [S_0]) / [rCYP]$$

where $[S_0]$ is the initial glyburide concentration (ranging from 0.01-20 μM) and [rCYP] is the concentration of the recombinant enzyme used in the incubation. Reaction velocities were plotted against initial glyburide concentrations ($[S_0]$), and kinetic parameters (K_m and V_{max}) were estimated from a least-squares regression fit to a Michaelis-Menten equation using the Graphpad Prism 6.04 software [38]. As mentioned previously, three separate experimental determinations were completed to estimate kinetic parameters for each of the CYP3A isoforms. Statistically significant differences between mean parameter estimates of different CYP3A isoforms were determined using one-way ANOVA analysis followed by the Tukey's multiple comparison test (n = 3 per CYP3A isoform).

For individual HFLM's, the Cl_{int} was calculated as previously described using the following equation [37, 38]:

$$Cl_{int} = k_{dep}/\text{microsomal protein concentration}$$

Linear correlations between glyburide Cl_{int}, CYP3A7 protein levels, 16α-OH DHEA formation, 1′-OH MDZ formation and 4′-OH MDZ formation were evaluated by estimating the Pearson correlation coefficient (r) using the Graphpad Prism 6.04 software.

Metabolite profile of glyburide in CYP3A supersomes, HFLMs, and HLMs and relative abundance by HPLC-MS/MS

The metabolite profile of glyburide was determined with CYP3A4, CYP3A5 and CYP3A7 supersomes as well as pooled HFLMs and pooled HLMs. Reaction mixtures contained 0.05 μM glyburide dissolved in methanol (< 1% v/v), 30 pmol/ml CYP3A supersomes or 0.8 mg/ml microsomal protein, and 100 mM potassium phosphate (KH_2PO_4) buffer (1 mM EDTA, pH 7.4), in a final volume of 200 μl. Incubations were performed according to section 2.5, except for two minor modifications: reactions were stopped at 30 min rather than 45 min, and 5 μl of supernatant were injected for HPLC-MS/MS analysis. One experiment was performed using duplicate determinations for each time point.

Metabolites M1-M5 were identified by HPLC-MS/MS using an Agilent series 1200 HPLC interfaced with an Agilent 6410 triple quadrupole mass spectrometer (Agilent Technologies, Palo Alto, CA). Separation of M1-M5, glyburide, and glipizide was achieved using an ACE C8 300 column (150 mm × 2.1 mm × 3 μ) with gradient elution. The mobile phases consisted of methanol (B) and water containing 0.1 % formic acid (A). The flow rate was set to 0.4 ml/min. The gradient was 40% methanol for the first 5 min, increased linearly to 90% for 4 min, held for 2 min at 90% methanol, and immediately decreased to 40%, and held at 40% for the remainder of the 15 min run time. The mass spectrometer was run in ESI positive ionization mode with a capillary voltage of 3500 V and a fragmentation voltage of 110 V for all metabolites and 87 V for glipizide. The drying gas temperature was 350º C, the nitrogen drying gas flow rate was 10.0 L/min, and the nebulizer pressure was 35 pound-force per square-inch-gauge. Since a standard for M5 is not commercially available, metabolite identification was based on elution order and ion transitions as previously described [39]. The following ion

transitions were monitored in MRM mode: *m*/z 510.2 >169.0, 367.0, and 369.0 for M1-M5, *m*/z 494.2 >169.0 for glyburide, and *m*/z 446.2 >321.1 for glipizide. HPLC-MS/MS data were processed using MassHunter (Agilent Technologies). Peak area ratios were used to compare relative abundance of metabolites between CYP3A supersomes, HFLMs, and HLMs, assuming that fragment ion signal to on-column injected molar amount is about the same for all the analytes.

16α-OH-DHEA formation in HFLMs and quantification by HPLC-MS

16α-OH-DHEA formation in HFLMs was performed as previously described with minor modifications [22]. Briefly, reaction mixtures contained 100 µM DHEA (dissolved in 100% v/v methanol, dried down under air, and reconstituted in HFLM protein/buffer mixture), 0.8 mg/ml HFLMs, and 100 mM potassium phosphate buffer (1 mM EDTA, pH 7.4), in a final volume of 100 µl. After pre-incubating in a shaking 37° C water bath for 5 min, reactions were initiated by adding NAPDH to a final concentration of 1 mM. Reactions were stopped at 0 and 10 min with 1 ml of ice-cold methanol. Incubations using HFLMs without NADPH at 0 and 10 min served as negative controls. Following the addition of 20 µl of progesterone (internal standard, 5.0 µg/ml in methanol), samples were briefly vortexed and centrifuged at 20,800 × g for 10 min at 4° C. The supernatant was transferred to a 96-well plate and 1 µl was injected for analysis by HPLC-MS. Due to the limited amount of fetal liver microsomal protein, only one depletion experiment was performed for each HFLM; however, duplicate determinations were performed for each time point. Under these conditions, the depletion of DHEA did not exceed 20%.

DHEA and 16α-OH-DHEA concentrations were quantified by HPLC-MS using an Agilent series 1100 HPLC interfaced with an Agilent G1956B single quadrupole mass

spectrometer (Agilent Technologies, Palo Alto, CA). Separation of DHEA and 16α-OH-DHEA was achieved using a Zorbax C18 extend column (50 mm × 2.1 mm × 5 μ) with gradient elution. The mobile phases consisted of methanol (B) and water containing 0.1 % formic acid (A). The flow rate was set to 0.3 ml/min. The gradient was 40% methanol for the first 3 min, increased linearly to 80% for 7 min, and held for 2 min at 80% methanol for the remainder of the 12 min run time. The mass spectrometer was run in API-ES positive ionization mode with a capillary voltage of 3750 V and a fragmentation voltage of 70 V for DHEA and 100 V for 16α-OH-DHEA and progesterone. The drying gas temperature was 350º C, the nitrogen drying gas flow rate was 10.0 L/min, and the nebulizer pressure was 35 pound-force per square-inch-gauge. Ions monitored were 271 *m*/z for DHEA, 315 *m*/z for progesterone, and 322 *m*/z for 16α-OH-DHEA. A calibration curve was prepared using potassium phosphate buffer as a matrix over the concentration range of 500 - 20,000 ng/ml (1.6 – 65 μM) DHEA. The lower limit of quantification in potassium phosphate buffer was 473.5 ng/ml with an accuracy of 103% and a precision of 11.4%.

1′-OH MDZ and 4′-OH MDZ formation in HFLMs and quantification by HPLC-MS/MS

1′-OH MDZ and 4′-OH MDZ formation in HFLMs was performed as previously described with minor modifications [31]. Briefly, reaction mixtures contained 8 μM midazolam dissolved in < 1% (v/v) methanol, 0.1 mg/ml HFLMs, and 100 mM potassium phosphate (KH_2PO_4) buffer (3 mM $MgCl_2$, 1 mM EDTA, pH 7.4), in a final volume of 250 μl. After pre-incubating in a shaking 37° C water bath for 5 min, reactions were initiated with 1 mM NADPH. Reactions were stopped at 0 and 5 min with 0.25 ml of ice-cold Na_2CO_3 solution (final pH 11).

Incubations using 0.1 mg/ml HLMs with and without NADPH at 0 and 5 min served as positive and negative controls, respectively. Following the addition of 50 µl of the internal standards ($^{15}N_3$-labeled 1′-OH MDZ and 4′-OH MDZ), samples were briefly vortexed and 3 ml ethyl acetate was added. Samples were then horizontally shaken for 20 min and centrifuged at 3700 × g for 20 min at room temperature. The supernatant was evaporated in a 37° C water bath with nitrogen gas. Residues were finally resuspended in 200 µl of 50:50 acetonitrile:water, 100 µl was transferred to a 96-well plate, and 10 µl was injected for analysis by HPLC-MS/MS. Duplicate determinations were performed for each sample. Under these conditions, the depletion of MDZ did not exceed 20%.

1′-OH and 4′-OH MDZ concentrations were quantified by HPLC-MS/MS using an Agilent series 1290 HPLC interfaced with an Agilent 6410B triple quadrupole mass spectrometer (Agilent Technologies, Palo Alto, CA). Separation of 1′-OH and 4′-OH MDZ was achieved using a Zorbax SB-C18 column (150 mm × 2.1 mm × 5 µ) heated to 35° C. Metabolites were separated with isocratic elution: 35% mobile phase B from 0-6 minutes, followed by 95% B at 6-9 minutes for column rinsing, and finally returned to 35% for the remainder of the 14 min run time. The mass spectrometer was run in ESP positive ionization mode with a capillary voltage of 1800 V and a fragmentation voltage of 150, 145, and 152 V for the internal standard, 1′-OH MDZ, and 4′-OH MDZ, respectively. The drying gas temperature was 350º C, the nitrogen drying gas flow rate was 11.0 L/min, and the nebulizer pressure was 35 pound-force per square-inch-gauge. The following ion transitions were monitored: *m/z* 342.1> 324.1 for 1′-OH MDZ, *m/z* 342.1> 297.1 for 4′-OH MDZ**,** and *m/z* 347.1> 329.2 for internal standards.

Glyburide fraction unbound in CYP supersomes and HFLMs

Protein binding of glyburide in CYP3A4, CYP3A5, and CYP3A7 supersomes as well as HFLMs and HLMs was determined by ultrafiltration using Microcon-10 kDa Centrifugal Filters with Ultracel-10 membranes (EMD Millipore Corporation, Billerica, MA). [^{3}H]-Glyburide (~1.5 ng) in methanol was aliquoted into 1.5 ml eppendorf tubes and evaporated to dryness. [^{3}H]-Glyburide was reconstituted in 100 mM potassium phosphate buffer (1mM EDTA, pH7.4) containing varying concentrations of glyburide (0.01, 0.05, and 20 μM) and protein concentrations identical to those used in depletion studies, in a total volume of 350 μl. Samples were briefly vortexed, and aliquots (110 μl) were transferred to ultrafiltration cartridges, equilibrated for 30 min at 37° C, and centrifuged at 1,000 × g for 10 min. Eight microliters of filtrate and unfiltered samples were counted on a liquid scintillation counter. The fraction unbound (f_u) of glyburide was calculated as the percentage of radioactivity of the filtrate to the radioactivity of the corresponding unfiltered incubation buffer/protein mixture. Triplicate determinations were performed for each sample. HLMs served as a positive control. Incubation buffer was used to determine non-specific binding of [^{3}H]-glyburide, which was 6.9 ± 3.7% (n = 9 replicates).

4.3 Results

Glyburide depletion kinetics of CYP3A supersomes

We first compared the kinetics of glyburide metabolism with recombinant CYP3A4, CYP3A5 and CYP3A7 supersomes. Substrate depletion kinetic parameters were estimated and the data are shown in Table 4-2. The kinetic profiles from a representative experiment are depicted in Figure 4-1. K_m and V_{max} values were estimated from three independent experiments.

The fraction unbound (f_u) remained constant for each CYP3A isoform over 0.01 – 20 μM glyburide. The f_u was 5-7% for CYP3A4 and CYP3A7 and ~15% for CYP3A5 (Table 4-2). Although apparent K_m values ($K_{m, app}$) did not significantly differ between CYP3A isoforms, K_m values corrected for protein binding ($K_{m, u}$) did, with CYP3A7 having the highest affinity to glyburide (in the nM range), followed by CYP3A4 and CYP3A5. CYP3A4 had the highest capacity to metabolize glyburide (V_{max} = 8.3 nmol/min/nmol P450), followed by CYP3A5 and CYP3A7 (V_{max} = 3.6 and 1.8 nmol/min/nmol P450, respectively). Consequently, $Cl_{int, u}$ of CYP3A4 was nearly 3-fold greater than that of CYP3A7 and 4-fold greater than that of CYP3A5 (37.1 versus 13.0 and 8.7 ml/min/nmol P450, respectively).

Human fetal liver demographics and CYP protein quantification

Estimated gestational age, fetal sex, race, post-mortem interval (time between death and tissue collection), genotype, and maternal medications or xenobiotics are listed for sixteen human fetal livers in Table 4-3. Nearly equal numbers of male and female fetal livers were collected (7 and 9, respectively). Estimated gestational age spanned from 13 to 21 weeks of gestation; however, most fetal livers were between the ages of 13 and 16 weeks of gestation. The composition of races among the fetal livers that were collected nearly reflects the composition of the population within the state of Washington. The top three maternal medications or xenobiotics recorded were alcohol, cigarettes, and marijuana. *CYP3A5*3/*3* and *CYP3A7*1/*1* were the most abundant variant CYP3A genotypes. Of the CYP isoforms quantified by HPLC-MS/MS, only CYP3A7 and P450 reductase were detected in quantifiable amounts; however multiple CYP isoforms were detected in pooled HLM quality controls. The CYP3A7 protein levels in HFLMs ranged between 10 and 160 pmol/mg protein (Figure 4-2). CYP3A5 protein was detectable in some of the HFLMs, but was not quantifiable due to a somewhat high LLOQ (lower limit of

quantification) (0.475 fmol/μg microsomal protein). The relationship between selected demographics and human fetal liver CYP3A7 protein levels was explored (Figure 4-2). CYP3A7 content did not appear to be sex-dependent, or affected by *CYP3A7*1C* and **2C* genotype (p = 0.45 and 0.40, respectively) (Figure 4-2). Given the small estimated gestational age range of the human fetal livers, it was not possible to evaluate the relationship between CYP3A7 protein content and gestational age or post-mortem intervals (all less than 6 hours) (Figure 4-2). Overall, none of these potential effectors significantly influenced protein levels of CYP3A7 in the human fetal liver samples of this study.

Metabolic profiles of glyburide generated by CYP3A supersomes, HFLMs, and HLMs

The primary metabolites of glyburide, M1-M5, are all mono-hydroxylated metabolites. Given the same CYP3A isoform concentration (30 pmol/ml), M5 was the dominant metabolite formed (of the metabolites measured) following a 30 min incubation with CYP3A4, CYP3A5 or CYP3A7 supersomes, the relative abundance of which was approximately 73, 57, and 96%, respectively (Figure 4-3, Table 4-4). Differences were observed between the relative abundance of M1-M5 across CYP3A isoforms. M5 appears to be predominant metabolite for all three CYP3A isoforms (57-96%); however, CYP3A7 produced ≤ 1% M1-M4 which was far less than 5-15% of M1-M4 formed by CYP3A4 or CYP3A5. The relative abundance of M1-M5 in CYP3A supersomes was independent of incubation time (30-90 min) and glyburide concentration (0.05-20 μM) (data not shown). With the same protein concentration (0.8 mg/ml), pooled HFLMs and pooled HLMs also predominantly formed M5 (97.0 and 64.9%, respectively) (Figure 4-4, Table 4-4). Interestingly, the metabolite profile in pooled HFLMs mirrored the

profile generated by CYP3A7. On the other hand, the metabolic profile from pooled HLMs mirrored that from CYP3A4 (Figures 4-3 and 4-4). However, the relative abundance of M1 in pooled HLMs on average was higher (~10%) than that in CYP3A4 or CYP3A5 (~5%). Again, the relative abundance of M1-M5 in HFLMs was not dependent on incubation time (30-90 min) or glyburide concentration (0.05-20 μM) (data not shown).

Correlation of glyburide depletion in HFLMs with CYP3A7 protein content, 16α-OH DHEA formation, and 4′-OH MDZ formation

Since M5 was the predominate metabolite formed by HFLMs, which cannot be quantified due to lack of commercially available standard, glyburide depletion as shown in Figure 4-5 was performed to estimate glyburide Cl_{int} in individual HFLMs. Glyburide depletion in HFLMs was NADPH-dependent, supporting the hypothesis that CYP3A7 in the fetal liver is the predominant enzyme responsible for glyburide metabolism. The average fraction unbound of glyburide across all sixteen HFLMs was 27.0 ± 7.9% (n = 3 replicates per liver) compared to 17.4 ± 1.4% (n = 3) in pooled HLMs ($p = 0.055$). In order to confirm that fetal CYP3A7 protein content in HFLMs was indeed correlated with CYP3A7 activity, DHEA metabolism to 16α-OH DHEA (a reaction specific to CYP3A7) was measured. We found that CYP3A7 protein levels were indeed highly correlated with 16α-OH DHEA formation (Pearson r = 0.76, $p < 0.001$) (Figure 4-6, panel A). CYP3A7 protein levels were also tightly correlated with Cl_{int} for glyburide depletion (Pearson r = 0.80, $p < 0.001$) (Figure 4-6, panel B), supporting the hypothesis that glyburide is primarily metabolized by CYP3A7 in human fetal livers. Figure 4-6, panel C also shows that glyburide depletion is directly correlated with 16α-OH DHEA formation (Pearson r = 0.80, $p < 0.001$). Midazolam, a probe CYP3A substrate, was also used to discern CYP3A7

activity. 1′-OH MDZ formation was moderately correlated with Cl_{int} for glyburide depletion (Pearson r = 0.52, p = 0.037) (Figure 4-7, panel A), while 4′-OH MDZ formation was highly correlated with glyburide Cl_{int} (Pearson r = 0.89, p < 0.001) (Figure 4-7, panel B) as well as CYP3A7 protein levels (Pearson r = 0.68, p = 0.004) (Figure 4-7, panel C). There was no correlation between the 1′-OH/4′-OH metabolite ratio and glyburide Cl_{int} (data not shown).

Glyburide depletion is not dependent on CYP3A5 genotype

We also examined whether CYP3A5 genotype impacts glyburide depletion and found that CYP3A5 genotype did not affect 16α-OH DHEA formation or glyburide Cl_{int} (Figure 4-8, panels A and B). The 1′-OH/4′-OH MDZ metabolite ratio was nearly two-fold larger for the single homozygous *CYP3A5*1/*1* expresser compared to the heterozygous (*CYP3A5*1/*3* and *CYP3A5*1/*6*) and homozygous (*CYP3A5*3/*3*, *CYP3A5*3/*6*, and *CYP3A5*6/*6*) variant genotypes, which are associated with decreased CYP3A5 protein levels [40] (Figure 4-8, panel C). Due to only one sample with the CYP3A5*1/*1 genotype, statistical analyses between groups was not performed.

4.4 Discussion

Glyburide is frequently used to treat GDM. However, a major concern of pregnant women using glyburide is the safety of the drug for the developing fetus. It is critical that we understand the mechanisms that control fetal exposure to glyburide, such as placental penetration and placental and fetal metabolism of glyburide. Previous studies including those from our laboratory have identified that ABC transporters such as BCRP play an important role in limiting transfer of glyburide across the placenta [16-18]. Placental metabolism of glyburide primarily by CYP19 has also been demonstrated [9, 10, 19]. Prior to this work, no studies have been done to

evaluate fetal metabolism of glyburide. Thus, the purpose of this study was to systematically investigate glyburide metabolism by human fetal livers.

Since CYP3A7 is known to be the predominant drug-metabolizing CYP enzyme in human fetal livers [21-23], we first characterized glyburide depletion kinetics of CYP3A7 supersomes and compared the data with those of CYP3A4 and CYP3A5 (Figure 4-1 and Table 4-2). CYP3A7 was able to catalyze glyburide depletion but with a relative lower (~65%) efficiency than CYP3A4. The $K_{m,\,u}$ values of CYP3A4 and CYP3A7 after correction for protein binding were comparable; however, the V_{max} of CYP3A4 was 4-5 times greater than that of CYP3A7, resulting in a nearly 3-fold difference in $Cl_{int,\,u}$ (Table 4-2). On the other hand, the $Cl_{int,,u}$ values of CYP3A5 and CYP3A7 were similar. Given the lower $Cl_{int,\,u}$ of CYP3A7 versus CYP3A4, quantifying CYP3A7 protein levels in human fetal livers is important in the effort to determine the overall contribution of CYP3A7 to glyburide metabolism in human fetal livers.

Thus, we performed absolute quantification of CYP enzymes in 16 individual HFLMs using a targeted mass spectrometry approach. Of the enzymes examined: CYP3A4, CYP3A5, CYP3A7, CYP2C9, CYP2C19, CYP2A6, and CYP2D6, only CYP3A7 protein levels were quantifiable in HFLMs. CYP3A5 was detectable in some of the HFLMs, but not quantifiable due to a somewhat high LLOQ. Other CYPs were not detectable at all. These results suggest that CYP3A7 is likely the major enzyme capable of metabolizing glyburide in human fetal livers, even if it has a relatively lower $Cl_{int,\,u}$ compared to CYP3A4. We noted that CYP3A7 protein levels in individual HFLMs were only slightly variable, ranging from approximately 50 to 160 pmol/mg protein with only one sample at around 10 pmol/mg protein (Figure 4-2). The protein levels of CYP3A7 in human fetal livers are in a similar range to the protein levels of CYP3A4 in human adult livers, but are much higher than those of CYP3A5 (up to 20 pmol/mg protein) [41].

Thus, CYP3A7 could significantly contribute to drug metabolism in human fetal livers, affecting fetal exposure to drugs. This study is the first to report CYP3A7 protein quantification by surrogate peptide-based HPLC-MS/MS in individual human fetal livers. The fetal livers were collected from women using medications and other substances. Alcohol, marijuana and cigarettes were the three most common substances used, though they did not seem to affect CYP3A7 microsomal protein levels. CYP3A7 protein content also did not seem to be affected by sex of the fetus, CYP3A7 genotype, estimated gestational age, or post-mortem interval (Figure 4-2). One fetal liver (ID# 25458) had a post-mortem interval of >24 hours and showed a notably lower level of CYP3A7 protein content (Figure 4-2). It is possible that the longer post-mortem interval would leave time for protein degradation to occur, and ultimately decrease CYP3A7 protein levels. Other factors may also play a role as another fetal liver (ID# 25217) with a post-mortem interval of 21 h possessed CYP3A7 protein levels comparable to other fetal livers with much shorter post-mortem intervals.

We then characterized the metabolic profiles of glyburide by CYP3A4, CYP3A5, CYP3A7, HFLMs, and HLMs. M5 was the predominant metabolite (of the metabolites measured) by CYP3A4, CYP3A5, and CYP3A7 with a relative abundance of 60-70% for CYP3A4 or CYP3A5 and of 96% for CYP3A7 (Figure 4-3 and Table 4-4). Likewise, of the metabolites measured, M5 accounted for nearly 97.0% of relative abundance in HFLMs versus 64.9% in HLMs (Figure 4-4 and Table 4-4). This pattern of metabolic profile again supports the notion that CYP3A7 is likely the major enzyme in human fetal livers responsible for glyburide metabolism. In a previous clinical study, steady-state concentrations of glyburide in women with GDM were reported to range from 3 nM to 250 nM over a 12-h dosing interval [11]. These concentrations are well below the apparent K_m of CYP3A7 but similar to its $K_{m,u}$. As glyburide

can cross the placenta and reach umbilical cord concentrations that are 70% of maternal concentrations at term [11], we anticipate that the predominant metabolite of glyburide produced by human fetal livers would be M5, followed by minimal levels of M1-M4. Extrahepatic fetal metabolism and placental metabolism may also influence the overall fetal metabolism and metabolite profile of glyburide in the fetus. Fetal adrenal metabolism has been reported for endogenous compounds such as testosterone [43]. CYP3A7 activity in fetal adrenal microsomes was evaluated via testosterone metabolism to 6β-OH testosterone; 6β-OH formation was 33% of that measured in fetal liver microsomes with matched tissues between 24-39 weeks of gestation [44]. Thus, fetal adrenal metabolism of glyburide by CYP3A7 may also contribute to overall fetal metabolism of glyburide, but is not expected to change the metabolite profile of glyburide in the fetus. Human term placenta has also been shown to metabolize glyburide, predominantly to M5 via CYP19 [9, 10, 20]. If M5 formed in the placenta can access the fetal circulation, placental metabolism could alter the overall metabolic profile of glyburide in the fetus. Although M5 is a major metabolite of both fetal and placental metabolism of glyburide, whether it is pharmacologically active is not known. This would be of considerable importance to investigate in future studies given that the other metabolites, M1 and M2b, are pharmacologically active [30].

After having established that CYP3A7 and HFLMs are capable of metabolizing glyburide, we performed further studies to confirm that CYP3A7 is the major enzyme in HFLMs responsible for glyburide metabolism using selective probe substrates. First of all, with 16 individual HFLMs, we found that 16α-OH DHEA formation, a reaction specific to CYP3A7, was highly correlated with CYP3A7 protein levels (Figure 4-6, panel A). Glyburide Cl_{int} was highly correlated with CYP3A7 protein levels (Figure 4-6, panel B) and 16α-OH DHEA

formation (Figure 4-6, panel C), supporting the conclusion that CYP3A7 is the enzyme responsible for glyburide metabolism in HFLMs.

We noted that HFLMs were also capable of metabolizing MDZ (Figure 4-7). It has been reported that the K_m values of CYP3A4 for 1′-OH MDZ and 4′-OH MDZ formation differ by a magnitude of 10 (2-6 μM versus 40-60 μM, respectively) [41]. The starting MDZ concentration in our incubations with HFLMs was 8 μM; therefore, if CYP3A4 or CYP3A5 were expressed in HFLMs, we might expect preferential formation of 1′-OH MDZ and the corresponding 1′-OH/4′-OH metabolite ratio to be far greater than 1. The metabolite ratio, however, was less than or around unity for 12 out of the 16 HFLMs (Figure 4-7, panel C), suggesting that CYP3A4 may not expressed in this set of fetal livers. In addition, glyburide Cl_{int} (Figure 4-7, panel B) and CYP3A7 protein content (Figure 4-7, panel C) were highly correlated with 4′-OH MDZ formation, confirming that CYP3A7 can catalyze 4′-OH MDZ formation. Considering CYP3A7's perhaps preferential formation of 4′-OH MDZ (given the MDZ incubation concentration used), and the fact that CYP3A5 protein was not quantifiable in these HFLMs, it is understandable why the 1′-OH/4′-OH MDZ ratio was ≤ 1 for the majority of HFLMs. For the metabolite ratios that were >1, CYP3A5 was likely present to a sufficient degree to form more 1′-OH MDZ, thus changing the metabolite ratio. The highest observed 1′-OH/4′-OH ratio (3.4) came from a fetal liver with the CYP3A5*1/*1 genotype, which is associated with expression of functional CYP3A5 (Figure 4-8, panel C). This supports the likelihood that CYP3A5 is present in some HFLMs and plays a role in the fetal metabolism of MDZ. The results of midazolam metabolism provide further evidence that CYP3A7 is the major CYP3A isoform in the fetal liver, and that CYP3A7 preferentially oxidizes substrates at sites that may be different from that of other CYP3A isoforms.

16α-OH DHEA formation was unaffected by CYP3A5 genotype (Figure 4-8, panel A), which is expected because 16α-OH DHEA formation is specific to CYP3A7 [20]. Given the low concentration of glyburide used in correlation studies (0.05 μM) and that the $K_{m,u}$ of CYP3A7 for glyburide is 2-3 times lower than that of CYP3A5 (Table 4-2), contribution of CYP3A5 to glyburide depletion would perhaps be unobservable. Therefore, glyburide Cl_{int} was not affected by *CYP3A5* genotype either. Given the low content of CYP3A5 in human fetal livers, contribution of CYP3A5 to fetal liver metabolism of glyburide is expected to be much lower than CYP3A7.

In summary, we have shown that CYP3A7 is substantially expressed in in human fetal livers and for the first time mediates metabolism of glyburide to the primary metabolite M5. Microsomal CYP3A7 protein content in human fetal livers was not affected by sex of the fetus, genotype, or gestational age, and correlated well with glyburide Cl_{int}, 16α-OH DHEA formation, and 4′-OH MDZ formation. These results are of significant clinical value for understanding and predicting fetal exposure to glyburide and informing fetal safety of the drug.

Tables and Figures for Chapter 4

Table 4-1. Optimized MS/MS parameters used for quantification of surrogate peptides and internal standards of CYP enzymes in trypsin digested microsomes

Enzyme	Peptide	Precursor Ion (m/*z*)	Product Ion (m/*z*)	Fragmentor (V)	Collision Energy (eV)	LLOQ (fmol on-column)
CYP3A4	LSLGGLLQPEKPVVLK	564.6	746	100	9	0.3
		564.6	689.4	100	10	
	LSLGGLLQPEKPVVLK	567.3	750	100	9	
		567.3	693.4	100	9	
CYP3A5	DSIDPYIYTPFGTGPR	900.0	995.7	130	28	1
		900.0	684.9	130	20	
	DSIDPYIYTPFGTGPR	904.9	1005.5	130	28	
		904.9	689.9	130	28	
CYP3A7	FNPLDPFVLSIK	695.4	918.4	110	16	0.1
		695.4	564.7	110	16	
	FNPLDPFVLSIK	699.4	926.5	110	16	
		699.4	568.8	110	16	
CYP2C9	GIFPLAER	451.9	585.4	75	7	0.15
		451.9	366.8	75	7	
	GIFPLAER	456.8	595.3	75	7	
		456.8	371.7	75	7	
CYP2C19	IYGPVFTLYFGLER	838.0	1145.4	145	28	1
		838.0	998.3	145	28	
	IYGPVFTLYFGLER	843.0	1155.6	145	28	
		843.0	1008.5	145	28	
CYP2A6	GTGGANIDPTFFLSR	777.1	982.5	130	22	0.4
		777.1	867.2	130	26	
	GTGGANIDPTFFLSR	781.9	992.5	130	26	
		781.9	877.5	130	26	
CYP2D6	GTTLITNLSSVLK	673.9	974.4	110	16	0.6
		673.9	861.3	110	16	
	GTTLITNLSSVLK	677.9	982.4	110	16	
		677.9	869.3	110	16	
CYP reductase	FAVFGLGNK	476.9	734.3	100	9	0.05
		476.9	635.3	100	9	
	FAVFGLGNK	480.8	742.4	100	9	
		480.8	643.4	100	9	

Underlined residues represent the internal standards with the labeled [$^{13}C_6{}^{15}N_2$]-lysine or [$^{13}C_6{}^{15}N_4$]-arginine.

Table 4-2. Glyburide depletion kinetics in CYP3A supersomes

	$K_{m, app}$ (μM)	$K_{m, u}$ (μM)	V_{max} (nmol/min/ nmol P450)	$Cl_{int, u}$ (ml/min/ nmol P450)	fu (%)
CYP3A4	3.1 ± 1.1	0.22 ± 0.08[a]	8.3 ± 4.8	37.1 ± 13.1[a,c]	7.1 ± 6.1
CYP3A5	3.0 ± 0.1	0.41 ± 0.01[a,b]	3.6 ± 0.3	8.7 ± 0.5[a]	13.6 ± 4.2[d]
CYP3A7	2.6 ± 0.9	0.15 ± 0.05[b]	1.8 ± 0.6	13.0 ± 3.0[c]	5.7 ± 3.9[d]

[a] $p < 0.05$ between CYP3A4 and CYP3A5; [b] $p < 0.01$ between CYP3A5 and CYP3A7; [c] $p < 0.05$ between CYP3A4 and CYP3A7; [d] $p < 0.05$ between CYP3A5 and CYP3A7; Shown are means ± SD of three independent experiments. Fraction unbound (fu) is reported as mean ± SD (n = 6). $K_{m, app}$ represents K_m apparent; $K_{m, u}$ represents K_m unbound; $Cl_{int, u}$ represents unbound intrinsic clearance

Table 4-3. Demographics of human fetal livers

ID	EGA (wk)	Sex	Race	PMI (hr)	CYP3A5 Genotype	CYP3A7 Genotype	Maternal Medications
25423	13	F	H	Unk	*3/*3	*1/*1	Unk
25421	13	F	CA	3:20	*3/*3	*1/*1	Alcohol, cigarettes
25422	13	F	NA	2:37	*1/*1	*1/*2C	Alcohol, cigarettes, marijuana
25448	13	M	Unk	Unk	*3/*6	*1/*2C	Unk
25458	14	M	CA	> 24:00	*1/*3	*1/*1	Alcohol, cigarettes, marijuana
25351	15	M	CA	6:13	*3/*3	*1/*1	Alcohol, levothyroxine
25279	15	M	PI, S	3:08	*1/*3	*1/*2C	Alcohol
25346	15	F	H	2:10	*3/*6	*1/*1C	Albuterol, alcohol, cigarettes, crystal methamphetamine, marijuana, acetaminophen/ hydrocodone
25452	15	F	CA	2:38	*1/*3	*1/*2C	Unk
25217	15	F	AA, H	21:00	*1/*6	*1/*2C	Unk
25435	15	F	CA, EI	1:07	*3/*3	*1/*1	Alcohol, cigarettes, crystal methamphetamine
25447	15	M	CA	4:36	*3/*3	*1/*1	Cigarettes
25449	15	F	CA	2:22	*3/*3	*1/*1	Ibuprofen, marijuana
25453	15	M	CA	5:20	*3/*3	*1/*1	Alcohol, ibuprofen, marijuana
25388	16	F	CA, H	Unk	*3/*3	*1/*1	Cigarettes, ibuprofen, marijuana, prenatal vitamins
25212	21	M	CA	5:15	*1/*3	*1C/*2C	Alcohol, birth control pill, amphetamine/ dextroamphetamine

EGA, estimated gestational age; Unk, unknown; H, Hispanic; CA, Caucasian; NA, Native American; PI, Pacific Islander; S, Samoan; AA, African-American; EI, East Indian; PMI, post-mortem interval

Table 4-4. Relative distribution (%) of glyburide's metabolic profile in CYP3A supersomes, HFLMs, and HLMs

	M1	M2a	M2b	M3	M4	M5
CYP3A4[a]	5.0 ± 1.2	5.6 ± 1.2	4.6 ± 1.3	7.4 ± 1.3	4.8 ± 1.1	72.6 ± 6.2
CYP3A5[a]	5.6 ± 0.3	8.0 ± 0.4	7.4 ± 0.8	8.6 ± 0.3	13.5 ± 0.9	57.0 ± 2.1
CYP3A7[a]	1.1 ± 0.05	0.5 ± 0.02	1.0 ± 0.1	1.0 ± 0.1	0.4 ± 0.2	96.1 ± 0.3
HFLM[b]	1.2 ± 0.4	0.2 ± 0.2	0.7 ± 0.3	0.9 ± 0.3	0.05 ± 0.2	97.0 ± 0.9
HLM[c]	10.5 ± 0.4	7.0 ± 0.5	6.0 ± 0.4	7.3 ± 0.4	4.4 ± 0.5	64.9 ± 0.8

Shown are means ± SD of CYP3A supersomes measured in duplicate from two separate experiments[a]; sixteen human fetal livers measured in duplicate from one experiment[b]; and pooled human liver microsomes measured in duplicate from two experiments[c].

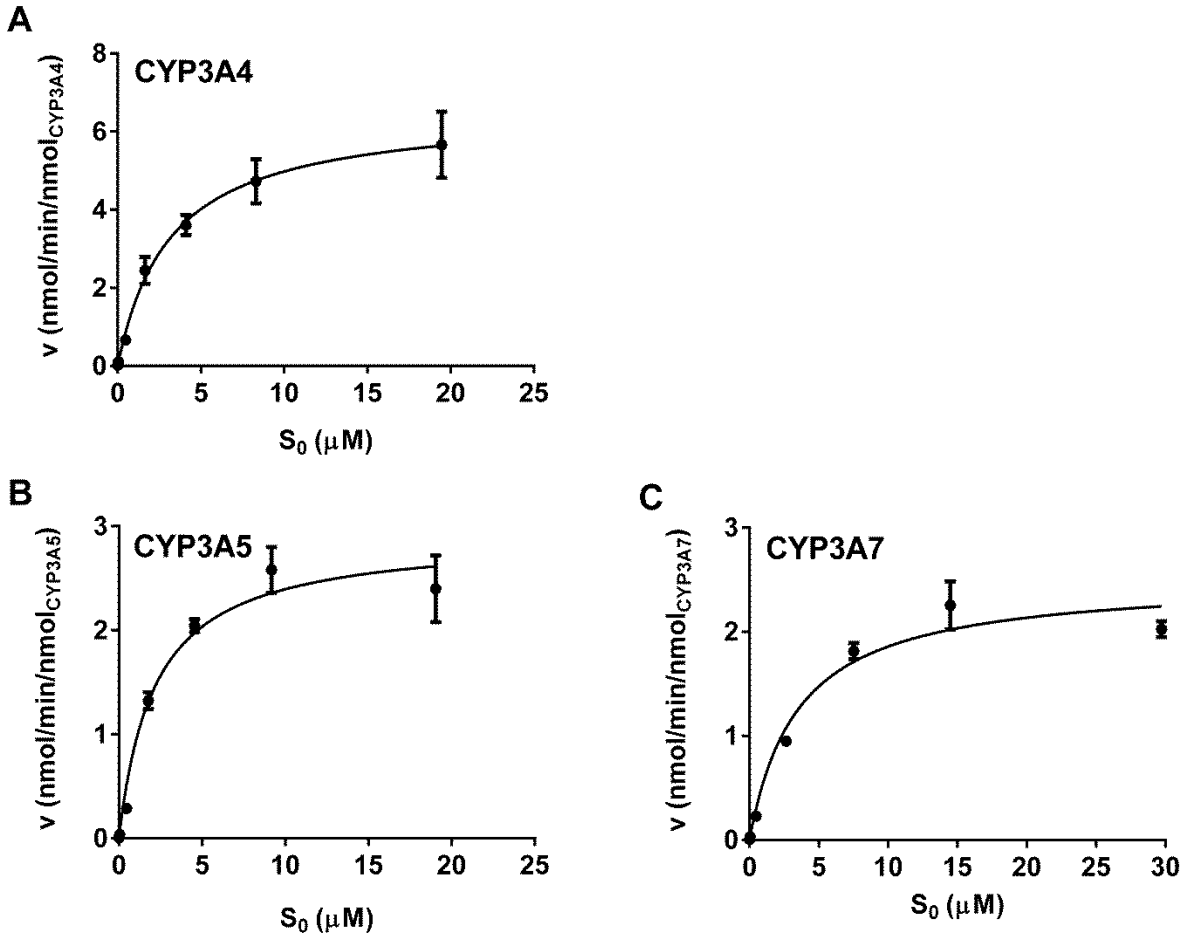

Figure 4-1. Representative kinetic profiles of glyburide depletion velocity versus initial glyburide concentration in CYP3A4 (A), CYP3A5 (B), and CYP3A7 (C) supersomes.

Shown are means ± SD of three replicate determinations per time point in a representative experiment. S_0, initial substrate (glyburide) concentration at time zero.

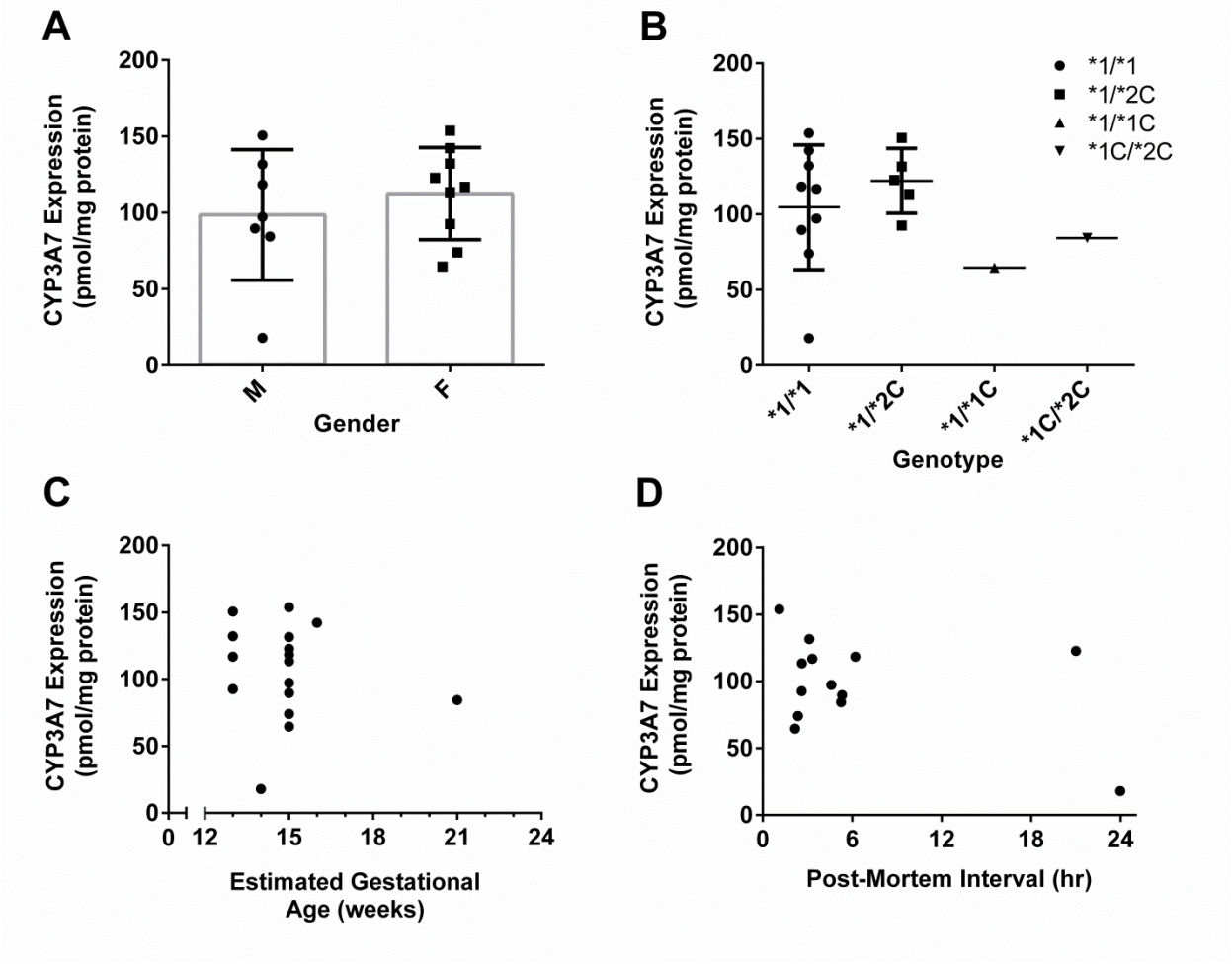

Figure 4-2. Effects of gender (A), CYP3A7 genotype (B), estimated gestational age (C), and post-mortem interval (D) on CYP3A7 protein content in sixteen human fetal livers.

Protein levels are shown as means of triplicate determinations from a single experiment. Using an unpaired Student's *t*-test ($p < 0.05$), no statistically significant differences in CYP3A7 protein levels were observed based upon gender ($p = 0.45$) or CYP3A7 genotype ($p = 0.40$). Statistical analyses were performed using the Graphpad Prism version 6.04 software.

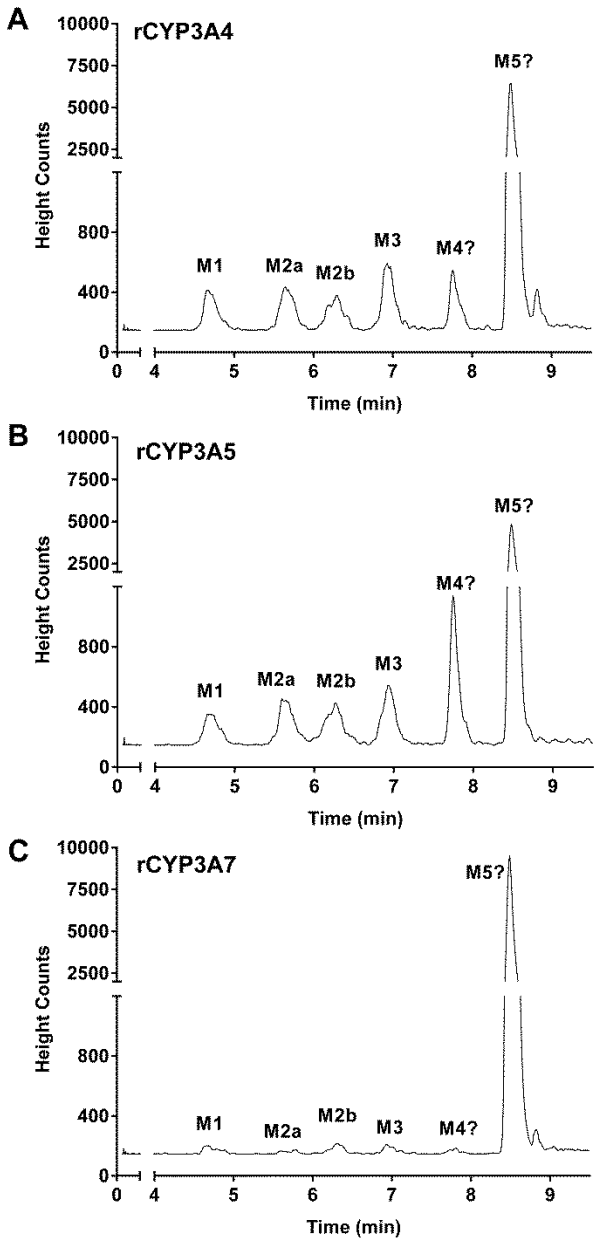

Figure 4-3. Representative metabolite profile of glyburide in CYP3A4 (A), CYP3A5 (B), and CYP3A7 (C) supersomes.

Mass ion chromatograms for extracts of supersome incubates showing the presence of the following metabolites: M1, M2a, M2b, M3, M4, and M5.

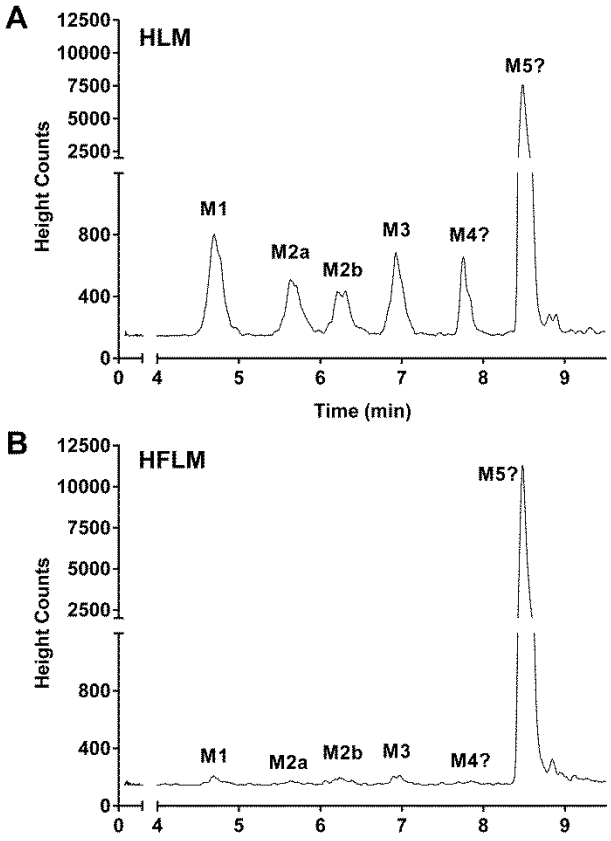

Figure 4-4. Representative metabolic profile of glyburide in human liver microsomes (A) and human fetal liver microsomes (B).

Mass ion chromatograms for extracts of supersome incubates showing the presence of the following metabolites: M1, M2a, M2b, M3, M4, and M5.

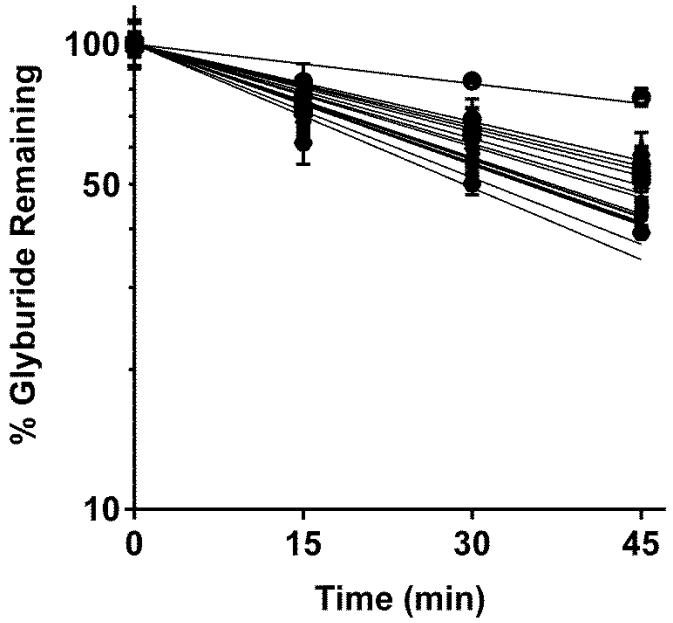

Figure 4-5. Time courses of glyburide depletion in human fetal liver microsomes.

Shown are means ± SD of sixteen individual HFLMs from a single experiment. Duplicate determinations were performed at all time points; however, the mean and SD was calculated from all 16 fetal livers.

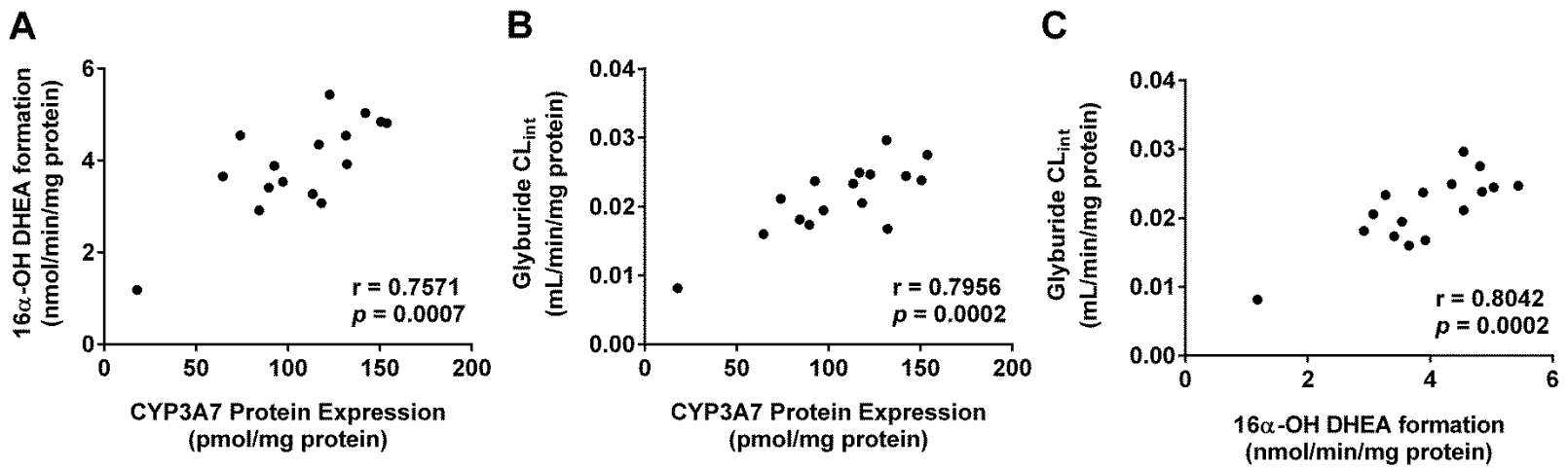

Figure 4-6. Correlation between CYP3A7 protein content and 16α-OH DHEA formation (A) or Cl_{int} of glyburide depletion (B), as well as correlation between Cl_{int} of glyburide depletion and 16α-OH DHEA formation (C) in human fetal liver microsomes.

Shown are means of duplicate incubations from single experiments. Statistically significant correlations ($p < 0.001$) were determined by the Pearson correlation analysis using the Graphpad Prism version 6.04 software.

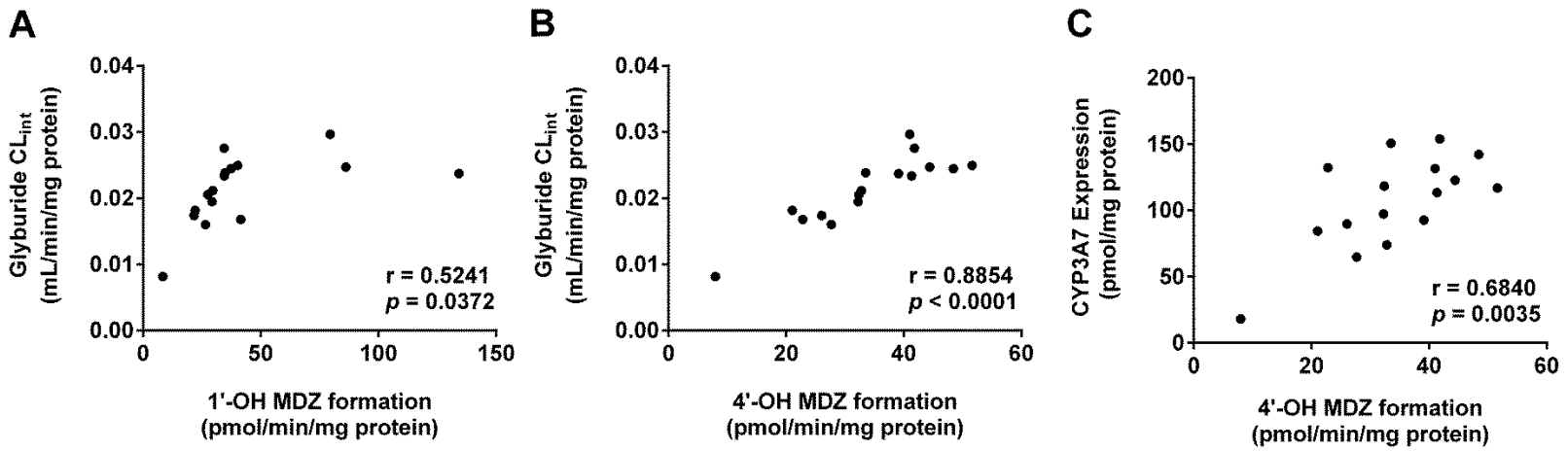

Figure 4-7. Glyburide Cl_{int} is correlated with 4′-OH midazolam formation in HFLMs.

Shown are means of duplicate incubations from single experiments. Statistically significant correlations ($p < 0.05$) between glyburide Cl_{int} and 1′-OH midazolam formation (A), 4′-OH midazolam formation (B), as well as correlations between CYP3A7 protein content and 4′-OH midazolam (C) were determined by the Pearson correlation analysis using the Graphpad Prism version 6.04 software.

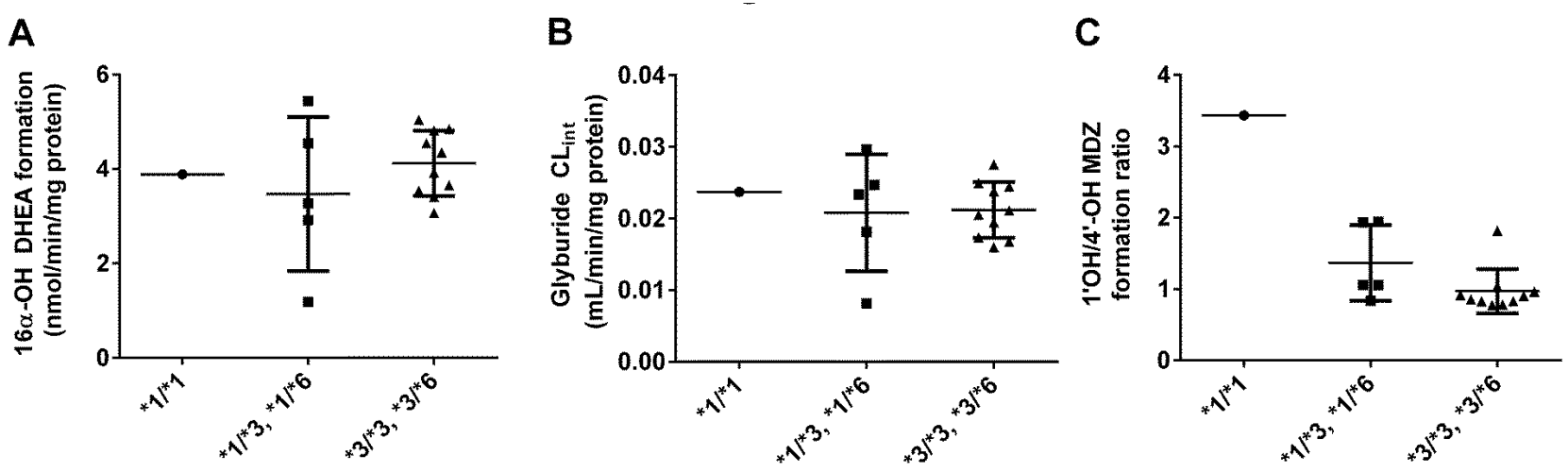

Figure 4-8. Effects of CYP3A5 genotype on 16α-OH DHEA formation (A), glyburide Cl_{int} (B), and 1′-OH/4′-OH midazolam formation ratios (C) in HFLMs.

Shown are means of duplicate incubations from single experiments.

References

[1] Paglia MJ, Coustan DR. Gestational diabetes: evolving diagnostic criteria. Curr Opin Obstet Gynecol. 2011;23:72-5.
[2] Jovanovic L, Pettitt DJ. Gestational diabetes mellitus. JAMA. 2001;286:2516-8.
[3] Camelo Castillo W, Boggess K, Sturmer T, Brookhart MA, Benjamin DK, Jr., Jonsson Funk M. Trends in glyburide compared with insulin use for gestational diabetes treatment in the United States, 2000-2011. Obstetrics and gynecology. 2014;123:1177-84.
[4] Coetzee EJ, Jackson WP. The management of non-insulin-dependent diabetes during pregnancy. Diabetes Res Clin Pract. 1985;1:281-7.
[5] Bertini AM, Silva JC, Taborda W, Becker F, Lemos Bebber FR, Zucco Viesi JM, et al. Perinatal outcomes and the use of oral hypoglycemic agents. J Perinat Med. 2005;33:519-23.
[6] Langer O, Conway DL, Berkus MD, Xenakis EM, Gonzales O. A comparison of glyburide and insulin in women with gestational diabetes mellitus. N Engl J Med. 2000;343:1134-8.
[7] Anjalakshi C, Balaji V, Balaji MS, Seshiah V. A prospective study comparing insulin and glibenclamide in gestational diabetes mellitus in Asian Indian women. Diabetes Res Clin Pract. 2007;76:474-5.
[8] Ogunyemi D, Jesse M, Davidson M. Comparison of glyburide versus insulin in management of gestational diabetes mellitus. Endocr Pract. 2007;13:427-8.
[9] Zharikova OL, Fokina VM, Nanovskaya TN, Hill RA, Mattison DR, Hankins GD, et al. Identification of the major human hepatic and placental enzymes responsible for the biotransformation of glyburide. Biochem Pharmacol. 2009;78:1483-90.
[10] Ravindran S, Zharikova OL, Hill RA, Nanovskaya TN, Hankins GD, Ahmed MS. Identification of glyburide metabolites formed by hepatic and placental microsomes of humans and baboons. Biochem Pharmacol. 2006;72:1730-7.
[11] Hebert MF, Ma X, Naraharisetti SB, Krudys KM, Umans JG, Hankins GD, et al. Are we optimizing gestational diabetes treatment with glyburide? The pharmacologic basis for better clinical practice. Clin Pharmacol Ther. 2009;85:607-14.
[12] Behravan J, Piquette-Miller M. Drug transport across the placenta, role of the ABC drug efflux transporters. Expert Opin Drug Metab Toxicol. 2007;3:819-30.
[13] Mao Q. BCRP/ABCG2 in the placenta: expression, function and regulation. Pharmaceutical research. 2008;25:1244-55.
[14] Ceckova-Novotna M, Pavek P, Staud F. P-glycoprotein in the placenta: expression, localization, regulation and function. Reprod Toxicol. 2006;22:400-10.
[15] Ni Z, Mao Q. ATP-binding cassette efflux transporters in human placenta. Curr Pharm Biotechnol. 2011;12:674-85.
[16] Zhou L, Naraharisetti SB, Wang H, Unadkat JD, Hebert MF, Mao Q. The breast cancer resistance protein (Bcrp1/Abcg2) limits fetal distribution of glyburide in the pregnant mouse: an Obstetric-Fetal Pharmacology Research Unit Network and University of Washington Specialized Center of Research Study. Mol Pharmacol. 2008;73:949-59.
[17] Gedeon C, Behravan J, Koren G, Piquette-Miller M. Transport of glyburide by placental ABC transporters: implications in fetal drug exposure. Placenta. 2006;27:1096-102.
[18] Hemauer SJ, Patrikeeva SL, Nanovskaya TN, Hankins GD, Ahmed MS. Role of human placental apical membrane transporters in the efflux of glyburide, rosiglitazone, and metformin. American journal of obstetrics and gynecology. 2010;202:383 e1-7.

[19] Zharikova OL, Ravindran S, Nanovskaya TN, Hill RA, Hankins GD, Ahmed MS. Kinetics of glyburide metabolism by hepatic and placental microsomes of human and baboon. Biochem Pharmacol. 2007;73:2012-9.
[20] Jain S, Zharikova OL, Ravindran S, Nanovskya TN, Mattison DR, Hankins GD, et al. Glyburide metabolism by placentas of healthy and gestational diabetics. Am J Perinatol. 2008;25:169-74.
[21] Komori M, Nishio K, Kitada M, Shiramatsu K, Muroya K, Soma M, et al. Fetus-specific expression of a form of cytochrome P-450 in human livers. Biochemistry. 1990;29:4430-3.
[22] Leeder JS, Gaedigk R, Marcucci KA, Gaedigk A, Vyhlidal CA, Schindel BP, et al. Variability of CYP3A7 expression in human fetal liver. J Pharmacol Exp Ther. 2005;314:626-35.
[23] Hakkola J, Raunio H, Purkunen R, Saarikoski S, Vahakangas K, Pelkonen O, et al. Cytochrome P450 3A expression in the human fetal liver: evidence that CYP3A5 is expressed in only a limited number of fetal livers. Biol Neonate. 2001;80:193-201.
[24] Schuetz JD, Beach DL, Guzelian PS. Selective expression of cytochrome P450 CYP3A mRNAs in embryonic and adult human liver. Pharmacogenetics. 1994;4:11-20.
[25] Zhou L, Naraharisetti SB, Liu L, Wang H, Lin YS, Isoherranen N, et al. Contributions of human cytochrome P450 enzymes to glyburide metabolism. Biopharm Drug Dispos. 2010;31:228-42.
[26] Chen H, Fantel AG, Juchau MR. Catalysis of the 4-hydroxylation of retinoic acids by cyp3a7 in human fetal hepatic tissues. Drug Metab Dispos. 2000;28:1051-7.
[27] Shimada T, Yamazaki H, Mimura M, Wakamiya N, Ueng YF, Guengerich FP, et al. Characterization of microsomal cytochrome P450 enzymes involved in the oxidation of xenobiotic chemicals in human fetal liver and adult lungs. Drug Metab Dispos. 1996;24:515-22.
[28] Yang HY, Lee QP, Rettie AE, Juchau MR. Functional cytochrome P4503A isoforms in human embryonic tissues: expression during organogenesis. Mol Pharmacol. 1994;46:922-8.
[29] Gedeon C, Anger G, Piquette-Miller M, Koren G. Breast cancer resistance protein: mediating the trans-placental transfer of glyburide across the human placenta. Placenta. 2008;29:39-43.
[30] Rydberg T, Jonsson A, Roder M, Melander A. Hypoglycemic activity of glyburide (glibenclamide) metabolites in humans. Diabetes Care. 1994;17:1026-30.
[31] Paine MF, Khalighi M, Fisher JM, Shen DD, Kunze KL, Marsh CL, et al. Characterization of interintestinal and intraintestinal variations in human CYP3A-dependent metabolism. J Pharmacol Exp Ther. 1997;283:1552-62.
[32] Brzezinski MR, Boutelet-Bochan H, Person RE, Fantel AG, Juchau MR. Catalytic activity and quantitation of cytochrome P-450 2E1 in prenatal human brain. J Pharmacol Exp Ther. 1999;289:1648-53.
[33] Thummel KE, Lee CA, Kunze KL, Nelson SD, Slattery JT. Oxidation of acetaminophen to N-acetyl-p-aminobenzoquinone imine by human CYP3A4. Biochem Pharmacol. 1993;45:1563-9.
[34] Kamiie J, Ohtsuki S, Iwase R, Ohmine K, Katsukura Y, Yanai K, et al. Quantitative atlas of membrane transporter proteins: development and application of a highly sensitive simultaneous LC/MS/MS method combined with novel in-silico peptide selection criteria. Pharmaceutical research. 2008;25:1469-83.
[35] Prasad B, Evers R, Gupta A, Hop CE, Salphati L, Shukla S, et al. Interindividual variability in hepatic organic anion-transporting polypeptides and P-glycoprotein (ABCB1) protein

expression: quantification by liquid chromatography tandem mass spectroscopy and influence of genotype, age, and sex. Drug Metab Dispos. 2014;42:78-88.
[36] Edson KZ, Prasad B, Unadkat JD, Suhara Y, Okano T, Guengerich FP, et al. Cytochrome P450-dependent catabolism of vitamin K: omega-hydroxylation catalyzed by human CYP4F2 and CYP4F11. Biochemistry. 2013;52:8276-85.
[37] Shuster DL, Risler LJ, Liang CK, Rice KM, Shen DD, Hebert MF, et al. Maternal-fetal disposition of glyburide in pregnant mice is dependent on gestational age. J Pharmacol Exp Ther. 2014;350:425-34.
[38] Nath A, Atkins WM. A theoretical validation of the substrate depletion approach to determining kinetic parameters. Drug Metab Dispos. 2006;34:1433-5.
[39] Ravindran S, Basu S, Gorti SK, Surve P, Sloka N. Metabolic profile of glyburide in human liver microsomes using LC-DAD-Q-TRAP-MS/MS. Biomedical chromatography : BMC. 2013;27:575-82.
[40] Lee SJ, Goldstein JA. Functionally defective or altered CYP3A4 and CYP3A5 single nucleotide polymorphisms and their detection with genotyping tests. Pharmacogenomics. 2005;6:357-71.
[41] Michaels S, Wang MZ. The Revised Human Liver Cytochrome P450 “Pie”: Absolute Protein Quantification of CYP4F and CYP3A Enzymes Using Targeted Quantitative Proteomics. Drug Metabolism and Disposition. 2014;42:1241-51.
[42] Godfrey KM, Haugen G, Kiserud T, Inskip HM, Cooper C, Harvey NC, et al. Fetal liver blood flow distribution: role in human developmental strategy to prioritize fat deposition versus brain development. PloS one. 2012;7:e41759.
[43] Wang H, Xu D, Peng RX, Yue J. Testosterone-metabolizing capacity and characteristics of adrenal microsomes in human fetus in vitro. Journal of pediatric endocrinology & metabolism : JPEM. 2010;23:143-52.
[44] Wang H, Ping J, Peng RX, Yue J, Xia XY, Li QX, et al. Changes of multiple biotransformation phase I and phase II enzyme activities in human fetal adrenals during fetal development. Acta pharmacologica Sinica. 2008;29:231-8.

Chapter 5: Glyburide and Metformin Pharmacodynamics (PD) in Women with Gestational Diabetes Mellitus (GDM): An Interim Analysis of Monotherapy versus Combination Therapy

5.1 Introduction

Gestational diabetes mellitus (GDM) complicates 5-14% of human pregnancies [1, 2]. Similar to type-2 diabetes mellitus (T2DM), the pathology of GDM can be explained by decreased pancreatic production/secretion of insulin, decreased insulin sensitivity, or a combination of the two. If left untreated, GDM poses significant risks to the mother, fetus, and neonate. Such risks include maternal hypertension, preeclampsia, and cesarean delivery, and fetal/neonatal morbidities such as macrosomia and hypoglycemia, as well as increased risk of metabolic syndrome, type-2 diabetes, and obesity for the offspring later in life [3, 4]. While insulin resistance naturally occurs in normal pregnancy, women with GDM experience insulin resistance beyond their ability to compensate with increased insulin production, leading to hyperglycemia. While insulin injection has been the standard of care for pharmacotherapeutic treatment of GDM, oral anti-diabetic agents such as glyburide and metformin have gained increasing popularity because of their ease of administration, lower cost, and comparable efficacy to insulin [5, 6]. Glyburide is a second generation sulfonylurea that inhibits ATP-dependent potassium channels on the cellular membrane of beta-islet cells in the pancreas, which

ultimately triggers the release of insulin [7]. Metformin, on the other hand, is a biguanide with a mechanism of action that is not fully understood, though it is believed to suppress glucose production and increase peripheral glucose uptake (an insulin sensitizer) [8].

It has been well established that physiological, biochemical and hormonal changes during pregnancy can alter the pharmacokinetics (PK) of drugs throughout gestation [9]. Thus, it is quite likely that the pharmacodynamics (PD) of drugs used to treat GDM are altered during pregnancy. Unfortunately, data is quite limited in regards to the PK/PD relationship of oral hypoglycemic agents such as glyburide and metformin during pregnancy, despite the fact that previous studies have shown that both glyburide and metformin exhibit altered PK during pregnancy. Specifically, the oral clearance of glyburide was found to double during the third trimester in women with GDM versus non-pregnant women with T2DM as controls, an effect thought to be due to increased hepatic CYP3A activity [10]. The renal clearance of metformin was also increased by 49% in mid-pregnancy and 29% in late pregnancy in women with GDM, type-2 diabetes, or polycystic ovary syndrome (all of which are conditions treated with metformin therapy) [11]. Despite this knowledge, the corresponding effects of decreased exposure on drug efficacy (PD) have not been fully characterized.

Insulin sensitivity and insulin secretion (beta-cell function) have been proposed as quantitative biomarkers to characterize glucose tolerance, and therefore have been used as PD biomarkers to evaluate oral hypoglycemic therapeutic efficacy [10, 12]. These indices can be estimated from serum glucose, insulin, and C-peptide concentrations following a glucose tolerance test dose, and provide mechanistic understanding of underlying disease pathology as well as response to drug therapies. Furthermore, insulin sensitivity and beta-cell function are believed to be related hyperbolically, i.e. reflecting the regulated feedback mechanisms that exist

between blood glucose and insulin [13]. Over the years, biomathematical models have been developed to describe the dynamic temporal relationship between serum glucose, insulin, and C-peptide concentrations in response to oral glucose and mixed meal tolerance tests (OGTTs and MMTTs) [14, 15]. One such class of these models is called the oral minimal model of glucose and C-peptide kinetics. Importantly, they have been implemented successfully to estimate insulin sensitivity and beta-cell function in pregnant women with GDM [10].

Considering the heterogeneous pathology of GDM (insulin resistance and/or beta-cell dysfunction) and the different mechanisms of action of glyburide and metformin, there may be individuals that would preferentially benefit from glyburide or metformin monotherapy, or require a combination of glyburide/metformin therapy to achieve optimal glycemic control. The purpose of the clinical study described herein was to characterize the PD of glyburide monotherapy, metformin monotherapy, or glyburide/metformin combination therapy in women with GDM compared to healthy pregnant women and non-pregnant women newly diagnosed with type-2 diabetes mellitus that were treated with metformin. Insulin sensitivity and beta-cell function were estimated from modeling of data acquired after mixed-meal tolerance tests (MMTTs) before and during chronic drug treatment. This chapter presents preliminary findings from an interim analysis as the study is currently still ongoing. Results from the full study will be used to optimize the design of a Phase II comparative trial of oral hypoglycemic therapy for the management of GDM.

5.2 Methods

Subjects

This ongoing prospective Phase I/II longitudinal PD study is supported by the National Institute for Child Health and Disorders (NICHD) and implemented through the network of Obstetric-Fetal Pharmacology Research Units (OPRU). Recruitment sites include University of Washington, University of Texas Medical Branch in Galveston, University of Pittsburgh, and University of Indiana. This study was approved by the Institutional Review Boards (IRBs) at each site and was conducted in accordance with their guidelines. There were three groups of women recruited for this study: pregnant women with GDM, non-pregnant women with T2DM, and healthy pregnant women. Pregnant women (singleton pregnancy), ages 18-45 years old, diagnosed with GDM between 20-32 weeks of gestation who failed diet therapy and required drug treatment according to the criteria listed in Table 5-1 were randomized to one of three treatment arms: glyburide monotherapy (GLY), metformin monotherapy (MET), or glyburide/metformin combination therapy (Combo). Treatment was initiated on or before 32 weeks of gestation. The control groups included (1) non-pregnant women, ages 18-45 years old, newly diagnosed with T2DM (hemoglobin A1C > 7%) who planned to be treated with metformin, and (2) healthy pregnant (HP) women (singleton pregnancy), ages 18-45 years old, between 20-32 weeks of gestation with normal 1 h glucose tolerance test (GTT) results. Women using medications that were expected to interact with glyburide or metformin, or alter blood glucose concentrations were excluded from the study. Additional exclusion criteria for women with GDM or T2DM included the following: serum creatinine > 1.2 mg/dL; hematocrit < 28%; allergy to glyburide, metformin, or sulfa-drugs; severe liver disease; congestive heart failure or

history of myocardial infarction; moderate to severe pulmonary disease; and adrenal or pituitary insufficiency. Likewise, healthy pregnant women with a hematocrit < 28% or known kidney, liver, heart, pulmonary, adrenal or pituitary disease were excluded from this study. Additionally, healthy pregnant women receiving hypoglycemic agents or corticosteroids were excluded. Demographics of available subjects as of September 17, 2014 are listed in Table 5-2. All subjects provided informed, written consent.

Figures 5-1, 5-2 and 5-3 are respective flow diagrams showing the dose titration regimens and study times for the GLY, MET, and Combo therapy groups. In the GLY treatment arm, subjects initially received 5 mg of glyburide daily. Doses were increased until blood glucose levels were considered controlled (based on criteria listed in Table 5-1), i.e., not to exceed a maximum dose of 26.25 mg of glyburide daily (Figure 5-1). In the MET treatment arm, subjects initially received 1 g of metformin daily, which could be increased to as much as 2 g daily to control blood glucose (Figure 5-2). Finally, in the Combo group, subjects received 5 mg of glyburide and 1 g of metformin daily, which could be increased to as much as 20 mg glyburide and 2 g metformin daily in order to maintain euglycemia (Figure 5-3). If subjects failed treatment based on criteria listed in Table 5-1, they were switched to insulin therapy.

PD study design

Insulin sensitivity (SI), beta-cell responsivity (Φ), and the resultant disposition index (DI) were estimated pre- and post-treatment (study day 1 and 2, respectively) using a mixed-meal tolerance test (MMTT) consisting of one can of Boost Plus® energy drink, two slices of whole wheat toast, and two teaspoons of margarine consumed within ten minutes. Subjects that failed treatment received a MMTT prior to switching to insulin therapy. Serial blood samples (4 mL

each) were collected over four hours to measure serum glucose, insulin, and C-peptide concentrations at the following time points: baseline (pre-MMTT, time = 0 min), as well as 10, 20, 30, 60, 90, 120, 150, 180, 210, and 240 min post-MMTT. Glucose concentrations were measured using the glucose oxidase/peroxidase assay [16]. Insulin and C-peptide concentrations were measured using previously described radioimmunoassays [17, 18].

PD modeling

The complicated interplay and feedback between insulin and glucose can be described in a piece-meal fashion by two separate stimulus-response models [19, 20]. The first model estimates insulin sensitivity (SI) by assuming serum insulin as the stimulus and changes in serum glucose concentration as the observed biological response (efficacy). The second model estimates pancreatic beta-cell function (Φ) by assuming serum glucose as the stimulus and changes in serum concentration of C-peptide as a surrogate for proximate (hepatoportal) released of insulin as the observed biological response. C-peptide concentration was used rather than insulin concentration because C-peptide and insulin are secreted from beta-cells into the portal vein in a 1:1 molar ratio, yet C-peptide does not undergo hepatic extraction as does insulin. These are referred to as the oral minimal models of glucose and C-peptide kinetics, respectively. The reciprocal feedback relationship between glucose utilization and insulin release is further recognized by the hyperbolic disposition Index (DI). A previous OPRU study utilized these oral minimal models for estimating SI, Φ, and DI in pregnant women with GDM [10].

Insulin sensitivity (SI): oral minimal model of glucose kinetics

Insulin sensitivity was estimated using the oral minimal model of glucose kinetics shown in Figure 5-4 [14, 19]. Briefly, glucose is absorbed through the gastrointestinal (GI) tract into the

bloodstream, where it distributes to the liver and peripheral tissues such as muscle and adipose for storage and/or consumption. Serum insulin (model stimulus) distributes into the remote insulin compartment (site of action), which represents the interstitial fluid of the liver and peripheral tissues. This model is described by two differential equations:

$$\frac{dG(t)}{dt} = \frac{Ra(t)}{V} - p_1(G(t) - G_b) - X(t)G(t) \qquad G(0) = G_b \qquad (\mathbf{5.1})$$

$$\frac{dX(t)}{dt} = -p_2X(t) + p_3(I(t) - I_b) \qquad X(0) = 0 \qquad (\mathbf{5.2})$$

Equation 5.1 describes changes in serum glucose concentration over time, which is driven by remote insulin concentration; Equation 5.2 describes changes in insulin action at the remote site over time, and is also driven by remote insulin concentration. *X(t)* refers to the concentration of insulin in the remote insulin compartment at time *t*, which is expressed in the form of a constant (min^{-1}) for first-order utilization of serum glucose by the peripheral tissues (mainly muscle). *G(t)* refers to serum glucose concentrations at time *t*. G_b refers to baseline glucose concentrations at $t = 0$. *Ra(t)/V* is the rate of appearance of glucose due to its absorption from the GI tract into systemic circulation. *Ra(t)* is further defined, however, by a piece-wise linear function with a set number of break points:

$$Ra(t) = \begin{cases} k_{i-1} + \dfrac{k_i - k_{i-1}}{t_i - t_{i-1}} \cdot (t - t_{i-1}) & \text{for } t_{i-1} \le t \le t_j, i = 1 \dots n \\ k_n \cdot e^{-\alpha t} & \text{for } t_i > t_n \end{cases} \qquad (\mathbf{5.3})$$

where k_i is the rate (slope) at time point t_i, and n is the number of break points. k_i is assumed to decline towards baseline according to the terminal exponential constant α after the last glucose sample at t_n. For the MMTT used in this study, there were ten intervals with eleven break points at 0, 10, 20, 30, 60, 90, 120, 150, 180, 210, and 240 minutes.

In equation 5.1, serum glucose concentration is depleted by (1) insulin action to promote peripheral utilization of glucose: $-X(t)G(t)$; and (2) glucose inhibition of its own production in the liver as well as stimulation of its uptake and utilization by the liver: $-p_1(G(t) - G_b)$. The rate constant p_1 (min^{-1}) is associated with glucose effectiveness (GE), a term describing glucose's ability to promote glucose uptake and utilization as well as inhibition of its production. GE is calculated by p_1V (dL/kg/min), where V is the volume of distribution of glucose. In order to make the model identifiable, V and p_1 were fixed to the population means 1.45 dL/kg and 0.015 min^{-1}, respectively [14]. Hence, $G(t)$ was solvable given an estimate of $X(t)$, which is calculated using equation 5.2 In equation 5.2, the rate constant p_2 (min^{-1}) governs the increase and decline of insulin action in the remote compartment. p_3 (min^{-2} per μU/mL) is a scaling factor that translates serum insulin concentration to a given magnitude of insulin action in the remote compartment. At $t = 0$ remote insulin concentration is set to zero to indicate that prior to the MMTT (baseline) there is no net insulin action. Lastly, insulin sensitivity (min^{-1} per μU/ml) was estimated using the following equation:

$$SI = \frac{p_3}{p_2} \qquad (\mathbf{5.4})$$

Several model assumptions were made in order to estimate insulin sensitivity. First, if glucose concentrations failed to return to basal levels at the end of the MMTT, it was assumed that Ra declined monoexponentially after the last time point at a previously reported rate of 0.017 min^{-1} [14]. It was also assumed that a known fraction ($f = 0.9$) of the ingested glucose dose was absorbed during the MMTT following splanchnic extraction [14, 21]. Additionally, parameter p_2 was previously difficult to estimate with precision, hence, a maximum *a posteriori* Bayesian estimation was used for p_2, assuming that the square root is normally distributed with mean 0.11 min^{-1} and CV 10% [22]. The measurement error associated with glucose

concentrations was assumed to be Gaussian (mean = 0, CV = 2%) and independent, as described previously [22]. Lastly, serum insulin concentration was assumed to be without error because it serves the input function.

Beta-cell responsivity (Φ): oral minimal model of C-peptide kinetics

Beta-cell function was measured using the oral C-peptide minimal model illustrated in Figure 5-5 [15]. Pancreatic secretion of insulin was biphasic in response to the rise in serum glucose generated by a MMTT. The first phase of insulin secretion, that of dynamic secretion (Φ_d), is an immediate response proportional to the rate of rise in serum glucose concentration (derivative of the glucose concentration with respect to time) over the first 60-90 min. The dynamic secretion phase is believed to be comprised of multiple steps including insulin localization to the beta cell membrane followed by exocytosis. The second phase, that of static secretion (Φ_s), is proportional to the elevation in glucose concentration above baseline; it represents a delayed response in insulin secretion caused by de novo synthesis, processing, and packaging of insulin. Glucose concentrations and the time derivative of the glucose concentration in-between sampling times were linearly-interpolated, error-free inputs for the oral C-peptide minimal model.

Serum C-peptide concentrations (pmol/L) were described using a two-compartment model and the following differential equations:

$$\frac{dCP_1(t)}{dt} = -k_{01}CP_1(t) - k_{21}CP_1(t) + k_{12}CP_2(t) + SR(t) \qquad CP_1(0) = 0 \qquad (\mathbf{5.5})$$

$$\frac{dCP_2(t)}{dt} = k_{21}CP_1(t) - k_{12}CP_2(t) \qquad CP_2(0) = 0 \qquad (\mathbf{5.6})$$

where k_{ij} represents various rate constants labeled in Figure 5-5, and CP_1 and CP_2 are C-peptide concentrations above basal levels in the central and peripheral compartments, respectively. The error associated with C-peptide measurement was assumed to be Gaussian (mean = 0) with an unknown, but constant variance.

Secretion rate, *SR(t)*, during a MMTT is comprised of static and dynamic secretion as shown in equation 5.7.

$$SR(t) = SR_s(t) + SR_d(t) \tag{5.7}$$

$SR_s(t)$ can be simplified as the provision ($Y(t)$) of C-peptide to pancreatic beta cells:

$$SR_s(t) = Y(t) \tag{5.8}$$

The change in provision over time is defined in equation 5.9:

$$\frac{dY(t)}{dt} = -\alpha\{Y(t) - \beta[G(t) - h]\} \qquad Y(0) = 0 \tag{5.9}$$

where α (min^{-1}) is the rate constant for the provision and β (min^{-1}) is the static phase sensitivity to glucose concentrations. *G(t)* refers to serum glucose concentrations at time *t*, and *h* is the threshold glucose concentration needed to elicit insulin secretion (typically, *h* is larger than G_b). When glucose concentrations increase, *Y(t)* approaches a steady-state value that is linearly related to *(G(t) – h)* by β. The time constant 1/α governs the approach of *Y* to steady-state. Dynamic secretion (SR_d) is defined in equation 5.10:

$$SR_d(t) = \begin{cases} k_d\left(1 - \dfrac{G(t) - G_b}{G_t - G_b}\right)\dfrac{dG}{dt} & if\ \dfrac{dG}{dt} > 0\ \ and\ \ G_b < G(t) < G_t \\ 0 & \text{otherwise} \end{cases} \tag{5.10}$$

k_d refers to the dynamic control of glucose on insulin secretion, and G_t is the glucose threshold concentration above which no additional increase in insulin secretion is possible. In this model of

dynamic insulin secretion, SR_d is proportional to the derivative of glucose; however, that proportionality is allowed to vary with changes in glucose concentrations.

The oral model provides three indices of beta-cell function: Φ_b, Φ_s, and Φ_d as defined by the following equations:

$$\Phi_b = \frac{(k_{01} CP_b)}{G_b} \tag{5.11}$$

$$\Phi_s = \beta \tag{5.12}$$

$$\Phi_d(t) = \begin{cases} k_d \left[1 - \frac{Peak\ G - G_b}{2(G_t - G_b)}\right] & if\ G_t > Peak\ G \\ \frac{k_d (G_t - G_b)}{2(Peak\ G - G_b)} & if\ G_b < G_t \leq Peak\ G \end{cases} \tag{5.13}$$

where $k_{01}CP_b$ is the baseline secretion rate and *Peak G* is the maximum glucose concentration during the MMTT. In some instances of estimating Φ_d, particularly for subjects in the T2DM and GDM groups, the estimate of G_t was less than G_b, which violates the conditions listed following equations 5.10 and 5.13. For those situations, we relied on a simpler model of dynamic insulin secretion, which assumes that the proportionality between SR_d and the derivative of glucose is constant [23]:

$$SR_d(t) = \begin{cases} k_d \frac{dG}{dt} & if\ \frac{dG}{dt} > 0\ and\ G(t) > G_b \\ 0 & \text{otherwise} \end{cases} \tag{5.14}$$

G_t values that were estimated again using equation 5.14 were no longer less than G_b, and no longer violated conditions used for calculation of SR_d. Using the simpler model in equation 5.14, Φ_d reduces to equation 5.15:

$$\Phi_d(t) = k_d \tag{5.15}$$

The static and dynamic indices can also be combined to form phi total (Φ_t) which is the average insulin secretion above basal secretion divided by the total glucose stimulus/exposure (area under the curve) still above threshold levels:

$$\Phi_t = \Phi_s + \frac{\Phi_d(Peak\ G - G_b)}{\int_0^{\infty}[G(t) - h]\,dt} \qquad (\mathbf{5.14})$$

Disposition index

The disposition index (DI) is the product of the insulin sensitivity index (SI) and the beta-cell function index (Φ_t). This assumed relationship between SI and Φ_t is referred to as the hyperbolic law of glucose tolerance and has provided insight into the underlying mechanisms of insulin insufficiency and resistance for glucose intolerance [13].

Calculations and statistical analysis

Kernel density plots (smoothed histograms) comparing time to attain glycemic control across GDM treatment groups were generated using R programming software [24]. Average time to glycemic control was calculated using R programming software; statistically significant differences in the average duration to glycemic control were determined by two-way analysis of variance (ANOVA) followed by the Tukey post-hoc test assuming a significance level of 0.05. Model parameters were estimated for individual subject datasets by nonlinear least squares regression using the SAAM II software (version 2.3, The Epsilon Group, Charlottesville, VA). Statistically significant differences in PD parameter estimates between study day 1 and 2 were estimated using a paired *t*-test and Wilcoxon signed-rank test.

5.3 Results

Demographics

Subject demographics were similar across treatment groups (Table 5-2). On average, subjects were approximately 30 years old, weighed 90 kg, and stood 160 cm tall. The majority of subjects were white and/or Hispanic. The average gestational age of pregnant subjects on SD 1 and SD 2 was 30.7 and 35.4 weeks of gestation, respectively. On average, subjects in the Combo group achieved glycemic control 10.7 days faster than the GLY group ($p = 0.0023$) (Figure 5-6). The average time to attain glycemic control was not statistically different between Combo and MET groups (4.6 days earlier, respectively, $p = 0.36$), nor was it different between MET and GLY groups (6.2 days earlier, respectively, $p = 0.17$) (Figure 5-6). This difference in average duration to glycemic control did not appear to relate to treatment failure, as the failure rate was the same for the GLY and Combo groups (~31%), and as high as 50% for the GDM MET group.

Serum glucose, insulin, and C-peptide concentrations

Averaged serum concentration-time profiles of glucose, insulin, and C-peptide following a four-hour MMTT are shown in Figure 5-7, 5-8, and 5-9, respectively for all five study groups pre- and post-drug treatment (referred to as study days SD 1 and SD 2). The shape of the serum glucose concentration-time profiles (Figure 5-7) remained consistent between SD 1 and SD 2 for all groups. Glucose concentrations at individual time points were lower on SD 2 in all groups except healthy pregnant (HP) women, who had no noticeable difference in the profiles between SD 1 and SD 2 (Figure 5-7, panel B). Following treatment, the shape of the insulin concentration-time profile shifted in the Combo and GLY groups (Figure 5-8). In the Combo group, insulin concentrations peaked 30 min earlier on SD 2 compared to SD 1; however, peak

concentrations (I_{max}) were not altogether different before and after treatment (149 and 143 μU/mL, respectively). In the GDM GLY group, the time associated with I_{max} (t_{max}) was 30 min later on SD 2 versus SD 1, rather than earlier; however, I_{max} was nearly identical on SD 1 and 2 (103 versus 102 μU/mL, respectively). Insulin levels remained unchanged between SD 1 and SD 2 for the HP and T2DM groups, but decreased on SD 2 for the Combo and MET groups. The shape of the C-peptide concentration-time profile was essentially unchanged by treatment for all groups (Figure 5-9). C-peptide concentrations increased on SD 2 compared to SD 1 or remained consistent with the SD 1 levels for all groups except for the MET group. Mean C-peptide concentrations following treatment on SD 2 were below the SD 1 baseline levels in the MET group.

Individual PD parameter estimates

Individual PD parameter estimates are listed by treatment group in Tables 5-3 through 5-7. To visualize the effect of treatment, Figures 5-10 through 5-16 provide line plots connecting individual parameter estimates (Φ_b, Φ_s, Φ_d, Φ_t, SI and DI) on SD 1 versus SD 2. In our preliminary analysis we found no statistically significant differences between pre- and post-treatment for the majority of parameters. Changes in Φ_s, Φ_d, Φ_t and SI between study days were not significant for any treatment group (Figures 5-11 through 5-15, respectively). Estimates of Φ_b increased from SD 1 to SD 2 in the GLY group ($p = 0.02$ with paired *t*-test; $p = 0.02$ with Wilcoxon sign-ranked test) and the HP group ($p < 0.001$ with paired *t*-test; $p < 0.001$ with Wilcoxon sign-ranked test) (Figure 5-10). Additionally, the DI increased from SD 1 to SD 2 in the Combo group ($p = 0.03$ with paired *t*-test; $p = 0.03$ with Wilcoxon sign-ranked test), but decreased in the HP group ($p = 0.04$ with paired *t*-test; $p = 0.06$ with Wilcoxon sign-ranked test) (Figure 5-16). Because of the limited number of subjects, particularly in the GDM groups as well

as the T2DM group, the trend (increasing or decreasing parameter estimates) between SD 1 and SD 2 is not well defined.

Hyperbolic disposition index curves

The hyperbolic relationship between beta-cell function and insulin sensitivity is illustrated by treatment group in Figures 5-17 through 5-21. For each treatment group, individual beta cell function (Φ_t) on each study day was plotted against the corresponding inulin sensitivity (SI) and the scatter-plot was fitted with the rectangular hyperbolic function; i.e., $\Phi_t = DI/SI$. In addition, a line was drawn connecting the individually plotted points from SD 1 to SD 2; these lines indicating the magnitude and direction of change in DI as a result of drug treatment and progression in gestation are herein referred to as vectors. Across the GDM treatment groups, most subjects' vector began at about the same starting position, which was most often the lower left region of the DI plot corresponding to low insulin sensitivity ($SI < 5 \cdot 10^{-4}$ min^{-1} μU^{-1} mL) and moderately low beta-cell function ($50 < \Phi_t < 150 \cdot 10^{-9}$ min^{-1}) (Figures 5-17 through 5-19). Subjects failing treatment (indicated in red) were present in all three GDM groups. Several subjects in the GDM groups displayed odd treatment vectors; they were characterized as odd for one of two reasons: either the SD 1 estimate of DI was already well-within the region of the hyperbolic curve corresponding to HP subjects, which calls into question the original GDM diagnoses, or the final SD 2 vector ended in the HP region, which calls into question why these subjects were declared to have failed their drug therapy.

We hypothesized that treatment with glyburide would increase Φ_t resulting in vertical, upward moving vectors; in contrast, treatment with metformin would increase SI, resulting in horizontal, rightward moving vectors. For the Combo group, we hypothesized diagonal vectors,

moving in the upper-right hand direction, which reflects improvements in both Φ_t and SI. Subjects in the GLY group (Figure 5-17) showed recognizable vertical vector movement, corresponding to slight increases in Φ_t. Subjects in the MET group (Figure 5-18) showed minimal rightward vectors only in a few subjects, especially if we were to exclude nearly one-half of the subjects who were declared failures on MET monotherapy. Contrary to our hypothesis, the Combo group showed mostly vertical vectors; in fact, some subjects showed remarkable increases in beta-cell function and little to no change in SI (Figure 5-19). The SD 2 hyperbolic curve for Combo and MET groups nearly overlapped with the control HP group on SD 2, which indicates achievement of glycemic control normal for pregnancy. Interestingly, the GLY curve on SD2 shifted diagonally to the left, away from the healthy pregnant group, indicating lack of improvement if not slight worsening of gestational diabetes.

There was a gestational age-dependent shift in the hyperbolic DI curve over the course of ~5.1 weeks between SD 1 and SD 2 in the healthy pregnant control group. Additionally, the distribution of DI estimates about the hyperbolic curves began as one, but split into two distinct clusters starting at SI estimates between 5 and $10 \cdot 10^{-4}$ min^{-1} μU^{-1} mL. One cluster deviated from the rectangular hyperbolic curve, flattening out at or below Φ_t values ~$100 \cdot 10^{-9}$ min^{-1}; the other cluster declined in sync with the hyperbolic curve towards $50 \cdot 10^{-9}$ min^{-1}. T2DM subjects at baseline were divided into two clusters, those with little to no insulin sensitivity (against the y-axis) and those with little to no beta-cell responsivity (against the x-axes). A few T2DM subject vectors were oddly placed relative to the range for healthy pregnant individuals. Considering the spare datasets and degree of disease severity in these subjects, the hyperbolic DI curves for the T2DM group were up against the x- and y-axis. Treatment with metformin did manage to improve subjects' insulin sensitivity as well as beta-cell function.

5.4 Discussion

In this chapter are presented preliminary data comparing the efficacy of glyburide monotherapy, metformin monotherapy, or combination therapy in women with GDM using quantitative indices of peripheral tissue sensitivity to insulin action and pancreatic beta-cell insulin release following mixed-meal tolerance tests. A key observation was the difference in the time to achieve glycemic control between the three GDM drug treatment groups, in the order of Combo ≈ MET > GLY. The bimodal shape of the kernel density plot comparing duration to glycemic control in the three GDM treatment arms (Figure 5-6) is perhaps caused by the scheduling of clinic visits (to evaluate glycemic control under a specified dose) and/or the number of dosing escalation options (4 options in the GLY and Combo group compared to 3 in the MET group). The failure rates (Table 5-2) seemed quite high across all groups (30-50%); however, the number of subjects in each group was relatively small (~16 subjects per group).

Serum glucose and insulin concentrations in the GLY group were similar to previously published data in women with GDM receiving glyburide [10]. Peak C-peptide concentrations, however, were approximately 1,000 pmol/L lower in the current GDM subjects compared to concentrations reported previously [10]. The cause is unclear, as the average glyburide dose was larger in this current study compared to the previous study (which would increase C-peptide levels). Though there may be too few subjects to evaluate differences in serum C-peptide at this time. Furthermore, it is interesting that subjects in the MET group had lower C-peptide concentrations post-treatment. Considering metformin's mechanism of action, one might expect insulin concentrations to be lower following treatment based on improved peripheral tissue uptake and disposal; however, lower C-peptide concentrations make it seem as though insulin production has decreased following treatment. We also expected significant differences in SI, Φ_t,

or DI before and after treatment, however there were essentially no statistically significant differences in PD parameter estimates between SD 1 and SD 2 in the three GDM drug treatment groups. It remains to be seen if statistically significant differences will emerge in the final analyses, given the low sample size and wide inter-subject variability of the current data.

There still seems to be a disconnection between the predictive capabilities of the hyperbolic DI curve for GDM disease pathology and subjects' clinical diagnostic criteria for GDM diagnoses and treatment failure. For example, some of the baseline SI and Φ_t estimates for GDM subjects were positioned within the domain of healthy pregnant subjects, calling into question how these women were diagnosed with GDM initially. Likewise, several subjects that supposedly failed therapy displayed treatment vectors that were located within the region of healthy pregnant subjects, again creating an incongruity between quantitative PD indices and treatment outcomes. The reasons for these issues may be because the MMTT occurs during one clinic visit, and therefore may not correlate with the clinical evaluation of GDM and drug treatment success or failure based on blood glucose monitoring and hyperglycemic symptoms, especially if GDM is mild. It is also perhaps possible that the relationship between SI and Φ_t is more complicated than a simple hyperbolic relationship. In fact, there is evidence to suggest that a more complicated relationship could be appropriate [25].

We had also expected the vectors connecting SD 1 and SD 2 in the DI plot to reflect the mechanism of action for the particular therapy administered. That was not always the case, however, as the direction and magnitude of the vectors was surprising for the GDM Combo and MET groups (Figures 5-17 through 5-19). In the Combo group there appeared to be a large synergistic effect on pancreatic beta-cell function (Φ_t) from the joint action of glyburide and metformin, whereas little effect on SI was evident. We had expected equal impact on SI and Φ_t

based on the two drugs' complementary mechanisms of action. This finding may trigger questions regarding metformin's mechanism of action that appears to improve pancreatic beta-cell function. In addition, this observation may explain why the initial efficacy, as judged by time to glycemic control and failure rates, were nearly comparable between the GLY and Combo groups. The other surprising finding was that metformin monotherapy had little to no impact on insulin sensitivity (Figure 5-18), although the effect may have been obscured by the high failure rate in this treatment group. It is possible that increased insulin resistance (decreased insulin sensitivity) throughout gestation, as evidenced by changes in the healthy pregnant hyperbolic curves from SD 1 to SD 2, works against metformin's mechanism action

Given the failure rates of drug treatment, duration to glycemic control, and the hyperbolic DI curves across treatment groups, the data analyzed herein suggest combination therapy for the treatment of GDM may provide further therapeutic benefit compared to glyburide and metformin monotherapy. The mechanism by which combination therapy provides therapeutic benefit remains a bit of a mystery at this point in time, as the synergistic effect of glyburide and metformin on beta-cell function was unexpected. These findings are valuable, however, for optimizing guideline recommendations for the use of oral anti-diabetic agents in pregnant women with GDM. With the clinical data we have to date, the current PD models do not predict the efficacy of glyburide and metformin for the treatment of GDM. However, the data are still incomplete, and current sample sizes are quite small. We await a full analysis of the entire data set that is expected to be completed in early 2015.

Tables and Figures for Chapter 6

Table 5-1. Conditional requirements for GDM diagnosis, drug treatment, drug treatment failure, and clinical control

Diagnosis of GDM	ANY of the following: • 1 h GTT: glucose > 185 mg/dL • 2 h GTT: ≥ 1 condition met: fasting ≥ 92 mg/dL, 1 h ≥ 180 mg/dL, 2 h ≥ 153 mg/dL • 3 h GTT: ≥ 2 conditions met: fasting ≥ 95 mg/dL, 1 h ≥ 180 mg/dL, 2 h ≥ 155 mg/dL, 140 mg/dL
Drug treatment required	ANY of the following: • Fasting glucose prior to 3 h GTT > 120 mg/dL • Failing 4 days of diet therapy (IF ≥ 3 occasions fasting glucose > 95 mg/dL, ≥ 75% 1 h postprandial glucose > 140 mg/dL, ≥ 75% 2 h postprandial glucose > 120 mg/dL, or ≥ 75% pre-prandial glucose > 110 mg/dL) • Failing 7 days of diet therapy (IF ≥ 25% fasting glucose > 95 mg/dL, ≥ 25% 1 h postprandial glucose > 140 mg/dL, ≥ 25% 2 h postprandial glucose > 120 mg/dL, or ≥ 25% pre-prandial glucose > 110 mg/dL)
Drug treatment failure	ANY of the following: • > 25% fasting glucose > 95 mg/dL • > 25% 1 h postprandial glucose ≥ 140 mg/dL • > 25% 2 h postprandial glucose ≥ 120 mg/dL • Any of the above plus intolerable GI side effects
Clinical control	• Fasting/preprandial glucose ≤ 95 mg/dL • 1 h postprandial glucose ≤ 140 mg/dL

GTT, Glucose Tolerance Test; h, hour; GI, gastrointestinal

Table 5-2. Demographics of GDM subjects (sorted by treatment), healthy pregnant subjects, and metformin-treated non-pregnant T2DM subjects

	GDM (n = 47)			Healthy Pregnant (n = 30)	T2DM (n = 12)
	Gly (n = 16)	Met (n = 15)	Combo (n = 16)		
Age (years)	30 ± 6	31 ± 4	30 ± 5	25 ± 5	31 ± 6
Body weight (kg)	90 ± 21	89 ± 15	94 ± 22	79 ± 13	92 ± 26
Height (cm)	160 ± 5	161 ± 5	161 ± 7	162 ± 8	158 ± 8
BMI (kg/m^2)	32 ± 8	32 ± 5	33 ± 8	27 ± 5	36 ± 7
Gestational age on SD 1 (weeks)	30.2 ± 2.0	31.0 ± 1.4	31.2 ± 1.8	30.4 ± 1.3	—
Gestational age on SD 2 (weeks)	35.4 ± 2.0	35.6 ± 1.2	34.9 ± 2.4	35.5 ± 1.0	—
Duration to glycemic control (days)	25 ± 13 (n = 11)	18 ± 9 (n = 7)	13 ± 7 (n = 11)	—	—
Failed treatment (%)	31% (n = 5)	50% (n = 7)	31% (n = 5)	—	—
Average Gly dose (mg orally twice daily)	4.2 ± 2.1 (range 2.5 - 8.75)	—	1.9 ± 0.6 (range 1.25 - 2.5)	—	—
Average Met dose (mg orally twice daily)	—	694 ± 251 (range 500 - 1000)	516 ± 75 (range 500 - 850)	—	900 ± 213 (range 500 - 1000)
Race/Ethnicity	3 Black 7 White 6 Hispanic/Latina/ White	1 Black 9 White 5 Hispanic/Latina/ White	3 Black 5 White 6 Hispanic/Latina/ White 1 American Indian or Alaska Native 1 Asian	5 Black 15 White 10 Hispanic/Latina/ White	2 Black 10 White 9 Hispanic/Latina/ White

Table 5-3. Individual PD parameter estimates of subjects with GDM receiving glyburide/metformin combination therapy

Study Day 1 (n = 16)							
Subject	**Φ_b (10^{-9} min^{-1})**	**Φ_d (10^{-9})**	**Φ_s (10^{-9} min^{-1})**	**Φ_t (10^{-9} min^{-1})**	**SI (10^{-4} min^{-1} μU^{-1} mL)**	**DI (10^{-13} min^{-2} μU^{-1} mL)**	**Peak G (mg/dL)**
02010080W *	10.07	392.79	76.43	79.06	0.12	9.49	244
02010100T *	17.29	1553.59	161.05	170.77	1.39	237.37	178
02010150E	13.32	1496.14	105.83	116.71	3.05	355.97	119
02010180S	18.44	6173.95	112.67	136.70	0.94	128.50	140
02020080Q	18.51	1677.46	90.83	100.36	1.08	108.39	161
02020090N *	7.09	1280.99	101.64	108.27	2.64	285.84	152
02020130E	18.58	905.51	97.37	103.73	1.09	113.06	165
02020180M	12.73	1386.75	108.03	116.07	2.24	259.99	163
02030060Q	10.98	3552.51	77.55	93.07	4.25	395.54	153
02030070N *	14.98	1043.57	73.54	80.12	0.99	79.32	198
02030090H	28.19	2392.07	79.90	94.70	0.48	45.45	173
02030700G	14.99	2505.21	169.10	192.30	0.76	146.15	152
02030710D	19.23	1613.75	99.92	109.94	1.27	139.63	220
02031220P	12.39	157.14	69.80	71.12	0.89	63.30	204
02040100B	9.74	1122.29	34.18	40.28	7.99	321.85	145
02040150J *	6.93	2592.07	203.20	213.99	5.00	1069.95	127
MEAN	**14.59**	**1865.36**	**103.81**	**114.20**	**2.14**	**234.99**	**168**
SD	**5.43**	**1432.09**	**42.17**	**45.22**	**2.07**	**251.40**	**34**

Study Day 2 (n = 13)							
Subject	**Φ_b (10^{-9} min^{-1})**	**Φ_d (10^{-9})**	**Φ_s (10^{-9} min^{-1})**	**Φ_t (10^{-9} min^{-1})**	**SI (10^{-4} min^{-1} μU^{-1} mL)**	**DI (10^{-13} min^{-2} μU^{-1} mL)**	**Peak G (mg/dL)**
02010080W *							
02010100T *							
02010150E	16.35	4594.30	289.95	317.27	3.56	1129.48	122
02010180S	17.12	2865.37	120.18	135.35	1.75	236.86	141
02020080Q	25.33	1379.50	126.64	135.21	1.44	194.71	139
02020090N *							
02020130E	12.34	1138.54	122.32	131.39	1.63	214.17	149

02020180M	16.97	916.58	85.83	94.11	1.26	118.58	177
02030060Q	9.98	1897.92	118.56	127.27	3.13	398.35	138
02030070N *	23.73	1172.70	111.68	118.35	1.21	143.21	159
02030090H	28.55	4960.23	313.92	347.50	1.40	486.49	125
02030700G	12.65	1582.37	62.56	72.73	0.98	71.27	187
02030710D	23.27	1391.65	32.66	41.65	2.22	92.47	138
02031220P	13.45	1483.35	160.86	170.58	2.19	373.58	152
02040100B	9.64	1539.35	83.75	90.27	7.08	639.11	135
02040150J *	7.07	609.48	215.20	217.24	9.65	2096.34	123
MEAN	**16.65**	**1963.95**	**141.85**	**153.76**	**2.88**	**476.51**	**145**
SD	**6.72**	**1359.48**	**83.94**	**90.57**	**2.60**	**566.42**	**20**

*Subjects that failed to achieve glycemic control; Φ_b, beta-cell response at baseline; Φ_d, dynamic phase beta-cell response; Φ_s, static phase beta-cell response; Φ_t, total beta-cell response; SI, insulin sensitivity; DI, disposition index; Peak G, maximum glucose concentration during MMTT.

Table 5-4. Individual PD parameter estimates of subjects with GDM receiving glyburide monotherapy

Study Day 1 (n = 16)							
Subject	**Φ_b (10^{-9} min^{-1})**	**Φ_d (10^{-9})**	**Φ_s (10^{-9} min^{-1})**	**Φ_t (10^{-9} min^{-1})**	**SI (10^{-4} min^{-1} μU^{-1} mL)**	**DI (10^{-13} min^{-2} μU^{-1} mL)**	**Peak G (mg/dL)**
02010090T *	15.18	1226.03	83.02	90.91	4.84	440.03	169
02010110Q *	10.17	1178.56	65.63	75.22	1.89	142.16	175
02010170V *	7.79	1130.45	58.59	67.83	2.53	171.60	169
02020100N	12.15	1136.83	96.99	105.73	1.72	181.86	164
02020160S	8.06	2051.06	74.28	86.41	1.94	167.63	153
02020110K	4.60	1230.24	47.03	57.24	6.94	397.26	161
02020170P *	10.90	1480.46	101.92	112.03	2.18	244.22	147
02020200J	19.99	4565.21	73.59	105.26	2.15	226.30	129
02020250R	15.74	2077.58	63.19	75.93	3.59	272.58	123
02030100H	11.81	1030.29	115.73	123.21	1.05	129.37	200
02030650S *	13.56	476.98	77.70	81.38	2.34	190.42	189
02030680J	9.24	908.65	75.59	82.25	3.32	273.05	163
02031200V	12.14	1427.20	94.91	102.48	1.43	146.54	177
02031210S	15.69	559.68	87.32	92.74	1.28	118.71	180
02031240J	5.77	1449.10	69.35	77.87	13.80	1074.64	179
02040010C	16.28	1101.51	75.62	82.71	0.82	67.82	166
MEAN	**11.82**	**1439.36**	**78.78**	**88.70**	**3.24**	**265.26**	**165**
SD	**4.17**	**936.72**	**17.46**	**17.39**	**3.22**	**237.23**	**20**

Study Day 2 (n = 13)							
Subject	**Φ_b (10^{-9} min^{-1})**	**Φ_d (10^{-9})**	**Φ_s (10^{-9} min^{-1})**	**Φ_t (10^{-9} min^{-1})**	**SI (10^{-4} min^{-1} μU^{-1} mL)**	**DI (10^{-13} min^{-2} μU^{-1} mL)**	**Peak G (mg/dL)**
02010090T *							
02010110Q *	19.50	1590.22	57.88	68.82	1.19	81.90	149
02010170V *							
02020100N	22.39	370.99	77.25	79.87	1.44	115.01	145
02020160S	10.89	1627.00	133.55	141.11	1.83	258.22	151
02020110K	5.28	995.86	180.85	186.08	8.20	1525.89	132
02020170P *	8.73	853.48	179.84	186.44	4.51	840.83	126

02020200J	23.13	1938.22	100.03	112.88	0.61	68.86	149
02020250R							
02030100H	20.62	992.93	73.69	81.23	0.71	57.67	158
02030650S *	22.75	619.28	44.05	48.75	1.07	52.16	180
02030680J	7.01	565.07	109.72	113.04	1.80	203.48	161
02031200V	13.15	916.35	82.12	87.13	0.79	68.84	163
02031210S	31.45	1420.59	66.00	78.35	1.21	94.81	131
02031240J	23.32	680.48	50.54	55.19	2.88	158.95	178
02040010C	17.56	722.70	79.86	83.98	1.12	94.06	157
MEAN	**17.37**	**1022.55**	**95.03**	**101.76**	**2.10**	**278.51**	**152**
SD	**7.77**	**476.91**	**44.96**	**44.84**	**2.12**	**429.49**	**17**

*Subjects that failed to achieve glycemic control; Φ_b, beta-cell response at baseline; Φ_d, dynamic phase beta-cell response; Φ_s, static phase beta-cell response; Φ_t, total beta-cell response; SI, insulin sensitivity; DI, disposition index; Peak G, maximum glucose concentration during MMTT.

Table 5-5. Individual PD parameter estimates of subjects with GDM receiving metformin monotherapy

Study Day 1 (n = 14)							
Subject	**Φ_b (10^{-9} min^{-1})**	**Φ_d (10^{-9})**	**Φ_s (10^{-9} min^{-1})**	**Φ_t (10^{-9} min^{-1})**	**SI (10^{-4} min^{-1} μU^{-1} mL)**	**DI (10^{-13} min^{-2} μU^{-1} mL)**	**Peak G (mg/dL)**
02010050I *	8.90	1534.88	76.93	86.96	4.04	351.30	135
02010070C *	9.16	477.67	54.54	58.32	4.26	248.44	151
02010130K *	13.02	1673.93	77.41	86.88	1.43	124.23	149
02020120H *	13.32	2411.37	74.62	93.32	1.53	142.78	170
02020140B *	14.72	1033.81	50.96	58.24	2.58	150.25	161
02020190J	15.01	2402.58	94.02	127.77	1.51	192.93	132
02020210G	11.03	887.61	68.33	74.93	1.80	134.88	174
02030080K	21.07	4620.80	123.48	158.15	2.54	401.70	119
02030630B	25.75	1024.51	115.95	123.19	0.86	105.94	175
02030660P	12.64	1059.37	77.65	84.79	1.50	127.18	204
02030640V	16.90	2276.64	91.45	108.45	0.81	87.84	166
02030720A	16.30	3268.09	117.56	135.40	8.81	1192.84	137
02040090B *	22.89	3118.10	133.95	152.87	0.49	74.91	141
02040140M *	7.32	1729.33	91.36	103.23	7.28	751.53	134
02010160B *							
02010210M							
02020260O *							
02030110E *							
02030120B *							
MEAN	**14.86**	**1965.62**	**89.16**	**103.75**	**2.82**	**291.91**	**153**
SD	**5.39**	**1138.11**	**25.52**	**32.05**	**2.49**	**315.71**	**23**

Study Day 2 (n = 12)							
Subject	**Φ_b (10^{-9} min^{-1})**	**Φ_d (10^{-9})**	**Φ_s (10^{-9} min^{-1})**	**Φ_t (10^{-9} min^{-1})**	**SI (10^{-4} min^{-1} μU^{-1} mL)**	**DI (10^{-13} min^{-2} μU^{-1} mL)**	**Peak G (mg/dL)**
02010050I *	12.47	1825.44	120.32	134.14	4.17	559.35	138
02010070C *	11.72	783.96	77.88	82.38	7.29	600.53	139
02010130K *	15.64	1759.89	80.13	93.38	2.17	202.64	142
02020120H *	15.38	2094.17	100.12	107.90	5.18	558.91	134
02020140B *							
02020190J	13.10	2150.04	102.45	117.15	1.22	142.92	143

02020210G	11.52	1584.46	60.53	72.81	2.96	215.50	146
02030080K	14.59	3612.68	130.14	163.67	3.47	567.94	140
02030630B	26.47	1650.36	109.12	125.80	2.20	276.75	153
02030660P	14.77	1452.88	91.15	100.10	2.20	220.23	150
02030640V	14.19	3938.80	95.29	111.29	8.74	972.71	127
02030720A	23.47	2694.90	126.85	143.76	2.69	386.71	129
02040090B *							
02040140M *	6.35	1647.04	90.73	101.77	4.91	499.70	148
02010160B *							
02010210M							
02020260O *							
02030110E *							
02030120B *							
MEAN	**14.97**	**2099.55**	**98.73**	**112.84**	**3.93**	**433.66**	**141**
SD	**5.33**	**906.58**	**20.76**	**25.94**	**2.26**	**239.35**	**8**

*Subjects that failed to achieve glycemic control; Φ_b, beta-cell response at baseline; Φ_d, dynamic phase beta-cell response; Φ_s, static phase beta-cell response; Φ_t, total beta-cell response; SI, insulin sensitivity; DI, disposition index; Peak G, maximum glucose concentration during MMTT.

Table 5-6. Individual PD parameter estimates of healthy pregnant women

Study Day 1 (n = 30)							
Subject	**Φ_b (10^{-9} min^{-1})**	**Φ_d (10^{-9})**	**Φ_s (10^{-9} min^{-1})**	**Φ_t (10^{-9} min^{-1})**	**SI (10^{-4} min^{-1} μU^{-1} mL)**	**DI (10^{-13} min^{-2} μU^{-1} mL)**	**Peak G (mg/dL)**
02010010U	11.65	5293.91	285.38	356.81	1.93	688.64	145
02010020R	13.75	5770.68	3.61	49.44	9.20	454.85	125
02010040L	19.21	2355.65	136.11	152.63	2.95	450.27	116
02010060F	12.32	7016.04	180.05	238.42	2.55	607.97	110
02010120N	11.86	1915.95	100.64	113.99	9.45	1077.23	117
02010190P	10.64	1454.18	81.05	95.61	3.72	355.67	168
02010200P	10.78	1357.79	82.50	93.55	25.20	2357.43	94
02020010O	7.47	2598.98	66.48	107.25	5.48	587.75	120
02020020L	4.45	1694.15	98.25	116.73	9.09	1061.07	109
02020030I	13.00	1832.70	130.14	144.58	3.08	445.30	131
02020040F	7.00	3568.77	82.98	100.88	14.80	1492.96	97
02020050C	7.49	2227.49	92.69	104.81	7.87	824.85	102
02020070T	9.55	2302.64	102.21	119.61	1.82	217.69	125
02020150V	3.15	1862.39	90.21	99.98	9.77	976.77	113
02020240U	8.29	2186.33	95.44	110.54	17.00	1879.21	104
02030010I	12.68	4890.23	79.63	113.84	5.12	582.88	99
02030020F	6.36	2300.98	82.47	98.59	13.40	1321.08	117
02030030C	16.33	1701.55	99.96	114.46	3.29	376.59	117
02030040W	15.57	6932.90	85.21	134.43	6.38	857.65	93
02030580N	10.62	3513.52	75.85	113.34	8.32	942.96	118
02030590K	22.82	3536.91	83.98	112.79	1.41	159.04	143
02031150K	6.99	2337.30	123.29	133.16	6.42	854.86	97
02031160H	7.57	1858.73	41.51	54.36	5.46	296.79	124
02040020W	3.93	1762.39	54.24	64.45	6.74	434.40	107
02040030T	7.27	1361.59	55.56	64.92	22.10	1434.65	105
02040040Q	14.50	1767.47	78.52	87.74	6.12	536.97	111
02040050N	8.90	1717.79	92.11	104.09	4.43	461.13	120
02040060K	7.67	1576.50	39.09	51.52	5.18	266.89	131
02040070H	11.80	1785.79	78.40	90.36	2.59	234.03	125
02040080E	8.20	2575.82	194.49	219.19	6.35	1391.88	119
MEAN	**10.39**	**2768.57**	**96.40**	**118.74**	**7.57**	**787.65**	**117**
SD	**4.42**	**1611.35**	**51.72**	**60.86**	**5.80**	**528.66**	**16**
Study Day 2 (n = 28)							

Subject	Φ_b (10^{-9} min^{-1})	Φ_d (10^{-9})	Φ_s (10^{-9} min^{-1})	Φ_t (10^{-9} min^{-1})	SI (10^{-4} min^{-1} μU^{-1} mL)	DI (10^{-13} min^{-2} μU^{-1} mL)	Peak G (mg/dL)
02010010U	14.94	3585.30	111.72	137.33	2.11	289.77	124
02010020R	22.62	3495.75	3.61	38.39	12.20	468.38	132
02010040L	21.93	4146.56	112.08	157.05	3.68	577.94	128
02010060F	13.02	4648.58	164.59	194.03	1.65	320.16	117
02010120N	14.85	2415.32	89.97	112.49	6.32	710.96	127
02010190P	10.83	2393.24	75.68	96.39	2.73	263.14	141
02010200P	14.87	3205.69	36.74	60.60	14.80	896.88	97
02020010O	9.36	4036.06	82.80	119.83	8.33	998.20	94
02020020L	6.93	2567.53	93.40	118.55	6.87	814.46	116
02020030I	15.21	2195.86	120.42	133.55	2.45	327.19	136
02020040F	9.13	2557.10	79.09	93.27	12.00	1119.24	100
02020050C	8.50	2207.70	92.69	110.38	10.50	1158.98	97
02020070T	11.27	1746.08	85.54	101.51	2.36	239.55	124
02020150V							
02020240U	14.83	1102.15	62.77	69.63	13.20	919.11	106
02030010I	18.25	3086.03	64.35	88.02	5.86	515.78	109
02030020F	9.25	2950.88	66.46	91.20	9.30	848.13	115
02030030C							
02030040W	19.85	5219.73	112.75	146.90	5.14	755.05	104
02030580N	10.29	4158.21	84.66	116.15	5.17	600.49	122
02030590K	30.38	3316.25	83.98	119.79	0.81	97.03	156
02031150K	6.81	1850.25	57.48	73.52	16.00	1176.31	114
02031160H	14.13	1414.51	39.70	50.04	9.01	450.85	108
02040020W	5.02	2008.36	58.28	70.35	4.39	308.83	113
02040030T	8.04	1430.63	61.71	73.24	13.70	1003.46	110
02040040Q	24.07	2048.76	81.41	94.31	5.23	493.24	119
02040050N	12.73	2789.30	91.58	115.28	5.44	627.11	122
02040060K	10.49	2488.28	70.75	83.89	5.13	430.38	106
02040070H	12.10	3056.30	88.11	105.50	3.95	416.74	113
02040080E	11.74	3425.49	164.57	183.66	4.52	830.16	102
MEAN	**13.62**	**2840.92**	**83.46**	**105.53**	**6.89**	**630.63**	**116**
SD	**5.87**	**1011.52**	**33.83**	**36.77**	**4.31**	**307.19**	**14**

*Subjects that failed to achieve glycemic control; Φ_b, beta-cell response at baseline; Φ_d, dynamic phase beta-cell response; Φ_s, static phase beta-cell response; Φ_t, total beta-cell response; SI,

insulin sensitivity; DI, disposition index; Peak G, maximum glucose concentration during MMTT.

Table 5-7. Individual PD parameter estimates of women with type-2 diabetes mellitus treated with metformin monotherapy

Study Day 1 (n = 14)							
Subject	**Φ_b (10^{-9} min^{-1})**	**Φ_d (10^{-9})**	**Φ_s (10^{-9} min^{-1})**	**Φ_t (10^{-9} min^{-1})**	**SI (10^{-4} min^{-1} μU^{-1} mL)**	**DI (10^{-13} min^{-2} μU^{-1} mL)**	**Peak G (mg/dL)**
02010140H	9.70	2684.72	3.61	16.29	9.07	147.76	174
02030220U	4.80	16.20	26.85	26.89	25.90	696.57	277
02030240O	2.44	11.69	5.39	5.44	2.40	13.07	469
02030250L	3.67	13.58	7.28	7.31	0.05	0.37	351
02030770I	4.14	471.99	81.51	84.31	9.43	795.08	188
02030780F	2.81	28.27	9.31	9.54	2.26	21.57	344
02031300R	2.58	16.20	7.94	8.03	8.31	66.75	313
02031330I	4.48	14.84	3.40	3.50	0.05	0.17	465
02031360W	14.08	1869.43	74.71	86.31	0.77	66.46	227
02040120S	9.94	22.63	28.76	28.89	0.57	16.47	249
02040130P	11.44	1786.50	48.94	61.95	0.40	24.78	191
02030230R	2.55	17.99	14.14	14.26	1.23	17.54	410
MEAN	**6.05**	**579.50**	**25.99**	**29.40**	**5.04**	**155.55**	**305**
SD	**4.08**	**957.73**	**27.83**	**30.61**	**7.51**	**279.54**	**105**

Study Day 2 (n = 12)							
Subject	**Φ_b (10^{-9} min^{-1})**	**Φ_d (10^{-9})**	**Φ_s (10^{-9} min^{-1})**	**Φ_t (10^{-9} min^{-1})**	**SI (10^{-4} min^{-1} μU^{-1} mL)**	**DI (10^{-13} min^{-2} μU^{-1} mL)**	**Peak G (mg/dL)**
02010140H							
02030220U	1.22	33.88	19.73	19.83	17.40	345.11	421
02030240O	4.14	28.62	21.17	21.58			345
02030250L	6.56	25.80	20.90	21.05	0.65	13.68	255
02030770I	4.11	467.72	60.97	63.58	11.70	743.84	198
02030780F	4.58	636.77	23.31	27.33	4.80	131.18	216
02031300R	1.82	14.75	15.77	15.88	10.30	163.53	287
02031330I	8.24	484.43	49.48	52.90	1.46	77.24	238
02031360W	16.14	1323.97	101.22	109.07	1.08	117.80	194
02040120S	11.85	123.40	3.61	4.03	12.20	49.14	180
02040130P	12.69	2468.61	63.06	80.24	0.77	61.78	154
02030230R							
MEAN	**7.14**	**560.80**	**37.92**	**41.55**	**6.71**	**189.26**	**249**

SD	**4.99**	**787.33**	**29.97**	**33.71**	**6.30**	**229.20**	**82**

*Subjects that failed to achieve glycemic control; Φ_b, beta-cell response at baseline; Φ_d, dynamic phase beta-cell response; Φ_s, static phase beta-cell response; Φ_t, total beta-cell response; SI, insulin sensitivity; DI, disposition index; Peak G, maximum glucose concentration during MMTT.

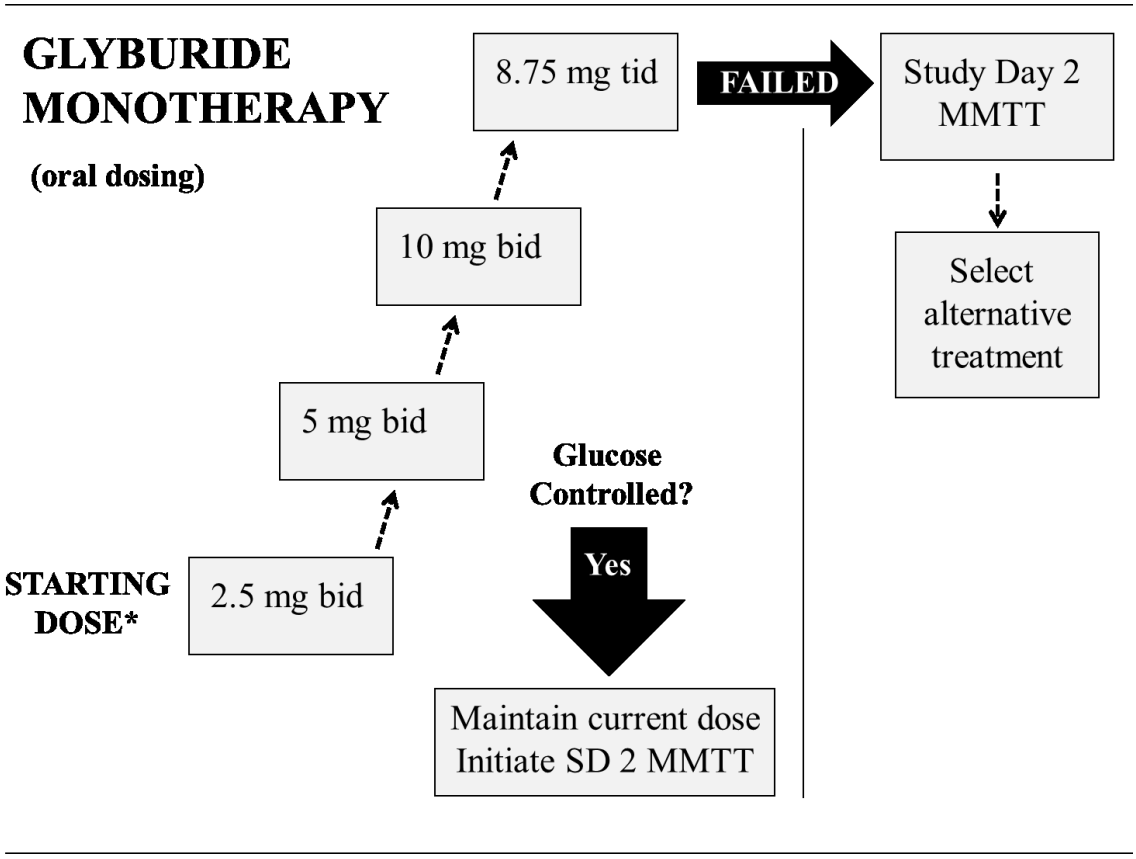

Figure 5-1. Glyburide monotherapy dosing regimen. Bid, twice daily; tid, three times daily. *Providers discretion can be used to start with a higher or lower dosage based on clinical situation.

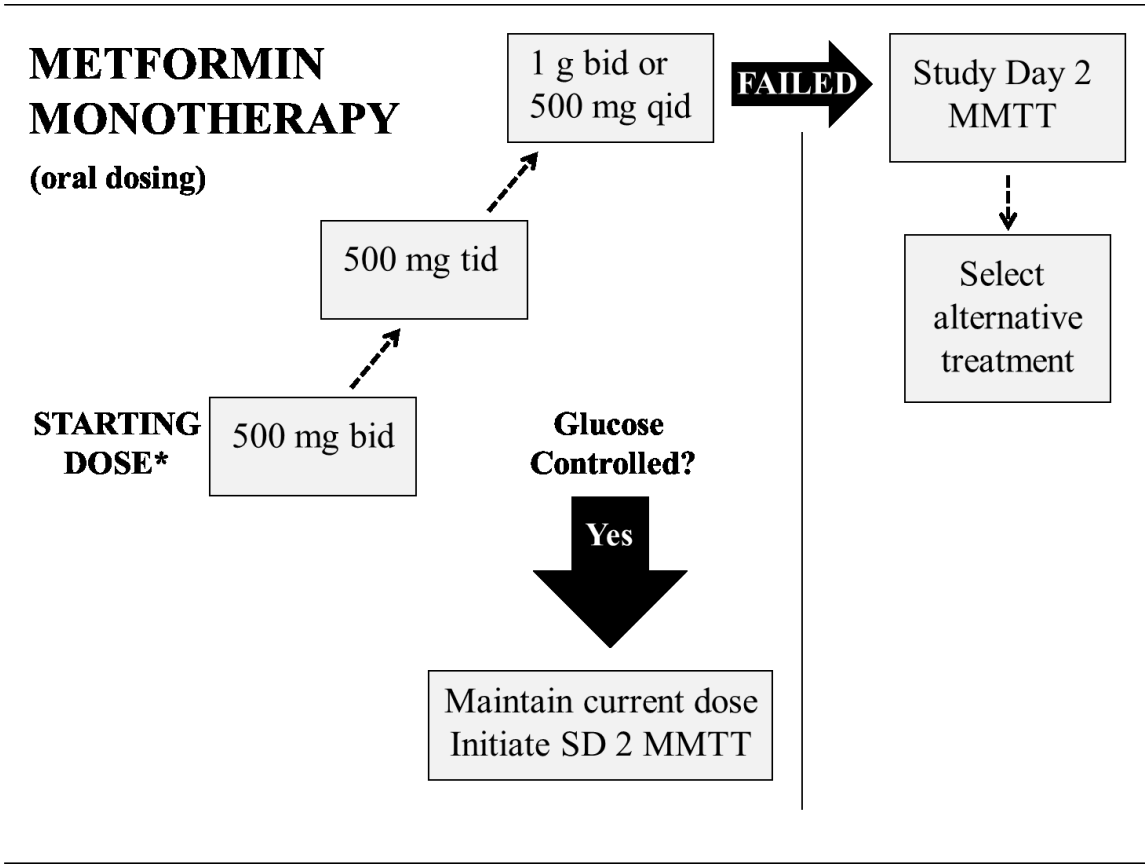

Figure 5-2. Metformin monotherapy dosing regimen. Bid, twice daily; tid, three times daily; qid, four times daily. *Providers discretion can be used to start with a higher or lower dosage based on clinical situation.

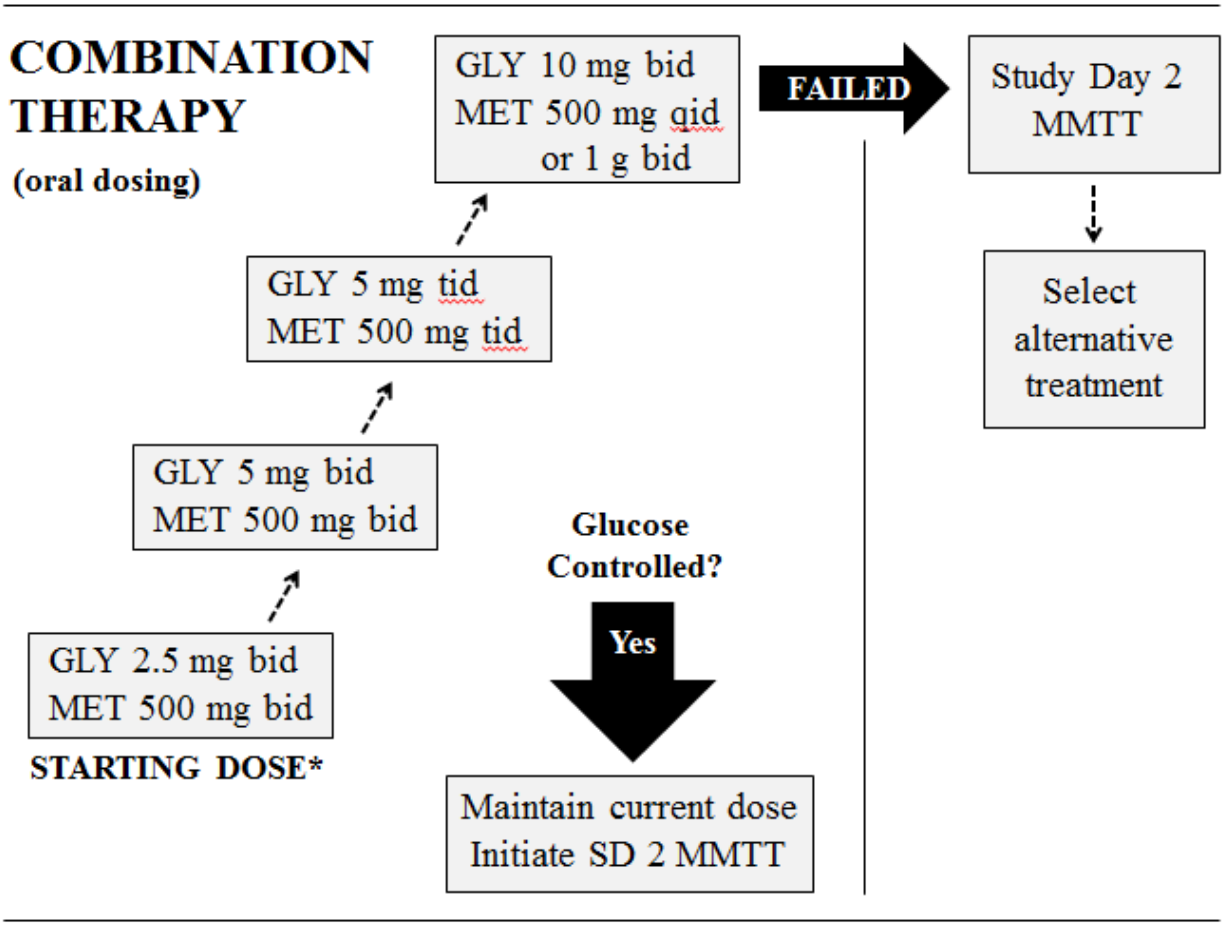

Figure 5-3. Glyburide (GLY) and Metformin (MET) combination therapy dosing regimen. Bid, twice daily; tid, three times daily; qid, four times daily. *Providers discretion can be used to start with a higher or lower dosage based on clinical situation.

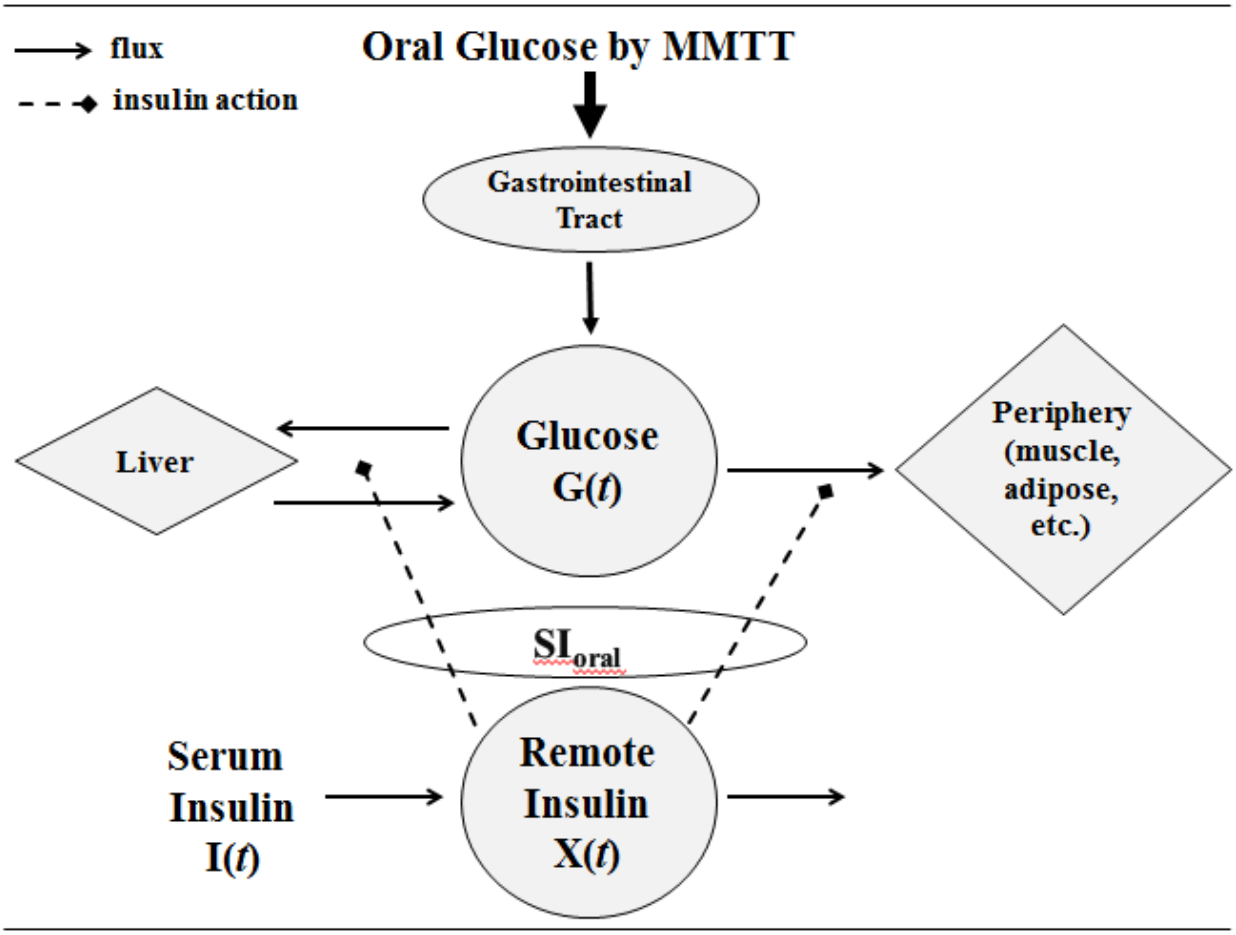

Figure 5-4. Oral minimal model of glucose kinetics following a MMTT. Adapted from [19].

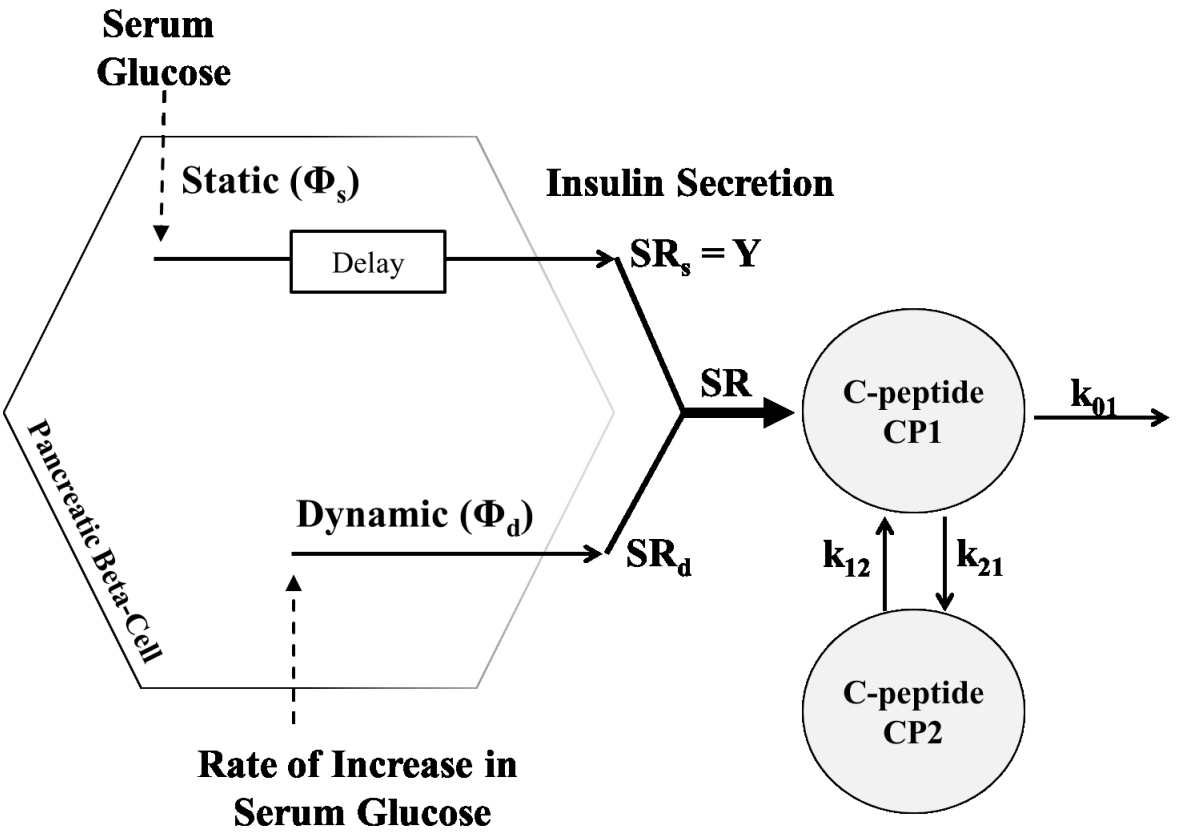

Figure 5-5. Oral C-peptide minimal model following a MMTT. Adapted from [19, 20].

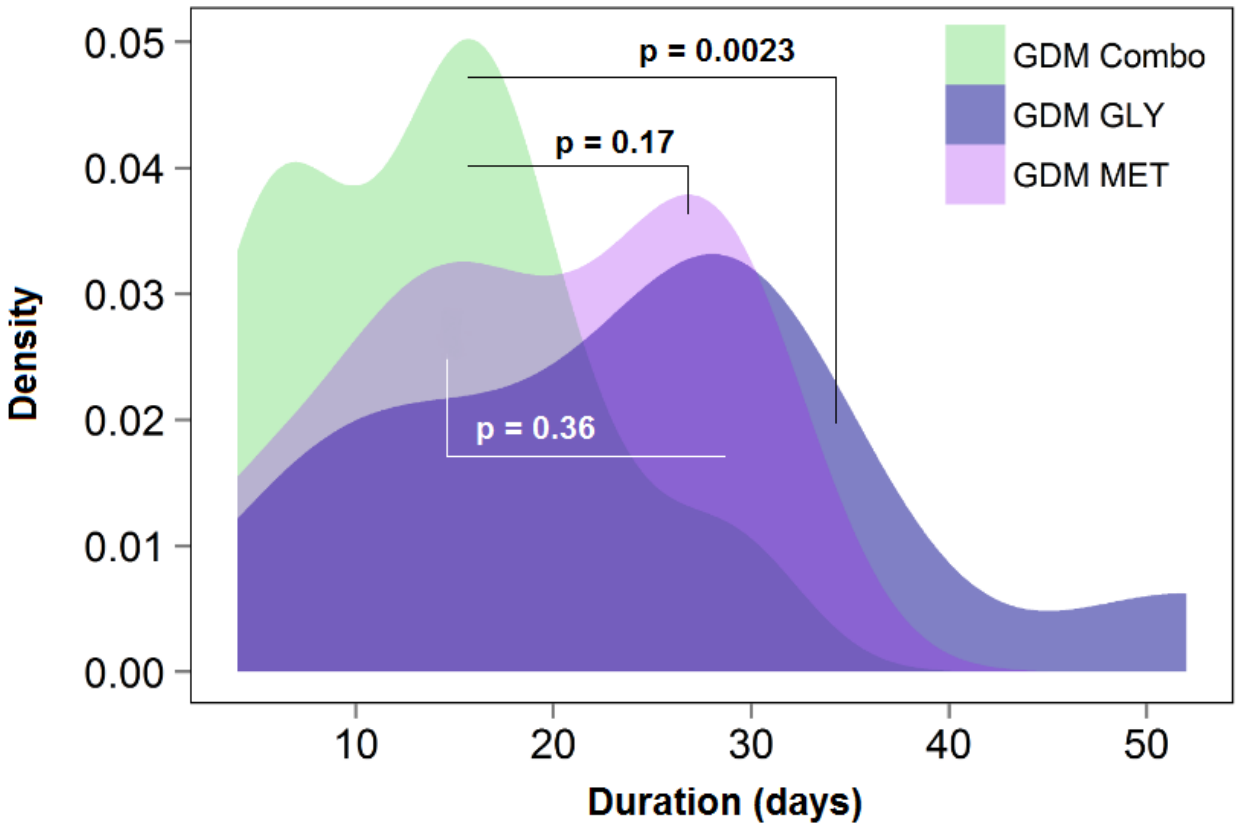

Figure 5-6. Kernel density plots comparing the duration to glycemic control between GDM combination therapy versus glyburide and metformin monotherapies. GDM Combo (green); GLY (dark purple); MET (lavender). Statistical comparisons between groups were performed using a two-way ANOVA with Tukey's post-hoc test assuming a significance level of 0.05.

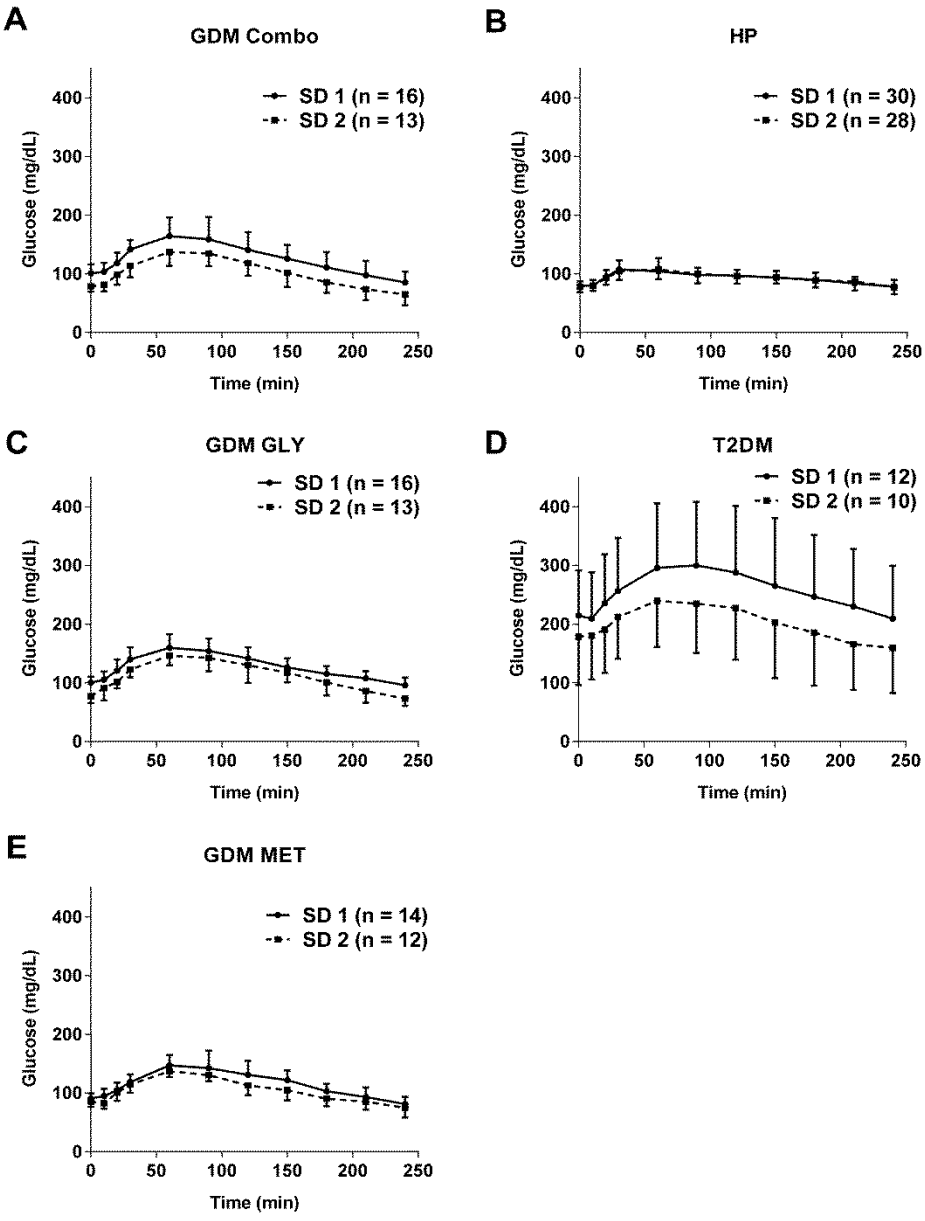

Figure 5-7. Glucose concentration-time profiles on study day 1 (SD 1) and study day 2 (SD 2) in women with GDM treated with glyburide/metformin combination therapy (A), glyburide monotherapy (C), or metformin monotherapy (E), as well as healthy pregnant women (B) and nonpregnant women with T2DM (D). Shown are means ± SD.

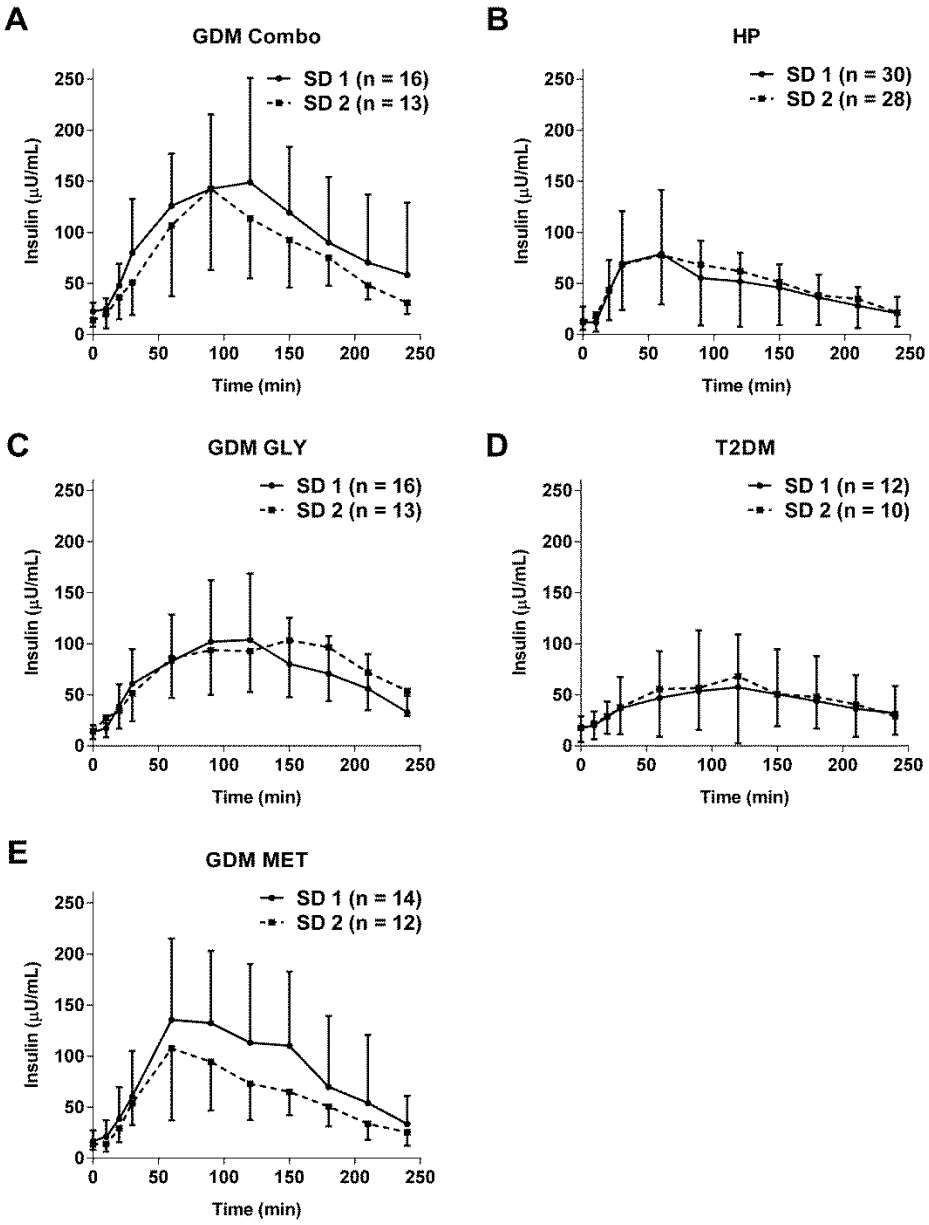

Figure 5-8. Insulin concentration-time profiles on study day 1 (SD 1) and study day 2 (SD 2) of women with GDM treated with glyburide/metformin combination therapy (A), glyburide monotherapy (C), or metformin monotherapy (E), as well as healthy pregnant women (B) and nonpregnant women with T2DM (D). Shown are means ± SD.

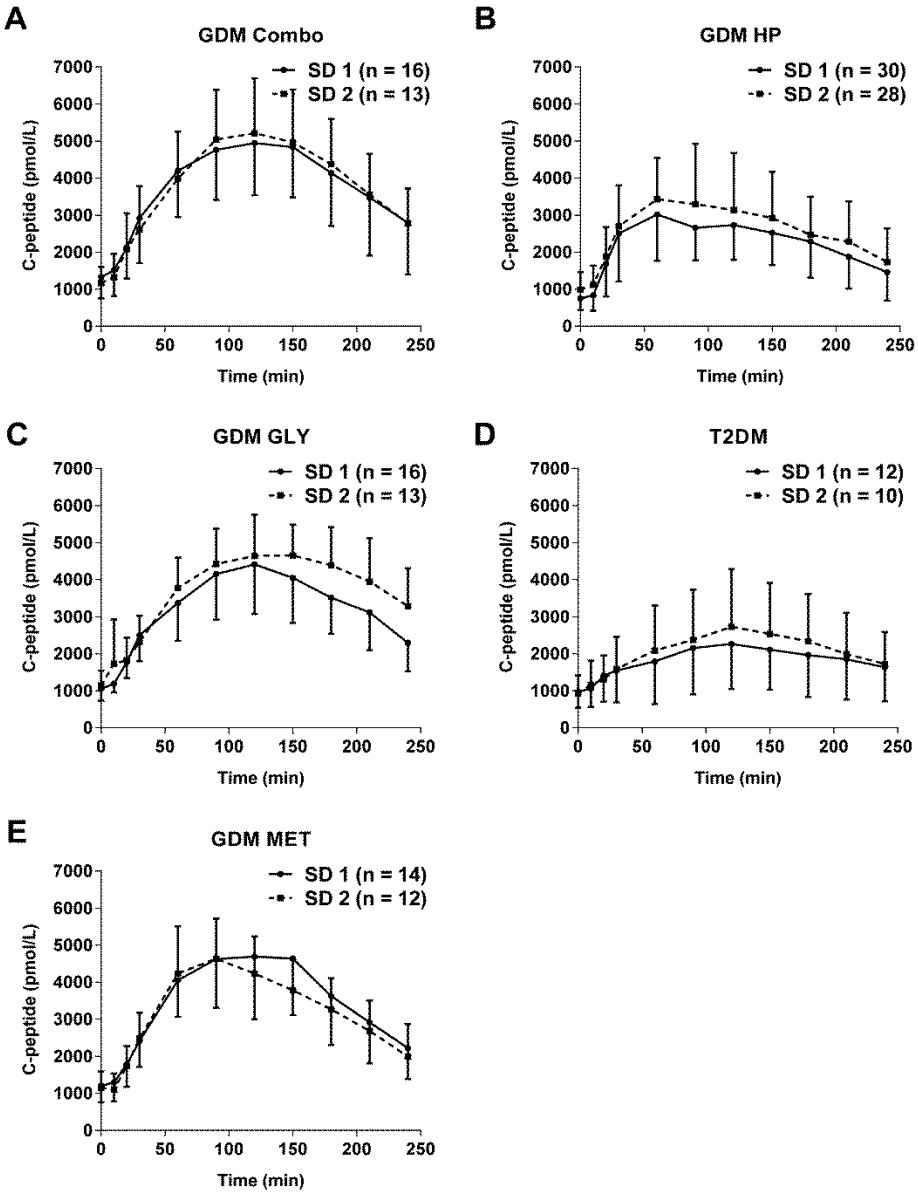

Figure 5-9. C-peptide concentration-time profiles on study day 1 (SD 1) and study day 2 (SD 2) in women with GDM treated with glyburide/metformin combination therapy (A), glyburide monotherapy (C), or metformin monotherapy (E), as well as healthy pregnant women (B) and nonpregnant women with T2DM (D). Shown are means ± SD.

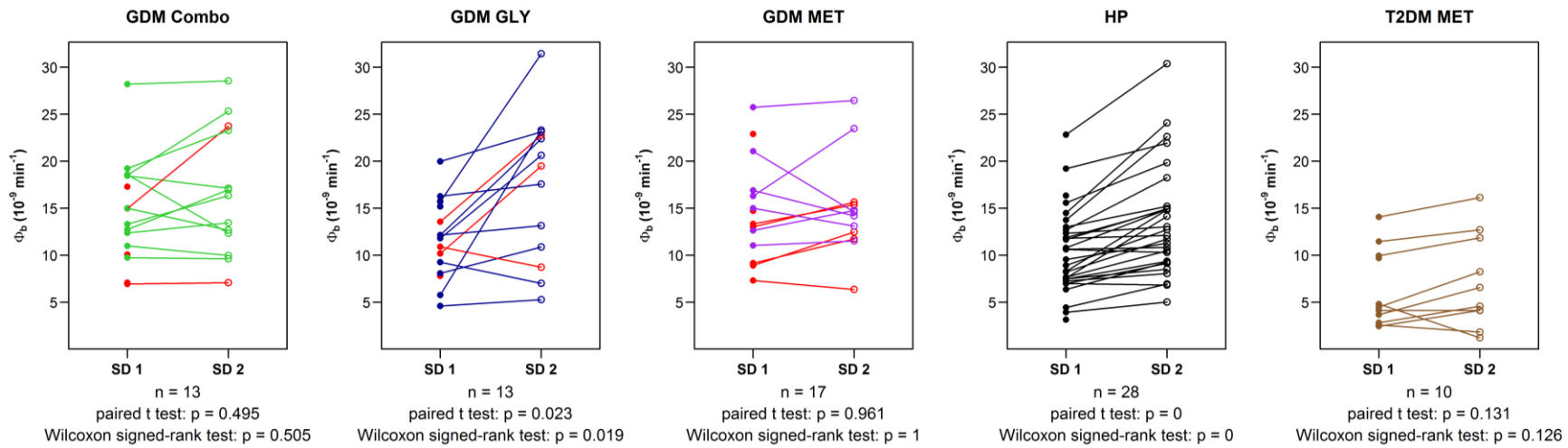

Figure 5-10. Changes in baseline beta-cell function (Φ_b) on study days (SD) 1 and 2. Subjects that failed to achieve glycemic control are shown in red color. P-values were calculated using a paired t-test as well as a Wilcoxon signed-rank test, and only included data from subjects that achieved glycemic control.

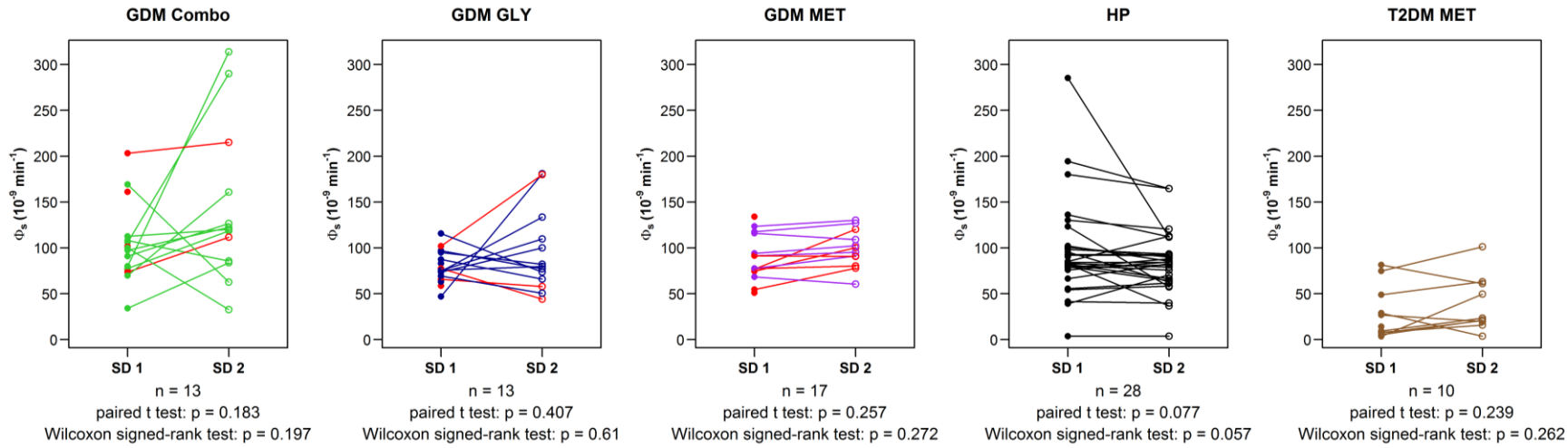

Figure 5-11. Changes in static beta-cell function (Φ_s) on study days (SD) 1 and 2. Subjects that failed to achieve glycemic control are shown in red color. P-values were calculated using a paired t-test as well as a Wilcoxon signed-rank test, and only included data from subjects that achieved glycemic control.

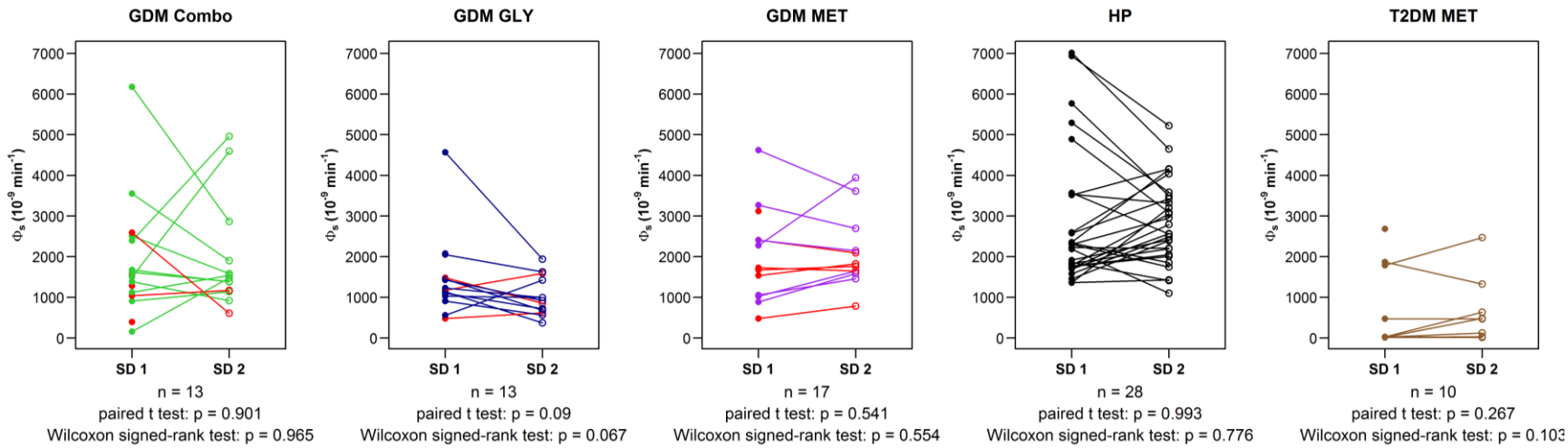

Figure 5-12. Changes in dynamic beta-cell function (Φ_d) on study days (SD) 1 and 2. Subjects that failed to achieve glycemic control are shown in red color. P-values were calculated using a paired t-test as well as a Wilcoxon signed-rank test, and only included data from subjects that achieved glycemic control.

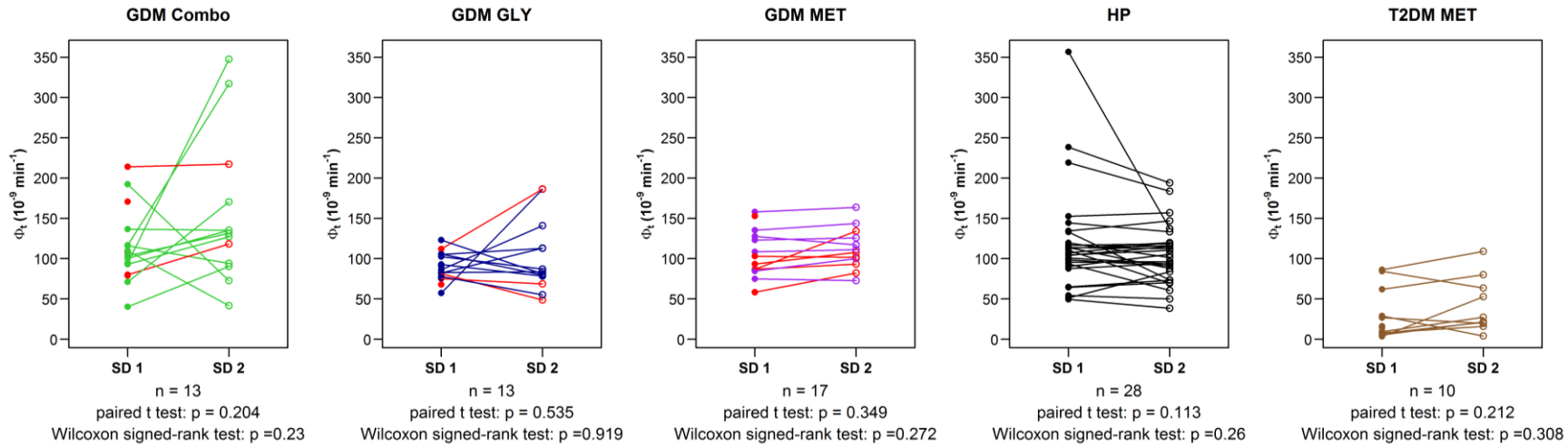

Figure 5-14. Changes in total beta-cell function (Φ_t) on study days (SD) 1 and 2. Subjects that failed to achieve glycemic control are shown in red color. P-values were calculated using a paired t-test as well as a Wilcoxon signed-rank test, and only included data from subjects that achieved glycemic control.

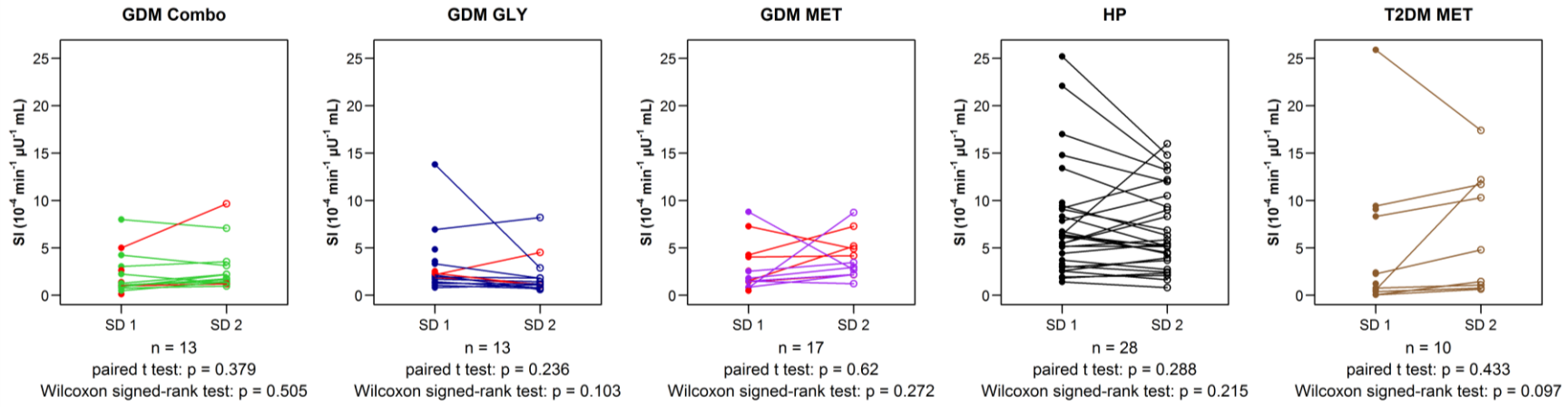

Figure 5-15. Changes in insulin sensitivity (SI) on study days (SD) 1 and 2. Subjects that failed to achieve glycemic control are shown in red color. P-values were calculated using a paired t-test as well as a Wilcoxon signed-rank test, and only included data from subjects that achieved glycemic control.

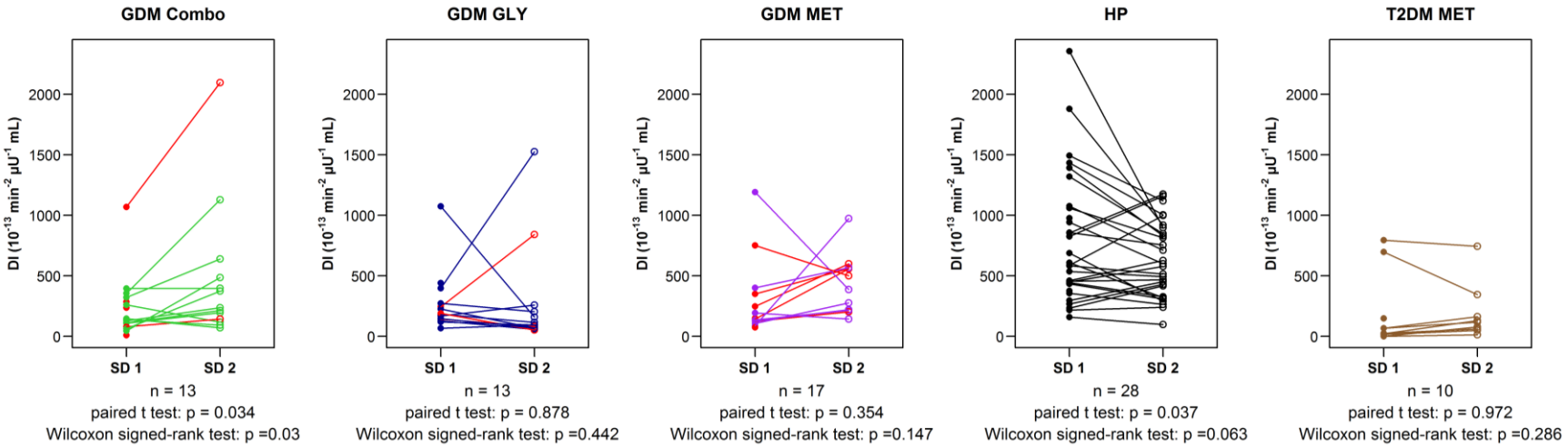

Figure 5-16. Changes in disposition index (DI) on study days (SD) 1 and 2. Subjects that failed to achieve glycemic control are shown in red color. P-values were calculated using a paired t-test as well as a Wilcoxon signed-rank test, and only included data from subjects that achieved glycemic control.

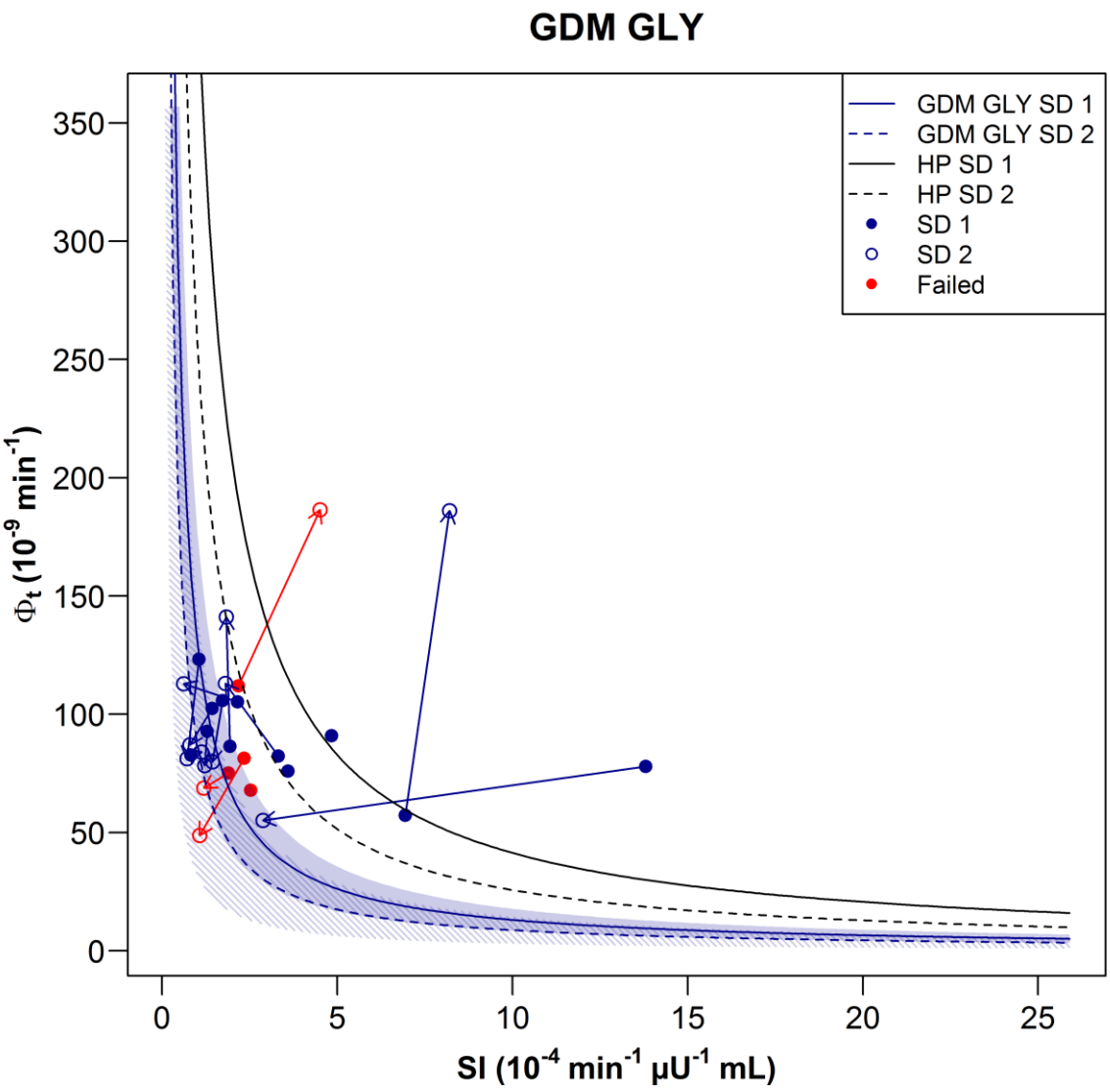

Figure 5-17. Hyperbolic disposition index (DI) curves pre- and post-treatment for GDM subjects receiving glyburide (GLY) monotherapy. Subjects that failed to achieve glycemic control are shown in red color. 95% confidence intervals (95%) of hyperbolic curve fits for GDM GLY SD 1 and SD 2 are shown as shaded blue areas.

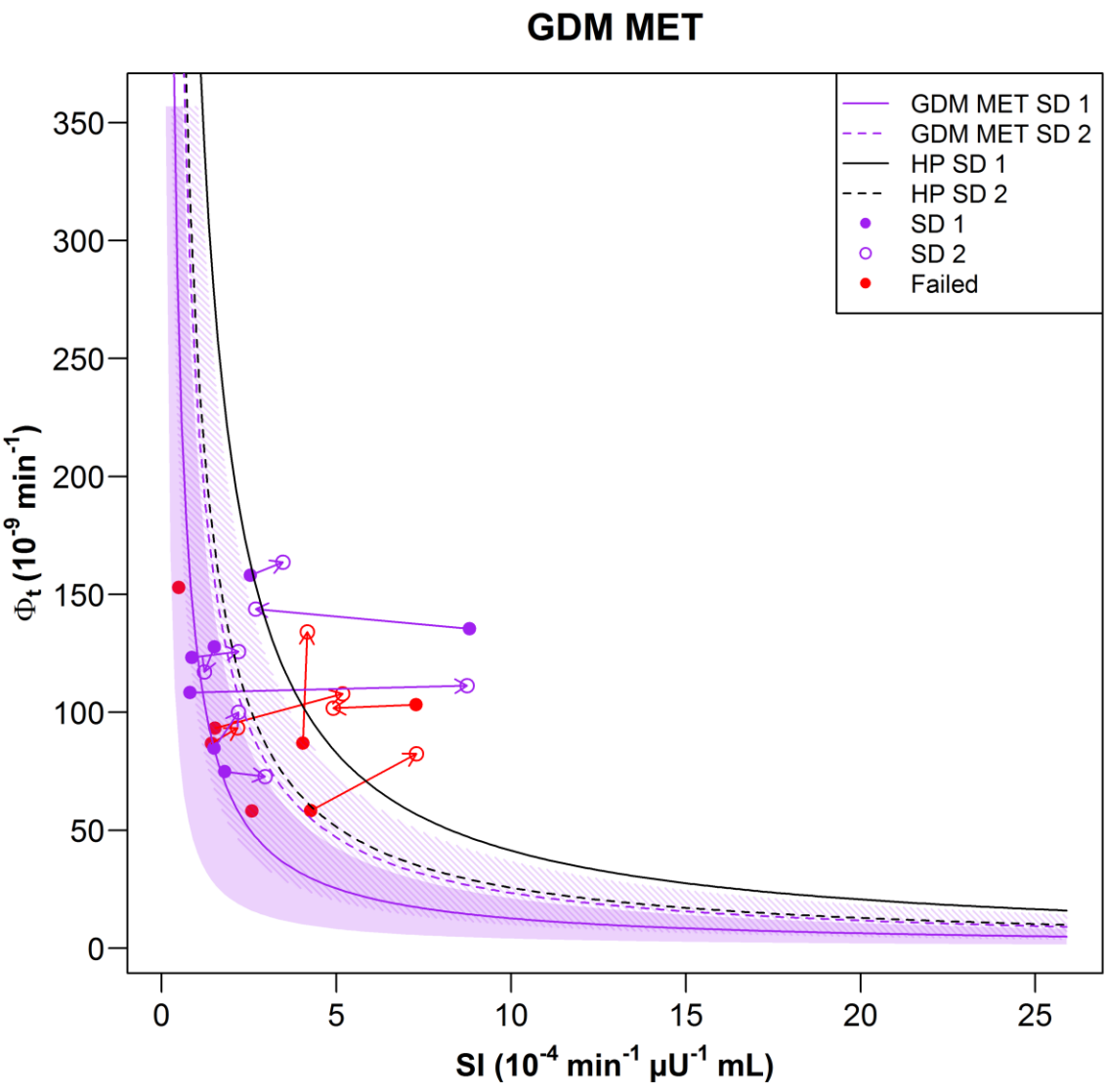

Figure 5-18. Hyperbolic disposition index (DI) curves pre- and post-treatment for GDM subjects receiving metformin (MET) monotherapy. Subjects that failed to achieve glycemic control are shown in red color. 95% confidence intervals (95%) of hyperbolic curve fits for GDM MET SD 1 and SD 2 are shown as shaded purple areas.

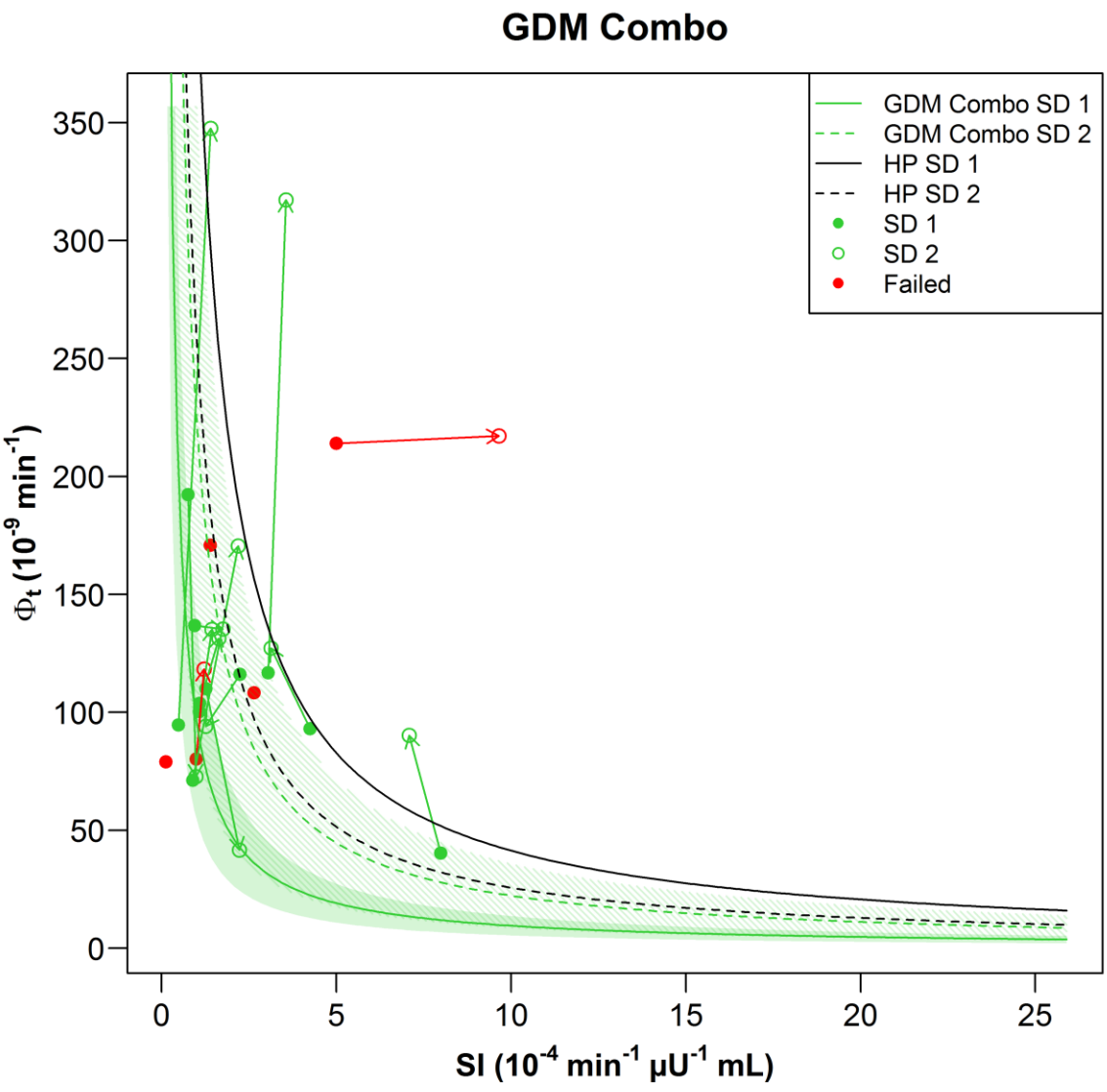

Figure 5-19. Hyperbolic disposition index (DI) curves pre- and post-treatment for GDM subjects receiving glyburide/metformin combination (Combo) therapy. Subjects that failed to achieve glycemic control are shown in red color. 95% confidence intervals (95%) of hyperbolic curve fits for GDM Combo SD 1 and SD 2 are shown as shaded green areas.

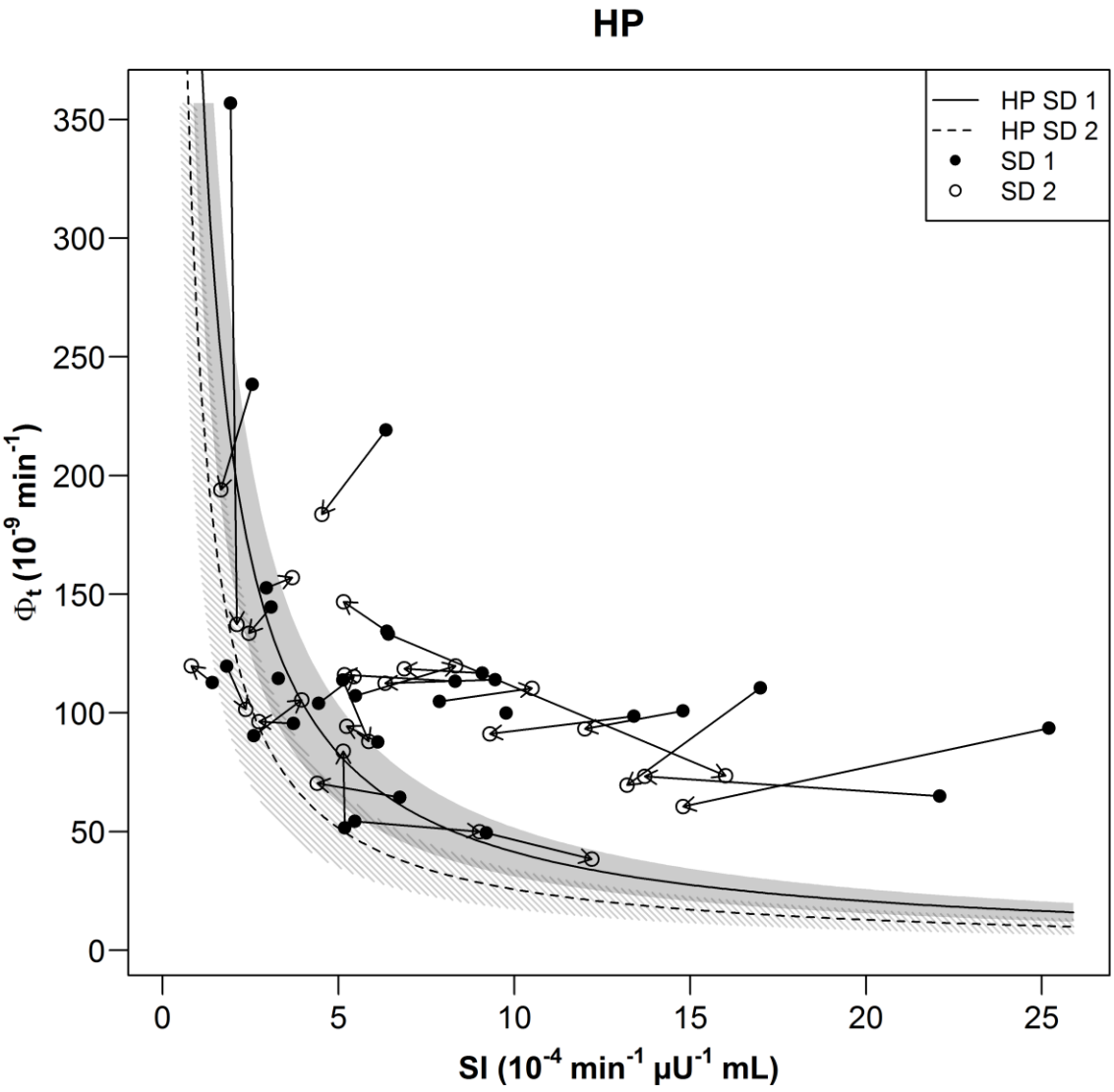

Figure 5-20. Hyperbolic disposition index curves for healthy pregnant (HP) subjects. 95% confidence intervals (95%) of hyperbolic curve fits for HP SD 1 and SD 2 are shown as shaded gray areas.

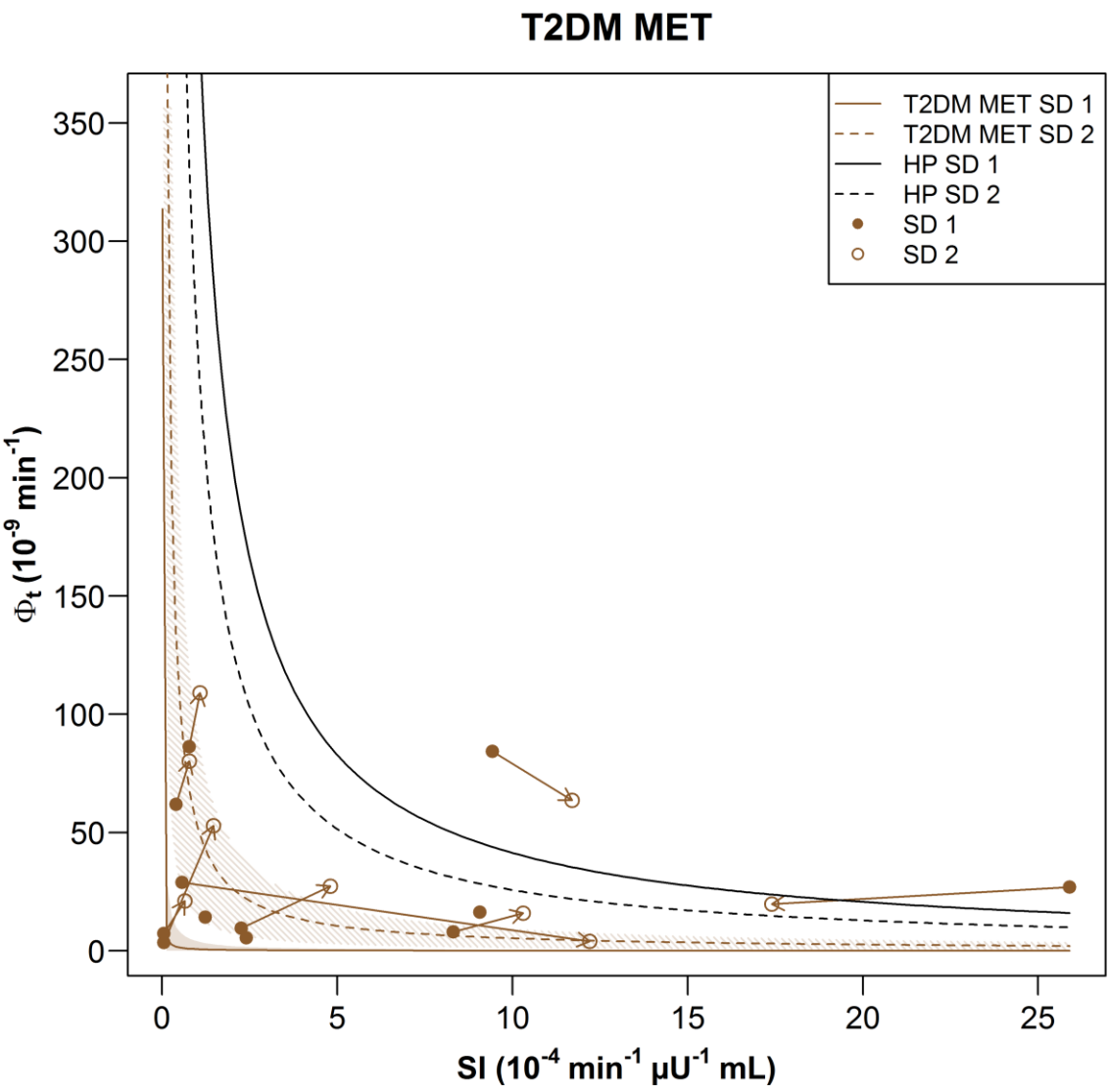

Figure 5-21. Hyperbolic disposition index curves pre- and post-treatment for T2DM subjects receiving metformin monotherapy. 95% confidence intervals (95%) of hyperbolic curve fits for T2DM SD 1 and SD 2 are shown as shaded brown areas.

References

[1] Jovanovic L, Pettitt DJ. Gestational diabetes mellitus. JAMA. 2001;286:2516-8.
[2] Paglia MJ, Coustan DR. Gestational diabetes: evolving diagnostic criteria. Curr Opin Obstet Gynecol. 2011;23:72-5.
[3] The Hyperglycemia and Adverse Pregnancy Outcome (HAPO) Study. Int J Gynaecol Obstet. 2002;78:69-77.
[4] ACOG Practice Bulletin. Clinical management guidelines for obstetrician-gynecologists. Number 30, September 2001 (replaces Technical Bulletin Number 200, December 1994). Gestational diabetes. Obstetrics and gynecology. 2001;98:525-38.
[5] Langer O, Conway DL, Berkus MD, Xenakis EM, Gonzales O. A comparison of glyburide and insulin in women with gestational diabetes mellitus. N Engl J Med. 2000;343:1134-8.
[6] Camelo Castillo W, Boggess K, Sturmer T, Brookhart MA, Benjamin DK, Jr., Jonsson Funk M. Trends in glyburide compared with insulin use for gestational diabetes treatment in the United States, 2000-2011. Obstetrics and gynecology. 2014;123:1177-84.
[7] Feldman JM. Glyburide: a second-generation sulfonylurea hypoglycemic agent. History, chemistry, metabolism, pharmacokinetics, clinical use and adverse effects. Pharmacotherapy. 1985;5:43-62.
[8] Kirpichnikov D, McFarlane SI, Sowers JR. Metformin: an update. Annals of internal medicine. 2002;137:25-33.
[9] Klieger C, Pollex E, Kazmin A, Koren G. Hypoglycemics: pharmacokinetic considerations during pregnancy. Ther Drug Monit. 2009;31:533-41.
[10] Hebert MF, Ma X, Naraharisetti SB, Krudys KM, Umans JG, Hankins GD, et al. Are we optimizing gestational diabetes treatment with glyburide? The pharmacologic basis for better clinical practice. Clin Pharmacol Ther. 2009;85:607-14.
[11] Eyal S, Easterling TR, Carr D, Umans JG, Miodovnik M, Hankins GD, et al. Pharmacokinetics of metformin during pregnancy. Drug Metab Dispos. 2010;38:833-40.
[12] Bergman RN, Phillips LS, Cobelli C. Physiologic evaluation of factors controlling glucose tolerance in man: measurement of insulin sensitivity and beta-cell glucose sensitivity from the response to intravenous glucose. The Journal of clinical investigation. 1981;68:1456-67.
[13] Bergman RN. Minimal model: perspective from 2005. Hormone research. 2005;64 Suppl 3:8-15.
[14] Dalla Man C, Caumo A, Cobelli C. The oral glucose minimal model: estimation of insulin sensitivity from a meal test. IEEE transactions on bio-medical engineering. 2002;49:419-29.
[15] Breda E, Cavaghan MK, Toffolo G, Polonsky KS, Cobelli C. Oral glucose tolerance test minimal model indexes of beta-cell function and insulin sensitivity. Diabetes. 2001;50:150-8.
[16] Bandi ZL, Fuller JB, Bee DE, James GP. Extended clinical trial and evaluation of glucose determination with the Eastman Kodak Ektachem GLU/BUN Analyzer. Clinical chemistry. 1981;27:27-34.
[17] Haffner SM, Mykkanen L, Stern MP, Valdez RA, Heisserman JA, Bowsher RR. Relationship of proinsulin and insulin to cardiovascular risk factors in nondiabetic subjects. Diabetes. 1993;42:1297-302.
[18] Wiedmeyer HM, Polonsky KS, Myers GL, Little RR, Greenbaum CJ, Goldstein DE, et al. International comparison of C-peptide measurements. Clinical chemistry. 2007;53:784-7.

[19] Cobelli C, Toffolo GM, Dalla Man C, Campioni M, Denti P, Caumo A, et al. Assessment of beta-cell function in humans, simultaneously with insulin sensitivity and hepatic extraction, from intravenous and oral glucose tests. American journal of physiology Endocrinology and metabolism. 2007;293:E1-E15.
[20] Toffolo G, Campioni M, Basu R, Rizza RA, Cobelli C. A minimal model of insulin secretion and kinetics to assess hepatic insulin extraction. American journal of physiology Endocrinology and metabolism. 2006;290:E169-E76.
[21] Caumo A, Bergman RN, Cobelli C. Insulin sensitivity from meal tolerance tests in normal subjects: a minimal model index. The Journal of clinical endocrinology and metabolism. 2000;85:4396-402.
[22] Dalla Man C, Caumo A, Basu R, Rizza R, Toffolo G, Cobelli C. Minimal model estimation of glucose absorption and insulin sensitivity from oral test: validation with a tracer method. American journal of physiology Endocrinology and metabolism. 2004;287:E637-43.
[23] Toffolo G, Breda E, Cavaghan MK, Ehrmann DA, Polonsky KS, Cobelli C. Quantitative indexes of beta-cell function during graded up&down glucose infusion from C-peptide minimal models. American journal of physiology Endocrinology and metabolism. 2001;280:E2-10.
[24] R Core Team. R: A language and environment for statistical computing. Vienna, Austria: R Foundation for Statistical Computing; 2014.
[25] Denti P, Toffolo GM, Cobelli C. The disposition index: from individual to population approach. American journal of physiology Endocrinology and metabolism. 2012;303:E576-86.

Chapter 6: Conclusion

Portions of this work were previously published in the following two manuscripts:

Shuster et al., *Drug Metabolism and Disposition* **41**:332–342, February 2013.

Shuster et al., *The Journal of Pharmacology and Experimental Therapeutics,* 350**(2)**:425-434, August 2014.

6.1 Chapter 2: Microarray Analysis

Pregnancy-induced changes in drug pharmacokinetics can be explained by changes in normal physiology as well as in the expression of drug-metabolizing enzymes and transporters. In Chapter 2, we determined gestational age-dependent mRNA expression profiles for all metabolic enzyme and transporter genes in the maternal liver, kidney, small intestine, and placenta of pregnant mice by microarray analysis. Specifically, we examined the expression of genes important for xenobiotic, bile acid, and steroid hormone metabolism and disposition, namely, cytochrome P450's (*Cyp*), UDP-glucuronosyltranserases (*Ugt*), sulfotransferases (*Sult*),

and ATP-binding cassette (*Abc*), solute carrier (*Slc*), and solute carrier organic anion (*Slco*) transporters.

Our data agreed quite well with previously published studies [1-3]. Overall, we found that *Cyp1a2*, most *Cyp2* isoforms, *Cyp3a11*, and *Cyp3a13* expression in the liver decreased on gestation days (gd) 15 and 19 compared to non-pregnant controls (gd 0). In contrast, *Cyp2d40*, *Cyp3a16*, *Cyp3a41a*, *Cyp3a41b*, and *Cyp3a44* in the liver were induced throughout pregnancy. In the placenta, *Cyp* expression on gd 10 and 15 was up-regulated compared to gd 19. Notable changes were also observed in *Abc* and *Slc* transporters. Our results revealed that *Abc* transporter gene expression in the maternal tissues and placenta was decreased during pregnancy. In particular, *Abcc3* in the liver, *Abcb1a* and *Abcc4* in the kidney, and *Abcc5* in the placenta were down-regulated on gd 15 and 19. Similarly, several *Slc* or *Slco* transporters important for drug disposition were moderately decreased during pregnancy (such as *Slco1b2* in the liver and *Slco4c1* in the kidney). Furthermore, *Slc22a3* (*Oct3*) and *Slc6a2* (*Net*) in the placenta were down-regulated and up-regulated, respectively, to a larger extent.

This was the first study to systematically characterize the gestational age-dependent gene expression profiles of all drug-metabolism enzyme and transporter families in maternal tissues and placenta in a pregnant mouse model. These data may have mechanistic relevance to drug disposition in human pregnancy, and thereby provide novel insights into potential changes in drug PK during pregnancy.

6.2 Chapter 3: Animal Dosing Study

Gestational diabetes mellitus (GDM) is a major complication of human pregnancy. One study estimated a 2-fold increase in the oral clearance of glyburide in women with GDM in the

third trimester of pregnancy compared to non-pregnant women with type-2 diabetes mellitus [4]. The time-course and mechanism by which pregnancy changes glyburide PK throughout gestation remain largely unexplained. In Chapter 3, we examined gestational age-dependent changes in the maternal-fetal disposition of glyburide and its primary metabolites using a pregnant mouse model. We found that the maternal plasma PK of glyburide changed in a gestational age-dependent manner, with the largest alterations occurring in mid-late gestation on gd 15 and 19. In particular, maternal glyburide CL, V_{β}, and V_{ss} steadily increased over gestation and were approximately doubled by mid-late gestation. We observed a steady increase in the glyburide depletion rate in mouse liver microsomes as gestation progressed, suggesting that the mechanism of increased glyburide CL is related to increases in hepatic metabolism. Increases in V_{ss} and V_{β} most likely reflect increases in total body water and fat content during pregnancy, and further suggest that distribution of glyburide into maternal tissues is increased during pregnancy.

Understanding maternal disposition of primary metabolites of glyburide was also important as some metabolites (e.g. M1 and M2b) are pharmacologically active [5, 6]. We had expected that increased glyburide CL across gestation would lead to increased formation of M1-M3, if they are all derived from pathways that are up-regulated. Instead, maternal metabolite/glyburide AUC ratios were quite small and relatively unchanged throughout gestation, suggesting there may be increases in the formation and elimination of these metabolites. The ultimate fate of glyburide's primary metabolites have not been well-characterized, though, therefore it is unknown whether these metabolites go on to be further conjugated, excreted in the bile, or secreted into the urine by the kidneys.

Total fetal exposure to glyburide was < 5% of maternal plasma exposure, and doubled on gd 19 versus gd 15. This change is consistent with the finding that protein expression of BCRP

in mouse placenta on gd 15 is 2-3 times greater than that on gd 19 [7]. As BCRP protein expression decreases from gd 15 to gd 19, glyburide penetration across the placenta to the fetus increases, and therefore causes potential safety concerns for fetal exposure during late pregnancy.

This was the first evidence of gestational age-dependent changes in maternal-fetal glyburide PK. These results indicate that maternal glyburide therapeutic strategies may require adjustments in a gestational-age dependent manner if these same changes occur in humans, though concerns of increased fetal exposure in late gestation also need to be addressed.

6.3 Chapter 4: Human Fetal Liver Metabolism

Glyburide is being increasingly prescribed for the treatment of gestational diabetes mellitus; however, fetal exposure to glyburide is not well characterized from a mechanistic perspective. Glyburide can cross the placenta and fetal concentrations at term reach levels that are nearly comparable to maternal levels [4]. Whether or not glyburide is metabolized in the fetus and by what mechanisms has yet to be determined. Therefore, in Chapter 4, we determined the kinetic parameters of CYP3A enzymes for glyburide depletion; characterized glyburide metabolism by human fetal livers using tissues collected during the first or early second trimester of pregnancy; and identified the major enzyme responsible for glyburide metabolism in human fetal livers. CYP3A4 had the highest metabolic capacity towards glyburide, followed by CYP3A7 and CYP3A5. M5 was the predominant metabolite generated by CYP3A7 and human fetal liver microsomes (HFLMs) with an approximately 96% relative abundance. While M5 was the dominant metabolite generated by CYP3A4, CYP3A5, and adult liver microsomes, M1-M4 were also present at significant, but low amounts. CYP3A7 protein levels in HFLMs were highly

correlated with glyburide Cl_{int}, 16α-OH DHEA formation, and 4′-OH MDZ formation. Likewise, glyburide Cl_{int} was highly correlated with 16α-OH DHEA formation. The genotype of CYP3A5 and CYP3A7, fetal sex, estimated gestational age, and post-mortem interval did not alter CYP3A7 protein expression or glyburide Cl_{int}. These results indicate that human fetal livers metabolize glyburide predominantly to M5 and that CYP3A7 is the major enzyme responsible for glyburide metabolism in human fetal livers. Until the pharmacologic activity of M5 is determined, as well as fetal metabolism in other tissues (e.g., fetal adrenal), the metabolic profile of glyburide and ultimately safety profile for use in pregnancy remain incomplete.

6.4 Chapter 5: PD Modeling

Similar to type-2 diabetes mellitus, the pathology of GDM can be explained by decreased pancreatic production/secretion of insulin, decreased insulin sensitivity, or a combination of both. In recent years, oral hypoglycemic agents such as glyburide and metformin have gained increasing popularity for the treatment of GDM, despite the fact that their PK is altered during pregnancy [4, 8-10]. Data is quite limited, however, regarding the PD of glyburide and metformin during pregnancy. Glucose control (efficacy) can be quantified using oral minimal models of glucose and C-peptide kinetics. In recent years, these models have successfully been implemented to estimate insulin sensitivity and beta-cell function in pregnant women with GDM [4]. In Chapter 5, we provide an interim analysis of the PD of glyburide monotherapy, metformin monotherapy, or glyburide/metformin combination therapy in women with GDM compared to healthy pregnant women and non-pregnant women with type-2 diabetes mellitus receiving metformin.

On average, subjects in the GDM combination (Combo) group achieved glycemic control 10.7 days faster than the glyburide (GLY) monotherapy group, but no statistically significant differences were observed between GLY and metformin (MET) monotherapy groups, nor between the Combo and MET groups. The failure rates seemed quite high across all groups as well: ~30% for Combo and GLY versus 50% for MET. Given the failure rates of drug treatment, duration to glycemic control, and the hyperbolic disposition index curves across treatment groups, the data suggest that combination therapy for the treatment of GDM may provide further therapeutic benefit compared to glyburide and metformin monotherapy. The mechanism by which combination therapy provides therapeutic benefit remains unknown, as the synergistic effect of glyburide and metformin on beta-cell function was unexpected. Since the number of subjects in each group was relatively small (~16 subjects per group), the data are currently incomplete and the full study is still ongoing.

Overall, the studies described in this thesis and the results obtained enhance mechanistic understanding of changes in maternal-fetal PK of glyburide and its metabolites during pregnancy, which is imperative for gestational age-dependent therapeutic strategies. The PD analysis of the clinical data for glyburide and metformin in pregnant women is essential for optimization of oral hypoglycemic therapy in the management of GDM.

References

[1] Zhang H, Wu X, Wang H, Mikheev AM, Mao Q, Unadkat JD. Effect of pregnancy on cytochrome P450 3a and P-glycoprotein expression and activity in the mouse: mechanisms, tissue specificity, and time course. Mol Pharmacol. 2008;74:714-23.
[2] Koh KH, Xie H, Yu AM, Jeong H. Altered cytochrome P450 expression in mice during pregnancy. Drug metabolism and disposition: the biological fate of chemicals. 2011;39:165-9.
[3] Hakkola J, Raunio H, Purkunen R, Pelkonen O, Saarikoski S, Cresteil T, et al. Detection of cytochrome P450 gene expression in human placenta in first trimester of pregnancy. Biochem Pharmacol. 1996;52:379-83.
[4] Hebert MF, Ma X, Naraharisetti SB, Krudys KM, Umans JG, Hankins GD, et al. Are we optimizing gestational diabetes treatment with glyburide? The pharmacologic basis for better clinical practice. Clin Pharmacol Ther. 2009;85:607-14.
[5] Rydberg T, Jonsson A, Roder M, Melander A. Hypoglycemic activity of glyburide (glibenclamide) metabolites in humans. Diabetes Care. 1994;17:1026-30.
[6] Balant L, Fabre J, Loutan L, Samimi H. Des 4-trans-hydroxy-glibenclamide show hypoglycemic activity? Arzneimittelforschung. 1979;29:162-3.
[7] Wang H, Wu X, Hudkins K, Mikheev A, Zhang H, Gupta A, et al. Expression of the breast cancer resistance protein (Bcrp1/Abcg2) in tissues from pregnant mice: effects of pregnancy and correlations with nuclear receptors. American journal of physiology Endocrinology and metabolism. 2006;291:E1295-304.
[8] Langer O, Conway DL, Berkus MD, Xenakis EM, Gonzales O. A comparison of glyburide and insulin in women with gestational diabetes mellitus. N Engl J Med. 2000;343:1134-8.
[9] Camelo Castillo W, Boggess K, Sturmer T, Brookhart MA, Benjamin DK, Jr., Jonsson Funk M. Trends in glyburide compared with insulin use for gestational diabetes treatment in the United States, 2000-2011. Obstetrics and gynecology. 2014;123:1177-84.
[10] Eyal S, Easterling TR, Carr D, Umans JG, Miodovnik M, Hankins GD, et al. Pharmacokinetics of metformin during pregnancy. Drug Metab Dispos. 2010;38:833-40.